Oceanologia

Official Journal of the Polish Academy of Sciences: Institute of Oceanology and Committee on Maritime Research

This journal is supported by the Ministry of Science and Higher Education, Warsaw, Poland

Indexed in: ISI Journal Master List, Science Citation Index Expanded, Scopus, Current Contents, Zoological Record, Thomson Scientific SSCI, Aquatic Sciences and Fisheries Abstracts, DOAJ

IMPACT FACTOR ANNOUNCED FOR 2015 IN THE 'JOURNAL CITATION REPORTS' IS 0.935; 5-year IF — 1.116

Publisher
Elsevier Sp. z o.o. 4/59,
02-796 Warsaw, Poland
Tel. +48 22 546 38 20, Fax. +48 22 546 38 21

Director of Journals Publishing
Ewa Kittel-Prejs

Publishing Editor
Joanna Lewczuk
j.lewczuk@elsevier.com
48 515 082 585, 48 22 546 38 24

Publishing Manager
Agnieszka Pawłowska
a.pawlowska@elsevier.com

Subscription and Distribution Manager
Jacek Sołtyk
prenumerata@elsevier.com
48 22 546 38 27, 48 510 134 282

Marketing & Promotion Manager
Anna Szkolut
a.szkolut@elsevier.com
48 22 546 38 40, 48 515 090 174

Advertising Pharma Solutions
Monika Giergielewicz
m.giergielewicz@elsevier.com
48 519 130 280

ISSN 0078-3234

Oceanologia (2016) 58, 249—263

Available online at www.sciencedirect.com

ScienceDirect

journal homepage: www.journals.elsevier.com/oceanologia/

ORIGINAL RESEARCH ARTICLE

Satellite observations of seasonal and regional variability of particulate organic carbon concentration in the Barents Sea

Malgorzata Stramska [a,b,*], **Jagoda Bialogrodzka** [b]

[a] *Institute of Oceanology, Polish Academy of Sciences, Sopot, Poland*
[b] *Department of Earth Sciences, Szczecin University, Szczecin, Poland*

Received 20 November 2015; accepted 13 April 2016
Available online 4 May 2016

KEYWORDS
Barents Sea;
Satellite remote sensing;
Ocean color;
Particulate organic carbon

Summary The Nordic and Barents Seas are of special interest for research on climate change, since they are located on the main pathway of the heat transported from low to high latitudes. The Barents Sea is characterized by supreme phytoplankton blooms and large amount of carbon is sequestered here due to biological processes. It is important to monitor the biological variability in this region in order to derive in depth understanding whether the size of carbon reservoirs and fluxes may vary as a result of climate change. In this paper we analyze the 17 years (1998—2014) of particulate organic carbon (POC) concentration derived from remotely sensed ocean color. POC concentrations in the Barents Sea are among the highest observed in the global ocean with monthly mean concentrations in May exceeding 300 mg m^{-3}. The seasonal amplitude of POC concentration in this region is larger when compared to other regions in the global ocean. Our results indicate that the seasonal increase in POC concentration is observed earlier in the year and higher concentrations are reached in the southeastern part of the Barents Sea in comparison to the southwestern part. Satellite data indicate that POC concentrations in the southern part of the Barents Sea tend to decrease in recent years, but longer time series of data are needed to confirm this observation.

* Corresponding author at: Institute of Oceanology, Polish Academy of Sciences, Powstańców Warszawy 55, Sopot 81-712, Poland. Tel.: +48 58 73 11 600; fax: +48 58 55 12 130.
E-mail address: mstramska@wp.pl (M. Stramska).
Peer review under the responsibility of Institute of Oceanology of the Polish Academy of Sciences.

Production and hosting by Elsevier

http://dx.doi.org/10.1016/j.oceano.2016.04.004

1. Introduction

The Barents Sea (BS) is an Arctic shelf sea. It is an important region for monitoring climate change and interactions between the atmosphere, the sea ice, and the ocean. This sea with its area of about 10% of the Arctic Ocean and an average depth of about 230 m is in large part free of sea ice even during the winter season and has a great influence on the Arctic. This is because BS is located on the main pathway of the heat transported by the ocean from low to high latitudes (e.g., Ådlandsvik and Loeng, 1991; Beszczynska-Möller et al., 2012; Smedsrud et al., 2013). The heat is transported with the relatively warm Atlantic Water (Fig. 1a) by the Norwegian Atlantic Current (NAC). Near Tromsøflaket, a bank located at the entrance to the Barents Sea, the NAC splits into two branches. One branch flows eastwards into the Barents Sea, and the other one flows northwards to Spitsbergen and Fram Strait (e.g., Furevik, 2001). The inflow of AW into the BS takes place through the Barents Sea Opening (BSO, Fig. 1a). The AW is exposed in the BS to the cold air. It becomes chilled and vertically mixed (Maslowski et al., 2004; Rudels et al., 2004; Schauer et al., 2002, 2008). In addition, there is the Norwegian Coastal Water (NCW) flowing along the Norwegian coast and over the continental shelf as the Norwegian Coastal Current (NCC). The vertical and horizontal extent of the NCC varies seasonally, and the front between the NCW and AW is characterized by eddies and meanders.

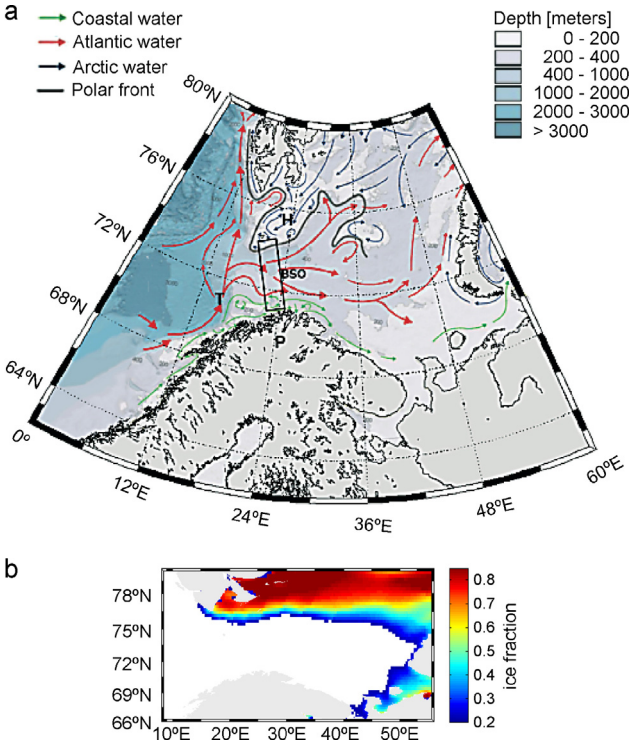

Figure 1 (a) Surface currents and bathymetry in the Barents Sea. Approximate position of the Barents Sea Opening (BSO) is indicated by a box, and letters T, H, and P indicate the location of Tromsoflaket, Hopen Island, and Porsangerfiorden. (b) The 33-year averaged (1982–2014) ice fraction in the study region in the month of May.

Tides are strong in the Barents Sea (the strongest in the Arctic apart from region near the Canadian Arctic Archipelago, Padman and Erofeeva, 2004) and they have substantial role affecting circulation and sea ice formation. Tidal mixing plays also a significant role for abyssal stratification and in controlling the water column structure on continental shelf. Interactions between tides and topography can stimulate topographic waves along the continental slope off the Northern Norway (Kowalik and Proshutinsky, 1995). This is an effective mechanism for cross slope exchange between the open sea and the shelf.

The atmospheric circulation over the BS is strongly influenced by cyclones advected from the North Atlantic. The strongest atmospheric pressure gradients are present in winter months, when southwesterly and westerly winds dominate in the southern part of the BS and southeasterly and easterly winds are frequently observed in the north (Terziev et al., 1990). The river runoff is small (163 km^3 $year^{-1}$) compared to other marginal seas of the Arctic Ocean. The Pechora River contributes most of the runoff (130 km^3 $year^{-1}$) (Lebedev et al., 2011).

Seasonal water mass transformations are driven by an intense vertical mixing due to cooling of the water masses over the entire Barents Sea in winter. In the Atlantic Water, the water column may become homogeneous down to 300 m due to vertical convection. Water mass transformations also include brine rejection processes caused by sea-ice formation in the northern and coastal BS (Schauer et al., 2002). In the spring, the water column stability in the Barents Sea is influenced by two mechanisms, ice melt and seasonal warming of the surface layer. Ice starts to melt in late April or early May, and a thin layer of melt water is progressively formed. This layer is usually more pronounced north of the Polar Front. Its thickness increases to 15–20 m during the summer and early autumn. The melt water surface layer is well-mixed and homogenous. In the Atlantic Water that is not covered by ice in winter, the stratification starts to develop when the sun begins to warm the surface layer. The stratification progresses very slowly. During summers a vertically homogeneous surface layer with about 10 m thickness is formed and some warming of the water can be observed down to 50–60 m. The Coastal Water along the Norwegian coast is, unlike the other main water masses in the Barents Sea, vertically stratified during the entire year. It preserves a weak vertical stability throughout the winter. In the spring and summer, the stratification increases because of the supply of fresh water and increased surface temperature.

It has been estimated that more than 50% of the Arctic Ocean winter heat loss occurs in the BS (Serreze et al., 2007). The oceanographic processes within the Barents Sea have a documented influence on the entire Arctic region and contribute significantly to the overall overturning in the Atlantic Ocean (Guemas and Salas-Melia, 2008; Semeneov et al., 2009). It has been shown that the Nordic and the Barents Seas are a significant sink for atmospheric carbon dioxide throughout the year (about 20–85 g C m^{-2} $year^{-1}$), while the export production due to biological productivity is in the range of 15–75 g C m^{-2} $year^{-1}$ (Skjelvan et al., 2005; Wassmann et al., 2006). Because there is a significant production of the dense (cold and salty) waters, the carbon contained in these waters can be sequestered for hundreds of years when the waters flow into the neighboring deep basins

of the Nordic Seas and Arctic Ocean (Dmitrenko et al., 2015; Lien and Trofimov, 2013; Lien et al., 2013). This means that the Barents Sea is an important region for studying ocean carbon cycle. Recently a comprehensive regional carbon budget has been constructed for the Barents Sea (see Kivimäe et al., 2010 and the references therein). This budget has been based on modeled volume flows and in situ data on dissolved inorganic carbon (DIC), dissolved organic carbon (DOC), and particulate organic carbon (POC) concentrations. The authors quantified many aspects of the regional carbon budget including fluxes due to advection, river and land sources, total CO_2 air–sea exchange, extra uptake of CO_2 in the polynyas, and burial in the sediments. One of the biggest uncertainties in the budget has been attributed to the variability of biological production and limited knowledge about spatial distribution and temporal variability of POC and DOC concentrations. An additional information about these quantities can be gained through ocean color remote sensing, which can complement in situ measurements.

The main goal in the present paper is to document spatial and temporal variability of POC concentrations in the surface waters of the Barents Sea using available satellite ocean color data. In particular we analyze the 17 years (1998–2014) time series of POC concentrations derived from data collected by the Sea-viewing Wide Field-of-view Sensor (SeaWiFS) aboard the OrbView-2 satellite and the Moderate Resolution Imaging Spectroradiometer deployed on the Aqua (EOS PM) satellite (MODIS-A). The BS is in large part ice-free all year round, thus permitting satellite observations of ocean color. Satellite POC data have been shown to have a similar performance as the chlorophyll data (Świrgoń and Stramska, 2015) and have been used to quantify particulate organic carbon reservoirs in different regions of the global ocean (e.g., for global estimates see Duforêt-Gaurier et al., 2010; Gardner et al., 2006; Stramska and Cieszyńska, 2015). Recall that POC particles include all living (e.g., phytoplankton, zooplankton) and non-living (e.g., detritus, fecal pellets) particles that contain organic carbon. The main source of POC particles in the open ocean is primary production. The information about variability and trends in POC biomass in the ocean can improve research on oceanic biological pump and its role in the sequestration of atmospheric carbon.

Satellite images of ocean color indicate that in the Barents Sea concentrations of POC reach impressively high values, and undergo significant interannual and regional variability. We will describe characteristic features of this variability, and investigate if this variability can be related to physical properties of the region, such as the sea surface temperature (SST), sea level anomalies (SLA), wind stress and ocean-atmosphere heat fluxes. We expect to find significant dependencies because phytoplankton blooms in the northern North Atlantic have been linked in the past to physical processes through in situ observations (e.g., see Marra et al., 2015, and the references therein), satellite data (e.g., Stramska, 2005) and phytoplankton models (e.g., Fasham et al., 1990; Stramska and Dickey, 1994; Stramska et al., 1995; Sverdrup, 1953; Tett and Edwards, 1984). Phytoplankton growth depends on available sunlight, water temperature, and nutrient availability. This can have important consequences for seasonal and climate related changes, and correlations in geographical patterns of SST and Chl.

The dependencies between mixing and phytoplantkton dynamics are different in different geographic regions. In the northern North Atlantic they can be summarized as follows (e.g., Stramska, 2005). (1) In winter/early spring there is enough nutrients in surface waters and there may be significant light energy at the top of the water column, but phytoplankton do not remain long enough near the surface to make significant growth. This is because water is being mixed over the mixed layer depths (MLD), which is relatively deep at this time of the year. (2) With the start of the seasonal stratification in spring and early summer, there are enough nutrients and light to support phytoplankton growth and initiation of phytoplankton bloom. It is an increased stabilization of the water column (increased SST) that allows phytoplankton to exploit higher irradiance intensities near the surface in early spring. Primary productivity increases and losses of biomass due to transport by mixing to deep waters decrease in comparison to the situation before bloom initiation. Therefore it seems that at this early phase of the phytoplankton bloom, there should be a positive correlation between SST and the biomass concentration in surface waters. Increased mixing of the water column will lead to decrease of the SST and of phytoplankton biomass in surface waters. This scenario has been supported in the past by in situ observations in the North Atlantic (see Marra et al., 2015, and the references therein). (3) In contrast, later in the season when waters are stratified, there is enough light but not enough nutrients to support net growth, and phytoplankton biomass decreases with increased stratification. At this stage we can expect that the warmer the surface water becomes in a given region (greater SST), the less mixing there is between surface and deeper, more nutrient-rich water. As surface water warms, the stratification becomes more pronounced, suppressing mixing and decreasing a transfer of nutrients from deeper to surface waters. Therefore phytoplankton productivity declines, and we would expect a negative correlation between SST and phytoplankton biomass in surface waters during this time of the year.

Regarding the long-term response of ocean productivity to rising temperatures (Henson et al., 2010), ocean models predict that increased SST will enhance stratification of the upper oceans (e.g., Hofmann et al., 2011), reducing the depth of the mixed layer and decreasing nutrient exchange with the deep ocean. Remote-sensing derived, globally averaged Chl *a* showed a significant negative relationship with density differences in the upper oligotrophic open ocean (Behrenfeld et al., 2006). Spatial patterns on a basin-scale for the stratified North Atlantic Ocean with SST ranging between 13 and 23°C are characterized by a strong inverse relationship between phytoplankton productivity and biomass with SST, mainly because nutrient supply is diminished in regions with higher SST (e.g., van de Poll et al., 2013).

2. Data sources and methods

Satellite remote sensing makes it possible to acquire large scale information about the oceans including dangerous and inaccessible regions. One such region is the Arctic, where temporal and spatial distribution of in situ observations has been irregular and insufficient, because of the inhospitable

conditions and harsh weather. Therefore, satellite remote sensing is a method of particular importance in the Arctic research. This article is based on analysis of interdisciplinary satellite data obtained from different sources for an important province of the Arctic, the Barents Sea. Our goal is to provide consistent description of POC concentration variability. Since the northern part of the Barents Sea is to a varying extent covered by sea ice (Fig. 1b), our analysis is more focused on the southern parts of the Barents Sea. To examine the correlations between different quantities, standard statistical methods have been used. Simple linear model for trends has been assumed, fitted to selected time series by a least square method and tested for statistical significance (Bendat and Piersol, 2010).

2.1. Ocean color data

The primary data set used in this study includes daily ocean surface POC concentrations derived from ocean color data collected by SeaWiFS and MODIS-Aqua. Each of these satellite missions provided global coverage of remote sensing reflectances in selected spectral bands in the visible and near-infrared spectral regions at approximately every 2 days (e.g., Franz et al., 2007; Siegel et al., 2013). Data have been processed by NASA using standard procedures (Franz et al., 2007; O'Reilly et al., 1998, 2000). These procedures involve atmospheric correction and removal of pixels with land, ice, clouds, or heavy aerosol load prior to calculation. For our study we have downloaded Level 3 POC data (Standard Mapped Images, SMI) with a nominal 9.2 km resolution at the equator, reprocessing versions R2010.0 and R2013.1 of SeaWiFS and MODIS-A data, respectively. This POC data product is derived by NASA with Stramski et al. (2008) algorithm, that allows to calculate POC concentrations from blue-to-green remote sensing reflectance band ratio. Comparisons of simultaneous satellite and in situ POC determinations in the global ocean can be found in Świrgoń and Stramska (2015). Approach to POC data analysis in the present study is similar to that described in Stramska (2014) and Stramska and Cieszyńska (2015). Therefore, we provide only a brief overview of these methods.

Daily POC concentrations [mg m^{-3}] were converted to the 21-day moving averages to fill in the missing data. At present it is difficult to precisely estimate the impact of data gaps due to clouds on average POC estimates presented on our maps. However, Racault et al. (2014) indicate that increased number of missing data in CZCS record in comparison to SeaWiFS has relatively low impact on quantities such as seasonal or annual mean chlorophyll concentrations. The estimates of the date of initiation of spring phytoplankton bloom or the duration of the growing season are more sensitive to gaps in ocean color data (Cole et al., 2012; Racault et al., 2014). Therefore we have limited our discussion to regional and seasonal means. From 21-day averaged data we estimated the monthly, annual, and the 17-year averaged POC concentrations. Data presented as spatial averages (including time series plots) represent the weighted averages from all pixels within the selected region. The weighted average accounts for the fact that pixel area at given latitude is equal to the cosine of this latitude multiplied by the pixel area at the equator (Campbell et al., 1995). The four regions, subjectively defined to show example time series of spatially averaged POC concentrations, are indicated in Figs. 2 and 5 as black boxes. The exact positions of these regions do not have any special significance, the regions have been defined mainly to illustrate temporal patterns of POC variability. We are interested in large-scale patterns, and using regional averages allows us to filter out the smaller scale variability. The geographical limits for each of the regions are as follows: region 1: 10.125–18.125°E and 71.375–74.375°N; region 2: 23.125–35.875°E and 72.0–75.0°N; region 3: 38.375–48.125°E and 69.375–72.875°N; region 4: 25.0–27.3°E and 70.95–71.45°N. For brevity we will use in this paper terms such as 'region 1 averages' or 'regional averages'. In all cases the regional averages were calculated only from pixels representing ocean surface. In the final POC dataset, data in years 1998–2002 are from SeaWiFS, in 2003–2007 represent average daily POC concentrations from SeaWiFS and MODIS-A, while in 2008–2014 are from MODIS-A observations. Estimates of multiyear trend in POC concentrations are based on data from one sensor (MODIS-A from 2003 to 2014) to avoid issues related to sensor intercalibrations.

Some of our results highlight seasonal POC variability in coastal waters. In coastal waters the standard NASA algorithms generally can be associated with increased errors in comparison to open oceans, because of optically more complex water composition (e.g., Woźniak, 2014; Woźniak et al., 2011). This is why we have decided to present additionally ocean color estimates of the vertical diffuse attenuation coefficient at 490 nm ($K_d(490)$). In this case $K_d(490)$ has been derived with the so called QAA algorithm (Lee et al., 2005a, b, 2007). The QAA algorithm has been validated in a wide range of oceanic and coastal regions and has been shown to have acceptable performance in optically complex waters (e.g., Doron et al., 2007; Lee et al., 2005a, 2007). Note that strictly speaking the vertical attenuation coefficient, $K_d(\lambda, z)$ is not a property of the water itself, but rather a descriptor of the underwater light field. It varies with depth and solar altitude (e.g., Mobley, 1994; Stramska and Frye, 1997). However in many studies $K_d(\lambda)$ has been treated as a quasi inherent optical property (quasi-IOP), because experimental data and inverse radiative transfer modeling efforts have shown that $K_d(\lambda)$ is strongly correlated with inherent optical properties, IOPs (see Kirk, 1984, 1991; Mobley, 1994). Thus, it is important to keep in mind that the spectral vertical attenuation coefficient ($K_d(\lambda)$) is significantly influenced by the variable concentrations of phytoplankton, colored dissolved organic matter (CDOM), and other optically active water components.

2.2. Sea surface temperature (SST) data

To illustrate regional variability and trends in sea surface temperature (SST) we have used the 33 years long data series (years 1982–2014) known as the National Oceanic and Atmospheric Administration (NOAA) Optimum Interpolation SST Version 2 data set (Reynolds et al., 2007). These SST data were provided by the NOAA/OAR/ESRL PSD, Boulder, Colorado, through their website at http://www.esrl.noaa.gov/psd/. These are daily records with spatial resolution of $0.25^\circ \times 0.25^\circ$, derived from the Advanced Very High Resolution Radiometer (AVHRR) infrared satellite measurements (Pathfinder data: from September 1981 to December 2005;

operational AVHRR: January 2006 onwards). In situ data from ships and buoys were used for a large-scale adjustment of satellite biases with respect to the in situ data, before data delivery by NOAA as the research quality data set. More details of the data processing methods can be found in Reynolds et al. (2007). Before applying the correction for bias, the satellite data have been classified into daytime and nighttime bins and they were corrected separately. Then, all the data have been reanalyzed jointly using the optimum interpolation (OI) procedure. The final data set represents the daily mean SST values and includes complementary information about the total SST error and information about ice fraction in a given pixel. Ice fraction equals 0 if there is no ice and equals 1 if sea surface is completely covered by sea ice. NOAA OISST SST data are currently the longest satellite data record that can be used to study long-term SST variability and trends. Note that the infrared satellite remote sensing SST algorithms can provide either a skin SST if they are based on radiative transfer models or a subskin SST if in situ observations have been used to adjust satellite retrievals (Merchant and LeBorgne, 2010). In the NOAA OI SST Version 2 data, the bias correction of the satellite data has been based on data from ships and buoys, therefore it can be interpreted as the bulk SST at about 0.5 m depth (Reynolds et al., 2007).

2.3. Sea level anomaly (SLA) data

To characterize the variability of sea level we have used sea level anomalies (SLA) extracted from the delayed time (DT) multimission global gridded data product available at AVISO (www.aviso.oceanobs.com). The SLA data are continuously updated by AVISO and referenced to the 20-year (1993–2012) mean sea surface height. For this study we have used the available DT SLA data, covering the time period from January 1, 1993 to December 31, 2014 (22 years). The SLA data have been interpolated by AVISO on $0.25^\circ \times 0.25^\circ$ spatial grid with 1-day temporal resolution, using computing methods based on objective analysis. Data have been corrected for instrumental noise, orbit determination error, atmospheric attenuation (wet and dry tropospheric and ionospheric influences), sea state bias, and tidal influence. The tidal aliasing is routinely corrected for by using tidal models that assimilate altimetry data (Le Provost, 2001). Detailed information about standard data processing methods is available at www.aviso.oceanobs.com. The error in the SLA data estimated by AVISO is about 1–2 cm. A comprehensive validation of a gridded satellite altimetry data product in the high-latitude seas, including the Barents Sea has been published by Volkov and Pujol (2012). The altimetric sea level determinations in coastal areas have been compared with available tide gauge records showing a good agreement in terms of the root-mean square differences, the amplitudes and phases of the seasonal cycle, and the long-term trend. Away from the coast the altimetry data have been found consistent with the mesoscale variability derived from drifter data.

2.4. Meteorological and hydrography data

To evaluate the role of atmospheric forcing we have used the meteorological data from the NOAA-CIRES Climate Diagnostic Center NCEP/NCAR (National Centers for Environmental Prediction and National Center for Atmospheric Research) Reanalysis 2. These data sets are based on state-of-the-art analysis/forecast system to assimilate global meteorological data from various available sources from 1948 to the present. In particular we have used the daily latent and sensible heat flux estimates, along with the net longwave and net shortwave radiation estimates to calculate the net heat flux at the sea surface. We have also used the wind stress data.

To discuss water properties we have used the World Ocean Atlas data (WOA 2013 version 2, www.nodc.noaa.gov/OC5/woa13/) provided by the National Ocean and Atmospheric Administration (NOAA) National Centers for Environmental Information (NCEI). The WOA consists of a climatology of fields of in situ ocean properties objectively analyzed for the World Ocean (Boyer et al., 2013). We have downloaded (1° grid) climatological monthly means of in situ temperature, salinity, and nitrate.

3. Results

3.1. Regional trends in SST and SLA

We start with a brief description of environmental conditions characterizing our study region. Fig. 2a and b shows the regional distribution of the 33-year averaged annual and May SST, respectively. Spatial SST distributions presented in Fig. 2a and b demonstrate significant influence of surface patterns of major oceanic currents shown in Fig. 1. The highest values of the 33-year average annual and May SST (about 8°C) are noted in the Norwegian Atlantic Current (NAC), while the lowest SST values (below 0°C) are detected in the northeastern part of the Barents Sea, a region which is covered by sea ice in winter. In Fig. 2c we have displayed spatial distribution of the 33-year averaged amplitude of the annual SST cycle. As can be seen in Fig. 2c the greatest amplitude of the seasonal SST cycle (about 8°C and more) is associated with the southeastern regions of the Barents Sea. These include regions located near Norway, within the shallower section of the Barents Sea where the water depth is below 300 m (compare with Fig. 1). The smallest amplitude of the 33-year averaged annual SST cycle ($\sim 3^\circ$C) is observed in the northern regions and in the West Spitsbergen Current. In Fig. 2d we have plotted spatial distribution of the standard deviations (STD) calculated from the 33-years long time series of the daily SST. These STDs were estimated after subtracting from the daily SST data the seasonal cycle and the multi-year trend. Thus, Fig. 2d illustrates the overall spatial variability of SST, unrelated to the seasonal cycle and multi-year trend. Note that the highest STD values (about 1.4°C) are documented near the Svalbard Archipelago and between Novaya Zemlya and the coastal regions near Russia. These high STD values can be due to the variable position of surface currents and frontal zones. The lowest STDs ($\sim 0.7^\circ$C) are associated with the AW inflow in the southwest part of our study region and are also observed in the northeastern region.

Time series of annually averaged SST data allowed us to estimate the 33-year annual and May SST trends, displayed in Fig. 2e and f. From the results shown in Fig. 2e and f it is clear that the trends (statistically significant at 95% confidence

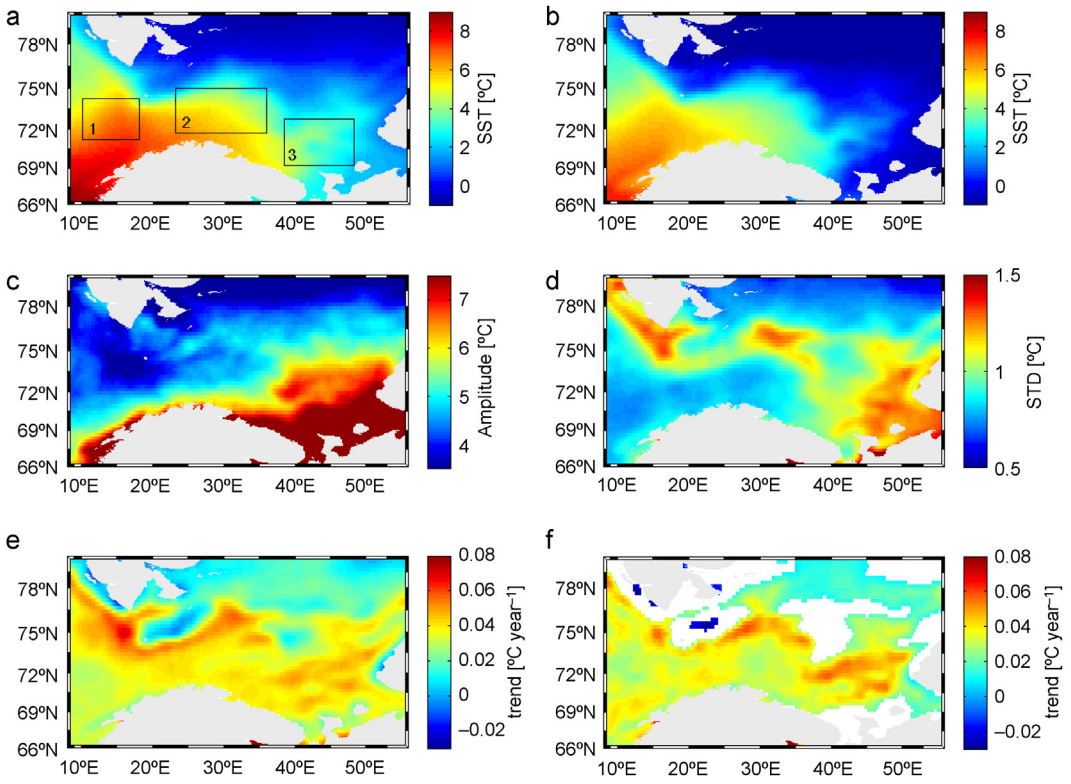

Figure 2 Maps based on the 33 years of SST data (1982–2014): (a) the 33-year mean SST, (b) the 33-year mean SST in the month of May, (c) the 33-year mean amplitude of the annual cycle, (d) standard deviation of SST anomalies, (e) trends in the annual mean SST, and (f) trends for the monthly mean SST in May. Only pixels with statistically significant ($p < 0.05$, 95% confidence level) trend have been displayed. Black boxes indicate study regions 1, 2, and 3 (see explanations in Section 2).

level, $p < 0.05$) of increasing annual and monthly mean SST (for the month of May) are detected in most of the area of the southern Barents Sea. Trends assume values of about 0.06°C year^{-1} (i.e., 0.6°C per decade) in the regions located west of the Hopen Island and between 0.04 and 0.06°C year^{-1} near the coastal regions off Norway. The trends in annually averaged SST are low or insignificant in the northern regions of the Barents Sea. Larger values of SST trend in the southern BS can be related to an increase of the volume and temperature of the Atlantic Water transported into the Barents Sea (Årthun et al., 2012). Recently, Oziel et al. (2016) showed that the volume of the Atlantic Water had approximately doubled between 1980 and 2011, and the domain occupied by the Atlantic Water extended further east and north. The authors indicate that although in the western part of the BS, the position of the Polar Front is constrained by the topography, in the eastern BS the position of the Southern Front (temperature front) is moving northward.

For comparison, according to Morice et al. (2012) linear trends in global surface temperature anomalies from 1979 to 2010 are approximately 0.17°C per decade, while northern/southern hemispheric trends are 0.24/0.10°C per decade. Luo et al. (2011) estimated linear trends for global, terrestrial, and ocean surface air temperatures (SAT) from 1982 to 2008 as 0.14, 0.21, and 0.10°C per decade, respectively. Using the 20 years (from January 1985 to December 2004) of the global Advanced Very High Resolution Radiometer Pathfinder data, the global SST trend has been estimated to be 0.18 and 0.17°C per decade based on the daytime or nighttime data respectively (Good et al., 2007). The warming trends estimated by us in the Barents Sea are greater than these global trends in most of the region located south from 76°N (see also Jakowczyk and Stramska, 2014).

Satellite altimetry sea level anomaly (SLA) data covering 22 years (1993–2014) have been used to investigate sea level variability in the study region. We have estimated regional pattern of statistically significant (95% confidence level, $p < 0.05$) trend in sea level (Fig. 3a). This trend varies spatially with values of about 2–4 mm year^{-1} in the southern Barents Sea. Similar trends for this region have been estimated before by Volkov and Pujol (2012), based on somewhat shorter SLA data record, covering the time from December 1992 to November 2010. For comparison, according to Nerem et al. (2010), the rate of globally averaged sea level rise is estimated currently as 3.1 mm year^{-1} (or 3.4 mm year^{-1} if correction for global isostatic adjustment is taken into account). Similar estimate of the global trend has been published by the Commonwealth Scientific and Industrial Research Organization (CSIRO, 3.2 mm year^{-1}, see www.cmar.csiro.au/sealevel/sl_hist_last_15.html), and by AVISO (3.2 mm year^{-1}, see www.aviso.oceanobs.com/en/news/ocean-indicators/mean-sea-level/). Thus, the sea level trend in the coastal regions of the southern Barents Sea is slightly higher than the globally averaged trend derived from satellite altimetry data. In Fig. 3b we have plotted standard deviation estimated from detrended SLA data. This result shows that the sea level variability is strongest in the southeastern Barents Sea. Note that this is almost the same region

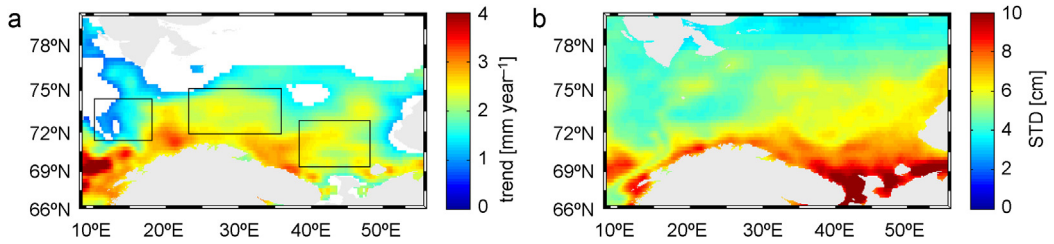

Figure 3 Sea level variability: (a) the 22-year trend (1993–2014) in the SLA data record. Only pixels with statistically significant ($p < 0.05$, 95% confidence level) trend have been displayed. (b) Standard deviations in the SLA data.

where we have observed relatively large annual amplitude and standard deviations of SST values (see Fig. 2).

It has been shown before that the major component in the variability of the altimetric and tide gauge sea level records in the BS region is the seasonal cycle (Volkov and Pujol, 2012). Its annual amplitude varies from about 7 to over 10 cm along the Norwegian coast. It has been confirmed by Volkov et al. (2013) that the sea level mass related variability in the central part of the BS is due to the combined effect of wind forcing balanced by the flow over the varying bottom topography (topographic influence). According to these authors wind forcing is the main reason for the observed time lag between the annual maxima in the Norwegian and Barents Seas.

3.2. POC concentrations

Maps displayed in Fig. 4 are summarizing the spring/summer variability of POC concentrations in the study region and show the 17-year averaged monthly data. The variability due to seasonal cycle is significant. The highest POC concentrations (more than 300 mg m^{-3}) can be found in the region located south from 76°N and between 22–50°E in May. West from about 22°E, at the edge of the Barents Sea and in the vicinity of the Norwegian Sea, the maximum annual POC concentrations are observed later in the year (in June), and on average these concentration do not reach as high values as they do in the region east from 22°E in May. It should be noted that the 17-year averaged POC monthly mean concentrations in the Barents Sea achieve quite high values when compared to global averages (see Stramska and Cieszyńska, 2015 for global estimates). For example it has been shown that the maximum seasonal POC concentration averaged over the entire North Atlantic Ocean is only about 110 mg m^{-3} and the annual mean is ~90 mg m^{-3}. The maximum values in different parts of the northern North Atlantic can exceed 300 mg m^{-3}. The Barents Sea is one of the few regions of the global ocean where such extreme values are regularly observed in satellite data.

When analyzing the characteristic features of POC concentration variability in the Barents Sea, we have noted that the temporal patterns of POC concentrations in the coastal regions off Norway are not synchronized with the progression of the seasonal cycle in the open waters of the southern Barents Sea. To show this in a better focus we present in Fig. 5 maps of monthly POC concentrations and vertical diffuse attenuation coefficient for downwelling irradiance at 490 nm (K_d(490)). We understand that ocean color POC estimates in coastal waters

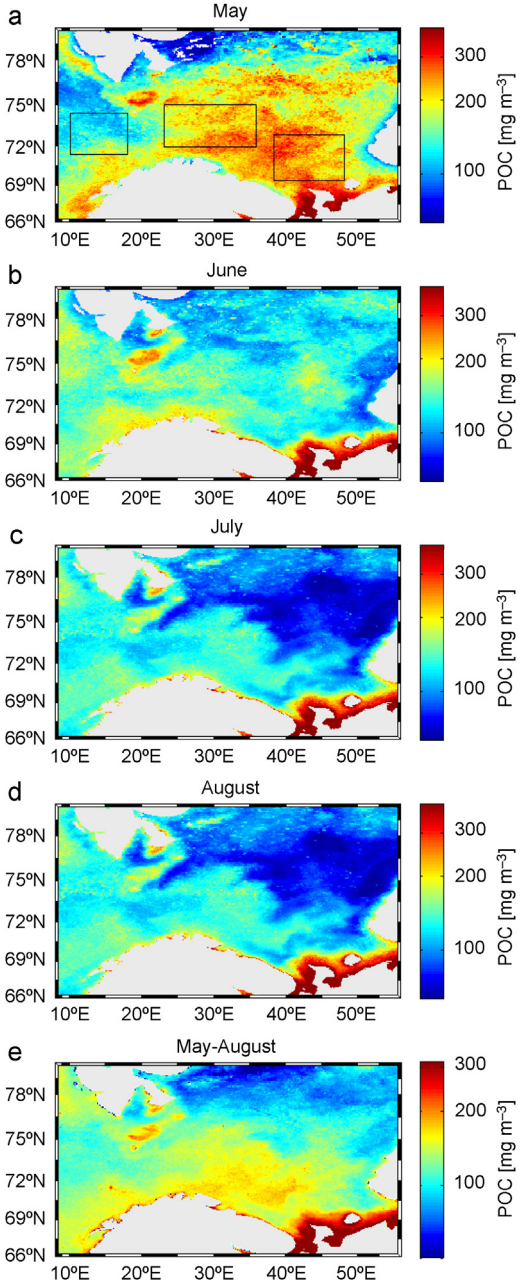

Figure 4 Maps of the 17-year averaged (1998–2014) surface POC concentrations in (a) May, (b) June, (c) July, (d) August, and (e) in summer (May–August).

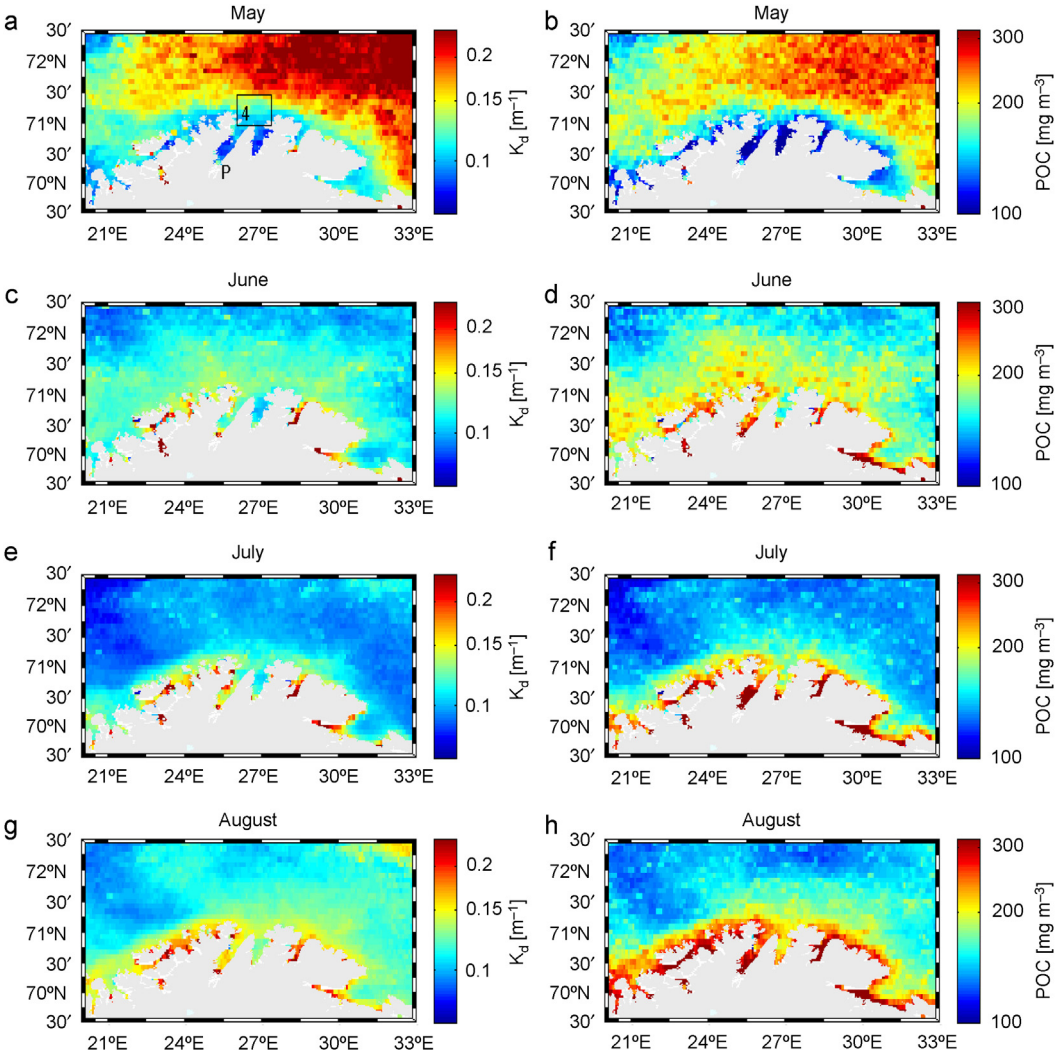

Figure 5 Maps of the 17-year averaged (1998–2014) (left panel) vertical diffuse attenuation coefficient at 490 nm, $K_d(490)$; (right panel) the monthly mean surface POC concentrations in the months of (a and b) May, (c and d) June, (e and f) July and (g and h) August. Black box in figure a indicates region 4.

may include larger errors than in the open ocean waters, but both $K_d(490)$ and POC estimates shown in Fig. 5 strongly suggest that in May coastal waters are characterized by rather low concentrations of optically active water components in comparison to the open ocean waters. These concentrations increase in coastal waters in June and in July. In August coastal waters are significantly more turbid than the open waters. A more quantitative interpretation of ocean color satellite data in coastal waters is out of scope if this paper, as coastal waters require a special approach including validations of local ocean color algorithms. We have recently carried out in situ experiments in one of the fjords shown in Fig. 5 (Porsangerfiorden) and we will address these problems in our next paper.

In order to stress the regional differences in seasonal cycles, we present in Fig. 6 the 17-year averaged daily time series of SST and POC concentrations averaged in the study regions 1, 2, 3, and 4. Region 1 is associated with the smallest amplitude of the seasonal SST cycle and the highest annual average SST value (Fig. 6a). The largest annual SST amplitude is observed in region 3. The differences between the 17-year averaged regional daily SST values in these two regions are more pronounced in the winter than in the summer. The SSTs in the winter season in coastal waters (region 4) have similar values as in region 2 but in the summer the SSTs in region 4 reach higher values than in region 1. In Fig. 6b we compare the time progression of the seasonal POC cycle in each of the regions. Since ocean color satellite data are missing due to low solar angles in winter, we limited this comparison to the time period of April through September. In Fig. 6b we can see that the rapid seasonal increase in POC concentration is observed on average earlier in the year and the maximum POC concentrations reach higher values in regions 2 and 3 than in regions 1 and 4. The seasonal progression of the cycle is similar in regions 2 and 3. Significant seasonal increase of POC concentration in region 2 and 3 is observed on average around year day 100 and it is accompanied by only a small increase in SST. Maximum SST values in the annual cycle are observed significantly later in the year (August) than the maximum POC concentrations (May). In comparison to regions 2 and 3, the seasonal increase in POC concentrations in region 1 is observed on average later in the year (days 115–125), the maximum concentrations are reached in June

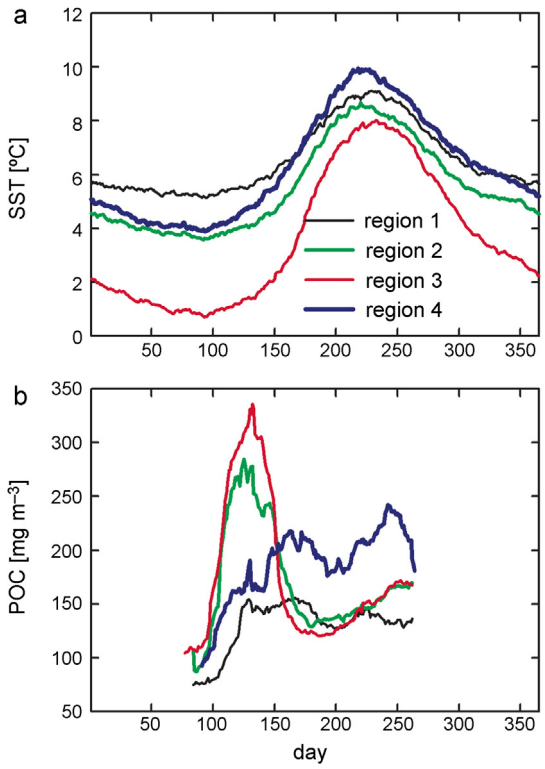

Figure 6 Comparison of the 17-year averaged (1998–2014) daily time series of (a) regionally averaged SST and (b) regionally averaged POC concentrations. The geographical positions of the regions are shown in Figs. 4a and 5a are explained in the text.

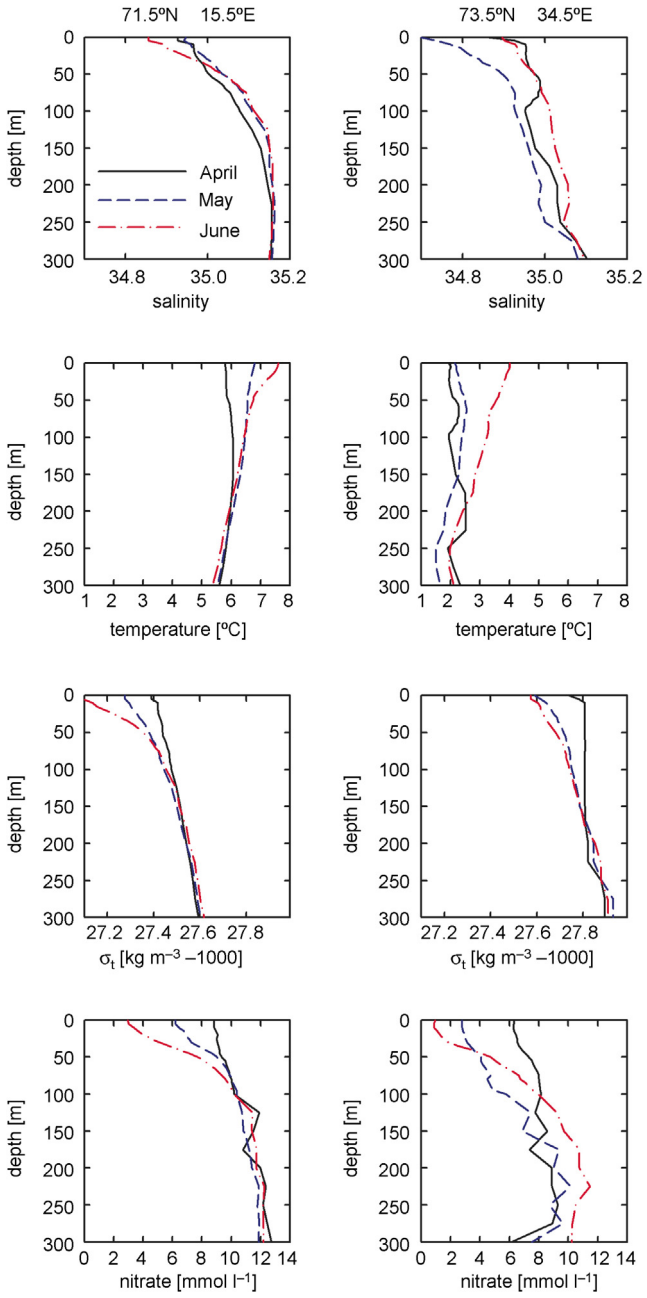

Figure 7 Comparison of the monthly climatology (based on WORLD OCEAN ATLAS 2013 version 2 objectively analyzed mean data on 1° grid from years 1995–2012) of water temperature, salinity, density $\sigma(t, s, 0)$, and nitrate concentration at grid points located within region 1 (left panel) and 2 (right panel).

and are lower than the annual maximum values in regions 2 and 3. In the coastal waters (region 4) the seasonal progression of POC cycle has a similar shape as in region 1, but it seems that higher POC concentrations are observed in coastal waters. Note, that the seasonal averages (May–August) of POC concentrations shown in Fig. 4e are significantly higher in the south-eastern part of the BS than in the western part of the study region. If we compare POC maps (Fig. 4) with SST and SLA maps (Figs. 2 and 3) we note that the region where seasonally averaged POC concentrations reach the spectacularly high values coincides with the area where the annual amplitude and standard deviation of SST as well as standard deviation of SLA are large. This suggests that the more variable thermal and dynamic environment, where vertical mixing of the water column is very intense, is also more prone to sustaining high production of POC particles.

Summarizing, the satellite POC concentrations in the open BS display seasonal variability that can be associated with the seasonal cycle in phytoplankton productivity and abundance. In the literature the Barents Sea has been described as a spring bloom system (Olsen et al., 2003; Rey, 1981). It has been shown that the exact timing of the phytoplankton bloom is somewhat variable and has significant regional variability throughout the Barents Sea. Usually the main bloom has been associated with the onset of seasonal stratification of the water column. The dominant algal group during the spring bloom are diatoms, and *Chaetoceros socialis* is often the most abundant species (Olsen et al., 2003; Rey, 1981). The concentrations of diatoms can reach up to several million cells per liter. When the silicate becomes limiting other algal groups such as flagellates take over. The most important flagellate species in the Barents Sea is *Phaeocyctis pouchetii*.

In order to derive a better understanding of the observed regional differences in the seasonal POC cycle in the BS we have plotted in Fig. 7 the vertical profiles of water temperature, salinity, density, and nitrate concentrations. These data represent climatology from WOA 2013 data sets for grid points located within regions 1 and 2. The lowest surface temperature in the upper part of the water column in both

regions is observed in April (we did not plot profiles for earlier months to improve the clarity of Fig. 7). Water salinity increases with depth, but generally water is less salty in region 2 than in region 1, while water temperature is lower in region 2 than in region 1. It is interesting to note that in April there is a small, but obvious decrease of salinity near the water surface in region 1 and 2, which translates to a decrease of water density that is more pronounced in region 2 than in region 1. It is also remarkable that water column density in region 2 is very well homogenized down till about 250 m, except for this small feature near the surface which is due to a decrease of water salinity. In region 2 in May, there is a further decrease of water salinity, which causes a decrease of water density and increases the stability of surface waters. This supports the notion that the inflow of melt water creates the opportunity for the onset of phytoplankton bloom. In May nitrate concentrations in region 2 are already significantly lower than in April (this decrease can be observed as deep as 120–150 m), which is consistent with our belief that significant primary production takes place here at this time of the year. In contrast to region 2, water column is weakly stratified in region 1 in April, but the mixed layer depth (defined by change in the water density, Monterey and Levitus, 1997) is still relatively deep (~150 m). In May surface water stratification increases, but if we look at the vertical profiles of nitrate concentrations, we can see that the change between April and May is smaller in region 1 and larger in region 2. This is in agreement with our observation that there is only small increase in the abundance of POC particles here in May.

Based on the presented data we suggest that the regional differences in the seasonal cycle of POC concentration to a large degree reflect regional differentiation in seasonal productivity and abundance of phytoplankton. These regional differences are determined by large scale air–sea interaction processes. Intense water column mixing during winter in the entire region pre-conditions it for the occurrence of intense seasonal phytoplankton blooms. The blooms start early in the study area 2, because the surface waters become stabilized when the low-salinity melt water is supplied. The fact that the water column is almost homogenous at the beginning of the spring, allows for efficient replenishing of nutrients at the time period when the bloom develops. At this time of the year the periods of calmer seas are alternating with stormy weather. Such conditions are very favorable for development of extreme phytoplankton blooms. The fact that the seasonal increase of POC concentration is observed later in study area 1 in comparison to study area 2 can be explained by lower supply of melt water in the area 1. Therefore, the initiation of the spring bloom in region 1 is delayed until the net heat flux is sufficient to stabilize the surface waters. However, the net heat flux in the spring also seems to favor more efficient warming of surface waters in region 2 than in region 1 (see Fig. 8). Note that according to NCEP convention negative heat flux indicates that the atmosphere is loosing and the ocean surface is gaining heat. Thus according to Fig. 8 in spring and summer (on average) more heat is transferred from the atmosphere to the ocean surface in region 2 than in region 1. In addition, the intensity of the spring blooms in region 2 is amplified by the fact that below the surface, the water column remains well mixed after the winter. Note that, since region 2 is located on the shelf with water depths of about 300 m or less, winter mixing reaches

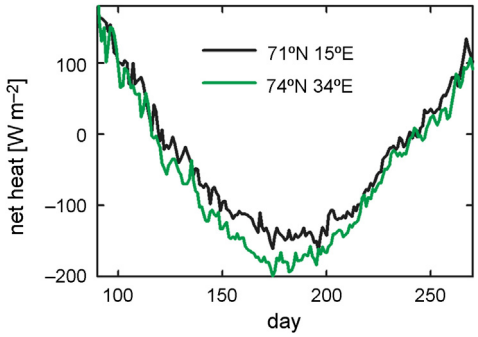

Figure 8 Comparison of the mean daily net heat flux at grid points located within region 1 and 2 (based on NCEP data from years 1998–2014 on sensible, latent, net shortwave and longwave radiation flux data).

the bottom water layer. This allows for efficient re-supply of nutrients from deep waters in winter and intermittent supply of nutrients in spring during storms. The main difference between region 1 and 2 is that region 1 is located in warmer AW waters in deeper ocean, and there is lower supply of low salinity waters. In addition, although there is an efficient mixing of warm advected water masses, water column does not appear to be as completely homogenous as in region 2. Phytoplankton biomass seems to increase in spring in response to seasonal warming of surface waters and this happens later than the onset of phytoplankton bloom in regions 2 and 3.

In addition to the seasonal cycle, satellite data allow us to trace the interannual variability of POC concentrations. This is shown in Fig. 9a, where regionally averaged May POC concentrations plotted as a function of the year have been compared. The highest POC concentrations are observed in year 2003. Interestingly, although the concentrations are generally lower in region 1 than in regions 2 and 3, nevertheless the patterns of interannual variability seem similar in all 3 regions. This is confirmed by scatter plots (Fig. 9b), that show statistically significant correlations between POC concentrations observed between regions 1 and 2 and between regions 1 and 3. In addition the seasonally (May–August) averaged POC concentrations are strongly influenced by the concentrations reached during the month when the maximum concentrations are observed. This is supported by the results summarized in Fig. 9c, where we can see a statistically significant correlation between May and seasonally averaged POC concentrations in regions 2 and 3. In region 1 the seasonally averaged POC concentrations correlate best with June POC concentrations. What is more, the interannual variability in POC concentrations can be linked to SST variability. We have analyzed different sets of data (heat fluxes, wind stress, air temperatures) and we have found out that the best, statistically significant correlation is observed between the minimum value of the regionally averaged SST in the winter season and the May POC concentrations (Fig. 9d). Correlations between April or May atmospheric or SST data and May POC concentrations were not statistically significant (not shown). This suggests that the interannual POC variability depends on winter pre-conditioning of the water masses. These could include more complete homogenization of the water column as well as production of more

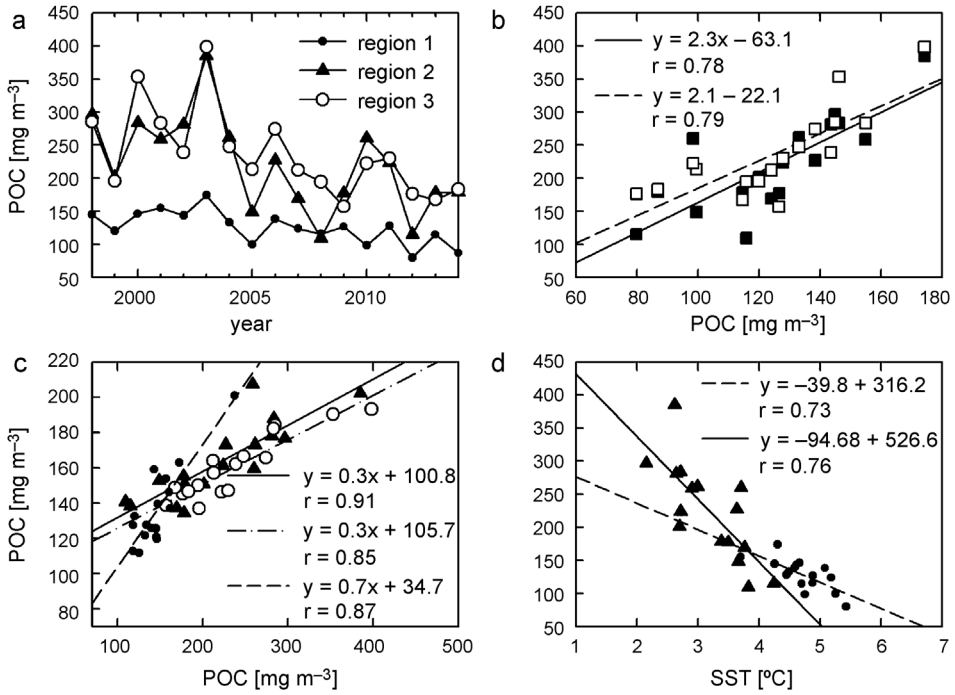

Figure 9 Interannual variability of POC concentration and SST in the study regions. (a) Time series regionally averaged of POC concentrations in the months of May in region 1 (black dots), 2 (black triangles) and 3 (open circles). (b) Relationships between the regionally averaged POC concentrations in May in different regions. Black squares and solid line are for region 2 plotted as a function of region 1, and open squares and dashed line are for region 3 versus region 1. Horizontal axis is for region 1. (c) Relationships between regional POC concentrations averaged over summer (May–August, shown on vertical axis) and the regional maximum monthly mean POC concentrations. Dashed line and dots are for POC concentrations in June in region 1, solid line and triangles are for POC concentrations in May in region 2, dash-dot-dash line and open circles are for POC concentrations in May in region 3. (d) Correlations between the regionally averaged POC concentrations in May and the regionally averaged annual minimum SST (dashed line and black dots are for region 1, solid line and triangles are for region 2).

sea ice in winter resulting in a better supply of melt water in the spring.

Because of the extremely high POC concentrations and efficient mixing of waters, the Barents Sea is potentially an important region for export of POC particles to deep waters. Note, that POC particles have low sinking velocities because their density is close to that of seawater. Traditionally, two processes have been attributed a major role for exporting POC. These are transport associated with the zooplankton ecosystem, and transport by gravitational settling of biogenic aggregates ballasted by heavy biomineral and lithogenic particles. Another potentially important mechanism for export of POC particles from surface waters is turbulent diffusion and mixing, in particular during energetic mixing episodes of surface waters in response to atmospheric forcing events (e.g., Stramska, 2010). This mechanism can play a particularly strong role in the Barents Sea.

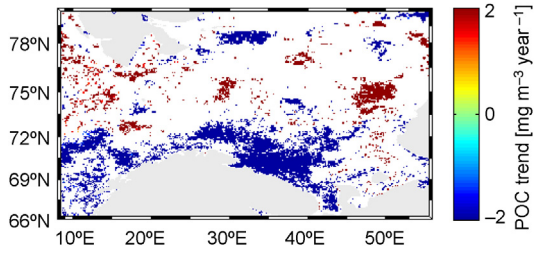

Figure 10 Map indicating pixels with statistically significant trend in surface POC concentrations ($p < 0.01$, 90% confidence level). Trend has been estimated using data from MODIS-Aqua (2003–2014).

Seasonally averaged POC concentrations can be used to investigate multiyear trends. We have tested if regional trends are statistically significant using data from MODIS-A (data from years 2003–2014). The results are presented in Fig. 10, where only pixels with statistically significant trends have been included. Trends of decreasing POC concentrations have been detected in few areas of the southern Barents Sea. This could be associated with less efficient mixing and more stable water masses in this polar province. It is generally expected that global climate change can slow the production of dense water masses due to less efficient creation of sea ice in this region. Increase in the SST has been confirmed by the analysis of the long-term SST data records. Note however that the results concerning POC trends need to be taken with caution and cannot be interpreted at this time as climate related change, because time series used in our calculations are too short for detection of climate trends.

4. Conclusions

Our main focus in this paper is in regional and seasonal variability of POC concentration in the region of the Barents

Sea. Since northern parts of the BS are covered by sea ice, our attention has been mostly on the southern part of the BS. Results presented in this paper have been based on ocean color satellite data supported by other interdisciplinary data sets available for research. The most important findings can be summarized in the following way.

- Seasonal increase in POC concentration in the southeastern Barents Sea is evident in May and is observed earlier in the year than in the southwestern side and in the neighboring waters of the Norwegian Sea. This is most likely associated with the stabilization of the surface waters by melt water beginning in April that allows for an early onset of phytoplankton bloom in the southeastern Barents Sea.
- In the southwestern edge of the Barents Sea and its vicinity, the seasonal increase of POC concentration is observed later in the year (end of May—June). This is likely associated with the fact that phytoplankton bloom in this area develops in response to water stratification taking place due to increased seasonal solar heating of surface waters. Seasonal increase of net heat flux gained by the ocean from the atmosphere and stabilization of the water column due to an increase in surface water temperature in this region is observed later in the year than the stabilization of surface waters in the southeastern Barents Sea by the advection of low salinity waters from melting sea ice.
- POC concentrations in the southeastern Barents Sea are among the highest observed in the global ocean. This can be linked to the fact that waters in this region become efficiently mixed during winters. The vertical mixing processes that take place during winters are important for transporting nutrient rich water to the surface, and this allows for high primary production in spring. In addition weak stratification of waters in May and June most likely allows for periodical replenishing the nutrients during storms and sustaining relatively high primary production and POC concentration through the summer months.
- Interannual variability of POC concentration in the open waters has been linked to lower SSTs observed in the winter season.
- In coastal waters the seasonal cycle of POC concentrations is not synchronized with the cycle observed in the open sea.
- We have shown that POC concentrations in the southern part of the Barents Sea tend to decrease in recent years. The decreasing trend has been detected with data from MODIS-Aqua from 2003 to 2014. This result needs to be taken with caution, as the ocean color time series are still too short to interpret this result as climate related trend.

Results presented in this paper strongly support the notion that seasonal restratification of the water column drives the changes in concentration of POC in surface waters from mid-winter lows to spring highs in the Barents Sea. In recent years there has been a renewed interest in Sverdrup's (1953) critical depth hypothesis (e.g., Behrenfeld, 2010; Chiswell, 2011). Conceptually, Sverdrup's hypothesis means that the balance between net phytoplankton production and the vertical mixing can determine the fate of phytoplankton populations in a variety of environments. Satellite data presented in our manuscript do not allow us to make calculations according to the model proposed by Sverdrup, since we do not have any data on grazing and community respiration. Nonetheless, our research supports the belief that mixing is critical for the temporal and spatial patterns observed in phytoplankton biomass in the Barents Sea.

Acknowledgments

The authors are grateful to all the persons involved in the programs providing free access to the data sets used in this study. The ocean color data were made available through the NASA Ocean Color Web (oceancolor.gsfc.nasa.gov/). The National Oceanic and Atmospheric (NOAA) Optimum Interpolation SST (OISST) Version 2 data set were made available by the NOAA Earth System Research Laboratory Physical Science Division (ESRL/PSD) and the meteorological data were obtained from the National Centers for Environmental Prediction and National Center for Atmospheric Research (NCEP/NCAR) Reanalysis Project at the NOAA/OAR/ESRL PSD (http://www.esrl.noaa.gov/psd/). World Ocean Atlas data (WOA 2013 version 2, www.nodc.noaa.gov/OC5/woa13/) were provided by the National Ocean and Atmospheric Administration (NOAA) National Centers for Environmental Information (NCEI). The altimeter data were processed by Ssalto/Duacs and distributed by AVISO, with support from Cnes (http://www.aviso). We would also like to thank Sebastian Meler from the IO PAN for help with data transfers.

Funding: This work was funded by the Norway Grants through the Polish-Norwegian Research Programme operated by the National Centre for Research and Development (NCBR contract No. 201985 entitled 'Application of in situ observations, high frequency radars, and ocean color, to study suspended matter, particulate carbon, and dissolved organic carbon fluxes in coastal waters of the Barents Sea'). Partial support for MS comes also from the statutory funds of the Institute of Oceanology of the Polish Academy of Sciences (IO PAN) and from the National Science Centre (NCN) in Poland through grant 2011/01/M/ST10/07728 'Global estimates of particulate organic carbon reservoir and export flux in the ocean based on satellite ocean color data'.

References

Ådlandsvik, B., Loeng, H., 1991. A study of the climatic system in the Barents Sea. Polar Res. 10 (1), 45—50, http://dx.doi.org/10.1111/j.1751-8369.1991.tb00633.x.

Årthun, M., Eldevik, T., Smedsrud, L.H., Skagseth, Ø., Ingvaldsen, R. B., 2012. Quantifying the influence of Atlantic heat on Barents Sea variability and retreat. J. Climate 25, 4736—4743.

Behrenfeld, M.J., 2010. Abandoning Sverdrup's critical depth hypothesis on phytoplankton blooms. Ecology 91 (4), 977—989, http://dx.doi.org/10.1890/09-1207.1.

Behrenfeld, M.J., O'Malley, R.T., Siegel, D.A., McClain, C.R., Sarmiento, J.L., Feldman, G.C., Milligan, A.J., Falkowski, P.G., Letelier, R.M., Boss, E.S., 2006. Climate-driven trends in contemporary ocean productivity. Nature 444 (7120), 752—755, http://dx.doi.org/10.1038/nature05317.

Bendat, J.S., Piersol, A.G., 2010. Random Data: Analysis and Measurement Procedures, 4th ed. Wiley, New Jersey, 640 pp.

Beszczynska-Möller, A., Fahrbach, E., Schauer, U., Hansen, E., 2012. Variability in Atlantic water temperature and transport at the entrance to the Arctic Ocean, 1997—2010. ICES J. Mar. Sci. 69 (5), 852—863, http://dx.doi.org/10.1093/icesjms/fss056.

Boyer, T.P., Antonov, J.I., Baranova, O.K., Coleman, C., Garcia, H.E., Grodsky, A., Johnson, D.R., Locarnini, R.A., Mishonov, A.V., O'Brien, T.D., Paver, C.R., Reagan, J.R., Seidov, D., Smolyar, I. V., Zweng, M.M., 2013. World Ocean Database 2013, NOAA Atlas NESDIS 72, S. Levitus, Ed., A. Mishonov, Technical Ed. Silver Spring, MD, http://dx.doi.org/10.7289/V5NZ85MT, 209 pp.

Campbell, J.W., Blaisdell, J.M., Darzi, M., 1995. Level-3 SeaWiFS Data Products: Spatial and Temporal Binning Algorithms. SeaWiFS Tech. Rep. Ser. 32, 73 pp.

Chiswell, S.M., 2011. Annual cycles and spring blooms in phytoplankton: don't abandon Sverdrup completely. Mar. Ecol. Prog. Ser. 443, 39–50, http://dx.doi.org/10.3354/meps09453.

Cole, H., Henson, S., Martin, A., Yool, A., 2012. Mind the gap: the impact of missing data on the calculation of phytoplankton phenology metrics. J. Geophys. Res.-Oceans 117 (C8), C08030, http://dx.doi.org/10.1029/2012JC008249.

Dmitrenko, I.A., Rudels, B., Kirillov, S.A., Aksenov, Y.O., Lien, V.S., Ivanov, V.V., Schauer, U., Polyakov, I.V., Coward, A., Barber, D.G., 2015. Atlantic water flow into the Arctic Ocean through the St. Anna Trough in the northern Kara Sea. J. Geophys. Res.-Oceans 120 (7), 5158–5178, http://dx.doi.org/10.1002/2015JC010804.

Doron, M., Babin, M., Mangin, A., Hembise, O., 2007. Estimation of light penetration, and horizontal and vertical visibility in oceanic and coastal waters from surface reflectance. J. Geophys. Res. 112 (C6), C06003, http://dx.doi.org/10.1029/2006JC004007.

Duforêt-Gaurier, L., Loisel, H., Dessailly, D., Nordkvist, K., Alvain, S., 2010. Estimates of particulate organic carbon over the euphotic depth from in situ measurements. Application to satellite data over the global ocean. Deep-Sea Res. Pt I 57 (3), 351–367, http://dx.doi.org/10.1016/j.dsr.2009.12.007.

Fasham, M., Ducklow, H.W., McKelvie, S.M., 1990. A nitrogen based model of plankton dynamics in the oceanic mixed layer. J. Mar. Res. 48 (3), 591–639.

Franz, B.A., Bailey, S.W., Werdell, P.J., McClain, C.R., 2007. Sensor-independent approach to the vicarious calibration of satellite ocean color radiometry. Appl. Optics 46 (22), 5068–5082, http://dx.doi.org/10.1364/AO.46.005068.

Furevik, T., 2001. Annual and interannual variability of Atlantic Water temperatures in the Norwegian and Barents Seas: 1980–1996. Deep-Sea Res. Pt I 48 (2), 383–404.

Gardner, W.D., Mishonov, A.V., Richardson, M.J., 2006. Global POC concentrations from in-situ and satellite data. Deep-Sea Res. Pt II 53 (5–7), 718–740, http://dx.doi.org/10.1016/j.dsr2.2006.01.029.

Good, S.A., Corlett, G.K., Remedios, J.J., Noyes, E.J., Llewellyn-Jones, D.T., 2007. The global trend in sea surface temperature from 20 years of Advanced Very High Resolution Radiometer Data. J. Climate 20, 1255–1264, http://dx.doi.org/10.1175/JCLI4049.1.

Guemas, V., Salas-Melia, D., 2008. Simulation of the Atlantic meridional overturning circulation in an atmosphere-ocean global coupled model. Part II: A weakening in a climate change experiment: a feedback mechanism. Clim. Dynam. 30 (7), 831–844, http://dx.doi.org/10.1007/s00382-007-0328-8.

Henson, S.A., Sarmiento, J.L., Dunne, J.P., Bopp, L., Lima, I., Doney, S.C., John, J., Beaulieu, C., 2010. Detection of anthropogenic climate change in satellite records of ocean chlorophyll and productivity. Biogeosciences 7 (2), 621–640, http://dx.doi.org/10.5194/bg-7-621-2010.

Hofmann, M., Worm, B., Rahmstorf, S., Schellnhuber, H.J., 2011. Declining ocean chlorophyll under unabated anthropogenic CO_2 emissions. Environ. Res. Lett. 6 (3), 1–7, http://dx.doi.org/10.1088/1748-9326/6/3/034035.

Jakowczyk, M., Stramska, M., 2014. Spatial and temporal variability of satellite-derived sea surface temperature in the Barents Sea. Int. J. Remote Sens. 35 (17), 6545–6560, http://dx.doi.org/10.1080/01431161.2014.958247.

Kirk, J.T.O., 1984. Dependence of relationship between inherent and apparent optical properties of water on solar altitude. Limnol. Oceanogr. 29 (2), 350–356.

Kirk, J.T.O., 1991. Volume scattering function, average cosines, and the underwater light field. Limnol. Oceanogr. 36 (3), 455–467.

Kivimäe, C., Bellerby, R.G.J., Fransson, A., Reigstad, M., Johannessen, T., 2010. A carbon budget for the Barents Sea. Deep-Sea Res. Pt I 57 (12), 1532–1542, http://dx.doi.org/10.1016/j.dsr.2010.05.006.

Kowalik, Z., Proshutinsky, A.Y., 1995. Topographic enhancement of tidal motion in the western Barents Sea. J. Geophys. Res.-Oceans 100 (C2), 2613–2637.

Le Provost, C., 2001. Ocean tides. In: Fu, L.-L., Cazenave, A. (Eds.), Satellite Altimetry and Earth Sciences: A Handbook of Techniques and Applications. Int. Geophys. Ser., vol. 69. Academic Press, San Diego, CA, pp. 267–304.

Lebedev, S., Kostyanoy, A.G., Ginzburg, A.I., Medvedev, D.P., Sheremet, N.A., Shauro, S.N., 2011. Satellite altimetry applications in the Barents and White seas. In: Vignudelli, S., Kostianoy, A.G., Cipollini, P., Benveniste, J. (Eds.), Coastal Altimetry. Springer-Verlag, Berlin, Heidelberg, 389–415.

Lee, Z.-P., Darecki, M., Carder, K.L., Davis, C.O., Stramski, D., Rhea, W.J., 2005a. Diffuse attenuation coefficient of downwelling irradiance: an evaluation of remote sensing methods. J. Geophys. Res. 110 (C2), C02017, http://dx.doi.org/10.1029/2004JC002573.

Lee, Z.-P., Du, K.P., Arnone, R., 2005b. A model for the diffuse attenuation coefficient of downwelling irradiance. J. Geophys. Res. 110 (C2), C02016, http://dx.doi.org/10.1029/2004JC002275.

Lee, Z.-P., Weidemann, A., Kindle, J., Arnone, R., Carder, K.L., Davis, C., 2007. Euphotic zone depth: its derivation and implication to ocean-color remote sensing. J. Geophys. Res. 112 (C3), C03009, http://dx.doi.org/10.1029/2006JC003802.

Lien, V.S., Trofimov, A.G., 2013. Formation of Barents Sea branch water in the northeastern Barents Sea. Polar Res. 32, 18905, http://dx.doi.org/10.3402/polar.v32i0.18905.

Lien, V.S., Vikebo, F.B., Skagseth, O., 2013. One mechanism contributing to co-variability of the Atlantic inflow branches to the Arctic. Nat. Commun. 4, 1488, http://dx.doi.org/10.1038/ncomms2505.

Luo, J.-J., Behera, S.K., Masumoto, Y., Yamagata, T., 2011. Impact of global ocean surface warming on seasonal-to-interannual climate prediction. J. Climate 24 (6), 1626–1646, http://dx.doi.org/10.1175/2010JCLI3645.1.

Marra, J.F., Dickey, T.D., Plueddemann, A.J., Weller, R.A., Kinkade, C.S., Stramska, M., 2015. Phytoplankton bloom phenomena in the North Atlantic Ocean and Arabian Sea. ICES J. Mar. Sci., http://dx.doi.org/10.1093/icesjms/fsu241.

Maslowski, W., Marble, D., Walczowski, W., Schauer, U., Clement, J. L., Semtner, A.J., 2004. On climatological mass, heat, and salt transports through the Barents Sea and Fram Strait from a Pan-Arctic coupled ice ocean model simulation. J. Geophys. Res. 109 (C3), C03032, http://dx.doi.org/10.1029/2001JC001039.

Merchant, C.J., LeBorgne, P., 2010. Retrieval of sea surface temperature from space, based on modeling of infrared radiative transfer: capabilities and limitations. J. Atmos. Ocean. Tech. 21 (11), 1734–1746, http://dx.doi.org/10.1175/JTECH1667.1.

Mobley, C.D., 1994. Light and Water. Radiative Transfer in Natural Waters. Academic Press, New York, 592 pp.

Monterey, G., Levitus, S., 1997. Seasonal variability of mixed layer depth for the World Ocean. NOAA Atlas, NESDIS 14, Washington, DC, 100 pp.

Morice, C.P., Kennedy, J.J., Rayner, N.A., Jones, P.D., 2012. Quantifying uncertainties in global and regional temperature change using an ensemble of observational estimates: the HadCRUT4 data set. J. Geophys. Res. 117 (D8), D08101, http://dx.doi.org/10.1029/2011JD017187.

Nerem, R.S., Chambers, D.P., Choe, C., Mitchum, G.T., 2010. Estimating mean sea level change from the TOPEX and Jason altimeter missions. Mar. Geod. 33 (Suppl. 1), 435–446, http://dx.doi.org/10.1080/01490419.2010.491031.

Olsen, A., Johannessen, T., Rey, F., 2003. On the nature of the factors that control spring bloom development at the entrance to the Barents Sea and their interannual variability. Sarsia 88 (6), 379–393, http://dx.doi.org/10.1080/00364820310003145.

O'Reilly, J.E., Maritorena, S., Mitchell, B.G., Siegel, D.A., Carder, K.L., Garver, S.A., Kahru, M., McClain, C.R., 1998. Ocean color chlorophyll algorithms for SeaWiFS. J. Geophys. Res. 103 (C11), 24937–24953, http://dx.doi.org/10.1029/98JC02160.

O'Reilly, J.E., Maritorena, S., Siegel, D.A., O'Brien, M.C., Toole, D., Mitchell, B.G., Kahru, M., Chavez, F.P., Strutton, P., Cota, G.F., Hooker, S.B., McClain, C.R., Carder, K.L., Muller-Karger, F., Harding, L., Magnuson, A., Phinney, D., Moore, G.F., Aiken, J., Arrigo, K.R., Letelier, R., Culver, M., 2000. Ocean color chlorophyll *a* algorithms for SeaWiFS, OC2 and OC4: Version 4. NASA Technical Memo 2000-206892, vol. 11. pp. 9–27.

Oziel, L., Sirven, J., Gascard, J.-C., 2016. The Barents Sea frontal zones and water masses variability (1980–2011). Ocean Sci. 12 (1), 169–184, http://dx.doi.org/10.5194/os-12-169-2016.

Padman, L., Erofeeva, S., 2004. A barotropic inverse tidal model for the Arctic Ocean. Geophys. Res. Lett. 31 (2), L02303, http://dx.doi.org/10.1029/2003GL019003.

Racault, M.-F., Sathyendranath, S., Platt, T., 2014. Impact of missing data on the estimation of ecological indicators from satellite ocean-colour time-series. Remote Sens. Environ. 152, 15–28, http://dx.doi.org/10.1016/j.rse.2014.05.016.

Rey, F., 1981. The development of the spring phytoplankton outburst at selected sites off the Norwegian coast. In: Sætre, R., Mork, M. (Eds.), The Norwegian Coastal Current. Univ. Bergen, 649–680.

Reynolds, R.W., Smith, T.M., Liu, C., Chelton, D.B., Casey, K.S., Schlax, M.G., 2007. Daily high-resolution-blended analyses for sea surface temperature. J. Climate 20 (22), 5473–5496, http://dx.doi.org/10.1175/2007JCLI1824.1.

Rudels, B., Jones, E.P., Schauer, U., Eriksson, P., 2004. Atlantic sources of the Arctic Ocean surface and halocline waters. Polar Res. 23 (2), 181–208, http://dx.doi.org/10.1111/j.1751-8369.2004.tb00007.x.

Schauer, U., Beszczynska-Möller, A., Walczowski, W., Fahrbach, E., Piechura, J., Hansen, E., 2008. Variation of measured heat flow through the Fram Strait between 1997 and 2006. In: Dickson, R.R., Meincke, J., Rhines, P. (Eds.), Arctic Subarctic Ocean Fluxes: Defining the Role of the Northern Seas in Climate. Springer, New York, 65–85.

Schauer, U., Loeng, H., Rudels, B., Ozhigin, V.K., Dieck, W., 2002. Atlantic water flow through the Barents and Kara seas. Deep-Sea Res. Pt I 49 (12), 2281–2298, http://dx.doi.org/10.1016/S0967-0637(02)00125-5.

Semeneov, V.A., Park, W., Latif, M., 2009. Barents Sea inflow shutdown: a new mechanism for rapid climate changes. Geophys. Res. Lett. 36 (14), L14709, http://dx.doi.org/10.1029/2009GL038911.

Serreze, M., Barrett, A., Slater, A., Steele, M., Zhang, J., Trenberth, K., 2007. The large-scale energy budget of the Arctic. J. Geophys. Res. 112 (D11), 1438–1445, http://dx.doi.org/10.1029/2006JD008230.

Siegel, D.A., Behrenfeld, M.J., Maritorena, S., McClain, C.R., Antoine, D., Bailey, S.W., Bontempi, P.S., Boss, E.S., Dierssen, H.M., Doney, S.C., Eplee, R.E., Evans, R.H., Feldman, G.C., Fields, E., Franz, B.A., Kuring, N.A., Mengelt, C., Nelson, N.B., Patt, F.S., Robinson, W.D., Sarmiento, J.L., Swan, C.M., Werdell, P.J., Westberry, T.K., Wilding, J.G., Yoder, J.A., 2013. Regional to global assessments of phytoplankton dynamics from the SeaWiFS mission. Remote Sens. Environ. 135, 77–91, http://dx.doi.org/10.1016/j.rse.2013.03.025.

Skjelvan, I., Olsen, A., Anderson, L.G., Bellerby, R.G.J., Falck, E., Kasajima, Y., Kivimae, C., Omar, A., Rey, F., Olsson, K.A., Johannessen, T., Heinze, C., 2005. A review of the biogeochemistry of the Nordic Seas and Barents Sea. In: Drange, H., Dokken, T., Furevik, T., Gerdes, R., Berger, W. (Eds.), The Nordic Seas: An Integrated Perspective Oceanography, Climatology and Modelling. American Geophysical Union, Washington, DC, 157–175.

Smedsrud, L.H., Esau, I., Ingvaldsen, R.B., Eldevik, T., Haugan, P.M., Li, C., Lien, V.S., Olsen, A., Omar, A.M., Otterå, O.H., Risebrobakken, B., Sandø, A.B., Semenov, V.A., Sorokina, S.A., 2013. The role of the Barents Sea in the Arctic climate system. Rev. Geophys. 51 (3), 415–449, http://dx.doi.org/10.1002/rog.20017.

Stramska, M., 2005. Interannual variability of seasonal phytoplankton blooms in the north polar Atlantic in response to atmospheric forcing. J. Geophys. Res. 110 (C5), C05016, http://dx.doi.org/10.1029/2004JC002457.

Stramska, M., 2010. The diffusive component of particulate organic carbon export in the North Atlantic estimated from SeaWiFS ocean color. Deep-Sea Res. Pt I 57 (2), 284–296, http://dx.doi.org/10.1016/j.dsr.2009.11.007.

Stramska, M., 2014. Particulate organic carbon in the surface waters of the North Atlantic: spatial and temporal variability based on satellite ocean colour. Int. J. Remote Sens. 35 (13), 4717–4738, http://dx.doi.org/10.1080/01431161.2014.919686.

Stramska, M., Cieszyńska, A., 2015. Ocean colour estimates of particulate organic carbon reservoirs in the global ocean – revisited. Int. J. Remote Sens. 36 (14), 3675–3700, http://dx.doi.org/10.1080/01431161.2015.1049380.

Stramska, M., Dickey, T.D., 1994. Modeling phytoplankton dynamics in the northeast Atlantic during the initiation of the spring bloom. J. Geophys. Res. 99 (c5), 10241–10253, http://dx.doi.org/10.1029/93JC03378.

Stramska, M., Dickey, T.D., Plueddemann, A., Weller, R., Langdon, C., Marra, J., 1995. Bio-optical variability associated with phytoplankton dynamics in the North Atlantic Ocean during spring and summer of 1991. J. Geophys. Res. 100 (C4), 6621–6632, http://dx.doi.org/10.1029/94JC01447.

Stramska, M., Frye, D., 1997. Dependence of apparent optical properties on solar altitude: experimental results based on mooring data collected in the Sargasso Sea. J. Geophys. Res. 102 (C7), 15679–15691, http://dx.doi.org/10.1029/97JC00886.

Stramski, D., Reynolds, R.A., Babin, M., Kaczmarek, S., Lewis, M.R., Röttgers, R., Sciandra, A., Stramska, M., Twardowski, M.S., Franz, B.A., Claustre, H., 2008. Relationships between the surface concentration of particulate organic carbon and optical properties in the Eastern South Pacific and Eastern Atlantic Oceans. Biogeosciences 5, 171–201, http://dx.doi.org/10.5194/bg-5-171-2008.

Sverdrup, H.U., 1953. On conditions for the vernal blooming of phytoplankton. J. Con. Cons. Perm. Int. Explor. Mer. 18 (3), 287–295.

Świrgoń, M., Stramska, M., 2015. Comparison of in situ and satellite ocean color determinations of particulate organic carbon concentration in the global ocean. Oceanologia 57 (1), 25–31, http://dx.doi.org/10.1016/j.oceano.2014.09.002.

Terziev, F.S., Girduk, G.V., Zykova, G.G., Dzhenyuk, S.L. (Eds.), 1990. Hydrometeorology and Hydrochemistry of the Seas of the USSR, vol. 1, Barents Sea, Issue 1, Hydrometerologicla Conditions. Hydrometeoizdat, Leningrad (in Russian).

Tett, P., Edwards, A., 1984. Mixing and plankton: an interdisciplinary theme in oceanography. Oceanogr. Mar. Biol. 22, 99–123.

van de Poll, W.H., Kulk, G., Timmermans, K.R., Brussaard, C.P.D., van der Woerd, H.J., Kehoe, M.J., Mojica, K.D.A., Visser, R.J.W., Rozema, P.D., Buma, A.G.J., 2013. Phytoplankton chlorophyll *a* biomass, composition, and productivity along a temperature and stratification gradient in the northeast Atlantic Ocean. Biogeosciences 10, 4227–4240, http://dx.doi.org/10.5194/bg-10-4227-2013.

Volkov, D.L., Landerer, F.W., Kirillov, S.A., 2013. The genesis of sea level variability in the Barents Sea. Cont. Shelf Res. 66, 92–104, http://dx.doi.org/10.1016/j.csr.2013.07.007.

Volkov, D.L., Pujol, M.-I., 2012. Quality assessment of a satellite altimetry data product in the Nordic, Barents, and Kara seas. J. Geophys. Res. 117 (C3), C03025, http://dx.doi.org/10.1029/2011JC007557.

Wassmann, P., Reigstad, M., Haug, T., Rudels, B., Carroll, M.L., Hop, H., Gabrielsen, G.W., Falk-Petersen, S., Denisenko, S.G., Arashkevich, E., Slagstad, D., Pavlova, O., 2006. Food webs and carbon flux in the Barents Sea. Prog. Oceanogr. 71 (2–4), 232–287, http://dx.doi.org/10.1016/j.pocean.2006.10.003.

Woźniak, S.B., 2014. Simple statistical formulas for estimating biogeochemical properties of suspended particulate matter in the southern Baltic Sea potentially useful for optical remote sensing applications. Oceanologia 56 (1), 7–39, http://dx.doi.org/10.5697/oc.56-1.007.

Woźniak, S.B., Meler, J., Lednicka, B., Zdun, A., Stoń-Egiert, J., 2011. Inherent optical properties of suspended particulate matter in the southern Baltic Sea. Oceanologia 53 (3), 691–729, http://dx.doi.org/10.5697/oc.53-3.691.

Oceanologia (2016) 58, 264—271

Available online at www.sciencedirect.com

ScienceDirect

journal homepage: www.journals.elsevier.com/oceanologia/

ORIGINAL RESEARCH ARTICLE

Detecting imprints of atmospheric waves in the Bering Sea with MODIS data

Marina Evdoshenko *

P.P. Shirshov Institute of Oceanology, Russian Academy of Sciences, Moscow, Russia

Received 11 November 2015; accepted 13 April 2016
Available online 29 April 2016

KEYWORDS
MODIS;
Remote sensing;
Ocean optics;
Water leaving radiance

Summary Satellite Moderate Resolution Imaging Spectroradiometer (MODIS) data of water leaving radiance of 859 nm with a spatial resolution of 250 m were used to investigate the impact of atmospheric gravity waves (AGWs), which manifested as stripes in clouds and on the sea surface. On the basis of an evaluation of the characteristics of AGWs and sea depth, it was shown that the surface stripes, or surface waves (SWs) were imprints of AGWs. Crests of SWs were like prolongations of cloud stripes on the combined radiance images testifying that SWs were shifted by minus a quarter of the period relative to AGWs.

1. Introduction

The possibility of processing the increased spatial resolution (250 m) data from Moderate Resolution Imaging Spectroradiometer (MODIS) has opened up new prospects (Franz et al., 2006). Particularly they concern more detailed observation of imprints of atmospheric phenomena, such as fronts, gravity waves, rain cells, convective cells and others, on the oceans' surface.

Atmospheric phenomena are usually invisible. Near infrared and optical radiance do not penetrate through clouds. However, at sufficiently high humidity atmospheric events can imprint in clouds and become visible on images of the radiance $L_t(\lambda)$ at the top of the atmosphere of level L1 (without the atmospheric correction). So, in the case of atmospheric gravity waves (AGWs), they display as “cloud streets” on $L_t(\lambda)$ images.

Atmospheric processes, that cause the variability of sea surface roughness, are usually investigated by their footprints on the sea surface with the help of satellite Synthetic Aperture Radar (SAR). Passive microwave radiation penetrates through clouds into the sea by no more than several millimeters so that surface snapshots of atmospheric impacts form SAR backscatter return (Valenzuela, 1978). Many papers

* Correspondence to: P.P. Shirshov Institute of Oceanology, Russian Academy of Sciences, 36, Nakhimovski prospect, Moscow 117997, Russia. Tel.: +7 4991245983; fax: +7 4991245983.
E-mail address: maarsio@bk.ru.
Peer review under the responsibility of Institute of Oceanology of the Polish Academy of Sciences.

ELSEVIER Production and hosting by Elsevier

http://dx.doi.org/10.1016/j.oceano.2016.04.003

are devoted to investigating atmospheric processes with the help of SAR, e.g. Alpers and Brummer (1994), Alpers and Huang (2011), Kozlov et al. (2014), Li et al. (2011), Vachon et al. (1994), Zheng et al. (1998).

In many published papers, atmospheric processes shown as cloudy structures have been examined in different geographical regions on the basis of MODIS true color $L_t(\lambda)$ images with a resolution of 250 m. Papers mentioned below contain some examples of signatures of atmospheric internal waves, coastally trapped atmospheric gravity waves, atmospheric vortex streets, atmospheric boundary rolls and convective cells: Da Silva and Magalhaes (2009), Liu et al. (2004), Li et al. (2008), Weigen et al. (2008).

One of the atmospheric impacts namely atmospheric gravity waves (AGWs) accompanied by corresponding changes in pressure, periodically force through the sea surface, modulating its level. This leads to a change in the normalized water leaving radiance $L_w(\lambda)$ (or remote sensing reflectance $Rrs(\lambda)$, which differs from $L_w(\lambda)$ by a factor of F_0 – mean solar irradiance) of level L2 (after the atmospheric correction). Under a clear sky, imprints of AGWs display on L_w images with sufficiently high resolution in the form of stripes of alternating brightness.

We have not found any papers where 250-m L_w images, obtained with MODIS, were used for identification of AGW signatures on the sea surface as surface waves (SWs). Also, we have not found any papers where a comparison of imprints of AGWs as cloud stripes on images of L_t and on the sea surface on images of L_w for a case of intermittent cloudiness was fulfilled on a single satellite picture. Therefore, the goal of this study was to obtain simultaneous 250-m MODIS images of AGW imprints in cloud and on the sea surface for some cases of their bright manifestations in different ocean regions. On the basis of an evaluation of a phase speed and a wavelength of AGWs, and water depth, we aimed to prove that found SWs were exactly imprints of AGWs, but not long surface gravity waves, and to reveal a phase shift between AGWs in cloud and the crests of SWs.

2. Material and methods

It is known that "normalized water-leaving radiance is that which would exit the sea surface if the Sun were at the zenith and if the atmosphere were absent" (Gordon et al., 1988). A layer width in which $L_w(\lambda)$ is formed varies with λ and is defined by the spectral dependence of the backscatter and the absorption coefficients of pure water and admixture.

Most MODIS optical radiance bands have spatial resolutions of 1 km, and only two bands I – at 645 nm and II – at 859 nm provide the resolution of 250 m. In clear ocean waters, $L_w(645)$ originates in a subsurface layer of 1–2 m, while $L_w(859)$ originates in the thin, topmost layer of about several centimeters due to the high absorption of pure water (Hale and Querry, 1973; Pegau et al., 1997). Our experience shows that imprints of atmospheric waves of small amplitude (up to some tens centimeters) are reproduced better by $L_w(859)$, than by $L_w(645)$ so we used only $L_w(859)$ data for our investigation.

Level L1a radiance MODIS data were obtained from http://oceancolor.nasa.gov, NOAA AVHRR L1 data – from http://www.class.ncdc.noaa.gov. MODIS level 2 radiance data were generated from level L1 data with the help of the SeaDAS software package, available on http://seadas.gsfc.nasa.gov. The process to generate 250-m data consists of several steps: obtaining a GEO file, generation of an L1b file and then generation of an L2 file, which includes radiance data and some product data, such as wind speed and direction. Wind components at a height of 10 m above the ocean were calculated for a given place and time by interpolating ancillary NCEP (National Centers for Environmental Prediction) data with the SeaDAS. Brightness and contrast of radiance images were enhanced slightly for better discernibility of AGWs in clouds and SWs.

3. Results

3.1. AGW packet in the Bering Sea

Optical scanners record imprints of AGWs on the ocean surface permanently (Evdoshenko, 2008, 2009). Consider their pronounced manifestations in the Bering Sea near St. Lawrence Island.

Appearance of cloud imprints in the Bering Sea at 22:45 on 6 June 2001 was caused by atmospheric solitary waves in the vicinity of St. Lawrence Island. That AGW packet propagating in the upwind direction was initially discovered in RADARSAT SAR image of arched atmospheric wave imprint on the sea surface and 250-m MODIS L_t-image of cloud waves (Li et al., 2004).

On 6 and 7 June 2001, the packet of quasi-stationary (standing) atmospheric waves was revealed as bow-shaped cloud stripes on several images of L_t of level L1 obtained from different satellite devices, including NOAA 14 AVHRR (Advanced Very High Resolution Radiometer), Terra MODIS (NASA's Earth Observing System – EOS AM) and OrbView-2 SeaWiFS (Sea-Viewing Wide Field-of-View Sensor). Images of standing atmospheric wave imprints in cloud, obtained from AVHRR at λ = 10.8 μm with a spatial resolution of 1 km, from MODIS at λ = 859 nm with resolution of 250 m and from SeaWiFS at λ = 670 nm with resolution of 1.1 km are shown in Fig. 1. One can see that the packet of AGWs existed for more than 10 h from the evening of 6 June up to the early morning of 7 June 2001.

The absence of the atmospheric cloud wave packet on AVHRR images of L_t at observations during the previous and following revolution periods of NOAA-14, each of which is equal to ~1 h 40 min, relative to the considered period of ~10 h, testified that the standing waves originated and disappeared rather abruptly. That is, solitary AGWs were formed only when the island was under the influence of the air break which propagated at low height.

St. Lawrence Island is 145 km long and 13–36 km wide. The highest mountain, with a maximum height H = 2207 m, is located in the middle of the island. Several mountains in its eastern part and a mountain at its western part are of lesser heights. Between the mountains are plateaus with numerous lagoons. Solitary, bow-shaped AGWs were obviously generated when the mountains blocked the cold arctic air break so that upstream waves arose as a secondary reflected flow. While passing freely through the plateaus to the leeward side of the island a part of the cold air break ramified and propagated downstream as cloud tails modulated by AGWs. On the lee side of the island cloudy AGWs turned around and moved downstream close to the meridian.

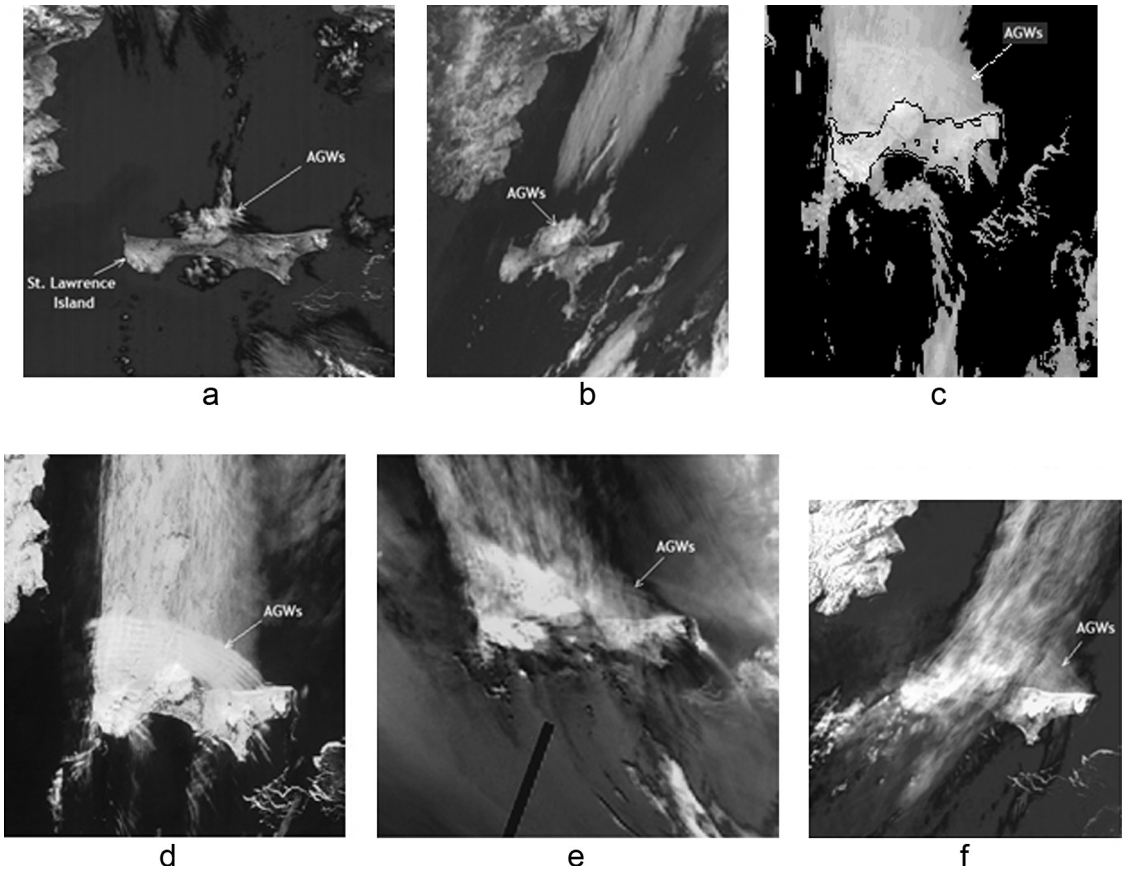

Figure 1 L_t-images from AVHRR at 17:15 on 6 June (a), AVHRR at 18:55 on 6 June (b), MODIS at 22:45 on 6 June (c), SeaWiFS at 0:35 on 7 June (d), AVHRR at 1:32 on 7 June (e) and AVHRR at 3:14 on 7 June (f).

An arctic cyclone, passing from the Arctic Ocean to the Bering Sea in the Pacific Ocean and provoking the movement of a cold air break to the south, was observed at 17:15 on 6 June on a MODIS 1-km image of L_t at 6.7 μm (channel 27). L_t(6700), reflecting the water vapor content at a height of 4.2 km (air pressure 600 hPa) showed that the northern tail end of the cyclone drew the cold air from the Arctic Ocean to St. Lawrence Island, the core of the cyclone being southward between St. Lawrence Island and the Aleutian Islands (see Fig. 2a).

Fig. 2b represents an enlarged MODIS L_t(859) image for the island surroundings. The AGW packet was revealed to the north and above the island as bow-shaped cloud stripes that were stretched from one end of the island to the other and resembled the island's arched southern boundary. The packet contained more than ten solitary waves, and the soliton wavelength was 4.75 km. To the south of the island several cloud tails appeared, consisted of a number of shorter, nearly linear cloud stripes that looked like a prolongation of the

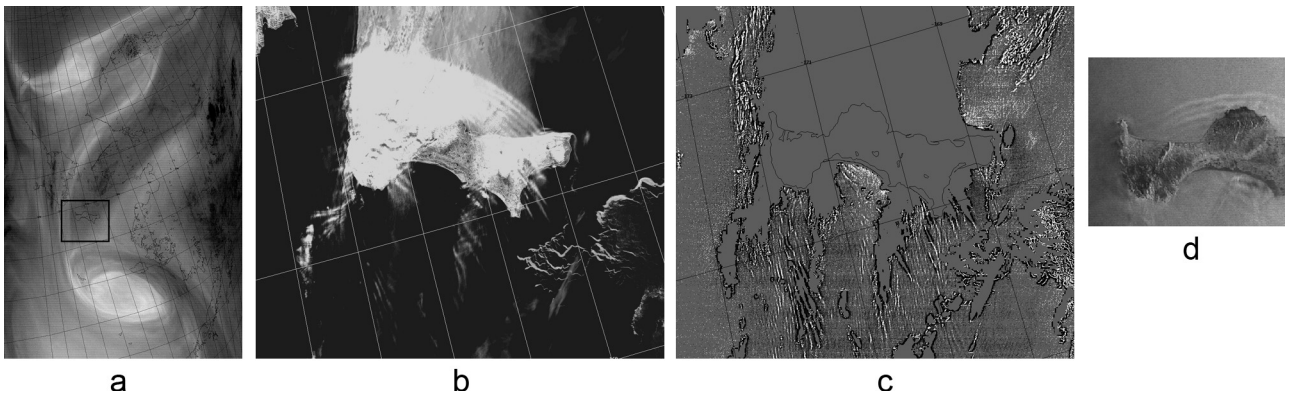

Figure 2 MODIS images at 22:45 on 6 June 2001: 1-km L_t(6700) (a), 250-m L_t(859) (b) and 250-m L_w(859) (c); coordinates of the box shown on (a) and regions shown on (b) and (c): 62.73°N, 174.14°W–63.97°N, 167.49°W; a RADARSAT ScanSAR wide B mode SAR image, acquired at 18:07:58 on 6 June 2001 (Li et al., 2004) (d).

arched waves to the north of the island. At the bottom right hand corner of Fig. 2b one can see a glacier.

The L_w(859) image shows AGW imprints as mainly longitude-oriented stripes of alternating brightness (or surface waves) southward of the island (see Fig. 2c). In contrast to the cloudy atmospheric wave appearance, when only one cloud stripe per period is visible, two stripes per period (light and dark) are visible in the case of surface imprints. The bright stripes symbolize wave crests, the dark ones symbolize wave troughs, the bright stripes being like continuations of cloud waves recognized on the L_w image as smooth gray stripes with pointed ends. Sea surface signatures that appeared as a great number of contrasting quasi-parallel stripes of different lengths and wavelengths were observable to the south of the island, at distances several times as great as the width of the island and attenuated with the distance. Their crest length reached hundreds of kilometers. Far from the island their wavelength decreased and was much smaller than that of the cloud arched waves to the north of the island. The minimum wavelength and the distinguishable crest width were limited by the scanner resolution, but undoubtedly signatures of lesser wavelength existed. Their crests are marked by dots instead of wider solid lines on Fig. 2c. To the south of the island, wavelengths of surface waves changed from ~1.5 km to ~4 km. Black boundaries on the image that restricted cloud areas can be explained by decreased values of L_w(859). They were obviously caused by the faults of the atmospheric correction.

A RADARSAT-1 SAR image of sea surface imprints of atmospheric waves with 100-m resolution, obtained at 18:07:58 on 6 June 2001, and presented in Li et al. (2004), is shown in Fig. 2d. On the image, imprints of AGWs on the sea surface in the form of arched waves to the north of the island are seen. Also visible are some signatures to the south from the island which coincide in direction with those appeared on MODIS L_w(859) image.

Fig. 3 represents L_t and L_w images of two smaller AGW packets in clouds and surface wave packets to the north and south from the island in the expanded scale. To the north from St. Lawrence Island arrows indicate a large, arched standing wave packet (LAGW), a smaller atmospheric wave packet (AGW) and a smaller SW packet. A smaller AGW packet propagated at an angle to the large, arched northern AGW packet (LAGW) and was evidently caused by a vertical velocity shear. Several tens waves are observable in the smaller, north-eastern AGW packet. The width of the packet is no less than 19 km, the wave crest length is no less than 3.4 km, and the wavelength is 0.9 km.

At the bottom of the L_t image, two wider AGW signatures of the bow-shaped packet (LAGW) are seen, and also surface waves (LSW) caused by them near the island's southern shore.

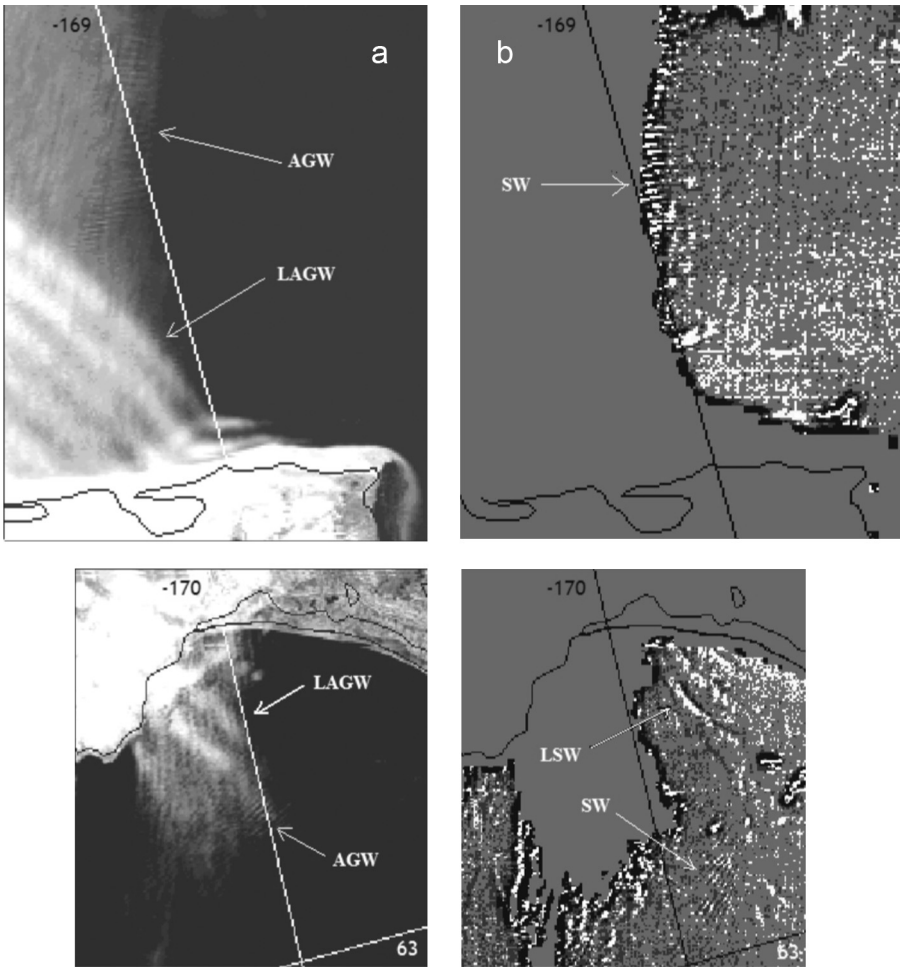

Figure 3 MODIS images: L_t(859) (a) and L_w(859) (b); upper — to the north and lower — to the south of St. Lawrence Island.

A small, southwestern AGW packet and a SW packet are visible on the L_t and L_w images. The packet width is no less than 23.6 km, the wave crest length is no less than 15 km, and the wavelength is 0.85 km. For both packets, SWs on L_w-images also appear to be like continuations of AGW cloudy signatures on L_t-images.

Images of $L_t(859)$ showed that cloudy waves of a smaller wavelength induced by AGWs were imposed on larger waves to the north and to the south from the island. This could be caused by different heights of AGWs in the low troposphere, so that cloudy waves were superimposed on each other on the image. Such phenomenon is observed frequently on satellite pictures and is also visible from the land.

The wind speed and direction were also calculated at 22:25 on 6 June 2001. A combined vector map is presented in Fig. 4. It is clear that the cold air outbreak with a wind speed of 11 m s^{-1} spread from the Arctic to the south. St. Lawrence Island was in the way of the stream and blocked it so that south from the island the wind speed did not exceed 8.5 m s^{-1} in the main stream. The island's blocking effect led to the origination of bow atmospheric waves that were directed to the north of the island against the air stream.

To disclose some peculiarities of the atmospheric–oceanic interactions, we represent the imposition in a difference mode of two images: $L_t(859)$ and $L_w(859)$ for a region of St. Lawrence Island (see Fig. 5). AGWs are shown in gray, and the crests of SWs that correspond to the highest L_w are shown in white. In Fig. 5 some combinations of SW crests (white arrows) and cloud stripes (black arrows) are presented.

In this paper, we present evidence that the surface waves were not long surface gravity waves but rather atmospheric wave imprint on the sea's surface. For this purpose, it is necessary to evaluate the phase speed of the atmospheric wave c_a and the speed of ocean surface gravity wave c_g that can propagate in the ocean of variable depth. c_a for the given site and time was calculated in Li et al. (2004) on the basis of the radiosonde upper air observation at nearby station Nome at Alaska at 12:00 on 6 June 2001. Using a forced, extended Korteweg-de Vries equation for a vertical profile of potential temperature, representing a two-layer system, the phase speed was evaluated as c_a = 8.9 m s^{-1} (Li et al., 2004). This

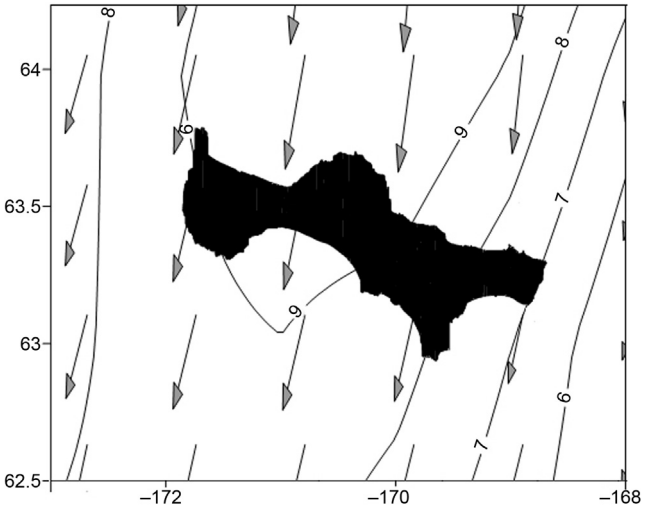

Figure 4 Wind speed (isolines) and wind direction (arrows) at a height of 10 m.

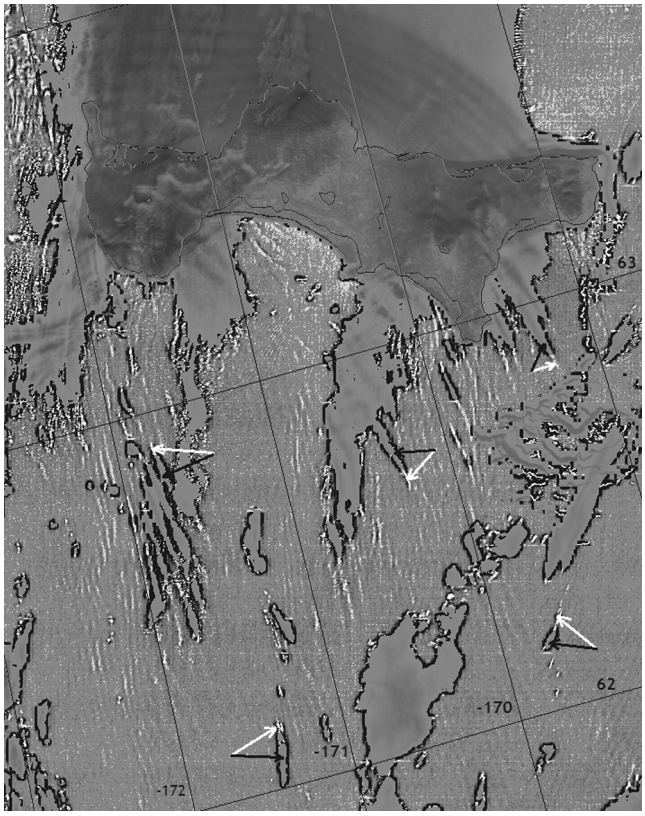

Figure 5 Imposition in a difference mode of $L_t(859)$ and $L_w(859)$ near St. Lawrence Island; some combinations of cloud-surface waves are denoted by black and white arrows.

value is close to the ocean wind speed near the island (see Fig. 4). As was shown previously, the wavelength of AGWs and SWs to the south of the island was from 1.5 km to 4 km. The depth in the region shown in Fig. 5 changes from h = 20 m near the island to h = 50 m near 62°N. When evaluating the phase speed for hypothetical surface gravity waves with a wavelength 1.5–4 km, we use an approximation of the dispersion relation for shallow waters, $c_g^2 = gh$, where g is the acceleration of gravity (Grimshaw et al., 1998). Calculations show that the speed c_g for such waves should be 14 m s^{-1} for the depth 20 m and 22 m s^{-1} for the depth 50 m, which is greater than the speed of AGWs. Moreover, as seen in Fig. 5, the locations of SW crests were generally like prolongations of AGW cloud imprints on the superimposed image, independent on depth, so we conclude that the SWs were exactly imprints of AGWs but not long gravity waves.

3.2. AGWs in the Gulf of Mexico

Another example of AGW imprints in clouds and on the sea surface was obtained with data from MODIS-Terra at 16:50 and MODIS-Aqua at 20:00 on 15 March 2008, in the Gulf of Mexico. A packet of atmospheric waves in the form of an undular bore was recorded as parallel white cloud stripes moving to the south. Desaturated true-color L_t-images of the bore are shown in the upper part of Fig. 6, on the left – obtained from MODIS-T and on the right – from MODIS-A. In the lower part of Fig. 6, the image of *Rrs*(859) of MODIS-A at 20:00 with increased brightness and contrast is shown. AGWs

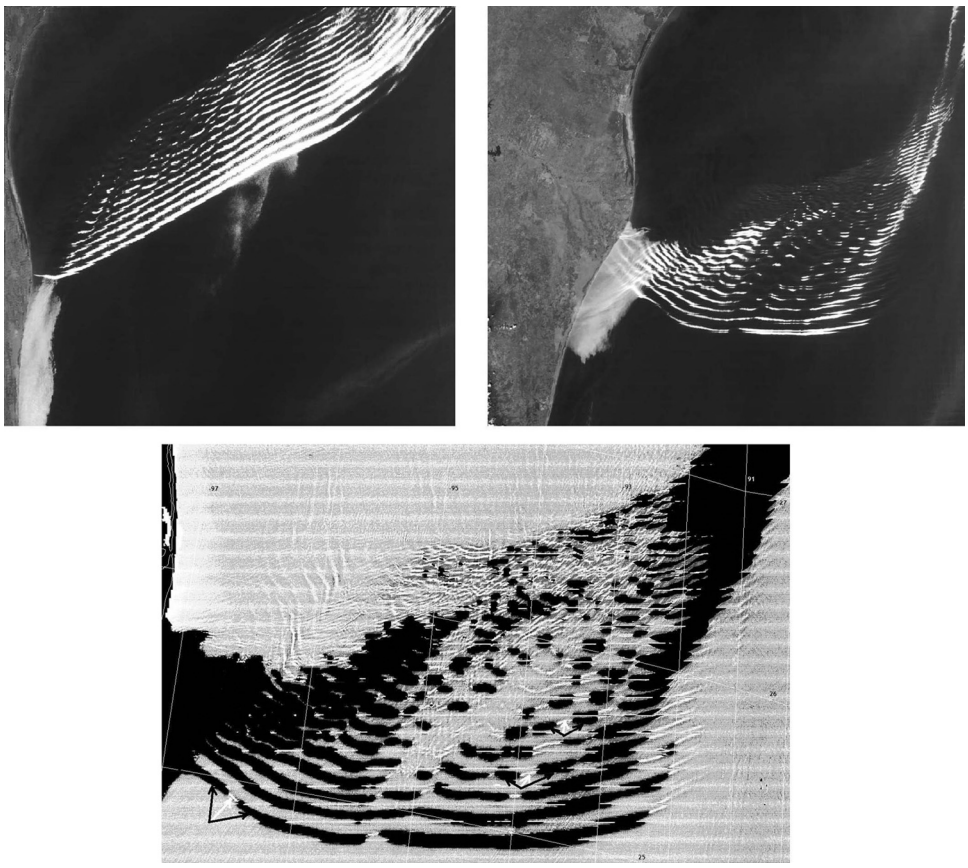

Figure 6 An undular bore wave packet in the Gulf of Mexico on 15 March 2008: above — desaturated true-color images of L_t, on the left — from MODIS-Terra at 16:50, on the right — from MODIS-Aqua at 20:00, below — a part of the increased *Rrs*(859) image at 20:00.

in clouds are presented in black and the crests of SWs in white. Some combinations of cloud-surface waves are denoted by black and white arrows. Defined by MODIS-T and MODIS-A data, the undular bore covered a distance of 83 km in 190 min. Thus the phase speed of AGWs was $c_a = 7\ \mathrm{m\ s^{-1}}$. The mean horizontal wavelength of AGWs defined by MODIS-A image was $\lambda_a = 10$ km, the same was the wavelength of surface waves λ_s. The depth h in the region varies from 100 m to 2000 m. As $h_{max} = 2$ km is no larger than a half of the wavelength λ_s, we used an approximation of the dispersion relation for shallow waters for evaluation of the phase speed of hypothetical long surface gravity waves (Grimshaw et al., 1998). For this case, $c_g = 30$—$140\ \mathrm{m\ s^{-1}}$, which is much greater than c_a. The crests of SWs were like prolongations of AGWs in clouds so we conclude that SWs could only be the imprints of AGWs, but not long gravity waves.

3.3. AGWs in the Carpentaria Gulf, Australia

One more example of AGWs and their impact on the sea surface is presented on the MODIS-Terra image obtained on 2 August 2002, at 01:00 in the Gulf of Carpentaria, to the north of Australia (sea Fig. 7). A desaturated, true-color

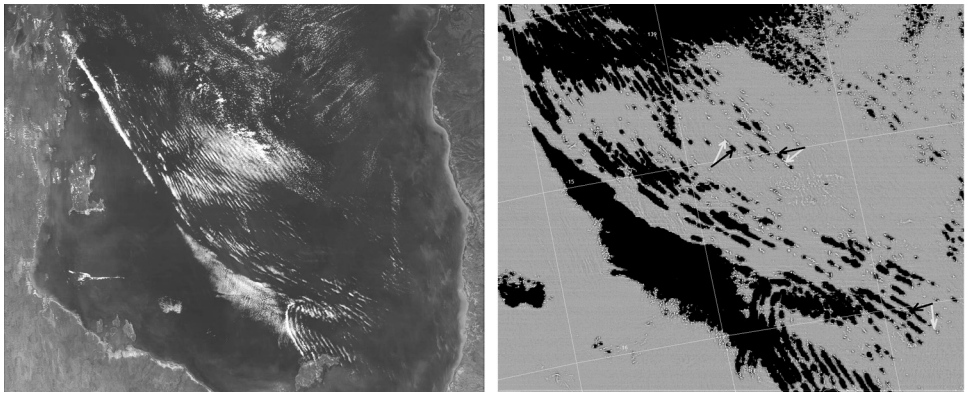

Figure 7 An undular bore on MODIS-Terra image obtained at 01:00 on 2 August 2002, in the Gulf of Carpentaria, Australia: on the left — a desaturated true-color image of L_t, on the right — a part of the increased *Rrs*(859) image.

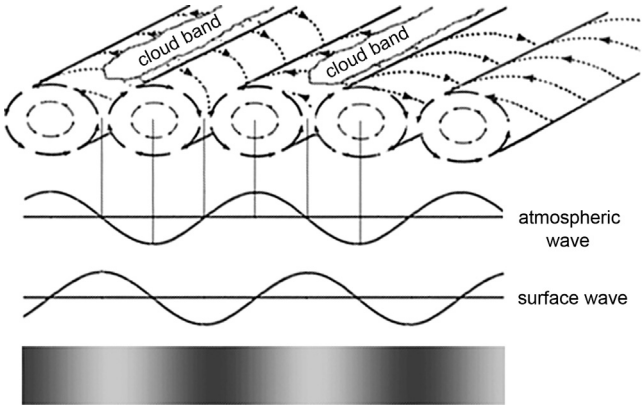

Figure 8 A scheme of the relative positioning of the AGW and the SW.

L_t-image of the gulf is shown on the left of Fig. 7. A typical phenomenon for this time of year is the Morning Glory — a powerful, solitary, low-level atmospheric wave that occurs as a roll cloud (shown in the left upper part of the image) with a number of waves. It represents an undular bore that appeared as parallel cloud stripes moving along the gulf. The image of *Rrs*(859) with increased brightness and contrast is presented on the right of Fig. 7. Cloudy AGWs are well defined as black stripes, and the crests of SWs as white stripes. The wavelength of AGWs and SWs was 7—10 km. SW crests were also like prolongations of the cloudy AGWs on the *Rrs*-image.

4. Discussion and conclusions

Thus, MODIS 250-m scanner returns at 859 nm are optimal for studying atmospheric waves by their traces in clouds and on the sea surface. These traces are mostly convenient to observe on ocean color scanner images in the case of intermittent cloudiness, when they imprint in adjacent parts of the region and are visible on a single satellite picture.

Signatures of AGWs propagating in the low troposphere were clearly manifested on images of normalized water leaving radiance L_w(859) (or remote sensing reflectance *Rrs*(859)). A studding of the nature of SWs was carried out. For this aim the phase speeds of AGWs were evaluated. On the basis of the wavelength of SWs and the values of variable ocean depth, the phase speeds of hypothetical ocean surface gravity waves were estimated in accordance with the dispersion relation, in the approximation of shallow waters. Evaluations showed that the phase speeds of hypothetical gravity waves should be much greater than the phase speeds of AGWs. Moreover, cloud imprints had prolongations in the crests of SWs. Therefore we conclude that the observed SWs could not be the long gravity waves but the imprints of AGWs. From this also follows that AGWs impact on the cloudy layer and on the sea surface instantly and simultaneously.

It is known from Gossard and Hooke (1975) that an AGW originates in a set of counter-rotating, nearly circular atmospheric vortices, so that the maximum and the minimum amplitudes of the AGW coincide with eddy axes. Between two adjacent, counter-rotating atmospheric vortices above the updraft part of the vortices' circulations, cloud bands can be formed, whereas sinking motions of atmospheric vortices correspond to areas free of cloud (Etling and Brown, 1993). Thus, if we consider the AGW, then cloud bands fit with areas where the AGW's vertical displacement is near zero (see the scheme in Fig. 8).

Figs. 5—7 show that the light stripes on L_w or *Rrs* images, which reflect the maximum amplitudes of AGWs, are a kind of prolongation of cloud stripes. This corresponds to a near zero displacement of AGWs so SWs were shifted by minus a quarter of the period relative to AGWs. This situation is shown on the scheme (Fig. 8) where cloud bands, reflected the AGW, and the SW, are presented in several projections. The scheme resembles a situation when a resonance of Proudman between AGWs and anemobaric waves on the ocean surface occurs (Levin and Nosov, 2009). From the cases considered, it follows that the resonant conditions are inherent for AGWs and their imprints on the sea surface in the form of SWs. Similar signatures are found to be manifested on L_w or *Rrs* images with a high spatial resolution obtained from MODISes flown on two NASA spacecrafts (Terra and Aqua) in different areas of the World Ocean regardless on depth.

Acknowledgement

This work is supported by grant of Russian Foundation for Basic Research N 08-05-00298-a.

References

Alpers, W., Brummer, B., 1994. Atmospheric boundary layer rolls observed by the synthetic aperture radar aboard the ERS-1 satellite. J. Geophys. Res. 99 (C6), 12613—12621.

Alpers, W., Huang, W., 2011. On the discrimination of radar signatures of atmospheric gravity waves and oceanic internal waves on synthetic aperture radar images of the sea surface. IEEE Trans. Geosci. Remote Sens. 49 (3), 1114—1126.

Da Silva, J., Magalhaes, J., 2009. Satellite observations of large atmospheric gravity waves in the Mozambique Channel. Int. J. Remote Sens. 30 (5), 1161—1182.

Etling, D., Brown, R., 1993. Roll vortices in the planetary boundary layer: a review. Bound.-Lay. Meteorol. 65 (3), 215—248.

Evdoshenko, M., 2008. Imprints of atmospheric events on the Caspian Sea surface by MODIS high resolution data. In: Proc. 9th Pan Ocean Remote Sensing Conf. (PORSEC 2008), Ocean Manifestation of Global Changes, 2—6 December 2008, Guangzhou, China, p. 42.

Evdoshenko, M., 2009. Using of MODIS high resolution data for study of atmospheric processes by their imprints on the sea surface. In: Proc. 4th Workshop on Remote Sensing of the Coastal Zone, Coasts and Climate Conflicts, 18—20 June 2009, Chania, Crete, Greece.

Franz, B., Werdell, P., Meister, G., Kwaitkowska, E., Bailey, S., Ahmad, Z., McClain, C., 2006. MODIS land bands for ocean remote sensing applications. In: Proc. Ocean Optics Conf. XVIII, 9—13 October 2006, Montreal, Canada.

Gordon, H., Brown, O., Evans, R., Brown, J., Smith, R., Baker, K., Clark, D., 1988. A semi-analytical radiance model of ocean color. J. Geophys. Res. 93 (D9), 10909—10924.

Gossard, E., Hooke, W., 1975. Waves in the Atmosphere: Atmospheric Infrasound and Gravity Waves — Their Generation and Propagation. Elsevier Sci. Publ., Amsterdam, 472 pp.

Grimshaw, R., Ostrovsky, L., Shrira, V., Spepanyants, Yu., 1998. Long nonlinear surface and internal gravity waves in a rotating ocean. Surv. Geophys. 19 (4), 289—338.

Hale, G., Querry, M., 1973. Optical constants of water in the 200-nm to 200-m wavelength region. Appl. Optics 12 (3), 555—563.

Kozlov, I., Romanenkov, D., Zimin, A., Chapron, B., 2014. SAR observing large-scale nonlinear internal waves in the White Sea. Remote Sens. Environ. 147, 99—107.

Levin, B., Nosov, M., 2009. Physics of Tsunamis. Springer Science & Business Media V.M., New York, 327 pp.

Li, X., Dong, X., Clemente-Colón, P., Pichel, W., Friedman, K., 2004. Synthetic aperture radar observation of the sea surface imprints of upstream atmospheric solitons generated by flow impeded by an island. J. Geophys. Res. 109, C02016.

Li, X., Zheng, W., Yang, X., Li, Z., Pichel, W., 2011. Sea surface imprints of coastal mountain lee waves imaged by synthetic aperture radar. J. Geophys. Res. 116, C02014.

Li, X., Zheng, W., Zou, C.-Z., Pichel, W., 2008. A SAR observation and numerical study on ocean surface imprints of atmospheric vortex streets. Sensors 8 (5), 3321—3334.

Liu, A.Q., Moore, G.W.K., Tsuboki, K., Renfrew, I.A., 2004. A high-resolution simulation of convective roll clouds during a cold-air outbreak. Geophys. Res. Lett. 31, L03101.

Pegau, W., Gray, D., Zaneveld, J., 1997. Absorption and attenuation of visible and near-infrared light in water: dependence on temperature and salinity. Appl. Optics 36 (24), 6035—6046.

Vachon, P.W., Johannessen, O.M., Johannessen, J., 1994. An ERS 1 synthetic aperture radar image of atmospheric lee waves. J. Geophys. Res. 99 (11), 22483—22490.

Valenzuela, G.R., 1978. Theories for the interaction of electromagnetic and oceanic waves: a review. Bound.-Lay. Meteorol. 13 (1), 61—85.

Weigen, X., Xilin, G., Li, X., 2008. Coastally trapped atmospheric gravity waves on SAR, AVHRR and MODIS images. Int. J. Remote Sens. 29 (6), 1621—1634.

Zheng, Q., Yan, X.-H., Klemas, V., Ho, C.-R., Kuo, N.-J., Wang, Z., 1998. Coastal lee waves on ERS-1 SAR images. J. Geophys. Res. 103 (C4), 7979—7993.

Oceanologia (2016) 58, 272–278

Available online at www.sciencedirect.com

ScienceDirect

journal homepage: www.journals.elsevier.com/oceanologia/

ORIGINAL RESEARCH ARTICLE

The effect of temperature and nitrogen deprivation on cell morphology and physiology of *Symbiodinium*

Buntora Pasaribu [c], Yu-Si Li [a], Ping-Chung Kuo [e], I-Ping Lin [e,g], Kwee Siong Tew [a,b], Jason T.C. Tzen [c], Yue Ken Liao [f], Chii-Shiarng Chen [a,b,d], Pei-Luen Jiang [a,b,*]

[a] *Graduate Institute of Marine Biotechnology, National Dong-Hwa University, Pingtung, Taiwan*
[b] *Taiwan Coral Research Center, National Museum of Marine Biology and Aquarium, Pingtung, Taiwan*
[c] *Graduate Institute of Biotechnology, National Chung-Hsing University, Taichung, Taiwan*
[d] *Department of Marine Biotechnology and Resources, National Sun Yat-Sen University, Kaohsiung, Taiwan*
[e] *Department of Biotechnology, National Formosa University, Yunlin, Taiwan*
[f] *Department of Forestry and Natural Resources, National Chiayi University, Chiayi, Taiwan*
[g] *Challenge Bioproducts Co. Ltd., Yunlin, Taiwan*

Received 4 June 2015; accepted 22 April 2016
Available online 10 May 2016

KEYWORDS
Symbiodinium;
Temperature;
Nitrogen deprivation

Summary Nutrients and temperature are the major elements in maintaining stable endosymbiotic relationships. The mechanisms and response of cultured *Symbiodinium* cells in the absence of nitrogen, and at various temperatures are still unclear. The present study investigated the influence of different temperatures and nitrogen-deprivation on free-living *Symbiodinium* cultures. The physiological responses of free-living *Symbiodinium* cells cultured at different temperatures during nitrogen deprivation under a 12:12 h light:dark were measured. *Symbiodinium* cell growth was significantly lower in response to lower temperatures. Transmission electron micrographs (TEMs) revealed the formation of lipid droplets induced by nitrogen deprivation under different temperatures. The results of this study will increase our understanding of adaptive responses occurring in *Symbiodinium* under environmental stress.

* Corresponding author at: Institute of Marine Biotechnology, National Dong Hwa University and National Museum of Marine Biology and Aquarium, 2 Houwan Road, Checheng, Pingtung 944, Taiwan. Tel.: +886 8 8825046; fax: +886 8 8825087.
E-mail address: villy@nmmba.gov.tw (P.-L. Jiang).
Peer review under the responsibility of Institute of Oceanology of the Polish Academy of Sciences.

Production and hosting by Elsevier

http://dx.doi.org/10.1016/j.oceano.2016.04.006

1. Introduction

Symbiodinium sp. is a unicellular microalga that has mutualistic associations with invertebrates such as corals and anemones (Davy et al., 2012). The coral host provides nutrients and carbon dioxide to *Symbiodinium* in hospite (Muscatine and Porter, 1977; Rodrigues and Grottoli, 2007). In return, these microalgae transfer more than 90% of their photosynthetically fixed carbon to the host cytoplasm where they reside (Muscatine, 1980). This mutualistic relationship enables coral to survive and remain healthy.

In more than a decade, the phenomenon of global climate change has contributed to the decline of coral reef around the world (Wilkinson, 2008). In such case, this change might generate huge impacts to the ocean ecosystem at all levels, such as higher mean sea water level, warmer ocean, stratified ocean, increasing CO_2 level in global scale, ice cover and ocean chemistry changes (Doney et al., 2009; Duce et al., 2008; Jackson et al., 2001; Kroecker et al., 2013; Poloczanska et al., 2013). The coral bleaching is expected to happen more frequently and become more severe due to the climate change. Environmental factors, such as nutrient levels and temperatures, play an important role in maintaining the stability of mutualistic associations between cnidarians and unicellular dinoflagellates (Belda et al., 1993; Hastie et al., 1992; Hoegh-Guldberg and Smith, 1989; Steen and Muscatine, 1987). It was reported that coral bleaching appeared in the seawater of southern Taiwan due to the exposure of temperature at 30–31°C (Mayfield et al., 2013, 2011). Furthermore, when corals were exposed at 14°C under the full sunlight, the reduction in photosynthetic ability caused the coral bleaching (Saxby et al., 2003). In terms of elevated sea temperature, the stability of corals and *Symbiodinium* endosymbiotic relationship is yet to be determined by anthropogenic stress factor such as coastal water quality (Wooldridge, 2014). Previous studies show that increasing nutrient levels, like dissolved nitrogen (N), in coastal water could induce some physiological impact on coral-dinoflagellate, for example, coral bleaching and reduced symbiont density (Koop et al., 2001; Marubini and Davies, 1996; Stimson, 1991; Szmant, 2002; Wiedenmann et al., 2013). For instance, the organic carbon supply by *Symbiodinium* to hosts could be established depending on nutrients from various sources including exogenous sea water, host catabolism and host heterotrophy (Steen, 1986; Szmant-Froelich and Pilson, 1984). Nitrogen, a major nutrient, is excreted as ammonium by the host (Rahav et al., 1989). Several investigations have reported that endosymbionts could survive in nitrogen-limited environments (Jiang et al., 2014; Peng et al., 2012). Therefore, nitrogen deprivation could alter symbiont physiologies (Weng et al., 2014). It is likely that symbiotic cnidarians may maintain the endosymbiont density through regulation of nitrogenous waste (McAuley, 1987; Rees, 1989). Moreover, temperature elevation alone can damage *Symbiodinium* cells in hospite (Sammarco and Strychar, 2013). It has been reported that the nutrient uptake in symbionts differed under different temperatures due to stress susceptibility among corals hosting different symbionts (Baker et al., 2013). There have been numerous studies using *Symbiodinium* treated with either differing temperatures or nitrogen deprivation (Jiang et al., 2014; Nitschke et al., 2015; Weng et al., 2014).

Several studies have reported that nitrogen starvation or other environmental stressors can affect growth, morphology, and metabolism of microalgae (Hockin et al., 2012; Pasaribu et al., 2014). For example, reduced nitrogen concentration increases lipid production in microalgae, which is stored in lipid droplets (Li et al., 2010; Piorreck et al., 1984). Recent studies have shown that increasing the temperature variation induced lipid content accumulation in *Nannochloropsis oculata* (Converti et al., 2009). Macedo and Alegre (2001) observed that lipid content increased in *Spirulina* cultured with nitrogen and decreased temperatures. However, the synergistic effects between nitrogen source and different temperature treatment on cellular mechanisms of *Symbiodinium* are poorly known.

The present study describes the influence of different temperatures and the absence of nitrogen in the medium on cultured free-living *Symbiodinium*. The aim was to examine changes in cellular biology, including cell proliferation, lipid classes, and ultrastructure in free-living *Symbiodinium*. *Symbiodinium* cell proliferation was slower when samples were cultured at temperatures of 15°C, than at 25 and 30°C. Results showed increased formation of different lipid droplets in *Symbiodinium* when cultured in extreme temperatures (i.e. 15 and 30°C).

2. Material and methods

2.1. *Symbiodinium* culture and treatment

The free-living *Symbiodinium* sp. (clade B) used in this study was obtained from National Museum of Marine Biology and Aquarium. They were maintained in the f/2 medium in filtered seawater (FSW) at room temperature under a photosynthetically active radiation (PAR) of 40 μmol m^{-2} s^{-1} in a 12-h light/12-h dark (12L/12D) cycle. For treatment, three-batch cultures were grown in the nitrogen-deficient artificial seawater with temperatures at 15, 25 and 30°C, separately.

2.2. *Symbiodinium* clade identification

The genetic identity (18S rDNA) of the cultured *Symbiodinium* was examined by PCR-RFLP (polymerase chain reaction-restriction fragment length polymorphism) analysis, and it was determined as clade B. *Symbiodinium* DNA was extracted using a plant genomic DNA extraction miniprep system (VIOGENE, Taipei). Basically, *Symbiodinium* nuclear small subunit (n18S-rDNA) was amplified by PCR from 3 replicate extracts of each of the two cultures using the primers, ss5z (an equimolar mixture of the oligonucleotides 5′-GCAGTTATAATT TATTTGATGGTCACTGCTAC-3′ and 5′-GCAGTTATAGTTTATTT-GATGGTTGCTGCTAC-3′) and ss3z (5′-AGCACTGCGTCAGTCC-GAATAATTCACCGG-3′). The PCR products were digested by restriction enzymes, *Taq* I and *Sau*3A I (Promega, USA). The digestion products were separated by electrophoresis on 1.5% 0.5× TAE (Amresco, USA) agarose gels, to generate the RFLP pattern. The RFLP pattern was compared to the literature (Rowan and Powers, 1991) to identify the clade of each culture.

2.3. Cell density determination

The *Symbiodinium* cell density was counted with haemocytometer based cell counting. Cell densities were determined daily by placing an aliquot of well-mixed culture suspension on a Neubauer hemocytometer (Marienfel, Germany) under a Axioskop2 Plus microscope (Zeiss, Germany) connected to a CCD camera (Photometrics, USA).

2.4. Lipid analyses

Lipid contents of three replicates from the nitrogen-deprived culture *Symbiodinium* cells with temperatures 15, 25 and 30°C were extracted by the Bligh and Dyer procedure (Bligh and Dyer, 1959). Neutral lipids from *Symbiodinium* cells were extracted with 150 μl of chloroform/methanol (2:1, v/v). After centrifugation, the lower chloroform fraction was collected for the analysis by thin layer chromatography (TLC) (Analtech, USA) with the solvent system modified from previous reports (Fuchs et al., 2007; Oku et al., 2003).

2.5. The transmission electron microscopy and imaging analysis

To investigate the morphological variability of *Symbiodinium* cultured in different temperatures under nitrogen deprivation, *Symbiodinium* cells were collected and fixed in 2.5% glutaraldehyde and 2% paraformaldehyde in 100 mM sodium phosphate containing 5% sucrose (pH 7.3) for 2.5 h at 4°C. They were then rinsed with 100 mM sodium phosphate buffer at 4°C. Cells were then post-fixed in 1% OsO_4 in 50 mM sodium phosphate (pH 7.3) for 1 h at 4°C. The cell aliquots were then washed three times for 15 min each with the same buffer and dehydrated by a graded ethanol series (50, 70, 80, 90, 95 and 100%) before embedding in LR white resin. Thin sections (70 nm) cut by a Leica Reichert Ultracut R were collected on nickel grids, post-stained with 2.5% uranyl acetate and 0.4% lead citrate, rinsed three times with water, and the samples were viewed on a JEM-1400 transmission electron microscope (JEOL, Japan).

3. Results and discussion

3.1. Morphology of free living cultured *Symbiodinium* cells

Symbiodinium spp. can be either autotrophic or symbiotic in cnidarians cells. Free-living *Symbiodinium* cells of 5—6 μm were brown-colored and coccoid-shaped (Fig. 1A). The size of cultured free-living *Symbiodinium* cells was equivalent to those of other free-living *Symbiodinium* species and clades (Blank and Huss, 1989). Generally, the morphology of cultured free-living *Symbiodinium* cells indicated they were smaller than symbiotic cells isolated from coral (Pasaribu et al., 2014). It has been reported that the most abundant *Symbiodinium* is coccoid yellow-brown (Freudenthal, 1962), and is smaller than cultured *Symbiodinium* (Jeong et al., 2014). In cultured free-living *Symbiodinium*, the intercalary bands were located at the cell surface (Fig. 1B). The intercalary bands are known as growth bands indicating cell growth, and occur with the addition of material along plate margins in some dinoflagellates (Graham and Wilcox, 2000).

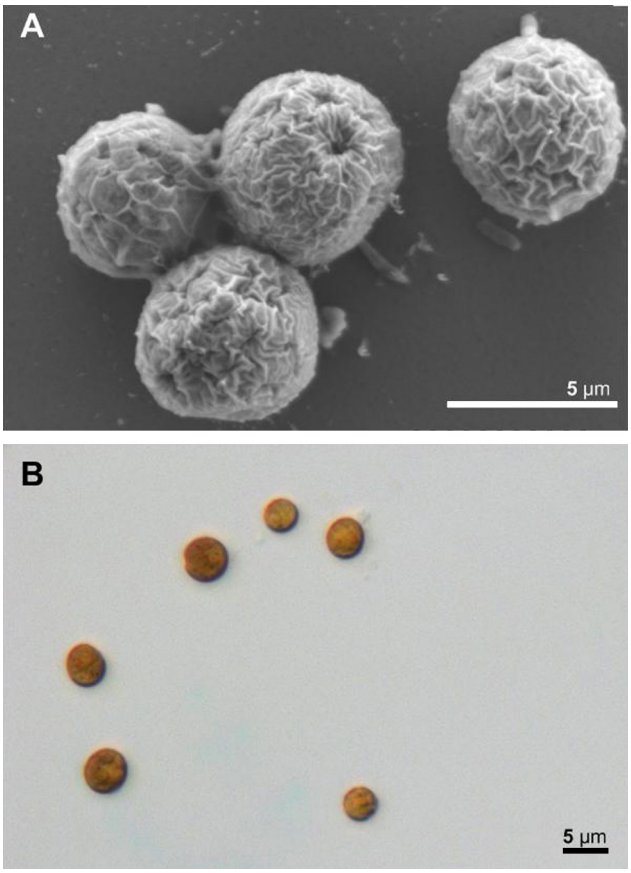

Figure 1 Microscopic examination of free-living cultured *Symbiodinium*. (A) Light microscopy of free-living cultured *Symbiodinium*. (B) Free-living cultured *Symbiodinium* observed under scanning electron microscopy.

3.2. Effect of temperature and nitrogen-deprivation on *Symbiodinium* cell growth

Temperature is an important factor for algal growth. It strongly influences cellular chemical composition, nutrient uptake, and growth rates of all algal species. After 5 days, *Symbiodinium* cells cultivated in a nitrogen-deprived medium proliferated more slowly and showed increased lipid contents, than those in a nitrogen-enriched medium (Jiang et al., 2014). To determine the most efficient way to cultivate *Symbiodinium* cells and induce lipid accumulation, free-living *Symbiodinium* cells were subjected to different temperatures under nitrogen-deprivation, and the cultures were counted using a hemocytometer. Fig. 2 shows that when cultured under nitrogen-starvation, *Symbiodinium* cells have slower growth at lower temperatures (15°C) than at normal temperatures (25°C). However, at high temperatures (30°C) growth rate was higher than at normal temperatures (25°C) (Fig. 2). As *Symbiodinium* cells cultured in nitrogen-deprived media showed inhibited growth with lower temperatures, higher temperatures were considered appropriate to achieve high cell concentrations. Different temperatures also affected phosphorus uptake in microalgae, with phosphorus

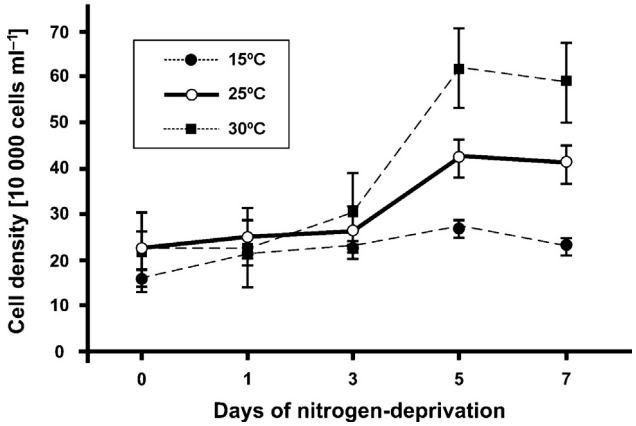

Figure 2 Growth curves of *Symbiodinium* cells cultivated at different temperatures under nitrogen deprivation. Temperature treatments (15, 25, and 30°C) were applied to free-living *Symbiodinium* sp. The data represents means ± SD (n = 3).

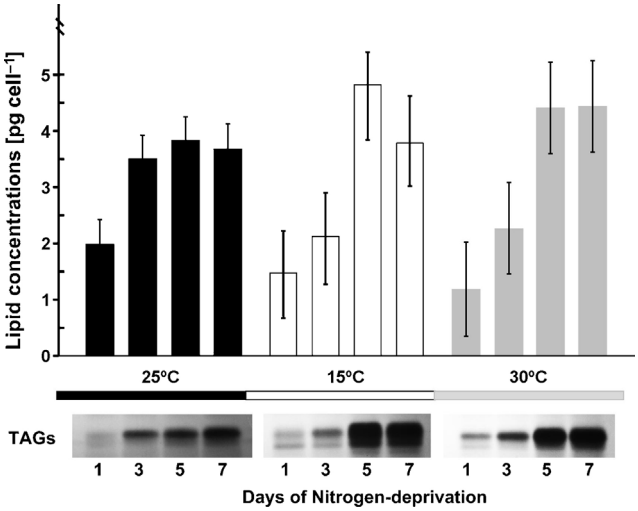

Figure 3 Thin layer chromatography (TLC) analysis of lipids extracted from *Symbiodinium* cells cultivated at different temperatures under nitrogen deprivation. The lipid comparison of free-living cultured *Symbiodinium* between three different temperatures under nitrogen deprivation.

accumulation increasing with higher temperatures compared to lower temperatures (Powell et al., 2008). Several microalgal species can grow in extreme environments, such as high temperatures of 30–35°C (Converti et al., 2009; Oliveira et al., 1999), however, some species do not grow efficiently in temperatures above 30°C and these temperatures are considered as heat stress (Bajguz, 2009). *Symbiodinium* cells had the best growth rates at normal temperatures (25°C) with nitrogen supply (Pasaribu et al., 2015); however, results from the present study indicated that *Symbiodinium* cells grew well in temperatures above 30°C in nitrogen-free media. Other studies have reported similar results that the optimum growth of *Symbiodinium* could exceed the thermal break-point (>32°C) (Kinzie et al., 2001; Strychar et al., 2005). Furthermore, the response to the temperature changes was an adaptive physiological adjustment of *Symbiodinium* (Sammarco and Strychar, 2013). It is feasible that *Symbiodinium* endosymbiont were present in nutrient-limited environment with respect to nitrogen source (Dubinsky and Berman-Frank, 2001; Wooldridge, 2010), therefore, the stability of coral-dinoflagellate was particularly supported by interaction of temperature and nutrient.

3.3. Temperature and nitrogen-deprivation induces neutral lipid accumulation in *Symbiodinium* cells

Nitrogen deprivation is a nutrient limitation that disrupts algal cell metabolism. Several studies reported that microalgae cultivation under environmental stress caused slow growth and lipid accumulation (Hu and Gao, 2005; Yeesang and Cheirsilp, 2011). Cultured free-living *Symbiodinium* cells were treated with low and high temperatures in a nitrogen-free medium for 7 days. The change in lipid content during the treatments was analyzed using thin-layer chromatography (TLC) (Fig. 3). There were no apparent differences between the temperatures during the experiment, and all temperature treatments induced neutral lipid (triacylglyceride [TAG]) accumulation on day 5. Previous studies demonstrated that nitrogen deprivation increased lipid content and lipid droplet accumulation in free-living *Symbiodinium* cells (Jiang et al., 2014). These findings were similar to those of the studies involving temperature and nutrient-starved green algae, *Spirulina* sp. and *N. oculata* (Converti et al., 2009; Macedo and Alegre, 2001).

3.4. Ultrastructure of lipid droplets in *Symbiodinium* cells

The main cause of coral bleaching is extreme temperatures and if the extreme temperature persists for a long period, corals begin to die. Sammarco and Strychar (2013) concluded that during exposure to the high temperatures for soft coral for 2 days, the *Symbiodinium* cells were apoptotic, but the hosts adapted to the high temperature. High water temperatures can affect the endosymbiotic *Symbiodinium* cells. In the free-living cultures, *Symbiodinium* cells were in contact with the environment directly. The cells slowly proliferated, and the morphology changed due to a lower temperature or upon nitrogen deprivation (Jiang et al., 2014; Pasaribu et al., 2015). When the temperature went up above 30°C, the free-living cultures of *Symbiodinium* cells did not change in terms of the growth during the nitrogen deprivation (Fig. 2). Synergistic effects of temperature and nitrogen source on cell morphology in the *Symbiodinium* cells were examined using transmission electron microscopy (TEM) (Fig. 4). After 5 days of culture in the nitrogen-deprived medium, the cell walls of *Symbiodinium* cells were thickened, and the lipid droplets (the major organelle) occupied most of the space in the cells (Fig. 4A and B). Lipid droplet formation was found in *Symbiodinium* cells with lipid accumulation in nitrogen-deprived conditions (Jiang et al., 2014). Lipid droplet accumulation in algae typically occurs during periods of environmental stress, including growth under nutrient-deficient conditions. Nitrogen-deprivation invariably caused a steady decline in the rate of cell growth. When algal cell divisions slow down, the synthesis of new membrane components might also slow down, and the cells transform fatty acids into triacylglycerols

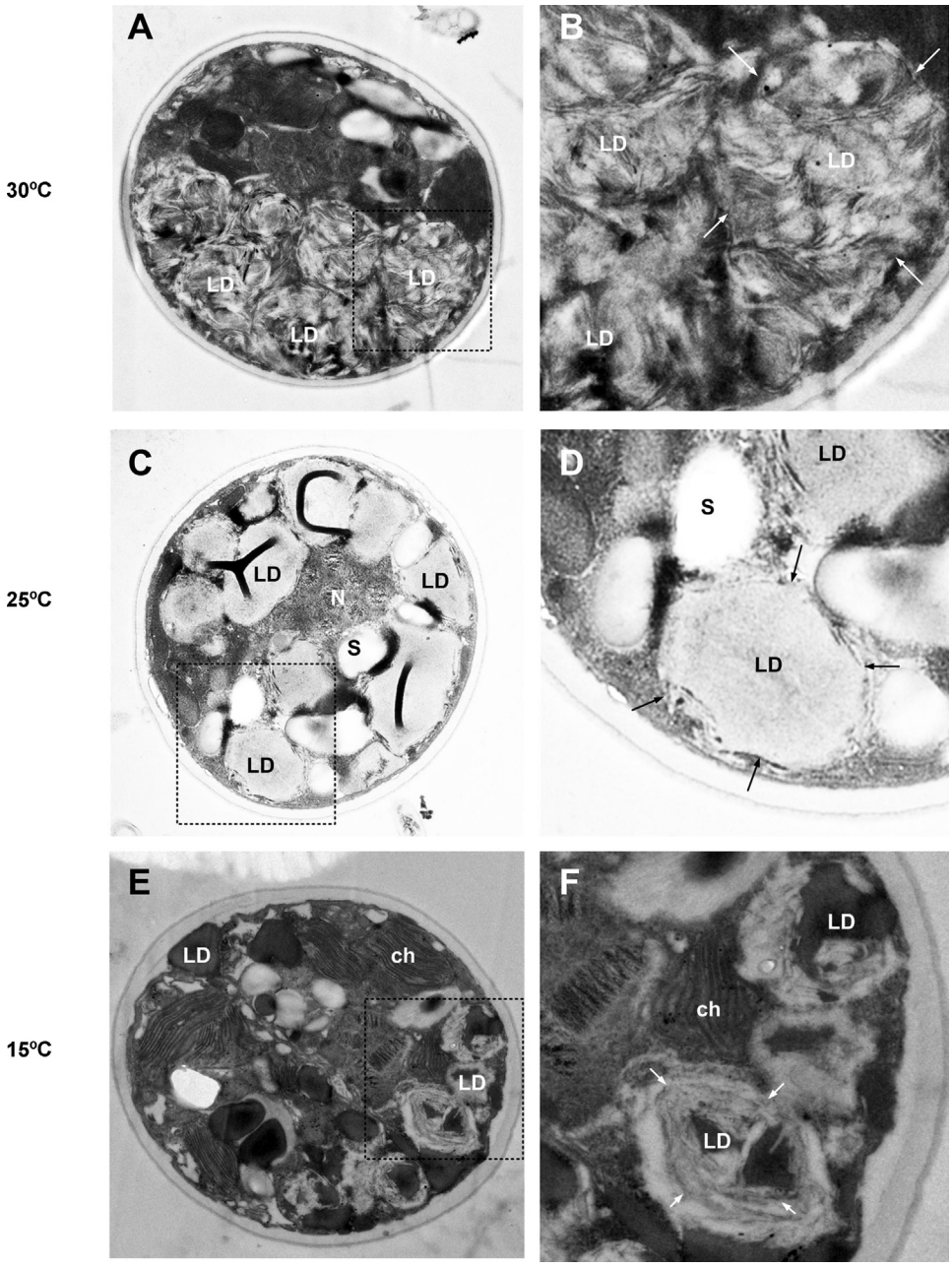

Figure 4 Morphology of *Symbiodinium* cells using transmission electron microscopy (TEM). (A and B) Ultrastructure of free-living *Symbiodinium* cells cultivated at 30°C using TEM. Free-living *Symbiodinium* cells cultivated at extreme temperatures (C and D: 25°C; E and F: 15°C). Abbreviations: LD, lipid droplet; Ch, chloroplast; N, nucleolus; S, starch granule.

(Jiang et al., 2014; Lin et al., 2012; Wang et al., 2009). Extreme temperature stress of low and high temperatures also induced lipid droplets in *Symbiodinium* cells (Fig. 4C and E). However, numerous inclusion bodies (see the arrowhead in Fig. 4D and F) appeared inside the lipid droplets on day 5 of the nitrogen-deprivation treatment, which were not found in the normal temperature treatment (Fig. 4B). The surface of lipid droplets in *Symbiodinium* cells seemed to be modified, suggesting that they might become relatively unstable. Bleaching induced similar morphological changes in *Symbiodinium* and its host (Dunn et al., 2007; Fujise et al., 2014). It was presumed that under extreme temperatures, *Symbiodinium* used lipids earlier to survive the environmental stress.

Acknowledgments

This work was supported by a grant from the Ministry of Science and Technology, Taiwan (MOST 104-2313-B-291-001 to P.-L. Jiang) and by intramural funding from NMMBA (1051016379).

References

Bajguz, A., 2009. Brassinosteroid enhanced the level of abscisic acid in *Chlorella vulgaris* subjected to short-term heat stress. J. Plant Physiol. 166 (8), 882–886.

Baker, D.M., Andras, J.P., Jordán-Garza, A.G., Fogel, M.L., 2013. Nitrate competition in a coral symbiosis varies with temperature among *Symbiodinium* clades. ISME J. 7 (6), 1248–1251.

Belda, C.A., Lucas, J.S., Yellowlees, D., 1993. Nutrient limitation in the giant clam zooxanthellae symbiosis: effect of nutrient supplement on growth of the symbiotic partners. Mar. Biol. 117 (4), 655–664.

Blank, R.J., Huss, V.A.R., 1989. DNA divergency and speciation in *Symbiodinium* (Dinophyceae). Plant Syst. Evol. 163 (3), 153–163.

Bligh, E.G., Dyer, W.J., 1959. A rapid method for total lipid extraction and purification. Can. J. Biochem. Physiol. 37 (8), 911–917.

Converti, A.A.A., Casazza, E.Y., Ortiz, P.P., Borghi, M.D., 2009. Effect of temperature and nitrogen concentration on the growth and lipid content of *Nannochloropsis oculata* and *Chlorella vulgaris* for biodiesel production. Chem. Eng. Process. 48 (6), 1146–1151.

Davy, K.S., Allemand, D., Weis, V.M., 2012. Cell biology of cnidarian-dinoflagellate symbiosis. Microbiol. Mol. Biol. Rev. 76 (2), 229–261.

Doney, S.C., Fabry, V.J., Feely, R.A., Kleypas, J.A., 2009. Ocean acidification: the other CO_2 problem. Annu. Rev. Mar. Sci. 1, 169–192.

Dubinsky, Z., Berman-Frank, I., 2001. Uncoupling primary production from population growth in photosynthesizing organisms in aquatic ecosystems. Aquat. Sci. 63 (1), 4–17.

Duce, R.A., LaRoche, J., Altieri, K., Arrigo, K.R., Baker, A.R., Capone, D.G., Cornell, S., Dentener, F., Galloway, J., Ganeshram, R.S., Geider, R.J., Jickells, T., Kuypers, M.M., Langlois, R., Liss, P.S., Liu, S.M., Middelburg, J.J., Moore, C.M., Nickovic, S., Oschlies, H., Pedersen, T., Prospero, J., Schlitzer, R., Seitzinger, S., Sorensen, L.L., Uematsu, M.M., Ulloa, O., Voss, M., Ward, B., Zamora, L., 2008. Impacts of atmospheric anthropogenic nitrogen on the open ocean. Science 320 (5878), 893–897.

Dunn, S.R., Schnitzler, C.E., Weis, V.M., 2007. Apoptosis and autophagy as mechanisms of dinoflagellate symbiont release during cnidarian bleaching: every which way you lose. Proc. R. Soc. B 274 (1629), 3079–3085.

Freudenthal, H.D., 1962. Symbiodinium gen. nov. and *Symbiodinium microadriaticum* sp. nov., a zooxanthella: taxonomy, life cycle and morphology. J. Protozool. 9 (1), 45–52.

Fuchs, B., Schiller, J., Sub, R., Schurenberg, M., 2007. A direct and simple method of coupling matrix-assisted laser desorption and ionization time-of-flight mass spectrometry (MALDI-TOF MS) to thin layer chromatography (TLC) for the analysis of phospholipids from egg yolk. Anal. Bioanal. Chem. 389 (3), 827–834.

Fujise, L., Yamashita, H., Suzuki, G., Sasaki, K., Liao, L.M., Koike, K., 2014. Moderate thermal stress causes active and immediate expulsion of photosynthetically damaged zooxanthellae (*Symbiodinium*) from corals. PLoS One 9 (12), e114321.

Graham, L.E., Wilcox, L.W., 2000. Algae. Prentice Hall, Upper Saddle River, NJ, 640 pp.

Hastie, L.C., Waston, T.C., Isamu, T., 1992. Effect of nutrient enrichment on *Tridacna derasa* seed: dissolved in organic nitrogen increases growth rate. Aquaculture 106 (1), 41–49.

Hockin, N.L., Mock, T., Mulholland, F., Kopriva, S., Malin, G., 2012. The response of diatom central carbon metabolism to nitrogen starvation is different from that of green algae and higher plants. Plant Physiol. 158 (1), 299–312.

Hoegh-Guldberg, O., Smith, J., 1989. The effect of sudden changes in temperature, light and salinity on the population density and export of zooxanthellae from the reef corals *Stylophora pistillata* Esper and *Seriatopora hystrix* Dana. J. Exp. Mar. Biol. Ecol. 129 (3), 279–303.

Hu, H., Gao, K., 2005. Response of growth and fatty acid compositions of *Nannochloropsis* sp. to environmental factors under elevated CO_2 concentration. Biotechnol. Lett. 28 (13), 987–992.

Jackson, J.B.C., Kirby, M.X., Berger, W.H., Bjorndal, K.A., Botsford, L.W., Bourque, B.J., Bradbury, R.H., Cooke, R., Erlandson, J., Estes, J.A., Hughes, T.P., Kidwell, S., Lange, C.B., Lenihan, H.S., Pandolfi, J.M., Peterson, C.H., Steneck, R.S., Tegner, M.J., Warner, R.R., 2001. Historical overfishing and the recent collapse of coastal ecosystem. Science 293 (5530), 629–637.

Jeong, H.J., Lee, S.Y., Kang, N.S., Yoo, Y.D., Lim, A.S., Lee, M.J., Kim, H.S., Yih, W.H., LaJeunesse, T.C., 2014. Genetics and morphology characterize the dinoflagellate *Symbiodinium voratum*, n. sp. (Dinophyceae) as the sole representative of *Symbiodinium* clade E. J. Eukaryot. Microbiol. 61 (1), 75–94.

Jiang, P.L., Pasaribu, B., Chen, C.S., 2014. Nitrogen-deprivation elevates lipid levels in *Symbiodinium* spp. by lipid droplet accumulation: morphological and compositional analyses. PLoS One 9 (1), e87416.

Kinzie III, R.A., Takayama, M., Santos, S.R., Coffroth, M.A., 2001. The adaptive bleaching hypothesis: experimental tests of critical assumptions. Biol. Bull. 200 (1), 51–58.

Koop, K., Booth, D., Broadbent, A., Brodie, J., Bucher, D., Capone, D., Coll, J., Dennison, W., Erdmann, M., Harrison, P., Hoegh-Guldberg, O., Hutchings, P., Jones, G.B., Larkum, A.W.D., O'Neil, J., Steven, A., Tentori, E., Ward, S., Williamson, J., Yellowlees, D., 2001. ENCORE: the effect of nutrient enrichment on coral reefs. Synthesis of results and conclusions. Mar. Pollut. Bull. 42 (2), 9–120.

Kroecker, K.J., Kordas, R.L., Crim, R., Hendriks, I.E., Ramajo, L., Singh, G.S., Duarte, C.M., Gattuso, J.M., 2013. Impacts of ocean acidification on marine organisms: quantifying sensitivities and interaction with warming. Glob. Change Biol. 19 (6), 1884–1896.

Li, X., Hu, H.Y., Yang, J., 2010. Lipid accumulation and nutrient removal properties of a newly isolated freshwater microalga, *Scenedesmus* sp. LX1, growing in secondary effluent. New Biotechnol. 27 (1), 59–63.

Lin, I.P., Jiang, P.L., Chen, C.S., Tzen, J.T.C., 2012. A unique caleosin serving as the major integral protein in oil bodies isolated from *Chlorella* sp. cells cultured with limited nitrogen. Plant Physiol. Biochem. 61, 80–87.

Macedo, R.V.T., Alegre, R.M., 2001. Influence of nitrogen content in the cultivation of *Spirulina maxima* in two temperature levels – Part II, Produção de Lipídios. Ciênc. Tecnol. Aliment. Campinas 21 (2), 183–186.

Marubini, F., Davies, P.S., 1996. Nitrate increases zooxanthellae population density and reduces skeletogenesis in corals. Mar. Biol. 127 (2), 319–328.

Mayfield, A.B., Chen, M.N., Meng, P.J., Lin, H.J., Chen, C.S., Liu, P.J., 2013. The physiological response of the reef coral *Pocillopora damicornis* to elevated temperature: results from coral reef mesocosm experiments in Southern Taiwan. Mar. Environ. Res. 86, 1–11.

Mayfield, A.B., Wang, L.H., Tang, P.C.C., Fan, T.Y., Hsiao, Y.Y., Tsai, C.L., Chen, C.S., 2011. Assessing the impacts of experimentally elevated temperature on the biological composition and molecular chaperone gene expression of a reef coral. PLoS One 6 (10), e26529.

McAuley, P.J., 1987. Nitrogen limitation and amino-acid metabolism of Chlorella symbiotic with green hydra. Planta 171 (4), 532–538.

Muscatine, L., 1980. Uptake, retention, and release of dissolved inorganic nutrients by marine alga-invertebrate associations. In: Cook, C.B., Pappas, P.W., Rudolph, E.D. (Eds.), Cellular Interactions in Symbiosis and Parasitism. Ohio Univ. Press, Columbus, 229–244.

Muscatine, L., Porter, J.W., 1977. Reef corals: mutualistic symbioses adapted to nutrient-poor environments. Bioscience 27 (7), 454–460.

Nitschke, M.R., Davy, S.K., Cribb, T.H., Ward, S., 2015. The effect of elevated temperature and substrate on free-living *Symbiodinium* cultures. Coral Reefs 34 (1), 161–171.

Oku, H., Yamashiro, H., Onaga, K., 2003. Lipid biosynthesis from [14C]-glucose in the coral *Montipora digitata*. Fish. Sci. 69 (3), 625–631.

Oliveira, M.A.C.L., Monteiro, M.P.C., Robbs, P.G., Leite, S.G.F., 1999. Growth and chemical composition of *Spirulina maxima* and *Spirulina platensis* biomass at different temperatures. Aquacult. Int. 7 (4), 261—275.

Pasaribu, B., Lin, I.P., Chen, C.S., Lu, C.Y., Jiang, P.L., 2014. Nutrient limitation in *Auxenochlorella protothecoides* induces qualitative changes of fatty acid and expression of caleosin as a membrane protein associated with oil bodies. Biotechnol. Lett. 36 (1), 175—180.

Pasaribu, B., Weng, L.C., Lin, I.P., Camargo, E., Tzen, J.T.C., Tsai, C. H., Ho, L.S., Lin, M.R., Wang, L.H., Chen, C.S., Jiang, P.L., 2015. Morphological variability and distinct protein profiles of cultured and endosymbiotic *Symbiodinium* cells isolated from *Exaiptasia pulchella*. Sci. Rep. 5, article no. 15353.

Peng, S.E., Chen, C.S., Song, Y.F., Huang, H.T., Jiang, P.L., Chen, W. N., Fang, L.S., Lee, Y.C., 2012. Assessment of metabolic modulation in free-living versus endosymbiotic *Symbiodinium* using synchrotron radiation-based infrared microspectroscopy. Biol. Lett. 8 (3), 434—437.

Piorreck, M., Baasch, K.H., Pohl, P., 1984. Biomass production, total protein, chlorophylls, lipids and fatty acids of freshwater green and blue-green algae under different nitrogen regimes. Phytochemistry 23 (2), 207—216.

Poloczanska, E.S., Brown, C.J., Sydeman, W.J., Kiessling, W., Schoeman, D.S., Moore, P.J., Brander, K., Bruno, J.F., Buckley, L.B., Burrows, M.T., Duarte, C.M., Halpern, B.S., Holding, J., Kappel, C.V., O'Connor, M.I., Pandolfi, J.M., Parmesan, C., Schwing, F., Thompson, S.H., Richardson, A.J., 2013. Global imprint of climate change on marine life. Nat. Clim. Change 3, 919—925.

Powell, N.A., Shilton, A.N., Pratt, S., Chisti, Y., 2008. Factors influencing luxury uptake of phosphorus by microalgae in waste stabilization ponds. Environ. Sci. Technol. 42 (16), 5958—5962.

Rahav, O., Dubinsky, Z., Achituv, Y., Falkowski, P.G., 1989. Ammonium metabolism in the zooxanthellate coral *Stylophora pistillata*. Proc. R. Soc. Lond. B: Biol. Sci. 236 (1284), 325—337.

Rees, T.A.V., 1989. The green hydra symbiosis and ammonium II. Ammonium assimilation and release by freshly isolated symbionts and cultured algae. Proc. R. Soc. B 235 (1281), 365—382.

Rodrigues, L.J., Grottoli, A.G., 2007. Energy reserves and metabolism as indicators of coral recovery from bleaching. Limnol. Oceanogr. 52 (5), 1874—1882.

Rowan, R., Powers, D.A., 1991. A molecular genetic classification of zooxanthellae and the evolution of animal-algal symbiosis. Science 251 (4999), 1348—1351.

Sammarco, P.W., Strychar, K.B., 2013. Responses to high seawater temperatures in zooxanthellate octocorals. PLoS One 8 (2), e54989.

Saxby, T., Dennison, W.C., Hoegh-Guldberg, O., 2003. Photosynthetic responses of the coral *Montipora digitata* to cold temperature stress. Mar. Ecol.-Prog. Ser. 248, 85—97.

Steen, R.G., 1986. Evidence of heterotrophy by zooxanthellae in symbiosis with *Aiptasia pulchella*. Biol. Bull. 170 (2), 267—278.

Steen, R.G., Muscatine, L., 1987. Low temperature evokes rapid exocytosis symbiotic algae by a sea anemone. Biol. Bull. 172 (2), 246—263.

Stimson, J., 1991. The temporal pattern and rate of release of zooxanthellae from the reef coral *Pocillopora damicornis* (Linnaeus) under nitrogen-enrichment and control conditions. J. Exp. Mar. Biol. Ecol. 153 (1), 63—74.

Strychar, K.B., Coates, M.C., Scott, P.W., Piva, T.J., Sammarco, P.W., 2005. Loss of symbiotic dinoflagellates (Symbiodinium; zooxanthellae) from bleached soft corals *Sarcophyton*, *Sinularia*, and *Xenia*. J. Exp. Mar. Biol. Ecol. 320 (2), 159—177.

Szmant, A.M., 2002. Nutrient enrichment on coral reefs: is it a major cause of coral reef decline? Estuar. Coast. Shelf Sci. 25 (4), 743—766.

Szmant-Froelich, A., Pilson, M.E.Q., 1984. Effects of feeding frequency and symbiosis with zooxanthellae on nitrogen metabolism and respiration of the coral *Astrangia danae*. Mar. Biol. 81 (2), 153—162.

Wang, Z.T., Ullrich, N., Joo, S., Waffenschmidt, S., Goodenough, U., 2009. Algal lipid bodies: stress induction, purification, and biochemical characterization in wild-type and starchless *Chlamydomonas reinhardtii*. Eukaryot. Cell 8 (12), 1856—1868.

Weng, L.C., Pasaribu, B., Lin, I.P., Tsai, C.H., Chen, C.S., Jiang, P.L., 2014. Nitrogen limitation induces lipid droplet accumulation and alters fatty acid metabolism in symbiotic dinoflagellates isolated from *Aiptasia pulchella*. Sci. Rep. 4 article no. 5777.

Wiedenmann, J., D'Angelo, C., Smith, E.G., Hunt, A.N., Legiret, F.E., Postle, A.D., Achterberg, E.P., 2013. Nutrient enrichment can increase the susceptibility of reef corals to bleaching. Nat. Clim. Change 3, 160—164.

Wilkinson, C., 2008. Status of Coral Reefs of the World: 2008. GCMN, Reef Rainforest Res. Centre, Townsville, 290 pp.

Wooldridge, S.A., 2010. Is the coral-algae symbiosis really mutually beneficial for the partners? Bioessays 32 (7), 615—625.

Wooldridge, S.A., 2014. Assessing coral health and resilience in a warming ocean: why looks can be deceptive. Bioessays 36 (11), 1041—1049.

Yeesang, C., Cheirsilp, B., 2011. Effect of nitrogen, salt, and iron content in the growth medium and light intensity on lipid production by microalgae isolated from freshwater sources in Thailand. Bioresour. Technol. 102 (3), 3034—3040.

Oceanologia (2016) 58, 279—291

Available online at www.sciencedirect.com

ScienceDirect

journal homepage: www.journals.elsevier.com/oceanologia/

ORIGINAL RESEARCH ARTICLE

Narrowband shortwave minima in spectra of backscattered light from the sea obtained from ocean color scanners as a remote indication of algal blooms☆

G.S. Karabashev*, M.A. Evdoshenko

Laboratory of Ocean Optics, Shirshov Institute of Oceanology RAS, Moscow, Russia

Received 27 December 2015; accepted 2 May 2016
Available online 13 May 2016

KEYWORDS
Algae;
Bloom;
Pigments;
Reflectance spectrum;
MODIS;
Baltic Sea

Summary We propose a new approach to indication of algal blooms. It stems from analysis of the multispectral satellite reflectance R_{rs} of areas where blooms were documented during recent decades. We found that spectra of algal blooms exhibit minima at wavelengths of channels of Moderate Resolution Imaging Spectroradiometer (MODIS) λ = 443 and λ = 488 nm (Baltic, Black, and Caspian seas), λ = 443 nm (Southwest Tropical Pacific (SWTP)), and λ = 443 nm and λ = 469 nm (Patagonian Continental Shelf (PCS)), attributable to absorption bands of chlorophyll *a* and accessory pigments. We quantified the minima using indices D1 = $R_{rs}(443) - R_{rs}(412)$ and D2 = $R_{rs}(488) - R_{rs}(469)$ and proved their diagnostic potential by comparing their distributions to that of $R_{rs}(555)$. Linear dependence of D1 upon chlorophyll *a* was found from MODIS data for the bloom of *Nodularia spumigena*. Time dependences of D1 and D2 point to the latter as a probable remote forerunner of cyanobacterial blooms. In the PCS, D1 and D2 proved to be too simplistic owing to diversity of spectral shapes at $\lambda < 550$ nm. Cluster analysis revealed close linkage of the latter and local oceanological conditions. Our findings bear witness to the diagnostic potential of the indices by virtue of their direct relation to pigment absorption and because the broadband background reflectance changes reduce when calculating the indices as a difference of spectrally

☆ Part of the paper was presented at the 8th International Conference "Current Problems in the Optics of Natural Waters", St. Petersburg, Russia, 8—12 September 2015.

* Corresponding author at: Laboratory of Ocean Optics, Shirshov Institute of Oceanology RAS, Nakhimovskiy prospekt, 36, Moscow 117997, Russia. Tel.: +7 499 1245996; fax: +7 499 1245983.
E-mail address: genkar@mail.ru (G.S. Karabashev).

Peer review under the responsibility of Institute of Oceanology of the Polish Academy of Sciences.

Production and hosting by Elsevier

http://dx.doi.org/10.1016/j.oceano.2016.05.001

close reflectances. Further studies are needed to convert the indices to band-difference algorithms for retrieving the bio-optical characteristics of algal blooms.

1. Introduction

The rapid growth of microalgae abundance in water basins is usually referred to as algal bloom. Extensive studies of blooms during last decades revealed recurrence of blooms in many areas of the oceans (Anderson, 2001; Sellner et al., 2003). A bloom may be induced by a set or a single algal species. The blooms occur in different climatic zones and cover the areas sizing from local scales to basin-wide ones. The period, when algal cells concentration in water exceeds a certain threshold level, determines the lifetime of a bloom. This period lasts from days to months. Radical changes in content and composition of suspended particles, dissolved organic matter, nutrients and other substances accompany the blooms because of vital activity of the microorganisms, their lifetime excretions, consumption, degradation, and final decomposition. These processes develop against a background of water dynamics events of different scales, which contributing into the intricacy of bloom patterns. The necessity to understand the latter is particularly urgent because some of the algae produce toxins and induce the harmful algal blooms (HABs) dangerous for aquatic biota and humans (Sellner et al., 2003).

The understanding of such cause-and-effect relations requires knowing the distributions of the relevant organisms and substances in time and space on periods from seconds to years and on scales from 10^0 to 10^6 m. To date, the problem of 'undersampling' (Munk, 2002) is far from being eliminated in biological oceanography since the labor-consuming laboratory treatment of water samples for studying the ecologically significant objects remains relevant (Balzano et al., 2015). The light absorbing and fluorescing chlorophyll and accessory pigments are inherent to the algae, which provides great scope for rapid remote sensing of algal abundance in different aquatic environments. In their pioneering work, Clarke et al. (1970) used an airborne spectroradiometer for recording the spectra of solar radiation, backscattered from the Sargasso Sea and coastal waters. In authors' judgment, the shape of these spectra demonstrated much potential for yielding information about algal chlorophyll in the near surface layer in spite of the fact that there were no radiance minima attributable to the absorption of light by algal pigments. At present, these potentialities are implemented as a system of satellite instrumentation, techniques, band-ratio algorithms, and discoveries described in thousands of publications. It is precisely the satellite information of global coverage that underlies the present day knowledge of geography, duration, and scales of algal blooms and inhomogeneities of optically significant admixtures in the World Ocean (McClain, 2001; Świrgoń and Stramska, 2015).

These successes were achieved thanks to orbiting multispectral ocean color scanners (OCSs) run by the NASA and ESA since 1978. Elimination of atmospheric contribution into the OCS products (atmospheric correction) makes them indispensable for ocean studies. The OCSs are distinguished by swaths more than 1000 km wide, ground sample distance (GSD) close to 1 km or less, and rated revisit time as short as 1–2 days which fits well to time and space scales of algal blooms. Such a consistency has been achieved at the expense of spectral resolution of the OCSs, which usually have several spectral bands in the visible range. This is insufficient for reliable identification of blooming algae from manifestation of individual absorption and fluorescence bands of algal chlorophyll and accessory pigments in the satellite reflectance spectra of the sea surface. At the same time, manifestations of this kind were occasionally reported in publications based on data of the shipborne hyperspectral radiometers.

When recording the R_{rs} spectra with a floating spectrometer in the Falkland Current frontal zone, Kopelevich et al. (2005) observed a broad minimum in the violet-blue range roughly at 440 nm where the absorption band of chlorophyll *a* belongs. This fact agrees well with information on blooms of various algae in the system of Falkland-Brazilian currents and the Patagonian Continental Shelf (Ferreira et al., 2013; Painter et al., 2010; Sabatini et al., 2012). Lubac and Loisel (2007) used a ship-borne spectrometer and recorded reflectance spectra having well-defined minimum in the blue-violet wavelength range. The minimum took place exclusively at stations in the English Channel where chlorophyll and cell counting in water samples provided evidence of the *Phaeocystis globosa* bloom. Similar shapes of the wavelength dependence of water-leaving radiance have been revealed by Soloviev (2005) when analyzing the images of the Caspian and Baltic Seas obtained with the OCS MODIS (Moderate Resolution Imaging Spectroradiometer) during blooms of *Nodularia spumigena* in summer 2005.

The MODIS determinations of sea surface reflectance have been improved in spectral resolution within the shortwave half of the visible spectrum upon data reprocessing version R2013.1. The updated estimates of R_{rs} are now available at the OceanColor website of NASA (http://oceancolor.gsfc.nasa.gov/) as Level 2 products at GSD = 1 km and wavelengths λ = 412, 443, 469, 488, 531, 547, 555, 645, 667, and 678 nm. Using the updated MODIS imagery for the same cyanobacterial bloom of 2005 in the Baltic Sea, we have found that better spectral resolution makes possible to discriminate the second shortwave reflectance minimum at 488 nm (Karabashev and Evdoshenko, 2015). Metsamaa et al. (2006) have measured the spectra of absorption coefficients of the cyanobacteria *Aphanizomenon flos-aquae* "*baltica*", *Anabaena circinalis* and *N. spumigena* as the main bloom-forming species in the Baltic Sea. In these organisms, the absorption of light peaks at 439 nm, exhibits weaker maximum at 479 nm, and tends to zero at 560 nm. The peak at 439 nm corresponds to the absorption maximum of the

chlorophyll *a*. The latter is universally present in the photosynthesis system of plants (the Soret band); the maximum at 479 nm points to the accessory pigments such as carotenoids or phycobilins (Wozniak and Dera, 2007). Poutanen and Nikkilä (2001) provided evidence of frequent occurrence of the carotenoids in the Baltic waters during last half-century.

The above findings give grounds to anticipate that an excess in the near-surface chlorophyll *a* concentration exhibits as minimal $R_{rs}(443)$ relative to $R_{rs}(412)$ and $R_{rs}(469)$ reflectances (reflectance deficit due to chlorophyll *a* absorption) while inequalities $R_{rs}(488) < R_{rs}(531)$ and $R_{rs}(488) < R_{rs}(469)$ indicate high content of accessory pigments (reflectance deficit due to accessory pigments). If quantified, these relationships appear promising for indication of algal blooms based on multispectral OCSs data in waters whose waters exhibit descending spectral slope at $\lambda < 500$ nm.

The differences $D1 = R_{rs}(443) - R_{rs}(412)$ and $D2 = R_{rs}(488) - R_{rs}(469)$ are the simplest quantitative indexes of variability of algal pigments directly calculable from measured multispectral reflectances. To our knowledge, the natural substances of non-algal origin, whose absorption bands resemble the algal pigments in spectral characteristics, are missing from marine environment. At the same time, there are other sources of reflectance deficit in the shortwave spectral range.

The sea surface spectral reflectance is predictable since the second half of the last century (Jerlov, 1976; Mobley, 1994; Morel, 1988). It is universally accepted that the sea surface reflectance dependence on wavelength of solar radiation relies on the ratio $R_{rs}(\lambda) \approx b_b(\lambda)/a(\lambda)$, where $b_b(\lambda)$ is the coefficient of total backscattering of light by suspended particles and water and $a(\lambda)$ is the sum of absorption coefficients of water and admixtures. The latter are the only components that are able to cause the reflectance deficit by definition. Absorbance of water proper is irrelevant to our aims because it is negligible at $\lambda < 500$ nm and universally constant as compared to the absorbance of admixtures.

The colored dissolved organic matter (CDOM), or "Gelbstoff", had been discovered and understood by Kalle (1963) as a substance, omnipresent in natural waters. The ubiquity of the CDOM means that it belongs to the refractory DOM at least partly. Dafner and Wangersky (2002) report that the residence time of dissolved organic carbon (DOC) makes up roughly 1300 years for the refractory DOC components in the surface layer of oligotrophic gyre. The extra CDOM is observable during blooms due to lifetime excretions and degradation of algae. For example, a two-fold increase of CDOM florescence intensity has been recorded in surface waters upon the local bloom authenticated by biological observations in March 1974 off Peru (Karabashev, 2008). It is known (Jerlov, 1976) that absorption of the CDOM exponentially grows with diminishing wavelength:

$$a_{CDOM}(\lambda) = a_{CDOM}(\lambda_0)e^{-S(\lambda-\lambda_0)}. \quad (1)$$

The slope S varies as 0.0165 ± 0.0035 in diverse waters depending on origin and residence time of the CDOM (Schwarz et al., 2002). The CDOM is difficult to trace in the clear ocean waters. Respectively, their spectral reflectance is inversely dependent on the wavelength from 400 to 700 nm. Measurable concentrations of CDOM in water, typical of oceanic periphery and inland seas, attenuate the shortwave reflectance to the extent that the reflectance spectrum takes the form of a unimodal curve having a positively sloping shortwave branch. Hence, the CDOM background widely varies in residence time and magnitude.

The atmospheric correction is a source of weakly selective bias in satellites R_{rs} estimates. Comparison of $R_{rs}(\lambda)$ from orbiting OSC and concurrent reflectance spectrum from a hyperspectral floating radiometer demonstrates that the difference of such spectra gradually increases towards the short- and longwave limits of the visible range (Burenkov et al., 2001). Dense accumulations of colored suspended mineral particles, the Aeolian fine sands from deserts alike, are able to affect the shape of the $R_{rs}(\lambda)$. However, the spectra of mass-specific absorption and scattering coefficients of mineral particles of different composition and dimensions exhibit no traces of fine structures from 400 to 700 nm (Stramski et al., 2007).

Thus, the totality of conceivable admixtures in natural seawater, excepting living algal cells, is a bearer of background absorption that adds up with the absorption of algal pigments. By virtue of higher spectral selectivity of pigments, subtraction of reflectances from spectrally close channels of an OSC reduces at least partly the contribution of non-algal background into the difference of reflectances involved. The same is true concerning partial reduction of the affect of atmospheric correction errors by subtraction. For this reasons, the indexes may be helpful as a new means for digesting already acquired multispectral information and as a simple tool for operative assimilation of data supplied by orbiting color scanners.

Our goals in this paper are two-fold. First, to propose the indices of algal pigments in seawater based on manifestations of pigments' shortwave absorption in data of satellite multispectral color scanners. Second, to give proofs of diagnostic potential of these indices as the first and necessary step prior to the development of an algorithm to retrieve some bio-optical parameters of algal blooms in seas and oceans.

We aspire to improve informativeness of currently functioning multispectral sensors and to make available the new information from global data sets collected with the help of these sensors during last decades. That is why we avoid considering the opportunities of hyperspectral remote sensing. It offers many advantages over the multispectral approach but for now is inferior to multispectral sensing in spatial coverage and revisit time. The latter are of primary importance for monitoring the algal blooms.

2. Material and methods

The algal blooms are unpredictable in time and space and difficult to explore in Baltic-size or larger water basins. Another difficulty is in the diversity of the bloom-forming species and their adaptive behavior leading to inadequacy of conventional techniques of water sampling (Kutser, 2004). Having regard to the reconnaissance nature of our goals, we took advantage of a less demanding approach. It is based on availability of published evidence on the intensity, species composition, and timing of blooms in certain marine areas during operation of MODIS sensors. Analytical treatment of archived MODIS imagery, corresponding to published

evidence in time and location, underlies our approach. The time span of MODIS operation since 2002 to the present and better spectral resolution in the visible are the key advantages of this sensor in reference to its forerunners and contemporaries among the OCSs.

2.1. Study areas

2.1.1. The Baltic Sea

This basin belongs to one of the best-studied inland seas of moderate latitudes. Here the cyanobacterial blooms occur in summer. They were extensively studied and documented during last decades under the aegis of HELCOM (Baltic Marine Environment Protection Commission – Helsinki Commission) and by individual researchers (Kahru et al., 2007; Vazyulya et al., 2014; Wasmund et al., 2013; etc.). It was established that the blooms are due to mass development of genera *Aphanizomenon*, *Nodularia* and *Anabaena*. The Baltic materials are the best in sufficiency for our aims thanks to availability of published information on species composition, time, extent, localization, and intensity of blooms during operation of MODIS sensors.

2.1.2. The Black Sea

Early summer blooms of the coccolithophore *Emiliania huxleyi* occur in the Black Sea (Burenkov et al., 2005; Cokacar et al., 2001; Karabashev et al., 2006b; Yasakova and Stanichnyi, 2012). They are beyond the scope of the present study because reflectance spectra of *E. huxleyi* blooms exhibit no traces of shortwave reflectance deficit (Karabashev and Evdoshenko, 2015). The first bloom of *N. spumigena* in the Black Sea has been recently observed in its NW shelf zone. This event has been described at length in Alexandrov et al. (2012) and is discussed in what follows.

2.1.3. The Caspian Sea

The blooms of *N. spumigena* happen from time to time in the South Caspian Sea. One of the most intensive blooms took place in August–September 2005. This is a valuable case of a single species bloom against a background of evolution of a mesoscale vortex. The satellite and conventional estimates of blooms' characteristics are given in Moradi (2014), Nasrollahzade et al. (2011) and Soloviev (2005).

2.1.4. The West Tropical Pacific (SWTP)

A comprehensive summary of aerial observations and/or bucket sampling of cyanobacteria from cruises and various transects made by the French Navy ships and the *r/v Alis* in the SWTP region from 1998 to 2010 is given in Dupouy et al. (2011). The later research (Biegala et al., 2014) corroborated the contribution of *Trichodesmium* sp. into the cyanobacterial bloom in this region. Using these sources as a guide, we examined the MODIS imagery of the SWTP in the box from 20°S, 163°E to 15°S, 169°E for December–February of 2007.

2.1.5. The Patagonian Continental Shelf (PCS)

Reflectance spectrum, recorded with floating hyperspectral radiometer in the Falkland Current frontal zone (Kopelevich et al., 2005), was initially the only incentive to consider the southwest Atlantic Ocean as an area where reflectance deficit in the blue-violet range may be traceable due to high density of phytoplankton population. The published evidence on physics and biology of the area corroborated this idea (Ferreira et al., 2013; Moreno et al., 2012; Sabatini et al., 2012; and others).

Upon some testing for occurrence of narrowband shortwave reflectance deficit and quality of satellite data, preference has been given to two images of the PCS collected with MODIS-Aqua sensor in May 2012 in the box from 44.5°S, 63°W to 41.5°S, 56°W.

2.2. Materials and data treatment

2.2.1. Initial data

Based on time and locations of blooms, known from publications or preliminary searching, we downloaded the digital images of relevant testing sites, obtained with the MODIS sensors and available at the NASA portal at http://oceancolor.gsfc.nasa.gov/. These archive materials involved the standard products of level L2 in current version for reflectances R_{rs} at wavelength λ = 412, 443, 469, 488, 531, 547, 555, 645, 667, and 678 nm and chlorophyll concentration chl_a. We preferred the MODIS Aqua data to the Terra imagery excepting few special cases.

The downloaded images were pre-processed with the SMCS browser (Sheberstov, 2015). It operates on Windows-systems, supports batch processing and visualization of data of different satellite sensors, and allows to control the data quality by means of flags and masks and to export fragments of digital images in desired coordinates and formats, convenient for further data treatment with dedicated software. When dealing with the SWTP data, we took advantage of the Giovanni online system, developed and maintained by the NASA GES DISC (Acker and Leptoukh, 2007). The system allowed us to compose the distributions of spectral reflectance R_{rs}(531) and bloom index D1 inside the box between 15°S, 162°E and 20°S, 169°E where MODIS data has been averaged in cells 4 km × 4 km over 8-day periods starting on December 3, 11, and 19, 2007.

2.2.2. Statistical analysis and visualization

We used the tools of descriptive statistics to compose and visualize the patterns of variability of relevant quantities in time and space. The K-means method of cluster analysis served to reduce the dimensionality of initial data sets in order to map the distribution of R_{rs} spectra over the PCS. The number of clusters K = 10 has been chosen as a trade off between intention to show the diversity of spectral shapes and necessity to limit the number of gradations of indexes for the sake of readability of the map. The average spectra of clusters (or centroids) served as keys for reading the map (Karabashev et al., 2006a).

We took advantage of linear regression analysis to find the dependence of index D1 upon the concentration of chlorophyll *a* when treating the data of the Caspian Sea bloom. Use has been made of the regional band-ratio algorithm for retrieving chlorophyll concentration from MODIS reflectances of the Caspian Sea (Kopelevich et al., 2013). This algorithm is based on ground truthing data obtained with the help of a floating spectroradiometer in the open Caspian Sea during summer seasons. The Caspian Sea level L2 data were averaged over a regular grid of cells 2 km × 2 km to remove irrelevant details of spatial distributions.

2.2.3. Adaptation of indices to reflectance spectra of waters of diverse transparency

In clear ocean waters, the spectral reflectance grows to the shortwave limit of the visible spectrum (see Section 1). This is the case of the SWTP region. We have to adopt the chlorophyll index D1 = $R_{rs}(443) - R_{rs}(469)$ in order to maintain the negativity of D1 as a feature of reflectance deficit due to chlorophyll *a* in waters of oceanic transparency. In such waters, $R_{rs}(443) - R_{rs}(412) < 0$ is a permanent property regardless of the deficit at 443 nm.

The PCS region is known as a meeting place of the open ocean and shelf waters. Therefore, we adopted D1 = $R_{rs}(443) - R_{rs}(469)$ as a chlorophyll *a* indication by analogy with the SWTP region. No spectra with the reflectance minimum at 488 nm have been found in both images of the PCS region. Instead, large fraction of pixels of the latter exhibited reflectance deficit at 469 nm. On these grounds, index D2 = $R_{rs}(469) - R_{rs}(488)$ has been tentatively adopted for accessory pigments in the PCS region. These adaptations should be kept in mind when comparing information from different testing sites.

3. Results

3.1. Extreme patterns of shortwave reflectance

The spectra in Fig. 1 belong to pixels having the lowest estimates of indices D1 or D2 among the pixels of an individual MODIS image. To reduce the effect of random errors, we reproduce the spectra having the lowest and second-lowest estimates of D1 and D2. The spectra are designated by abbreviation of testing site name and digital code. For instance, blt11 in panel *1* designates the spectrum from the Baltic Sea having the lowest index D1, blt12 points to the spectrum having the second-lowest D1 and blt22 means the spectrum with the second-lowest D2. Thus, Fig. 1 displays the initial spectral shapes unaffected by our data processing.

The spectra from inland seas (panels *1*–*3* in Fig. 1) are similar in wavelength of their main maxima in the green. The amplitudes of these maxima are 4–5 times as high as reflectance level of the same waters under bloom-free conditions. In the Baltic Sea, there is evident difference between shapes of spectra $R_{rs}(\lambda)$, having maximal D1 or D2. The same spectra are virtually indistinguishable in the Black and Caspian Seas.

The SWTP spectra feature the simplest shape having well-reproducible minimum at 443 nm. The same minimum is present in spectra of the PCS regions but much larger reflectance deficit is evident at 469 nm.

3.2. Variability of the indices

3.2.1. Baltic Sea bloom in July 2005

This bloom is one of the most intensive cyanobacterial Baltic blooms for last decades in spatial coverage, sea surface reflectance level, and biological characteristics (Wasmund et al., 2013). Satellite images of this bloom frequently illustrate materials dedicated to nature conservation.

The maps in Fig. 2 reproduce the pixel-by-pixel distributions of indices D1 and D2 along with $R_{rs}(555)$ from the MODIS image of the Eastern Gotland Basin of July 10, 2005, when the bloom was close to culmination. The distributions exhibit similar structures despite the fact that indices D1 and D2 are

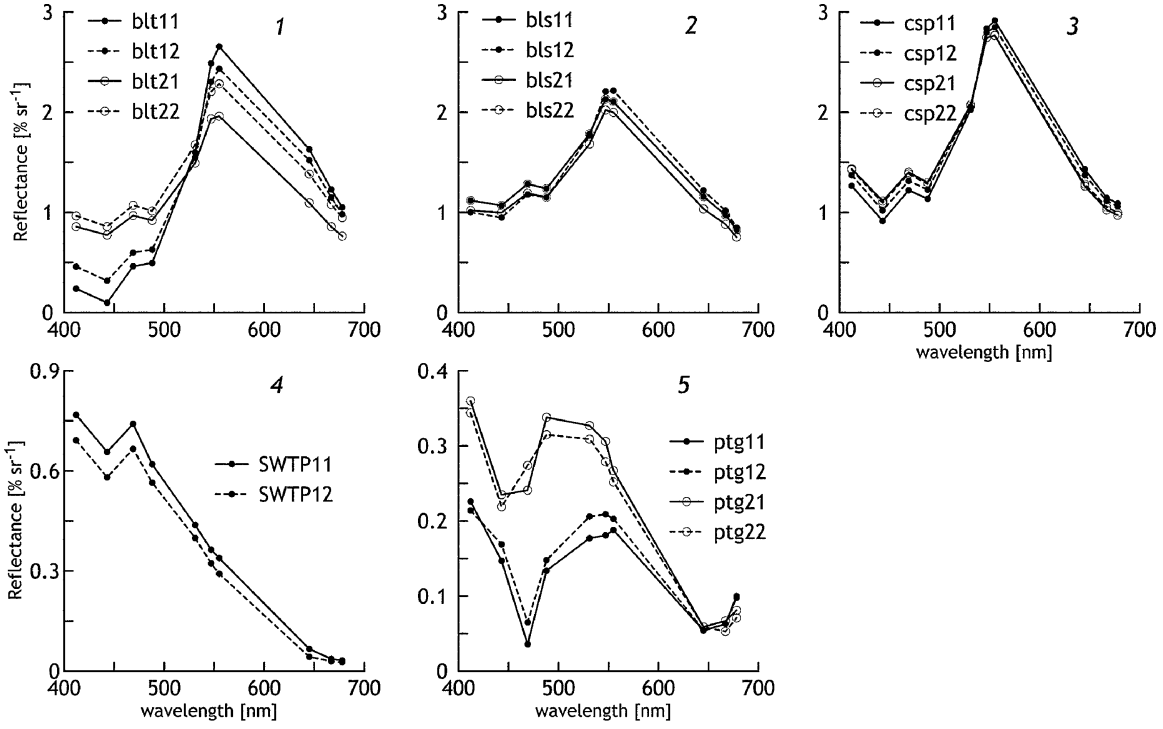

Figure 1 Reflectance spectra having the lowest (11) and the second-lowest (12) minima at λ = 443 nm and the lowest (21) and the second-lowest (22) minima at 488 nm during blooms in the following aquatic areas. Panel *1*: the Baltic Sea (blt) from 18°E, 55°N to 21°E, 58°N, MODIS Aqua, July 10, 2005; Panel 2: the Black Sea (bls) from 30.9°E, 46.0°N to 31.7°E, 46.5°N, MODIS Aqua, July 7, 2010; Panel *3*: the Caspian Sea (csp) from 49.5°E, 37.5°N to 52°E, 38.75°N, MODIS Aqua, September 1, 2005; Panel *4*: the SWTP (SWTP) from 168°E, 20°S to 169°E, 19°S, MODIS Terra, December 10, 2007; Panel 5: the PCS waters (ptg) from 63°W, 44.5°S to 58°W, 41.5°S, MODIS Aqua, May 18, 2012.

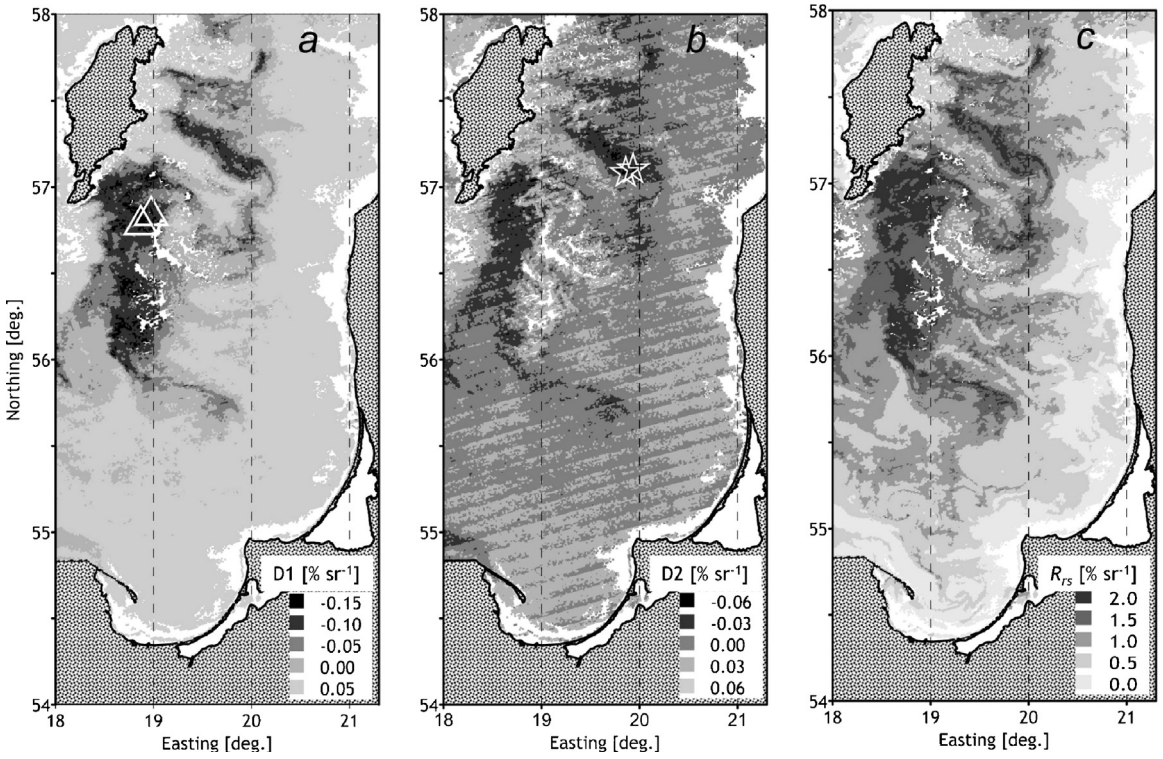

Figure 2 The distributions of indices D1 [% sr^{-1}] (*a*), D2 [% sr^{-1}] (*b*), and reflectance R_{rs}(555) [% sr^{-1}] (*c*), pixel-by-pixel calculated from the MODIS image of the East Baltic Sea of July 10, 2005. White triangles in panel *a* mark the pixels having spectra blt11 and blt12 in panel *1* of Fig. 1. Stars in panel *b* mark the pixels having spectra blt21 and blt22 in panel *1* of Fig. 1.

much lower in amplitude and lack precision as compared to the R_{rs}(555) estimates. It is notable that the pixels of the lowest and second-lowest estimates of D1 belong to the bloom maximum between 56°N and 57°N whereas analogous pixels of D2 reflectance deficit occurred within another maximum divorced from the former one.

To judge the time dependence of the spectral features of these blooms, use has been made of MODIS images of testing site in the East Gotland Basin of the Baltic Sea from 18.34°E, 55.16°N to 20.54°E, 57.87°N (see Fig. 2). The images were obtained in July 2005 for year days (YD) 185, 186, 187, 190, 191, 192, and 194. After calculating the D1 and D2 for every pixel of an image of a particular YD, we plotted the histograms of these indices along with the histograms of R_{rs}(555) as a proxy for bloom intensity (Fig. 3). The displacements of the high-end wing of the histograms for R_{rs}(555) and the

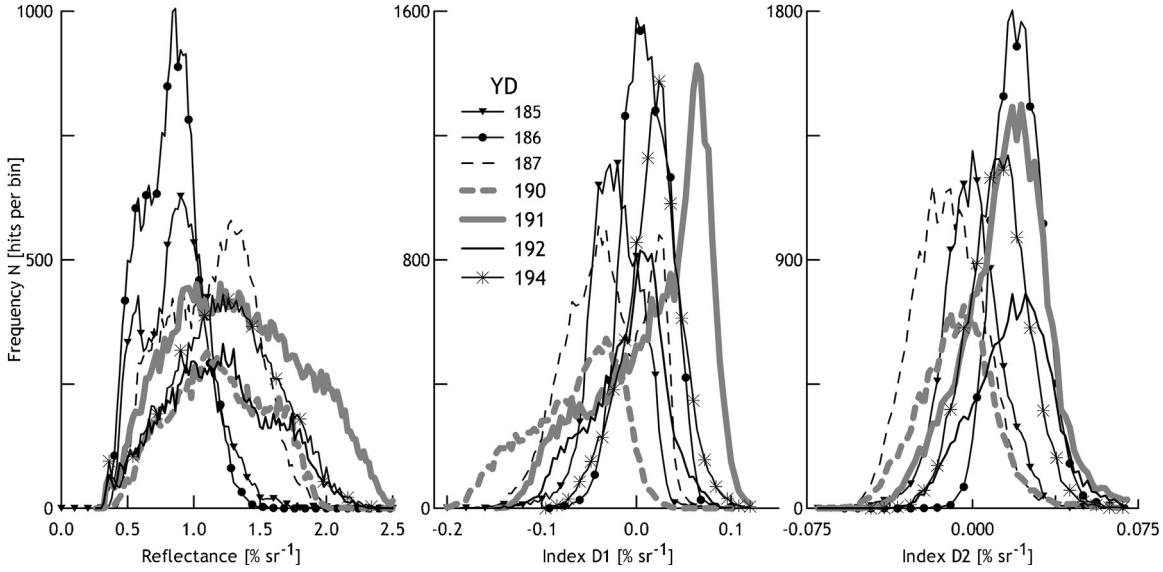

Figure 3 The histograms of reflectance R_{rs}(555) and indices D1 and D2 calculated from the MODIS images of the same testing site from 18.341°E, 55.155°N to 20.537°E, 57.867°N in the East Gotland Basin for year days (YD) 185, 186, 187, 190, 191, 192, and 194 in 2005. *N* designates the frequencies of occurrence of values of respective variables in bins of the *X*-axes.

low-end wings of the histograms for D1 and D2 during bloom period indicate extreme bloom intensity in terms of these quantities regardless of probable inconstancy of the amount of pixels of acceptable quality within the same testing site.

The $R_{rs}(555)$ histograms 185 and 186 in Fig. 3 belong to the same range of $R_{rs}(555) < 1.5\%\ sr^{-1}$, which roughly corresponds to the medium level blooming. The fraction of the highest $R_{rs}(555) > 2\%\ sr^{-1}$ was the most numerous on the YD 191, which is the day of bloom's peak in terms of the $R_{rs}(555)$ level. The lowest fraction of $D1 < -0.15$ was the most populated on YD 190 while the lowest D2 were the most abundant on YD 187 (Fig. 3). This means that the reflectance deficit at 443 and 488 nm was one or several days ahead of the highest reflectance peak at 555 nm. Notice that histograms of D1 and D2 for YDs 192 and 194 returned to their earlier ranges on YDs 185 and 186 whereas considerable fraction of $R_{rs}(555) > 1.5\%\ sr^{-1}$ survived until YD 194.

3.2.2. Caspian Sea bloom of August–September 2005

Initially, the bloom shows up as a combination of quasi-linear elements distinguished from the background by slightly higher $R_{rs}(555)$ (panel *1* in Fig. 4). In 2 weeks, a mesoscale cyclonic vortex develops in the west of the testing site, and the whole bloom takes the shape of a comet with the vortex as its head in the west and filament-like structures as its tail in the east (panel *2* in Fig. 4). This evolution took place beyond the reach of coastal influences and in a deep basin, which excludes the contribution of near-bottom resuspended sediments into water surface reflectance. Under these conditions, the variations of D1 and $R_{rs}(555)$ were inversely correlated lengthwise in the zonal profile at 38.18°N (horizontal arrow in panel *2*) which is evident from distributions of D1 and $R_{rs}(555)$ in panel *3*. Notice that the western part of testing site on YD 230 appears as a bloom-free space.

Consider now the reflectance spectra in Fig. 5, plotted from data at the center of the vortex (L = 72 km for YD 230 and 244, left panel) and at site of L = 90 km where $R_{rs}(555)$ peaks (right panel). It is evident that spectra *1–3* are more or less similar to each other in shape and magnitude while spectrum *4* exceeds them at least three-fold in amplitude. Spectrum *3* is lower in amplitude than the spectra *1* and *2*. It is worth noting that $D2 < 0$ and $D1 > 0$ under fore-bloom conditions on YD 230 (spectrum *1* in Fig. 5) while $D1 < D2 < 0$ at the time of bloom culmination (spectrum *4* in Fig. 5).

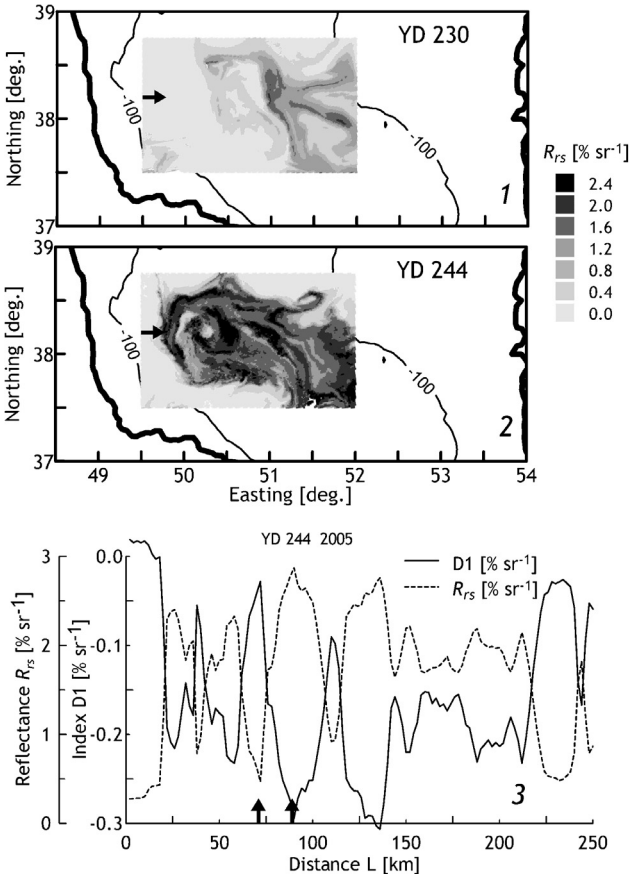

Figure 4 Distributions of reflectance $R_{rs}(555)$ and index D1 in the South Caspian Sea of August 18 (YD 230) and September 1 (YD 244), 2005. Panels *1* and *2* display the localization of the bloom relative to 100 m depth contour at initial and culmination stages of the bloom. The horizontal arrows mark the starting point of the zonal profiles of D1 and $R_{rs}(555)$ in panel *3* passing through the center of the anticyclonic vortex at 38.18°N. The left vertical arrow in panel *3* indicates the distance L = 72 km from starting point of profile to $R_{rs}(555)$ minimum at vortex center while the right arrow marks the position of $R_{rs}(555)$ maximum east of the vortex center.

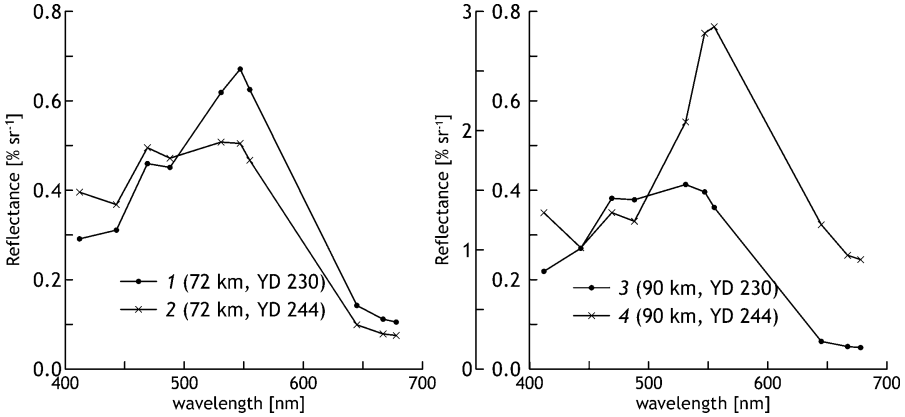

Figure 5 Left panel: reflectance spectra at site of vortex center (72 km) prior to (*1*, YD 230) and during (*2*, YD 244) the bloom. Right panel: the same but at site of $R_{rs}(555)$ maximum east of vortex center (see Fig. 4). Spectrum *4* belongs to reflectance range 0–3% sr^{-1}.

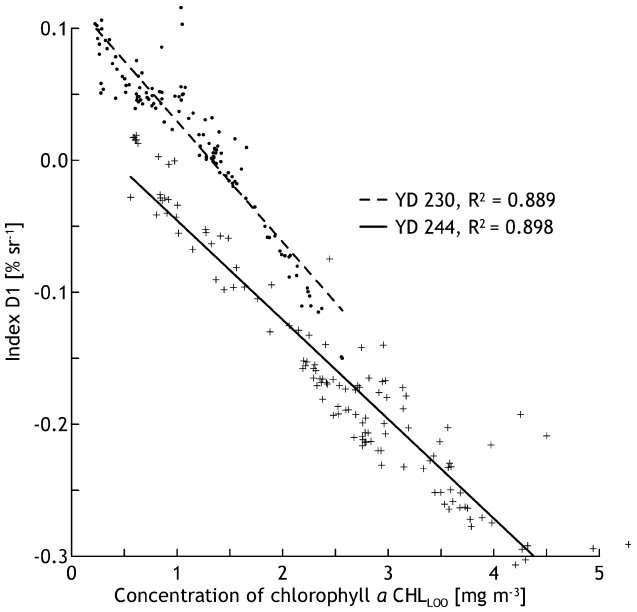

Figure 6 Dependences of index D1 on concentration of chlorophyll *a* CHL_{LOO} (regressions D1(CHL_{LOO})), found from MODIS reflectances at *X*-coordinates of the profile in panel *3*, Fig. 4. Regional algorithm (2) has been used to estimate CHL_{LOO}. The dashed regression line and dots correspond to data of YD 230, 2005; the solid regression line and crosses are for YD 244, 2005. R^2 represent the estimates of coefficients of determination. For details, see text.

Evolution of the bloom against a background of mesoscale vortex resulted in strong intermittence of content of optically significant admixtures in the zonal profile across the vortex' center. This and localization of the profile far away of coastal zone and shallows provide favorable conditions for testing the concentration dependence of indices. The standard algorithms for calculating the chlorophyll *a* content from satellite reflectance are famed for poor performance in waters of inland seas (Blondeau-Patissier et al., 2014). Upon the abortive attempt to use the MODIS standard product chl_a for finding dependence of D1 on chlorophyll *a*, we took advantage of the regional algorithm (Kopelevich et al., 2013) for estimating the content of chlorophyll *a* from MODIS $R_{rs}(488)$ and $R_{rs}(555)$ at *X*-coordinates of the profile in Fig. 4, panel *3*. The formula is of the form

$$CHL_{LOO} = 0.573\left(\frac{R_{rs}(488)}{R_{rs}(555)}\right)^{-2.39}. \quad (2)$$

The subscript LOO stands for the Laboratory of Ocean Optics. In Fig. 6, regressions D1(CHL_{LOO}) exemplify the results for YD 230 and YD 244, 2005. In the same profile, the standard estimates of MODIS chlorophyll chlor_a are characterized by 14.03 mg m^{-3} for the mean and from 2.1 to 37.6 mg m^{-3} for the range. Finally, we calculated the regressions D2(CHL_{LOO}) and found larger data scatter and reduces R^2 to 0.563 for YD 230 and to 0.763 for YD 244 as compared to $R^2 = 0.9$ in the case of D1(CHL_{LOO}).

3.2.3. The SWTP bloom

Fig. 7 shows the reflectance spectra at different levels of index D1, calculated from distributions found with the help of the Giovanni online system in the SWTP region. These distributions indicate gradual advancement of higher reflectance to the west of the Vanuatu Archipelago but they were depreciated because of data gaps due to cloudiness. Presenting results as averaged spectra instead of 2D patterns spares space but keeps the main outcomes.

In Fig. 7, the shape of spectra, having positive D1, is typical of the clearest ocean waters. The negativity of D1 decreased with time faster during the first half of the 24-day period against a background of growth of R_{rs} at $\lambda > 500$ nm. In spite of data losses, the spectra having D1 < 0 survived until the end of this period. This means that the spectra in panel *4* of Fig. 1 are not accidental and characterize one of the

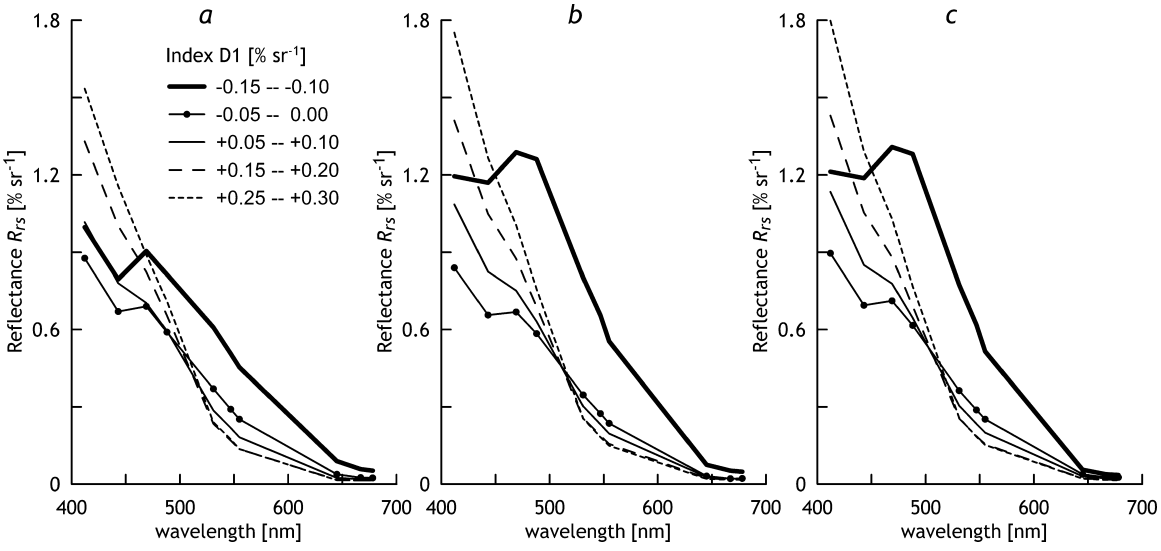

Figure 7 Average reflectance spectra $R_{rs}(\lambda)$ from gridded MODIS-Aqua data in the SWTP box between 20°S, 163°E and 15°S, 169°E for 8-day periods starting on December 3 (*a*), December 11 (*b*), and December 19 (*c*), 2007 (see Sections 2.2.1 and 2.2.3). The spectra have been calculated from MODIS data subsets whose estimates of index D1 hit the intervals $-0.15 < D1 < -0.10$, $-0.05 < D1 < 0.0$, $+0.5 < D1 < +0.10$, $+0.15 < D1 < +0.20$, and $+0.25 < D1 < +0.30$ (for details see text).

inherent features of bloom in the SWTP region in December 2007.

3.2.4. The PCS patterns

Diversity of spectral shapes is the most remarkable feature of the PCS. The cluster analysis has helped us to reduce this diversity to observable level. Fig. 8c demonstrates that the spectra ptg11 and ptg12 (Fig. 1) belong to the same domain of cluster 6 and spectra ptg21 and ptg22 belong to the same domain of cluster 7. In our view, such consistency of geography and spectral shapes involved provides evidence of objective character of clustering outcomes because the ptg-spectra and centroids of spectral clusters have been found using different criteria and procedures.

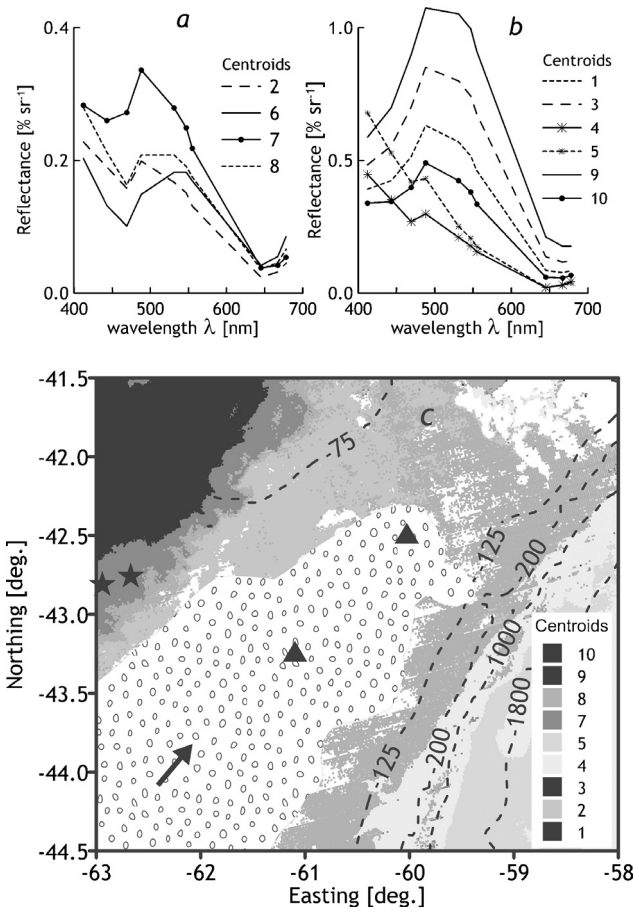

Figure 8 Cluster analysis of reflectance spectra $R_{rs}(\lambda)$ as applied to the MODIS-A image of the PCS from 44.5°S, 63°W to 41.5°S, 58°W, collected on May 18, 2012. Panels *a* and *b* serve as a key for reading the map in panel *c*. Panel *a* shows mean spectra (centroids) of four clusters having minima at 443 nm (centroid 7) and at 469 nm (centroids 2, 6, 8). Panel *b* displays the centroids of the off-shelf clusters 4 and 5 and the inner-shelf clusters 1, 3, 9, 10 (all in black in panel *c*) having centroids peaks at 488 nm. In panel *c*, the numbers of gray shades correspond to numbering of centroids in panels *a* and *b*. The gravel pattern in the map indicates the domain of cluster 6 having the lowest $R_{rs}(469)$. The arrow indicates the direction of general water transport in the area. The triangles and stars mark the sites of pixels having spectra ptg11, ptg12 and ptg21, ptg22 in panel 5, Fig. 1, respectively. The depth contours (dashed, [m]) are based on the data processed with the GEBCO Grid Demonstrator v. 2.13.

The K-means clustering of reflectance spectra on the pixel-by-pixel bases revealed three groups of spectral types. They are given in panels *a* and *b* of Fig. 8. The outer PCS between 75 and 125 m isobaths was dominated by pixels of cluster 6 (gravel pattern in the map, Fig. 8). Among the spectra in Fig. 8*a*, the cluster 6 is distinguished by the lowest $R_{rs}(469)$. The spectra of clusters 2 and 8 have minima at 469 nm too but their amplitude is lower as compared to that of the cluster 6. Clusters 4 and 5 belong to pixels in the continental slope area. The similarly shaped centroids of clusters 1, 3, 9, 10 belong to the inner part of the PCS west of the 75 m isobath.

The centroid of cluster 7 in panel *a* is the only spectrum having minimum at 443 nm. The domain of cluster 7 interfaces the outer and inner shelf areas. After subdividing the set of spectra of cluster 7 into 10 sub-clusters, we have found that the pixels, having spectral minima at 443 nm, outnumber those having minima at 469 nm among the pixels of interfacing domain. We have found no indications of pixels having spectral minimum at 488 nm over the whole PCS area shown in panel *c*, Fig. 8.

It should be mentioned that spectra of the MODIS image of May 2, 2012 of the PCS area has been clustered using the same procedure. The set of ten centroids was certainly similar to that of May 18 excepting underpopulated clusters whose spectra recall the centroids 6, 2, 8 in Fig. 8, panel *a*. The domain of spectrum *6* extended, at most, to 61°W. To all appearance, the image of May 2 reproduced the same bloom at earlier stage of evolution. We omitted respective results to spare space.

4. Discussion

4.1. Variety of reflectance deficit in the blue-violet range

The CDOM presence in water is easy to recognize in the above satellite reflectance spectra in panel *b*, Fig. 8. The spectra 1, 3, 9, 10 correspond to waters, rich in suspended matter and CDOM. They belong to inner shelf (black shade in panel *c*) and exhibit reflectance decline following the growth of CDOM absorption from green to violet.

The spectra of this kind are typical of waters of low and moderate transparency (inland seas, shelf areas, shallows, climatic upwelling areas, etc.). Here reflectance deficit of algal origin adds up with the deficit due to CDOM. When calculating the indices D1 and D2 as differences of R_{rs} of neighbor channels of MODIS sensor, we substantially reduce the affect of inconstancy of the CDOM background but the latter survives in the case of using the ratios of R_{rs} of the same channels instead of differences.

Another sort of reflectance deficit arises due to atmospheric correction errors. They are coincidentally frequent in the areas of higher CDOM content. Such errors are easy to discriminate when they are large to an extent that negative spectral reflectances appear among the pixels' attributes. As a rule, this is typical of reflectances from channels at $\lambda < 500$ nm and $\lambda > 600$ nm, but the absence of negative estimates of R_{rs} does not mean that pixels' attributes are

free of such errors. Again, quantifying the algal reflectance deficit as difference of R_{rs} of neighbor channels substantially reduces the damage caused by errors of atmospheric correction. These circumstances are favorable for diagnostic applications of indices D1 and D2.

4.2. Diagnostic potential of indices D1 and D2

The use of index D1 as a measure of content of chlorophyll *a* in water is justifiable by the fact that the absorption band of this pigment peaks roughly at 443 nm (Wozniak and Dera, 2007). From the very beginning of satellite remote sensing of seas and oceans in the visible range, any orbital multispectral sensor is equipped with a channel, centered at 443 nm. As for the index D2, its diagnostic capability is less definite. Among previously named carotenoids and phycobilins, there are pigments whose absorption bands peak near 488 nm. The same is true concerning such accessory pigment as chlorophyll *c*. It is worth to notice that spectral shapes, having well defined minima at 443 and 488 nm, took place in the Baltic, Black, and Caspian Seas. From the previously mentioned, it may be seen that *N. spumigena* was always present among the species responsible for blooming event in all three seas. The same species was the only contributor into the blooms in the Black and Caspian Seas.

The SWTP spectra, deprived of D2 minima, resulted from blooming of *Trichodesmium* sp. These are the grounds to anticipate that changes in negative estimates of D2 are mainly due to the reflectance deficit caused by accessory pigments of *N. spumigena*. If this is the case, one might expect certain disagreements of D1 and D2 behavior in space and time due to differences of functions of main and accessory pigments.

In Fig. 2, the pairs of pixels, having the lowest and second-lowest D1 and D2, are tens of kilometers apart from each other. Besides, they belong to structural elements that differ in extent and orientation. According to histograms in Fig. 3, describing the time dependence of cyanobacterial bloom of 2005 in the Baltic Sea, the estimates of D2 has reached their lowest level ahead of D1 and the lowest D1 estimates occurred ahead of $R_{rs}(555)$ culmination. Qualitatively, this sequence appears natural because the estimates of $R_{rs}(555)$ depend on total content of backscattering particles, including remains of algal cells, while D1 and D2 relate to living organisms.

The case of the Caspian Sea (Fig. 4) allows to distinguish the following stages of bloom event: prior-to-bloom conditions (western part of the area in panel *1*), a "young" bloom (eastern part of the area in panel *1*), the bloom in the prime of life (western part of the area in panel 2), and the bloom of advanced age (east of the same area). This sequence corresponds to gradual development of bloom in the east according to several images, collected prior and upon YD 230, and to later evolution of the bloom against a background of the westwards bound mesoscale vortex. It is worth noting that $D2 < 0$ and $D1 > 0$ under fore-bloom conditions on YD 230 (spectrum *1* in Fig. 5) while $D1 < D2 < 0$ at the time of bloom culmination (spectrum *4* in Fig. 5). This is another independent argument in support of the above evidence of earlier occurrence of $D2 < 0$ relative to timing of $D1 < 0$ at the initial stage of bloom development.

Under the fore-bloom conditions (YD 230), the estimates of D1 remained weakly positive but D2 fluctuated at zero level. When passing to the next stage, the D1 estimates jumped from 0.1 to $-0.15\%\ sr^{-1}$ and gradually declined to zero. The estimates of D2 exhibited the same changes but within narrower limits.

The panel *3* in Fig. 4 demonstrates strong intermittence of estimates of D1 lengthwise in the zonal profile across the vortex center (YD 244). Respective estimates of D2 fluctuated from 0 to −0.1 levels. The similarity of the Caspian and Baltic blooms of 2005 is in the fact that negative D2 appeared slightly ahead of negative D1. We anticipate that this peculiarity is inherent to blooms of *N. spumigena* regardless of specific features of environment and may be used for early warning of highly harmful *N. spumigena*.

The outcomes of regression analysis of the Caspian Sea bloom substantiate the hopes of diagnostic capabilities of index D1. Regardless of maturity of the bloom, regression lines for YDs 230 and 244 are indistinguishable in their linearity and estimates of R^2 (Fig. 6). The latter means that chlorophyll concentration was virtually the only contributor into the variations of D1 estimates along the zonal profile across the bloom. However, the regression lines go closely in parallel but they do not coincide. This may be due to the specific features of algorithms for retrieving the chlorophyll concentration from the satellite reflectances. The Caspian bloom significantly enhanced the shortwave reflectance deficit due to CDOM and shifted the wavelength of reflectance maximum to 555 nm (compare spectra 2 and 4 in Fig. 5). These affects may be due to surface scums which are characteristic of blooms of *N. spumigena* and were detected at mature stages of the bloom in the south Caspian Sea in 2005 (Moradi, 2014).

Relationship of regressions $D1(CHL_{LOO})$ and $D2(CHL_{LOO})$ (see Section 3.2.2) fit well to the assumed partial co-variance of main and accessory pigments at the time of bloom development. Index D1 and CHL_{LOO} closely co-varied during early and mature stages of the bloom, as it should be when comparison characteristics depend on the same carrier (algal chlorophyll in our case). The lowest correlation links index D2 and CHL_{LOO} in the beginning of bloom and correlation of intermediate strength describes their coupling at later stage of blooming. This sequence agrees with the above conclusion concerning leading behavior of D2 relative to D1 during initial stage of a bloom.

4.3. The special case of the Patagonian Continental Shelf

In the inland seas, the CDOM reflectance deficit exceeded the algal one (the D1 and D2 minima are superimposed on the descending slope of $R_{rs}(\lambda)$) while CDOM deficit was negligible in the SWTP and D1 minimum interrupted monotonous growth of reflectance with diminishing wavelengths. In the PCS proper (cluster 6 in panel *c*, Fig. 8), the algal and CDOM reflectance deficits were more or less comparable in amplitude.

Three features are worth to noting. First, cluster 6 is the most populated among clusters whose centroids are given in panel *a*, Fig. 8. Second, this centroids are the only that exhibit R_{rs} maximum at $\lambda > 650$ nm, usually attributable to fluorescence of chlorophyll *a*. Third, centroid 6 exhibits the highest magnitude of reflectance minimum at 469 nm. The same minimum is traceable in centroids of clusters 4 and 5,

whose general view is similar to general view of R_{rs} spectra in the SWTP region. The clusters 4 and 5 are common in the zone of continental slope tens of miles east off the outer shelf. To all appearance, absorption peak at 469 nm was a characteristic feature of the PCS bloom in May 2012, and traced the lateral water exchange between the shelf proper and the zone of continental slope.

The broad shortwave R_{rs} minimum, recorded with the help of a hyperspectral ship-borne instrument in the Falkland-Brazilian current system (Kopelevich et al., 2005), recalls the centroid 6 in Fig. 8, panel *a*. Spectrum *6* belongs to four spectral types characteristic of water of the outer shelf area. In total, they substantially differ from spectral shapes of inland seas and SWTP region.

The spectral properties of centroids in panel *a* of Fig. 8 may be regarded as a result of partial superposition of absorption bands of chlorophyll *a* and accessory pigments whose absorption band peaks closer to 469 nm than to 488 nm. Such pigments can be inferred from Wozniak and Dera (2007). An alternative interpretation follows from findings of Welschmeyer (1994). Based on recent acknowledgment of the presence of chlorophyll *b* in marine phytoplankton, the author demonstrates that the shortwave absorption bands of chlorophylls *a*, *c*2, and *b*, extracted from algal cultures, peak from 430 to 460 nm and partially superimpose each other. When recorded with a low-resolution instrument in living algal cells, this triplet may appear as a single broad band, red-shifted by 10–30 nm relative to absorption maximum of chlorophyll *a*.

A question arises: whether we are dealing with a single species as a carrier of the whole set of pigments involved or a number of species as carriers of individual pigments from the similar set. In our view, the presence of spectral types 4 and 5, found far beyond the outer shelf and marked by the same reflectance deficit, as spectrum *6* (Fig. 8), provides evidence in favor of the first choice. Otherwise, we have to admit that different algal species were equally successful in surviving the lateral water exchange between the regions of the outer shelf and continental slope.

4.4. Limitations and difficulties

The abovementioned failure to find the reflectance deficit due to chlorophyll in R_{rs} spectra during coccolithophore summer bloom in the Black Sea arises out of the fact that the backscattering of light by the calcite shells of these algae is disproportionally strong relative to content of pigments in their cells. This is a fundamental distinction of the coccolithophores. Therefore, reflectance deficit approach is universally inapplicable to the blooms of the coccolithophores. At the same time, the satellite monitoring of blooms of other species against a background of high content of coccolithophores and/or coccoliths may be successful because the background components of reflectances are reducible when estimating D1 and D2 by subtraction of spectrally close reflectances.

We failed to find manifestations of shortwave reflectance deficit in certain regions of a fortiori highest content of chlorophyll, CDOM, and suspended particles (Curonian Lagoon of the Baltic Sea in summer, the inner PCS areas (spectra 1, 3, 9, 10 in panel *b*, Fig. 8) and the like). At the same time, there is an example of well-marked reflectance deficit in the blue-violet range according to MODIS data obtained quasi-concurrently with the recording of smooth R_{rs} spectrum by means of a floating hyperspectral spectrometer (Fig. 13, panel d, sta 17F in the east of the Gulf of Finland (Vazyulya et al., 2014)). Based on the shape of longwave hyperspectral reflectance, the authors assume the contribution of cyanobacterial bloom into the spectral shapes of Baltic waters during their observations. The Baltic cyanobacteria tend to produce the surface scums and to scatter over subsurface thickness depending on the environmental conditions and time of day. This and other adaptive mechanisms of the cyanobacteria create enormous difficulties in obtaining adequate information concerning their abundance and distribution (Kutser, 2004). It is permissible to assume that surface accumulation of cyanobacteria took place at sta 17F and the floating spectrometer, being partially submerged, underestimated the content of their pigments in the surface film while the MODIS radiometer sensed both the film and the underlying layer.

5. Conclusion

The main outcome of our study is an initiation of a new approach to monitoring the algal blooms in seas and oceans by means of multispectral color scanners. We quantified manifestations of shortwave reflectance deficit, caused by absorption of solar radiation by algal photosynthetic pigments. Difference of reflectances from a pair of neighbor spectral channels, one of which is tuned to absorption band of a specific pigment, served as a measure of the deficit. The threshold of bloom detection in terms of concentration of chlorophyll *a* is close to 0.4–0.5 mg m^{-3} and corresponds to slightly positive estimates of index D1 in the case of a cyanobacterial bloom (Fig. 4).

The difference-based index is advantageous over indications based on reflectance ratios because subtraction of spectrally close reflectances reduces the bias due to broadband reflectance deficit caused by the CDOM absorption and atmospheric correction errors. The disadvantage of the same index is in higher random errors inherent to subtraction results. To our knowledge, the algal pigments are the only natural substances in aquatic environment whose absorption bands have the half-width making up only a fraction of the blue-violet range. If this is the case, the manifestations of narrow-band reflectance deficit are attributable exclusively to the algal pigments.

The indices presented here may already be applied to current satellite monitoring of algal blooms and to treatment of archived data of orbital multispectral sensors. In three of four non-PCS cases, we were dealing with the blooms contributed by *N. spumigena*. The latter was the major contributor into the Caspian and Black Seas blooms. This species attracts attention as one of the most frequent and harmful cyanobacteria. The prospect of using the D2 estimates as a forerunner of *N. spumigena* blooms follows from the enhancement of D2 ahead of D1 during blooms in the Baltic and Caspian Seas. Our visual inspection of R_{rs} spectra in early summer MODIS images of different Baltic Sea regions revealed frequent occurrence of close-to-zero reflectance deficit at λ = 488 nm during years of moderate and strong blooms.

More works will have to be done to recognize the full worth of the diagnostic potential of the reflectance deficit due to algal pigments. Highly variable spectral patterns of the PCS region give notice of broader range of problems that may become accessible if narrow-band manifestations of reflectance deficit will be quantified by more precise and adequate models than the simplistic difference of two reflectances. In any case, a definitory formula has to involve the subtraction of measured or simulated background reflectance from level L2 data in order to retrieve the content of pigments from shortwave manifestations of algal absorption in reflectance field. This procedure may be regarded as a band-difference retrieval algorithm by analogy with the current band-ratio algorithms. Given the above advantages and limitations of the proposed indices, the former algorithm may be useful supplement to the latter ones.

Acknowledgement

This research was supported by grant no. 14-17-00451 from the Russian Science Foundation. The ocean color data were made available through the National Aeronautics and Space Administration (NASA) OceanColor Web (http://oceancolor.gsfc.nasa.gov/).

References

Acker, J.G., Leptoukh, G., 2007. Online analysis enhances use of NASA Earth science data. EOS Trans. AGU 88, 14–17.

Alexandrov, B.G., Terenko, L.M., Nesterova, D.A., 2012. The first case of a water bloom by *Nodularia spumigena* Mert. ex Born. et Flah. (Cyanophyta) in the Black Sea. Algologia 22 (2), 152–165.

Anderson, D.M., 2001. Phytoplankton blooms. In: Steele, J.H., Turekian, K.K., Thorpe, S.A. (Eds.), Encyclopedia of Ocean Sciences. Academic Press, London, 2179–2192.

Balzano, S., Ellis, A.V., Le Lan, C., Leterme, S.C., 2015. Seasonal changes in phytoplankton on the north-eastern shelf of Kangaroo Island (South Australia) in 2012 and 2013. Oceanologia 57 (3), 251–262, http://dx.doi.org/10.1016/j.oceano.2015.04.003.

Biegala, I.C., Aucan, J., Desnues, A., Rodier, M., Dupouy, C., Raimbault, P., Douillet, P., Hunt, B., Pagano, M., Clavere-Graciette, A., Bonnefous, A., Roumagnac, M., Gasol, J., Periot, M., Schenkels, O., Sharma, P., Harlay, J., Eldin, G., Cravatte, S., Marin, F., Varillon, D., Bonnet, S., Roubaud, F., Jamet, L., Gérard, P., Goyaud, A., Legrand, H., Gouriou, Y., Ganachaud, A., 2014. The South Pacific Ocean Time Series (SPOT) station: a first focus on diazotrophs community. In: 140312-Poster ASLO 2014 SPOT.

Blondeau-Patissier, D., Gower, J.F.R., Dekker, A.G., Phinn, S.R., Brando, V.E., 2014. A review of ocean color remote sensing methods and statistical techniques for the detection, mapping and analysis of phytoplankton blooms in coastal and open oceans. Prog. Oceanogr. 123, 123–144.

Burenkov, V.I., Kopelevich, O.V., Pautova, L.V., 2005. Possible causes of the increased content of suspended particles in the northeastern part of the Black Sea in June. Oceanology 45 (Suppl. 1), 39–50.

Burenkov, V.I., Vedernikov, V.I., Ershova, S.E., Kopelevich, O.V., Sheberstov, S.V., 2001. Use of the SeaWiFS satellite scanner data on the ocean color for the estimation of the bio-optical characteristics of the Barents Sea waters. Oceanology 41 (4), 461–468.

Clarke, G.L., Ewing, G.C., Lorenzen, C.J., 1970. Spectra of backscattered light from the sea obtained from aircraft as a measure of chlorophyll concentration. Science 167 (3921), 1119–1121, http://dx.doi.org/10.1126/science.167.3921.1119.

Cokacar, T., Kubilay, N., Oguz, T., 2001. Structure of *Emiliania huxleyi* blooms in the Black Sea surface waters as detected by SeaWiFS imagery. Geophys. Res. Lett. 28 (24), 4607–4610.

Dafner, E.V., Wangersky, P.J., 2002. A brief overview of modern directions in marine DOC studies. Part II – Recent progress in marine DOC studies. J. Environ. Monit. 4, 55–69.

Dupouy, C., Benielli-Gary, D., Neveux, J., Dandonneau, Y., Westberry, T.K., 2011. An algorithm for detecting *Trichodesmium* surface blooms in the South Western Tropical Pacific. Biogeosciences 8, 3631–3647.

Ferreira, A., Stramski, D., Garcia, C.A.E., Garcia, V.M.T., Ciotti, A.M., Mendes, C.R.B., 2013. Variability in light absorption and scattering of phytoplankton in Patagonian waters: role of community size structure and pigment composition. J. Geophys. Res. Oceans 118, 698–714, http://dx.doi.org/10.1002/jgrc.20082.

Jerlov, N.G., 1976. Marine Optics. Elsevier, Amsterdam, 233 pp.

Kahru, M., Savchuk, O.P., Elmgren, R., 2007. Satellite measurements of cyanobacterial bloom frequency in the Baltic Sea: interannual and spatial variability. Mar. Ecol. Prog. Ser. 343, 15–23, http://dx.doi.org/10.3354/meps06943.

Kalle, K., 1963. Ueber das Verhalten und die Herkunft der in der Gewaessern und in die Atmosphaere immer vorhandenen himmelblauen Fluoreszenz. Dtsch. Hydrogr. Z. 16 (4), 153–166.

Karabashev, G.S., 2008. Assessing biological-physical interaction in the upper ocean from space: advantages and pitfalls. In: Mertens, L.P. (Ed.), Biological Oceanography Research Trends. Nova Science, New York, 177–192.

Karabashev, G.S., Evdoshenko, M.A., 2015. Spectral features of cyanobacterial bloom in the Baltic Sea from MODIS data. Sovremennye problemy distantsionnogo zondirovaniya. Zemli iz kosmosa 12 (3), 158–170, (in Russian).

Karabashev, G.S., Evdoshenko, M.A., Sheberstov, S.V., 2006a. Normalized radiance spectrum as a water exchange event diagnostics. Int. J. Remote Sens. 27 (9–10), 1775–1792.

Karabashev, G.S., Sheberstov, S.V., Yakubenko, V.G., 2006b. The June maximum of normalized radiance and its relation to the hydrological conditions and coccolithophorid bloom in the Black Sea. Okeanologiya 46 (3), 331–343, [Oceanology 46(3), 305–317].

Kopelevich, O.V., Burenkov, V.I., Goldin, Yu.A., Sheberstov, S.V., 2005. Bio-optical studies in the Atlantic ocean combining satellite and ship measured data. In: Proc. III Int. Conf. "Current problems in optics of natural waters" (ONW'20005), Saint-Petersburg, 193–198.

Kopelevich, O.V., Sheberstov, S.V., Sahling, I.V., Vazyulya, S.V., Burenkov, V.I., 2013. Bio-optical Characteristics of the Barents, White, Black, and Caspian Seas from Data of Satellite Ocean Color Scanners, http://optics.ocean.ru.

Kutser, T., 2004. Quantitative detection of chlorophyll in cyanobacterial blooms by satellite remote sensing. Limnol. Oceanogr. 49, 2179–2189.

Lubac, B., Loisel, H., 2007. Variability and classification of remote sensing reflectance spectra in the Eastern English Channel and Southern North Sea. Remote Sens. Environ. 110, 45–58.

McClain, C., 2001. Ocean color from satellites. In: Steele, J.H., Turekian, K.K., Thorpe, S.A. (Eds.), Encyclopedia of Ocean Sciences. Academic Press, London, 1945–1959.

Metsamaa, L., Kutser, T., Strombeck, N., 2006. Recognizing cyanobacterial blooms based on optical signature: a modelling study. Boreal Environ. Res. 11, 493–506.

Mobley, C.D., 1994. Light and Water. Radiative Transfer in Natural Waters. Academic Press, San Diego, 592 pp.

Moradi, M., 2014. Comparison of the efficacy of MODIS and MERIS data for detecting cyanobacterial blooms in the southern Caspian Sea. Mar. Pollut. Bull. 87 (1–2), 311–322, http://dx.doi.org/10.1016/j.marpolbul.2014.06.053.

Morel, A., 1988. Optical modeling of the upper ocean in relation to its biogenous matter content (case I waters). J. Geophys. Res. 93 (C9), 10749–10768.

Moreno, D.V., Pérez Marrero, J., Morales, J., Llerandi García, C., Villagarcía Úbeda, M.G., Rueda, M.J., Llinás, V., 2012. Phytoplankton functional community structure in Argentinian continental shelf determined by HPLC pigment signatures. Estuar. Coast. Shelf Sci. 100, 72–81.

Munk, W., 2002. The evolution of physical oceanography in the last hundred years. Oceanography 15 (1), 135–141.

Nasrollahzade, H.S., Makhlough, A., Pourgholam, R., Vahedi, F., Qanqermeh, A., Foong, S.Y., 2011. The study of *Nodularia spumigena* bloom event in the southern Caspian Sea. Appl. Ecol. Environ. Res. 9 (2), 141–155.

Painter, S.A., Poulton, A.J., Allen, J.T., Pidcock, R., Balch, W.M., 2010. The COPAS'08 expedition to the Patagonian Shelf: physical and environmental conditions during the 2008 coccolithophore bloom. Cont. Shelf Res. 30, 1907–1923.

Poutanen, E.-L., Nikkilä, K., 2001. Carotenoid pigments as tracers of cyanobacterial blooms in recent and post-glacial sediments of the Baltic Sea. AMBIO 30 (4), 179–183, http://dx.doi.org/10.1579/0044-7447-30.4.179.

Sabatini, M.E., Akselman, R., Reta, R., Negri, R.M., Lutz, V.A., Silva, R.I., Segura, V., Gil, M.N., Santinelli, N.H., Sastre, A.V., Daponte, M.C., Antacli, J.C., 2012. Spring plankton communities in the southern Patagonian shelf: hydrography, mesozooplankton patterns and trophic relationships. J. Mar. Syst. 94, 33–51, http://dx.doi.org/10.1016/j.jmarsys.2011.10.007.

Schwarz, J.N., Kowalczuk, P., Kaczmarek, S., Cota, G.F., Mitchell, B. G., Kahru, M., Chavez, F.P., Cunningham, A., McKee, D., Gege, P., Kishino, M., Phinney, A.D., Raine, R., 2002. Two models for absorption by coloured dissolved organic matter (CDOM). Oceanologia 44 (2), 209–241.

Sellner, K.G., Doucette, G.J., Kirkpatrick, G.J., 2003. Harmful algal blooms: causes, impacts, and detection. J. Ind. Microbiol. Biotechnol. 30 (7), 383–406, http://dx.doi.org/10.1007/s10295-003-0074-9.

Sheberstov, S.V., 2015. System for batch processing of oceanographic satellite data. Sovremennye problemy distantsionnogo zondirovaniya. Zemli iz kosmosa 12 (6), 154–161, (in Russian).

Soloviev, D., 2005. Identification of the extent and causes of cyanobacterial bloom in September–October 2005 and development of the capacity for observation and prediction of HAB in the southern Caspian Sea using remote sensing technique, http://www.caspianenvironment.org/newsite/DocCenter/2006/HABrepFinalFull_corrected_compressed_pictures.doc.

Stramski, D., Babin, M., Wozniak, S.B., 2007. Variations in the optical properties of terrigenous mineral-rich particulate matter suspended in seawater. Limnol. Oceanogr. 52 (6), 2418–2433.

Świrgoń, M., Stramska, M., 2015. Comparison of in situ and satellite ocean color determinations of particulate organic carbon concentration in the global ocean. Oceanologia 57 (1), 25–31, http://dx.doi.org/10.1016/j.oceano.2014.09.002.

Vazyulya, S.V., Khrapko, A.N., Kopelevich, O.V., Burenkov, V.I., Eremina, T.I., Isaev, A.V., 2014. Regional algorithms for the estimation of chlorophyll and suspended matter concentration in the Gulf of Finland from MODIS-Aqua satellite data. Oceanologia 56 (4), 737–756, http://dx.doi.org/10.5697/oc.56-4.737.

Wasmund, N., Busch, S., Gromisz, S., Höglander, H., Jaanus, A., Johansen, V., Jurgensone, I., Karlsson, C., Kownacka, J., Kraśniewski, W., Olenina, I., 2013. Cyanobacteria biomass. HELCOM Baltic Sea Environment Fact Sheet. Online.17-Feb-15, http://www.helcom.fi/baltic-seatrends/environment-fact-sheets/.

Welschmeyer, N.A., 1994. Fluorometric analysis of chlorophyll *a* in the presence of chlorophyll *b* and pheopigments. Limnol. Oceanogr. 39 (8), 1985–1992.

Wozniak, B., Dera, J., 2007. Light Absorption in Sea Water. Springer Science, Business Media, New York, 463 pp.

Yasakova, O.N., Stanichnyi, S.V., 2012. Anomal'noe tsvetenie *Emiliania huxleyi* (Prymnesiophyceae) v Chernom more v 2012 g. (Anomalous blooming of *Emiliania huxleyi* (Prymnesiophyceae) in the Black Sea in 2012). Mors'kii ekologichnii zhurnal 11 (4), 54 pp., (in Russian).

Oceanologia (2016) 58, 292—301

Available online at www.sciencedirect.com

ScienceDirect

journal homepage: www.journals.elsevier.com/oceanologia/

ORIGINAL RESEARCH ARTICLE

Size-selective microzooplankton grazing on the phytoplankton in the Curonian Lagoon (SE Baltic Sea)

Evelina Grinienė [a,b,*], Sigitas Šulčius [c], Harri Kuosa [d]

[a] Open Access Centre for Marine Research, Klaipėda University, Klaipėda, Lithuania
[b] Marine Science and Technology Centre, Klaipėda University, Klaipėda, Lithuania
[c] Laboratory of Algology and Microbial Ecology, Nature Research Centre, Vilnius, Lithuania
[d] Finnish Environment Institute (SYKE), Marine Research Centre, Helsinki, Finland

Received 18 August 2015; accepted 5 May 2016
Available online 19 May 2016

KEYWORDS
Ciliates;
Pico- and nanophytoplankton;
Dilution experiments;
Phytoplankton pigments;
Predator—prey interactions

Summary Dilution experiments were performed to estimate phytoplankton growth and microzooplankton grazing rates at two sites: freshwater (Nida) and brackish water (Smiltyne) in the Curonian Lagoon (SE Baltic Sea). Using the size-fractionation approach and dilution experiments, we found that the microzooplankton community was able to remove up to 78% of nanophytoplankton (2—20 μm) standing stock and 130% of the total daily primary production in the brackish waters of the lagoon, and up to 83% of standing stock and 76% of the primary production of picophytoplankton (0.2—2 μm) in the freshwater part. The observed differences were attributed to the changes in ciliate community size and trophic structure, with larger nano-filterers (30—60 μm) dominating the brackish water assemblages and pico-nano filterers (<20 μm and 20—30 μm) prevailing in the freshwater part of the lagoon.

1. Introduction

Microzooplankton (size category 20—200 μm) grazers, usually dominated by protists, are considered to be one of the most important phytoplankton mortality factors in aquatic systems. They can remove up to 60—75% (about 2/3) of daily primary production (PP), with the remaining 1/3 being chanelled directly through mesozooplankton or lost by viral lysis, settling and advection processes (Calbet, 2008; Landry and Calbet, 2004; Schmoker et al., 2013). Due to the high

* Corresponding author at: Open Access Centre for Marine Research, Klaipėda University, H. Manto Str. 84, LT-92294 Klaipėda, Lithuania. Tel.: +370 63538585.
E-mail address: evelina.griniene@apc.ku.lt (E. Grinienė).
Peer review under the responsibility of Institute of Oceanology of the Polish Academy of Sciences.

Production and hosting by Elsevier

http://dx.doi.org/10.1016/j.oceano.2016.05.002

metabolic rate and short generation time, microzooplankton may play a pivotal role in determining the overall rates of grazing, nutrient regeneration and secondary production, especially during periods when they are most abundant (Weisse, 1990).

Ciliates tend to dominate microzooplankton communities in estuaries and reach very high abundances (up to 72 800 cells L^{-1}) (Gallegos, 1989; Quinlan et al., 2009). Even though their preferred prey falls within the 5–25 μm size-class, ciliates can feed even on the smallest phytoplankton, i.e. picofraction (<2 μm) (Hansen et al., 1994). Thus ciliates may be an important link in the transfer of carbon from picophytoplankton to higher trophic levels (Quinlan et al., 2009), especially during the summer when copepod production is at its highest (Dzierzbicka-Głowacka et al., 2015). In addition, a number of nano-sized (2–20 μm) ciliates are widening the effect of microzooplankton towards smaller prey size.

Size-selective grazing by ciliates has important implications for the food-web structure and nutrient cycling, especially in coastal regions, where efficient grazing on small-sized phytoplankton, called Fast-Growing-Low-Biomass, is observed (Sun et al., 2007). Moreover, different size groups of the phytoplankton community also have specific responses to grazing by ciliates.

Using the dilution technique (Landry and Hassett, 1982), the estimated grazing impact on phytoplankton is frequently masked by the abundant large phytoplankton fraction, not suitable for grazers, which is frequently dominant in coastal eutrophic waters (Gallegos et al., 1996). Therefore, the size-fractioning is suggested in coastal and estuarine areas, where the less abundant small phytoplankton fraction can have high turnover rates and contribute significantly to the secondary production of microzooplankton (Gallegos et al., 1996).

The information available on the trophic role of ciliates as grazers in the transitory ecosystems with changing riverine discharges and salinity regimes is limited. The dilution method for microzooplankton grazing estimation has been used only in a few Baltic Sea studies (Aberle et al., 2007; Lignell et al., 2003; Moigis and Gocke, 2003; Reckermann, 1996). Setälä and Kivi (2003) used field data combined with experimentally derived species-specific clearance rate information to assess ciliate community grazing in the open Baltic Sea. Reckermann (1996) estimated that microzooplankton carbon consumption rates exceeded mesozooplankton grazing in the Gotland Sea by 10 times, and in the estuarine Pomeranian Bay by 25–30 times.

The Curonian Lagoon is one of the most heavily eutrophicated coastal areas of the Baltic Sea (Gasiūnaitė et al., 2008). This transitory ecosystem is characterised by high primary production and the domination of toxic cyanobacteria during summer/autumn (Gasiūnaitė et al., 2005; Krevš et al., 2007; Sulčius et al., 2015). In the estuarine part the overall phytoplankton biomass markedly decreases with increasing salinity (Gasiūnaitė et al., 2008). An important feature of this system is the heterogeneity of the pelagic communities induced by the non-stable salinity gradient. The microzooplankton community in the lagoon is dominated by the ciliates, while heterotrophic dinoflagellates comprise only a minor fraction (<1%) of the total dinoflagellate abundance (Olenina I., personal communication). The detailed ciliate taxonomical composition of the Curonian Lagoon was described by Mažeikaitė (1978, 2003) and revised to include the brackish water ciliate assemblage by Grinienė et al. (2011). Recent observations show significant differences in the community structure of ciliated protozoan between the brackish water and freshwater parts of the lagoon (Grinienė, 2013). In this study it was demonstrated that very small nano-ciliates (<20 μm) compose more than 60% of total freshwater ciliate assemblage, while in the brackish water community the share of nano-ciliates is only 15% of the total abundance. The larger size fraction (20–60 μm) dominates the brackish water ciliate assemblage (Grinienė, 2013).

In this study we applied dilution experiments and phytoplankton size-fractionation to experimentally evaluate the differences in microzooplankton and phytoplankton community structures, grazing and growth rates between the freshwater and brackish water parts of the lagoon. The experiments were made with two communities representing the two extremes of the habitat: a high salinity sample from an area (Smiltyne) with extreme salinity variability, and a freshwater sample from an area (Nida) with constant low salinity regime. Our hypothesis is that the grazing efficiency varies according to the grazer community structure (size and grazing mode).

2. Material and methods

2.1. Study area

The Curonian Lagoon (SE Baltic Sea) is a shallow (mean depth 3.8 m) eutrophic water basin connected to the Baltic Sea by the narrow Klaipeda strait. The southern and central parts of the lagoon contain fresh water due to discharge from the Nemunas River. The salinity in the northern part varies from 0 to 7 due to seawater intrusions, which are usually restricted to the northern part of the lagoon, rarely propagating more than 40 km (Dailidienė and Davulienė, 2008). Seawater inflows with a residence time of 1–6 days are most common (Gasiūnaitė, 2000). In terms of hydraulic regime-based zonation, the northern part of the lagoon and Nemunas River avandelta are classified as transitory, while the central part is classified as stagnant and intermediate (Ferrarin et al., 2008).

According to the intensive weekly study in 2007–2008 the seasonal dynamics in the fresh water site (Nida) ciliates follows the model of temperate eutrophic lakes with four seasonal phases: winter, early spring, late spring and summer/autumn (Grinienė, 2013). Summarising, during the winter time ciliate growth is limited by low biomass of phytoplankton. In the early spring, when small sized phytoplankton prevails, ciliate assemblage is dominated by small naked oligotrichs and prostomatids. After the late spring diatom bloom, ciliate assemblage shifts to medium sized nano-filterers (tintinnids). The functional and taxonomic diversity of ciliates increases toward the summer, which points to the exploitation of a wide size range of food. Small sized naked oligotrichs (pico-nano fraction feeders) and peritrichs (mainly pico-fraction feeders) were most abundant in summer and autumn. Despite this ciliate community structure is homogenous during whole period (June–October) forming the same summer/autumn cluster (Grinienė, 2013).

The structural differences between the seasonal clusters were significant and shown by ANOSIM global *R* statistics

Table 1 Analysis of similarity (ANOSIM) of the four seasonal assemblages in Nida site (from Grinienė, 2013).

Assemblages	*R* statistics	Significance level, *p*
Winter, early spring	0.96	<0.01
Early spring, late spring	0.91	<0.01
Late spring, summer/autumn	0.74	<0.01
Summer/autumn, winter	0.88	<0.01

approaching 1 with the highest differences were observed between spring and winter assemblages, and also between the two spring assemblages (Table 1).

In the brackish water site (Smiltyne) significant negative salinity effect on the ciliate community is observed (Grinienė, 2013). Summarising, the total abundance of ciliates correlated negatively with salinity in this site ($r = -0.42$, $N = 34$, $p < 0.05$). Two ciliate assemblages, according to salinity intervals 0–2 PSU and ≥4 PSU, could be distinguished. The global *R* statistics from ANOSIM of these assemblages demonstrated that the overall differences between them were statistically significant (global $R = 0.939$, $p < 0.01$). Structurally, these assemblages were very different in species composition, size and feeding mode.

2.2. Dilution experiment setup and sample analysis

Water samples for the experiments were collected from two sites: freshwater (Nida) on 29 August and brackish water (Smiltyne) on 10 October 2009. Water was collected from a depth of 0.5 m into two 50 L carboys and transported to the laboratory.

The particle-free water (FW) was prepared by filtering lagoon water sequentially through a plankton mesh with a pore size of 20 μm, intermediate 2-μm and 0.7-μm GF/F filters and finally a 0.2-μm Millipore filter under slight air pressure. The length of the filtration process depends on the concentration of phytoplankton and suspended solids, and it took 20 and 5 h at the Nida and Smiltyne sites, respectively. The whole lagoon water (WW) was collected the next day in the Nida and Smiltyne experiments and was gently poured through a 150-μm mesh to remove mesozooplankton. Visual observation before experiments was conducted to assure that the 150-μm-sized mesh removed mesozooplankton and that the filtration through the mesh did not have a negative effect on the vitality of ciliates, especially aloricated forms. The WW was diluted by FW to four target dilutions in ratios of 1:0 (no dilution), 3:1, 1:1 and 1:3 (dilution factor or decimal fraction of WW: 1, 0.75, 0.5 and 0.25, respectively) in 3 L transparent plastic bottles. The incubation volume was 3 L and all treatments were carried out in triplicate. All bottles were incubated *in situ* at a depth of 0.5 m for 24 h. During the experiment on 10 October 2009, altogether 6 bottles out of 12 were lost during the night-time storm.

At the start and at the end of both experiments, 500 ml from each experimental bottle were sampled for nutrient (nitrate, nitrite, ammonium, phosphate and silicate) analysis, 25–30 ml for nano- and picofractions of chlorophyll *a* and 300 ml for microzooplankton counts.

The sample for nanophytoplankton (2–20 μm) chlorophyll *a* was filtered through a 20-μm mesh and concentrated onto a 2-μm Millipore polycarbonate filter. The remaining filtrate was concentrated on a 0.2-μm Millipore polycarbonate filter for picophytoplankton (0.2–2 μm) chlorophyll *a* measurement. All filters were kept frozen at −20°C and analysed within 2 months.

Total chlorophyll *a* concentration in the initial water samples was determined fluorimetrically (FluorProbe II). Pigments of nano- and picofractions were measured by high-performance liquid chromatography (HPLC) at the Baltic Sea Research Institute, Warnemünde, Germany. The samples were analysed according to Barlow et al. (1997). Pigments were detected by absorbance at 440 nm using a Biotek (545 V) diode array detector and identified by retention time and online visible spectra (350–750 nm) obtained from scans by the diode array detector. Chlorophylls were further detected by a Jasco (FP-1520) fluorescence detector (440 and 660 nm excitation and detection wavelengths, respectively). The chromatograms are processed using the Biotek Kroma 3000 software. Pigment concentrations were calculated by the peak area.

Nutrients were analysed at the Baltic Sea Research Institute (Warnemünde, Germany) according to standard methods (Grasshoff et al., 1983).

Ciliate counts were performed in Lugol fixed samples by Utermöhl's (1958) method. Volumes of 10–25 ml were settled for at least 24 h in Utermöhl's chambers. Ciliates were counted, measured and identified with an inverted microscope at 200× magnification. The entire content of each Utermöhl chamber was surveyed, and an additional subsample was counted if the total number was <150 organisms.

Rotifers and copepod nauplii were counted using a microscope at 40× magnification in the Bogorov chamber.

Ciliate-size groups (<20 μm, 20–30 μm, 30–60 μm and >60 μm) and trophic groups (pico-filterers, nano-filterers, pico/nano-filterers, omnivorous feeding on heterotrophic flagellates, algae or ciliates, and predators feeding on other ciliates) were distinguished according to Mironova et al. (2012). *Mesodinium rubrum* (*Myrionecta rubra*) was observed in the Smiltyne site experiment but not included in the total ciliate abundance counts, because it appears to function mostly as an autotroph.

2.3. Data analysis

Dilution experiment data analysis was performed according to Landry and Hassett (1982). The apparent growth rate of prey (*AGR*) was estimated using the function (1):

$$AGR\ (\mathrm{day}^{-1}) = \frac{\ln(Chla_t/Chla_0)}{t}, \quad (1)$$

where $Chla_t$ and $Chla_0$ are the final and initial concentration of chlorophyll *a* [μg L^{-1}] and *t* is the time of incubation [day]. *AGR* was estimated for both pico- and nanosize fractions.

The rates of growth and grazing mortality were calculated by the linear regression of *AGR* versus actual dilution factor. The absolute value of the slope of the regression is the grazing rate by microzooplankton *g* [day^{-1}] and ordinal intercept (y-intercept) of the regression is the growth rate of phytoplankton in the absence of grazing *k* [day^{-1}].

Significant negative slope (one-tailed t-test, $p < 0.05$) suggests a measurable grazer effect on phytoplankton growth. In cases of statistically non-significant regression, grazing rates were not determined and the phytoplankton growth rates were obtained from averaged *AGR* among all dilution treatments (Twiss and Smith, 2012).

The standing stock of phytoplankton biomass as chlorophyll *a* [μg L^{-1}] removed daily P_i [% day^{-1}] and phytoplankton potential production grazed daily P_p [% day^{-1}] were calculated using equations (2) and (3) presented in James and Hall (1998):

$$P_i = 1 - e^{-g}, \quad (2)$$

$$P_p = \frac{(e^k - e^{k-g})}{(e^k - 1)}, \quad (3)$$

where k is the growth rate of phytoplankton and g is the grazing rate of microzooplankton estimated from the linear regression.

To determine clearance rates (y) for total ciliate community and different trophic groups, a biovolume-dependent equation (4) established for the Baltic Sea (Setälä and Kivi, 2003) was applied:

$$y = 0.1493 \times x^{0.906}, \quad (4)$$

where x is the estimated spherical diameter (ESD) of the ciliate.

3. Results

3.1. Environmental parameters and nutrient concentrations

The different environmental parameters, nutrient concentration and microzooplankton abundances are given in Table 2. At the fresh water site (Nida) salinity was 0, whereas at the brackish water site (Smiltyne) it was 6.2. The difference in water temperature between sites was 7.6°C. Due to the high initial concentrations of both inorganic nitrogen (nitrate + nitrite + ammonium) and phosphorus (phosphate) as well as silicate no nutrient limitation happened during the incubations (Table 2). The lowest end values were above 1 μmol L^{-1} and 0.5 μmol L^{-1} for inorganic nitrogen and phosphorus, respectively (Table 2).

3.2. Phytoplankton community structure

We used high-performance liquid chromatography (HPLC) estimations of phytoplankton pigment signatures to determine the community structure of phytoplankton fractions. The total chorophyll *a* concentration was 6 times higher in freshwater (30.3 μg L^{-1}) than in brackish water (4.7 μg L^{-1}) (Table 2). The relative abundance of different phytoplankton size groups within the community, represented by the chlorophyll *a* concentrations, differed between freshwater and brackish water areas. In the freshwater site the share of >20 μm, nano- (2–20 μm) and picofraction (0.2–2 μm) was 47.7%, 46.4% and 5.9% of total chlorophyll *a* concentration, respectively. The nanofraction of chlorophyll *a* dominated the brackish water site with 59.8% of total chlorophyll *a*, while the share of >20 μm fraction was 38.2% and that of picofraction only 1.9% of the total.

Table 2 Environmental parameters and microzooplankton abundance at initial whole lagoon water (WW) at two research sites.

Parameters	Freshwater site	Brackish water site
Temperature [°C]	18.6	11
Salinity	0	6.2
Dissolved oxygen [mgO_2 L^{-1}]	16.6	10.1
Nitrate [μmol L^{-1}]	0.09	7.02
Nitrite [μmol L^{-1}]	0.03	0.31
Silicate [μmol L^{-1}]	1.95	11.81
Ammonium [μmol L^{-1}]	3.37	5.15
Phosphate [μmol L^{-1}]	1.88	0.98
Total chlorophyll *a* [μg L^{-1}]	30.3	4.7
Pico-fraction chlorophyll *a* [μg L^{-1}]	1.8	0.09
Nano-fraction chlorophyll *a* [μg L^{-1}]	14.1	2.8
Microzooplankton abundance[a]:		
Ciliates [ind. L^{-1}]	30 667	9800
Copepod nauplii [ind. L^{-1}]	115	24
Rotifers [ind. L^{-1}]	75	–

[a] Not including heterotrophic dinoflagellates and silicoflagellates.

The pigment composition gives an indication of the systematic composition of phytoplankton, but it cannot be considered quantitative. At both sites the picofraction of phytoplankton was represented only by chlorophyll *a*, whereas the nanofraction of phytoplankton contained additional pigments and varied between sites (Fig. 1). Lutein (green algae), alloxanthin (cryptophytes), β-carotene (for all phytoplankton taxonomic groups) and divinyl chlorophyll *a* (cyanobacteria) were found in the nanofraction at the freshwater (Nida) site, while at the brackish water (Smiltyne) site 19′-hexanoyloxyfucoxanthin (prymnesiophytes) and zeaxanthin (cyanobacteria) were recorded. In addition to chlorophyll *a*, fucoxanthin (diatoms) was detected in the nanofraction at both sites. Phytoplankton *AGR* calculations were performed using only chlorophyll *a* (as indicator of the whole phytoplankton community) data. Other pigments were detected only in undiluted water (dilution factor 1) or weakly diluted treatment (dilution factor 0.75), and they could not be used in *AGR* calculations. However, the pigment results indicate that the autotrophic communities remained stable during the experiments.

3.3. Microzooplankton community structure

At both experimental sites microzooplankton was dominated by ciliates (99% of total abundance), while the number of metazoans was very low, composing 1% of the total microzooplankton abundance at both experimental sites (Table 2). In the brackish water site nano-filterers feeding on nanosized phytoplankton were dominated by medium-sized (30–60 μm) tintinnid *Tintinnopsis* sp., large naked oligotrich *Strombidium*

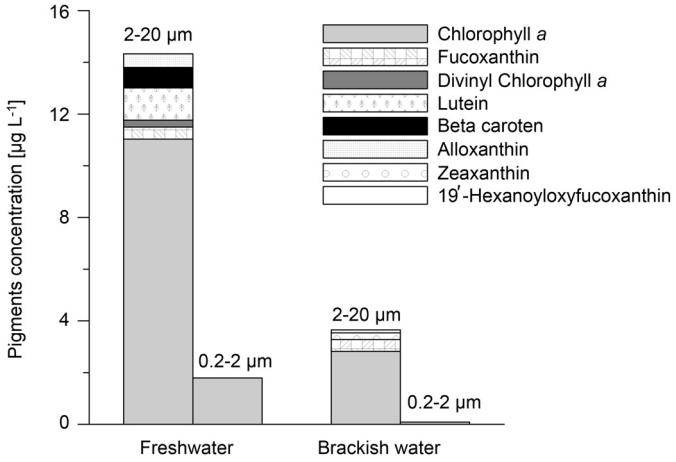

Figure 1 Pigments concentrations of pico- and nanophytoplankton at experimental sites.

conicum, *Strombilidium gyrans* and *Lohmaniella* sp. and large (>60 μm) ciliates (*Codonella relicta*, *Tintinnopsis kofoidi*): they shared 48% of the total ciliate abundance (Fig. 2). Small ciliates (<20 and 20—30 μm) were composed of *Mesodinium* cf. *acarus*, *Strobilidium* spp., *Urotricha* sp. and *Lohmaniella oviformis*.

In the freshwater site small-sized (<20 and 20—30 μm) pico/nano-filterers (*Strobilidium* spp., *Tintinnopsis* cf. *nana*, *Halteria* sp.) and pico-filterers (*Cyclidium* spp., *Vorticella* spp.) prevailed. Together these functional groups composed 77% of the total abundance (Fig. 2). Medium-sized ciliates (30—60 μm) were represented mainly by tintinnids *Tintinnidium pusillum*, *Tintinnopsis tubulosa* and *Codonella cratera*, and they composed 23% of the total ciliate abundance. Predators represented by *Didinium nasutum*, found only in the brackish water site, shared 4% of the total ciliate abundance. These could affect experiments by selectively preying on other ciliates, but at this low number the effect is considered to be minor.

3.4. Growth and grazing rates of phytoplankton

In the freshwater site the grazing rate (g = 1.8 day^{-1}) on the picofraction of the phytoplankton community exceeded the

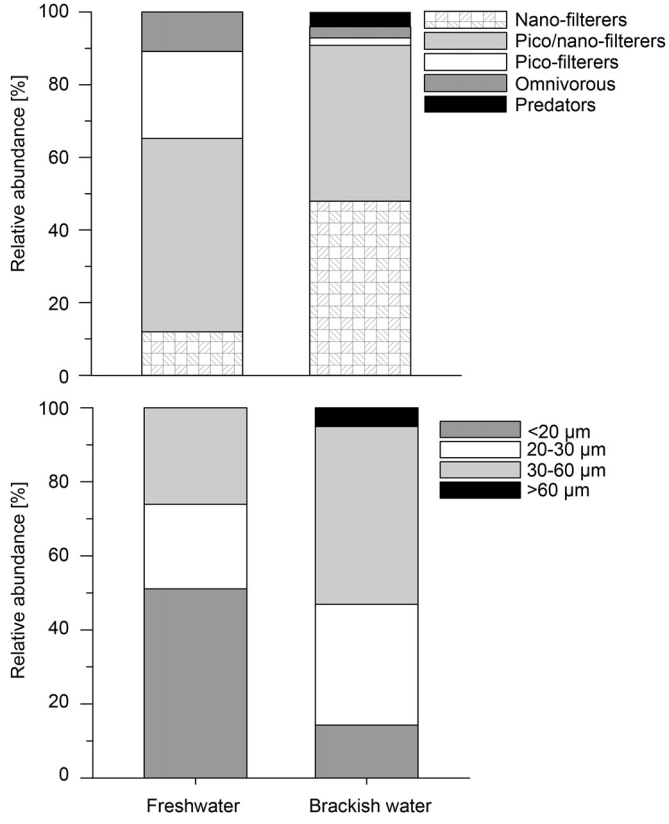

Figure 2 Relative abundance of ciliate functional and size classes at experimental sites.

Table 3 Growth rates of the phytoplankton pico- and nanofractions $k \pm$ SE [day^{-1}] and microzooplankton grazing rates $g \pm$ SE [day^{-1}] based on chlorophyll *a*. R^2, coefficient of determination; *N*, number of observations. The significance level of regression (i.e. slope, *g*, was significantly differed from zero, $p < 0.05$) is indicated by *p*-value; n.s., non significant.

Site	Fraction [μm]	*k*	*g*	R^2	*p*-value	*N*
Freshwater	0.2–2	1.33 ± 0.36	-1.83 ± 0.53	0.55	<0.01	12
	2–20	0.19 ± 0.19	-0.35 ± 0.29	0.15	n.s.	10
Brackish water	0.2–2	-1.09 ± 0.60	2.19 ± 0.90	0.59	n.s.	6
	2–20	0.92 ± 0.28	-1.52 ± 0.42	0.77	<0.05	6

prey growth rate ($k = 1.3$ day^{-1}) (Table 3), indicating high microzooplankton pressure on this size class. The microzooplankton grazing pressure on picoalgae expressed by the percentage of grazed biomass as standing stock (P_i) and percentage of grazed potential production (P_p) was 83% and 76%, respectively.

In the freshwater site the grazing rate of nanophytoplankton was not estimated, because no significant linear relationship was observed between the apparent growth rate (*AGR*) of this fraction and the dilution factor, i.e. the slope (microzooplankton grazing rate, *g*) did not differ significantly from zero (Fig. 3; Table 3). However, the growth rate of the nanofraction of phytoplankton can be calculated as the average of apparent growth rates among all dilution treatments (average ± SE) and replicates ($N = 10$), and it was near zero (-0.02 ± 0.08 day^{-1}).

The *AGR* of the picofraction increased linearly with the dilution factor at the brackish water site and regression analysis resulted in a positive slope, which did not differ statistically from zero (Fig. 3; Table 3); therefore the microzooplankton grazing rate (*g*) is not interpretable. However, the growth rate (0.28 ± 0.3 day^{-1}) was only less than ¼ of the growth rate calculated in the freshwater site, indicating significant differences in the activity of the picosize fraction.

The growth rate of nanoalgae at the brackish water site was 0.9 day^{-1} and largely exceeded the nanophytoplankton growth rate in the freshwater site. The grazing rate (1.5 day^{-1}) was higher than the growth of the prey community, however, while the actual values were lower (Table 3; Fig. 3). In the brackish water site microzooplankton grazed on 78% of the nanophytoplankton standing stock per day and 130% of potential daily production.

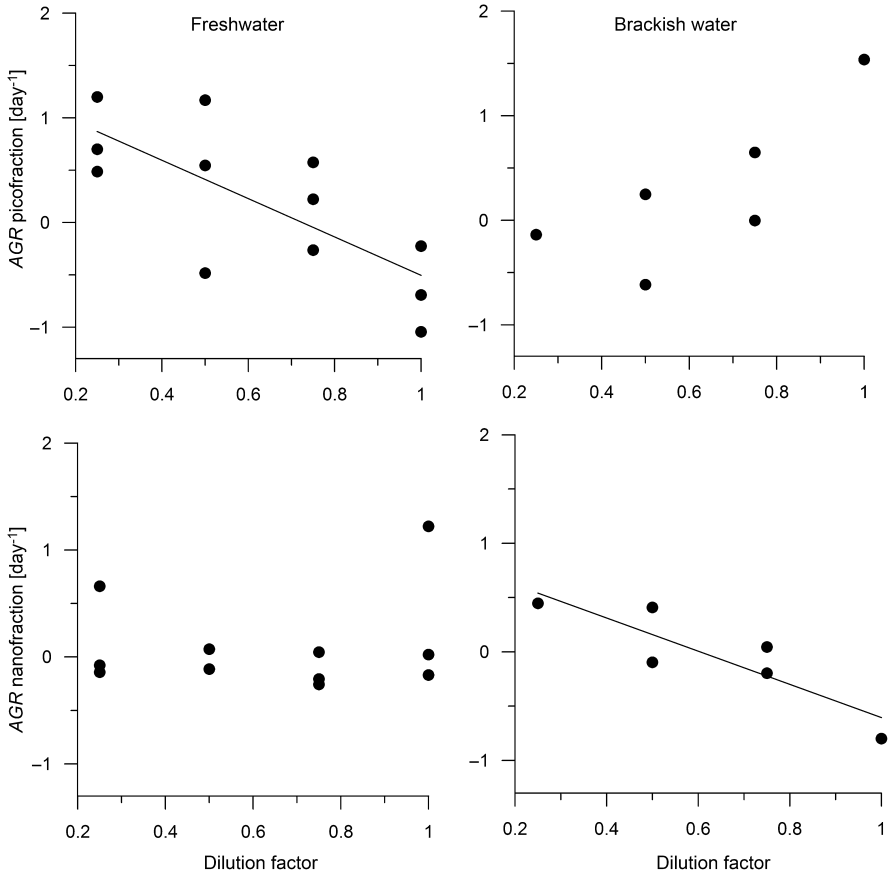

Figure 3 Relationship between dilution factor and apparent growth rate (*AGR*) of chlorophyll *a* of pico- and nanofractions at both sites. Only significant slopes are presented in the graph.

4. Discussion

Dilution experiments have been performed over the past three decades to examine the grazing impact of microzooplankton, ranging from the open sea to coastal zones and estuaries (data reviewed by Landry and Calbet, 2004 and Schmoker et al., 2013). This relatively simple and standard technique is useful for comparative microzooplankton grazing rate studies among the geographic regions, as well as revealing the role of microzooplankton in time series of ecological processes (Gallegos, 1989).

However, for the estimation of microzooplankton grazing on phytoplankton in the Baltic Sea the dilution technique has been applied to a lesser extent (Aberle et al., 2007; Lignell et al., 2003; Moigis and Gocke, 2003; Reckermann, 1996). Moigis and Gocke (2003) used the dilution method as an alternative to the ^{14}C and O_2 methods for primary production estimation, but they did not take into account the grazers' community. The grazing rate by microzooplankton varied from 0.21 to 0.41 day^{-1} in Kiel Fjord.

Reckermann (1996) found high microzooplankton grazing rates on ultraphytoplankton (<5 μm) both in the Gotland Sea and the Pomeranian Bay. In the Gotland Sea in 1994, the microzooplankton (<200 μm) grazing pressure on *Synechococcus* was higher than on eukaryotic pico- and nanophytoplankton. Generally, microzooplankton grazing on *Synechococcus* was over 100% of gross production grazed per day and pico- and nanoeukaryotic production was not completely grazed. In the Pomeranian Bay, microzooplankton grazing on ultraphytoplankton varied from considerably exceeding daily growth to rather low values (176–51%). In the study by Lignell et al. (2003) the microzooplankton grazing rate on the whole phytoplankton community varied between 0.05 and 0.30 day^{-1}. However, in both studies the total phytoplankton community rather than different size classes was measured, which may mask the effect of the size-selective microprotozoa grazing or even genus/species level as is evidenced by Aberle et al. (2007) in their mesoscosm study.

The significant estimates of ciliate grazing rates on phytoplankton pico- and nanofractions were obtained at freshwater (Nida) and brackish water (Smiltyne) sites, respectively. Grazing rates exceeded the growth rate of phytoplankton fractions ($g > k$), suggesting that phytoplankton production and biomass accumulation is controlled by microzooplankton, as it was frequently observed by other authors (Burkill et al., 1987; Landry et al., 1995; Lehrter et al., 1999; McManus and Ederington-Cantrell, 1992; Verity et al., 1993).

The grazing rate of the picofraction at the freshwater site is in the range reported in the other regions (Table 4). Ciliates consumed 76% of potential picophytoplankton production at this freshwater site. The dominance of small pico- and pico/nano-filterers in the freshwater site suggests that predation on the picophytoplankton fraction can be high, but it could be tested visually by observing autotrophic picofraction cells via epifluorescence microscopy or flow cytometry. The calculated clearance rate as the daily clearance percentages (% of the water volume cleared in 24 h) by pico/nano-filterers in this site was very similar (70%) to potential picophytoplankton production removed by ciliates calculated from the dilution experiment. This finding is in good agreement with the study by Rassoulzadegan et al. (1988) as they found that small ciliates (<30 μm) consist of 72% picoplankton and 28% nanoplankton.

In contrast, the dilution experiment provided no statistically significant estimates of grazing rate (g) for phytoplankton nanofraction at the freshwater site. The *AGR* of the nanofraction was very similar in all dilution treatments (Fig. 3), which indicates the absence of microzooplakton grazing. This is supported by the low number of nano-filterers in the initial water at the beginning of the experiment (Fig. 2). The low average value of *AGR* (-0.02 ± 0.08) indirectly points at a slowly growing nanophytoplankton community, which can be

Table 4 Published results of microzooplankton grazing in other regions. Growth rates of the phytoplankton pico- and nanofractions k [day^{-1}] and microzooplankton grazing rates g [day^{-1}], P_p, potential consumption of primary production [% day^{-1}]; N, number of dilution experiments.

Location	Salinity	Fraction [μm]	k	g	P_p	N	Reference
Curonian Lagoon	0	0.2–2	1.33	1.83	76	1	This study
	6.2	2–20	0.92	1.52	130	1	
Chesapeake Bay	20	0.2–2	2.10	1.92	97	1	Sun et al. (2007)
		2–20	0.61	0.41	73	1	
Delaware Inland Bay	15	0.2–2	2.05	0.7	58	1	
		2–20	0.81	0.77	97	1	
Delaware Bay	16	0.2–2	1.83	1.78	99	1	
		2–20	0.84	0.32	48	1	
Gulf of Alaska	–	<5	0.42	0.48 (0.02–1.07)	102 (±29)	39	Strom et al. (2007)
		5–20	0.34	0.39 (0.05–0.92)	102 (±32)		
Manukau estuary (New Zealand)	28–33	<5	0.2–1.8	0.3–1.3	30–230	12	Gallegos et al. (1996)
		5–22	0.2–1.8	0–0.8	0–98		
Upper St. Lawrence River (US)	–	0.2–2	0.2–1.8	0–1.1	–	12–38	Twiss and Smith (2012)
		2–20	0.1–1.3	0–1.2	–		

a result of viral lysis, the presence of toxic material or other unknown inhibitory metabolites that could be released during preparation of the filtered water (Stoecker et al., 2015).

The grazing rate of the nanofraction at the brackish water (Smiltyne) site exceeded grazing rates in other estuarine ecosystems by two- or threefold (Table 4). Ciliates consumed 130% of the nanophytoplankton production at the brackish water site. The calculated total ciliate community clearance rate as daily percentage was lower — 71%, but 41% was due to nano-filterers. This is not surprising as nanophytoplankton chlorophyll *a* concentration was 30 times (Table 2) higher than picophytoplankton chlorophyll *a*, and ciliate assemblage was dominated by medium-sized ciliates (Fig. 2) composed of naked oligotrichs *Strombilidium gyrans*, *Strombidium conicum* and tintinnid taxa *Tintinnopsis* sp.; all of them prefer to feed on small nano-sized algae (Appendix A, Table A1). Gallegos et al. (1996) used the dilution technique combined with size fractioning and found that the highest grazing rates of the phytoplankton fraction of 5—22 μm coincided with tintinnid abundance increase in ciliate assemblage. The tendency of higher consumption rates is usually reported in dilution experiments where nutrients are not added (Landry and Hassett, 1982). The adding of nutrients is recommended at the start of the experiment to keep the phytoplankton growth unlimited (Gallegos, 1989; Landry et al., 1995). In this study nutrients were not added, assuming high rates of N and P loading in the Curonian Lagoon during autumn, when experiments were conducted and to avoid increased mortality of delicate protists during experiments (Gifford, 1988; Landry and Hassett, 1982).

In the Smiltyne site, the *AGR* of the picofraction increased linearly with the dilution factor (theoretically impossible case); with the highest *AGR* values at nondiluted treatment (Fig. 3), similar results were reported previously (Gallegos, 1989; Lignell et al., 2003; Modigh and Franzè, 2009). Positive slopes are usually attributed to the complex cycling of nutrients between internal and external pools, mixotrophy or filtration contamination and trophic cascade effect (review by Calbet and Saiz, 2013). The last explanation could be the reason for the positive *AGR* of the picofraction trend along the dilution factor in our data, suggesting that nano-filterers, which dominated in the brackish water site (Fig. 2), intensively grazed not only on the autotrophic nanofraction of phytoplankton, but also on heterotrophic flagellates, which belong to the same size spectra (2—20 μm) and are one of the main pico-fraction feeders, thereby releasing the phytoplankton picofraction from predator control. Unfortunately, the number of heterotrophic nanoflagellates (HNF) was not estimated in this study, making the ciliate protozoa grazing estimates overestimations to some degree. HNF counts should also be included in the dilution experiments in the Baltic Sea. A similar food web effect was suggested to affect the dilution experiments in mesocosms (Lignell et al., 2003), but it was not found in the experiments conducted in the Baltic Sea by Reckermann (1996).

5. Conclusion

The dilution experiment approach revealed a significant ciliate grazing effect on the nano-fraction of phytoplankton in the brackish water, and on the pico-fraction in the freshwater community. This pattern is related to the differences in ciliate community size structure: larger nano-filterers dominate in the brackish water assemblages, whereas pico/nano-filterers prevail in freshwater. Thus it is important to monitor the species composition and/or size-class division of specific ciliate communities to estimate their size-selective grazing effect. This is also important for constructing more detailed carbon flow models in the Baltic Sea ecosystem.

Acknowledgements

We would like to thank Dr. Maren Voß and Dr. Frederike Korth from the Leibniz Baltic Sea Research Institute (IOW) for their help in nutrient and pigment analysis. We are grateful to Dr. Ričardas Paškauskas for his help during experimental manipulations and Dr. J. Lesutienė for her comments on the manuscript.

The current study was supported by the BIO-C3 (Biodiversity changed investigating causes, consequences and management implications) MARSEC within the BONUS, the joint Baltic Sea Research and Development programme funded jointly by the EU Seventh Framework Programme and the Research Council of Lithuania (Grant Agreement No. BONUS-1/2014), and by a grant (No. MIP-036/2012) from the Research Council of Lithuania and the Academy of Finland.

Appendix A. Supplementary data

Supplementary data associated with this article can be found, in the online version, at doi:10.1016/j.oceano.2016.05.002.

References

Aberle, N., Lengfellner, K., Sommer, U., 2007. Spring bloom succession, grazing impact and herbivore selectivity of ciliate communities in response to winter warming. Oecologia 150 (4), 668—681.

Ayo, B., Santamaria, E., Latatu, A., Artolozaga, I., Azua, I., Iriberri, J., 2001. Grazing rates of diverse morphotypes of bacterivorous ciliates feeding on four allochthonous bacteria. Lett. Appl. Microbiol. 33 (6), 455—460.

Barlow, R.G., Mantoura, R.F.C., Cummings, D.G., Fileman, T.W., 1997. Pigment chemotaxonomic distributions of phytoplankton during summer in the western Mediterranean. Deep-Sea Res. Pt. II 44 (3—4), 833—850.

Burkill, P.H., Mantoura, R.F.C., Lewellyn, C.A., Owens, N.J.P., 1987. Microzooplankton grazing and selectivity of phytoplankton in coastal waters. Mar. Biol. 93, 581—590.

Burkovskii, I.V., 1976. Ecology of the White Sea Tintinnida (Ciliata). Zool. J. 55, 497—507.

Calbet, A., 2008. The trophic roles of microzooplankton in marine systems. ICES J. Mar. Sci. 65, 325—331.

Calbet, A., Saiz, E., 2013. Effects of trophic cascades in dilution grazing experiments: from artificial saturated feeding responses to positive slopes. J. Plankton Res. 35 (6), 1183—1191.

Dailidienė, I., Davulienė, L., 2008. Salinity trend and variation in the Baltic Sea near the Lithuanian coast and in the Curonian Lagoon in 1984—2005. J. Mar. Syst. 74 (S), 20—29.

Dzierzbicka-Głowacka, L., Kalarus, M., Musialik-Koszarowska, M., Lemieszek, A., Żmijewska, M.I., 2015. Seasonal variability in the population dynamics of the main mesozooplankton species in the Gulf of Gdańsk (southern Baltic Sea): production and

mortality rates. Oceanologia 57 (1), 78–85, http://dx.doi.org/10.1016/j.oceano.2014.06.001.

Fenchel, T., 1987. Ecology of Protozoa: The Biology of Free-living Phagotrophic Protists. Springer-Verlag, Berlin, Heidelberg, 197 pp.

Ferrarin, C., Razinkovas, A., Gulbinskas, S., Umgiesser, G., Bliūdžiutė, L., 2008. Hydraulic regime-based zonation scheme of the Curonian Lagoon. Hydrobiologia 611 (1), 133–146.

Foissner, W., Berger, H., 1996. A user-friendly guide to the ciliates (Protozoa, Ciliophora) commonly used by hydrobiologists as bioindicators in rivers, lakes, and waste waters, with notes on their ecology. Freshwater Biol. 35 (2), 375–482.

Gaedke, U., Wickham, S., 2004. Ciliate dynamics in response to changing biotic and abiotic conditions in a large, deep lake (Lake Constance). Aquat. Microb. Ecol. 34 (3), 247–261.

Gallegos, C.L., 1989. Microzooplankton grazing on phytoplankton in the Rhode River, Maryland: nonlinear feeding kinetics. Mar. Ecol.-Prog. Ser. 57, 23–33.

Gallegos, C.L., Vant, W.N., Safi, K.A., 1996. Microzooplankton grazing of phytoplankton in Manukau Harbour, New Zealand. New Zeal. J. Mar. Freshwater Res. 30 (3), 423–434.

Gasiūnaitė, Z.R., 2000. Coupling of the limnetic and brackishwater plankton crustaceans in the Curonian Lagoon (Baltic Sea). Int. Rev. Hydrobiol. 85 (5–6), 653–661.

Gasiūnaitė, Z.R., Cardoso, A.C., Heiskanen, A.S., Henriksen, P., Kauppila, P., Olenina, I., Pilkaitytė, R., Purina, I., Razinkovas, A., Sagert, S., Schubert, H., Wasmund, N., 2005. Seasonality of coastal phytoplankton in the Baltic Sea: influence of salinity and eutrophication. Estuar. Coast. Shelf Sci. 65 (1–2), 239–252.

Gasiūnaitė, Z.R., Daunys, D., Olenin, S., Razinkovas, A., 2008. The Curonian Lagoon. In: Schiewer, U. (Ed.), Ecology of Baltic Coastal Waters. Ecological Studies 197. Springer-Verlag, Berlin, Heidelberg, 197–215.

Gifford, D.J., 1988. Impact of grazing by microzooplankton in the Northwest Arm of Halifax Harbour, Nova Scotia. Mar. Ecol.-Prog. Ser. 47, 249–258.

Grasshoff, K., Ehrhardt, M., Kremling, K., 1983. Methods of Seawater Analysis, 2nd ed. Verlag Chemie, Berlin, 419 pp.

Grinienė, E., 2013. Functional role of plankton ciliates in a eutrophic coastal lagoon. (Ph.D. thesis). Klaipėda Univ., 123 pp.

Grinienė, E., Mažeikaitė, S., Gasiūnaitė, Z.R., 2011. Inventory of the taxonomical composition of the plankton ciliates in the Curonian Lagoon (SE Baltic Sea). Oceanol. Hydrobiol. Stud. 40 (4), 86–95.

Hansen, B., Bjørnsen, P.K., Hansen, P.J., 1994. Prey size selection in planktonic zooplankton. Limnol. Oceanogr. 39 (2), 395–403.

James, M.R., Hall, J.A., 1998. Microzooplankton grazing in different water masses associated with the subtropical convergence round the South Island, New Zealand. Deep-Sea Res. Pt. I 45 (10), 1689–1707.

Jonsson, P.R., 1986. Particle size selection, feeding rates and growth dynamics of marine planktonic oligotrichous ciliates (Ciliophora: Oligotrichina). Mar. Ecol.-Prog. Ser. 33, 265–277.

Kivi, K., Setälä, O., 1995. Simultaneous measurement of food particle selection and clearance rates of planktonic oligotrich ciliates (Ciliophora: Oligotrichina). Mar. Ecol.-Prog. Ser. 119, 125–137.

Krevš, A., Koreivienė, J., Paškauskas, R., 2007. Phytoplankton production and community respiration in different zones of the Curonian lagoon during the midsummer vegetation period. Transit. Waters Bull. 1 (1), 17–26.

Landry, M.R., Calbet, A., 2004. Phytoplankton growth, microzooplankton grazing, and carbon cycling in marine systems. Limnol. Oceanogr. 49 (1), 51–57.

Landry, M.R., Hassett, R.P., 1982. Estimating the grazing impact of marine microzooplankton. Mar. Biol. 67, 283–288.

Landry, M.R., Kirshtein, J., Constantiou, J., 1995. A refined dilution technique for measuring the community grazing impact of microzooplankton, with experimental tests in the central equatorial Pacific. Mar. Ecol.-Prog. Ser. 120, 53–63.

Lehrter, J.C., Pennock, J.R., McManus, G.B., 1999. Microzooplankton grazing and nitrogen excretion across a surface estuarine-coastal interface. Estuaries 22 (1), 113–125.

Lignell, R., Seppälä, J., Kuuppo, P., Tamminen, T., Andersen, T., Gismervik, I., 2003. Beyond bulk properties: responses of coastal summer plankton communities to nutrient enrichment in the northern Baltic Sea. Limnol. Oceanogr. 48 (1), 189–209.

Lindholm, T., 1985. *Mesodinium rubrum* – a unique photosynthetic ciliate. Adv. Aquat. Microbiol. 3, 1–48.

Mažeikaitė, S.I., 1978. Zooplankton of the northern part of the Curonian Lagoon in 1974 and 1975. Acad. Sci. Lithuanian SSR 64, 55–56, (in Russian).

Mažeikaitė, S.I., 2003. Freshwater Plankton Heterotrophic Protists of Lithuania. Press of the Botany Institute, Vilnius, 222 pp., (in Lithuanian).

McManus, G.B., Ederington-Cantrell, M.C., 1992. Phytoplankton pigments and growth rates, and microzooplankton grazing in a large temperate estuary. Mar. Ecol.-Prog. Ser. 87, 77–85.

Mironova, E.I., Telesh, I.V., Skarlato, S.O., 2012. Diversity and seasonality in structure of ciliate communities in the Neva Estuary (Baltic Sea). J. Plankton Res. 34 (3), 208–220.

Modigh, M., Franzè, G., 2009. Changes in phytoplankton and microzooplankton populations during grazing experiments at a Mediterranean coastal site. J. Plankton Res. 31 (8), 853–864.

Moigis, A.G., Gocke, K., 2003. Primary production of phytoplankton estimated by means of the dilution method in coastal water. J. Plankton Res. 25 (10), 1291–1300.

Quinlan, E.L., Jett, C.H., Philips, E.J., 2009. Microzooplankton grazing and the control of phytoplankton biomass in the Suwannee River estuary, USA. Hydrobiologia 632 (1), 127–137.

Rassoulzadegan, F., Laval-Peuto, M., Sheldon, R.W., 1988. Partitioning of the food ration of marine ciliates between pico- and nanoplankton. Hydrobiologia 159, 75–88.

Reckermann, M., 1996. Ultraphytoplankton and protozoan communities and their interactions in different marine pelagic ecosystems (Arabian Sea and Baltic Sea). (Ph.D. thesis). Rostock Univ., 152 pp.

Schmoker, C., Hernández-León, S., Calbet, A., 2013. Microzooplankton grazing in the oceans: impacts, data variability, knowledge gaps and future directions. J. Plankton Res. 35 (4), 691–706.

Setälä, O., Kivi, K., 2003. Planktonic ciliates in the Baltic Sea in summer: distribution, species association and estimated grazing impact. Aquat. Microb. Ecol. 32 (3), 287–297.

Stoecker, D.K., Nejstgaard, J.C., Madhusoodhanan, R., Pohnert, G., Wolfram, S., Jakobsen, H.H., Šulčius, S., Larsen, A., 2015. Underestimation of microzooplankton grazing in dilution experiments due to inhibition of phytoplankton growth. Limnol. Oceanogr. 60 (4), 1426–1438.

Strom, S.L., Macri, E.L., Olson, M.B., 2007. Microzooplankton grazing in the coastal Gulf of Alaska: variations in top down control of phytoplankton. Limnol. Oceanogr. 52 (4), 1480–1494.

Strüder-Kypke, M.C., Kypke, E.R., Agatha, S., Warwick, J., Motagnes, D.J.S., 2003. The "user friendly" guide to coastal planktonic ciliates. The Planktonic Ciliate Project by University of Liverpool, http://www.liv.ac.uk/ciliate/intro.htm.

Sun, J., Feng, Y., Zhang, Y., Hutchins, D.A., 2007. Fast microzooplankton grazing on fast-growing, low-biomass phytoplankton: a case study in spring in Chesapeake Bay, Delaware Inland Bays and Delaware Bay. Hydrobiologia 589 (1), 127–139.

Šulčius, S., Pilkaitytė, R., Mazur-Marzec, H., Kasperovičienė, J., Ezhova, E., Błaszczyk, A., Paškauskas, R., 2015. Increased risk of exposure to microcystins in the scum of the filamentous cyanobacterium Aphanizomenon flos-aquae accumulated on the western shoreline of the Curonian Lagoon. Mar. Pollut. Bull. 99 (1–2), 264–270.

Twiss, M.R., Smith, D.E., 2012. Size-fractionated phytoplankton growth and microzooplankton grazing rates in the upper St. Lawrence River. River Res. Appl. 28 (7), 1047—1053.

Utermöhl, H., 1958. Zur Vervollkommnung der quantitativen Phytoplankton-Methodik. Mitteilungen/Int. Verein. Theor. Angew. Limnol. 9, 1—38.

Verity, P.G., Stoecker, D.K., Sieracki, M.E., Nelson, J.R., 1993. Microzooplankton grazing of primary production at 140°W in the equatorial Pacific. Deep-Sea Res. Pt. II 43 (4—6), 1227—1256.

Weisse, T., 1990. Trophic interactions among heterotrophic microplankton, nanoplankton, and bacteria in Lake Constance. Hydrobiologia 191 (1), 111—122.

Oceanologia (2016) 58, 302–316

Available online at www.sciencedirect.com

ScienceDirect

journal homepage: www.journals.elsevier.com/oceanologia/

ORIGINAL RESEARCH ARTICLE

Eutrophication influence on phytoplankton community composition in three bays on the eastern Adriatic coast

Mia Bužančić *, Živana Ninčević Gladan, Ivona Marasović, Grozdan Kušpilić, Branka Grbec

Institute of Oceanography and Fisheries, Split, Croatia

Received 31 December 2015; accepted 6 May 2016
Available online 20 May 2016

KEYWORDS
Phytoplankton;
Chlorophyll *a*;
Biodiversity;
The eastern Adriatic coast

Summary This study shows the influence of eutrophication pressure on the phytoplankton community structure, abundance and biodiversity in the investigated bays with different hydromorphological features. Šibenik Bay is a highly stratified estuary of the karstic river Krka; Kaštela Bay is a semi-enclosed coastal bay, which is influenced by the relatively small river Jadro; and Mali Ston Bay is located at the Neretva River estuary, the largest river on the eastern part of the Adriatic Sea. All of the areas are affected by urban pressure, which is reflected in the trophic status of the waters. The greatest anthropogenic influence was found in Kaštela Bay while the lowest influence was found in Mali Ston Bay. In this study, the highest biomass concentration and maximum abundance of phytoplankton were recorded at the stations under the strongest anthropogenic influence. Those stations show a dominance of abundance compared to the biomass and a dominance of opportunistic species, which is reflected in the lower biodiversity of phytoplankton community. Diatoms were the most represented group of the phytoplankton community in all three bays, followed by the dinoflagellates. Diatoms that were highlighted as significant for the difference between the bays were *Skeletonema marinoi* in Šibenik Bay, *Leptocylindrus minimus* in Kaštela Bay and the genus *Chaetoceros* spp. in Mali Ston Bay. Dinoflagellates were more abundant at the stations under the strongest anthropogenic influence, and most significant were *Prorocentrum triestinum* in Kaštela Bay and *Gymnodinium* spp. in Šibenik Bay and Mali Ston Bay.

* Corresponding author at: Institute of Oceanography and Fisheries, Šetalište I. Meštrovića 63, P.O. Box 500, 21000 Split, Croatia. Tel.: +385 21 408000; fax: +385 21 358650.
E-mail address: buzancic@izor.hr (M. Bužančić).
Peer review under the responsibility of Institute of Oceanology of the Polish Academy of Sciences.

Production and hosting by Elsevier

http://dx.doi.org/10.1016/j.oceano.2016.05.003

1. Introduction

Phytoplankton biomass and community composition were analyzed in three bays on the eastern Adriatic coast, with different hydrological and trophic statuses. Phytoplankton is very sensitive to changes in its environment and, therefore, provides good insight into water quality before it becomes visible on higher trophic levels and the excessive eutrophication of certain areas commences (Brettum and Andersen, 2005). Eutrophication is an enrichment of water with nutrients, primarily nitrogen and phosphorus, which stimulates primary production. In some cases, that leads to visible blooms and accumulation of submerged and floating organic material in the water (Vollenweider, 1992). Eutrophication can have natural and anthropogenic origins. A natural one occurs due to substrate remineralization, upwelling and increase of rivers inflow. Resuspension of particulate matter can enhance primary production because of the intrusion of the pore water rich with nutrients from the sediments into the bottom layer and consequentially into the whole water column (Guinder et al., 2015; Su et al., 2015). A previous study of the investigated areas shows that sediment resuspension is one of the sources of ammonia, nitrate and phosphate regeneration (Barić et al., 2002). Upwelling brings nutrient rich waters from the deeper layers, and rivers' inflow bring the bulk of total nitrogen to the sea. Anthropogenic eutrophication occurs due to various human activities in the vicinity of the coastal area, such as the inflow of urban and industrial wastewaters, rinsing of agricultural land and atmospheric pollution. A causal link between anthropogenic sources of nutrients and the eutrophication of the system is generally accepted (McQuatters-Gollop et al., 2009; Smith, 2006), although it is very important to take into account systems-specific features of a certain area to distinguish changes in the ecosystem resulting from natural seasonal and interannual dynamics. Given the scale, the eutrophication process could be beneficial for the ecosystem, but it could have adverse effects depending on the different characteristics of each ecosystem (Crossetti et al., 2008; Marasović and Pucher-Petković, 1985; Skejić et al., 2014; Su et al., 2015). The beginning of eutrophication causes an increase in phytoplankton biomass, but the composition of the phytoplankton community becomes more uniform. Certain species disappear, while at the same time, opportunistic species of phytoplankton begin to dominate (McQuatters-Gollop et al., 2009). Species diversity is reduced because of the competitive exclusion between species, whereas with a slight increase of eutrophication, competition is relaxed, thus resulting in increased diversity. With a further increase in eutrophication, diversity drops again because of species reduction due to stress (Spatharis et al., 2007). Eutrophication tends to favour small and fast-growing organisms, which usually means that the proportion of the dominant taxa to the total biomass is relatively low, meaning that the biodiversity values are higher than when large-sized taxa dominate (Uusitalo et al., 2013).

In highly eutrophicated systems, the trophic chain is lacking higher links, and autotrophic processes exceed heterotrophic, which significantly affects the balance of the system (Richardson et al., 1998). The responses of phytoplankton to the eutrophication process have been reported mostly through chlorophyll *a* concentrations (Edwards et al., 2003; Gowen et al., 1992; Vollenweider, 1976). The phytoplankton biomass (chl *a*) is a common indicator of eutrophication because it provides consistent insights of a certain area, but it should be monitored with the compositional changes of the community structure (McQuatters-Gollop et al., 2009; Ninčević Gladan et al., 2015). The Water Framework Directive (WFD) (European Commission, 2008) states that phytoplankton and its biodiversity are one of the crucial biological elements in the assessment of the ecological status of the sea. Previous studies of researched bays along the eastern Adriatic coast, revealed that these are the areas with the highest nutrient concentration and primary productivity. These are the semi-enclosed areas and salt-wedge estuaries with a high urban nitrogen and phosphorus loading, and a high natural nitrate and silicate loading by the rivers' inflow (Barić et al., 1992; Legović et al., 1994). In previous studies, the trophic status of investigated bays has been determined using the phytoplankton abundance and volume (Čalić et al., 2013; Marasović and Ninčević, 1997; Viličić, 1989).

The aim of this study is to determine a difference between the stations considering the specific nutrients, to quantify the potential anthropogenic pressures and to determine the relationship between abiotic parameters and biomass. In addition, we determine the similarity of the phytoplankton community regarding the abundance of species and define how much individual species affect the diversity observed between the investigated stations. The aim is to establish the relationship between biomass and phytoplankton abundance and use it as a way to define the level of disturbance in the investigated areas. Overall, the aim of this study is to investigate the impact of anthropogenic pressures on phytoplankton community structure and biodiversity.

2. Material and methods

2.1. Study area

Šibenik Bay is a highly stratified estuary of the karstic river Krka, with small tidal amplitudes and permanently brackish surface water (Svensen et al., 2007). The Krka River is one of the most pristine European rivers, characterized by low concentrations of nutrients and extremely low input of terrigenous material (Legović et al., 1994). Freshwater discharge from the Krka River has been systematically monitored since 1947 (Bonacci and Ljubenkov, 2005), and it can vary between 5 and 565 $m^3 s^{-1}$ with an annual average discharge of 52.9 $m^3 s^{-1}$ (1950–1998). The Krka River estuary is a typical salt-wedge, highly stratified estuary (Žutić and Legović, 1987) that is 25 km long and relatively narrow except for two wider parts, Prokljan Lake and Šibenik harbour. The depth gradually increases from 5 to 43 m at the mouth. The town of Šibenik is located in the estuary's middle reach, and it is the only source of direct anthropogenic eutrophication (Gržetić et al., 1991; Legović et al., 1994). Šibenik harbour has reduced exchange with the waters of the open sea, and it is under a direct anthropogenic influence (Kušpilić, 2005). The phytoplankton community in the estuary is dependent on seasonal cycles of temperature and salinity (winter–spring and summer–autumn), and on the degree of eutrophication, which can

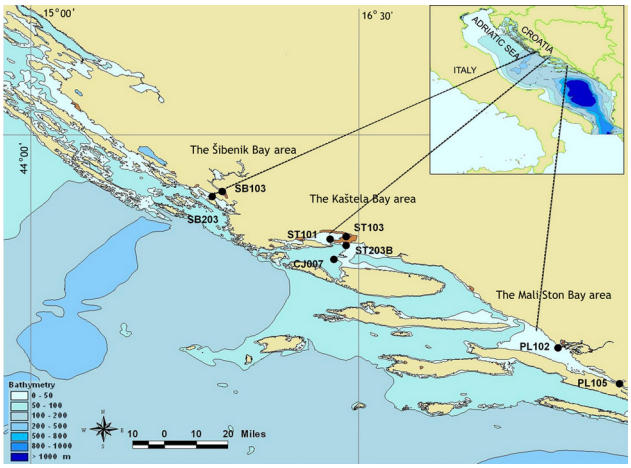

Figure 1 The investigated areas with sampling stations.

be of natural or anthropogenic origin. Decomposition of freshwater phytoplankton greatly contributes to natural eutrophication and the regeneration of nutrients in the upper reaches of the estuary, whereas in the lower parts, the eutrophication favours anthropogenic sources (Legović et al., 1994; Svensen et al., 2007; Viličić et al., 1989). Previous studies of this area show that the main source of nitrates and orthosilicates is the Krka River, while the total phosphorus is mainly of anthropogenic origin from the Šibenik urban area (Legović et al., 1994). In this area, samples were taken at two stations, SB103 and SB203, which were 35 m and 25 m deep, respectively (Fig. 1).

Kaštela Bay is a semi-enclosed coastal bay, the largest in the middle part of the eastern Adriatic coast, 15 km long and 6 km wide, with an average depth of 23 m. It communicates with the adjacent channel through an inlet that is 1.8 km wide and 40 m deep. The most important fresh water source is the Jadro River, a relatively small river with an average annual discharge of 8 $m^3 s^{-1}$, which discharges into the eastern part of the bay (Ljubenkov, 2015). The discharge of several submarine springs is of a lower intensity. Kaštela Bay is under the strong impact of untreated municipal and industrial effluents. Previous studies show that anthropogenic eutrophication and nutrient inflow from the Jadro River cause frequent summer algal blooms with the development of toxic dinoflagellates (Marasović et al., 1991). Regularity in spring–autumn maximum abundances was found, but there was also evidence that algal biomass and community structure changed over time. An increase of abundance and phytoplankton biomass have been recorded in mid-1980 to mid-1990's period, following the decrease (Ninčević Gladan et al., 2009). Previous studies also show a regularity of layout in the size fractions. Smaller pico and nano fractions contributed more to community composition in the outer more open part of the bay, while larger micro fractions occurred in the inner and more eutrophicated part (Marasović and Ninčević, 1997).

In this area, samples were taken at four stations, two located within the bay (ST101, ST103) and the other two just outside of the bay (ST203B, CJ007) (Fig. 1). The outer stations were included in the research to determine the reach of anthropogenic influence to the surrounding area. The depth of the investigated stations ST101, ST103, ST203B and CJ007 were 37 m, 12 m, 35 m and 50 m, respectively.

Mali Ston Bay is deeply cut between the mainland and the Pelješac Peninsula, and it is located at the end of the Neretva Channel. The area is influenced by a considerable freshwater discharge from the Neretva River, the largest river on the eastern part of the Adriatic Sea, and several submarine springs situated inside Mali Ston Bay. The average annual discharge of the Neretva River is 332 $m^3 s^{-1}$ (Orlić et al., 2006). Neretva River estuary is classified as the salt-wedge type, where due to small tidal currents, the advection of the river water is much larger than the introduction of seawater through tidal mixing. The bay generates estuarine circulation with a brackish water output current on the surface, while saline water enters below the halocline from the open sea. This area is sparsely populated, so the anthropogenic impact on the bay is low. Previous studies show that the principal regulator of production conditions in Mali Ston Bay is the specific, constant and strong exchange of water within the bay and the open sea, the strong impact of the Neretva River and the karstic submarine springs (Viličić, 1989). According to the nutrient concentration, the transparency of the water column and the quantity of phytoplankton, Mali Ston Bay may be classified as a moderate natural eutrophicated system (Jasprica and Carić, 1994; Jasprica et al., 2012; Skejić et al., 2015; Viličić, 1989; Viličić et al., 1998). Thanks to the hydrographic features and favourable primary production, the bay has been well known for cultivated mussels since ancient times, and today it presents one of the most important places for shellfish farming in Croatia. In this area, samples were taken at two stations PL102 and PL105, 21 m and 8 m deep, respectively (Fig. 1).

2.2. Sampling methods

Sampling was performed during 2005, with the intent of capturing the seasonal cycle of phytoplankton in a certain area. In Kaštela Bay, sampling was performed monthly in a period from January to December, while in Šibenik and Mali Ston Bay, the study covers 8 months of sampling (January, May, June, July, August, September, November, December). Physical and chemical parameters (salinity, temperature, nutrients) were sampled simultaneously with phytoplankton samples to make a more complete ecological characterization of the study area. Sampling and determination of phytoplankton, physical and chemical parameters were conducted using standard oceanographic methods (Strickland and Parsons, 1972). Temperature and salinity were measured with a Seabird-25 CTD probe. Dissolved oxygen was determined by the Winkler method of thiosulphate titration. Dissolved inorganic nutrient concentrations were measured photometrically with an AutoAnalyzer III system (Bran + Luebbe), using modified automated methods according to Grasshoff (1976). Chlorophyll *a* concentrations were measured using the fluorometric method from 90% acetone extracts (Strickland and Parsons, 1972), and the results were expressed as mg chl *a* m^{-3}. Phytoplankton abundance and community composition have been determined according to the Utermöhl method (Utermöhl, 1958). Water samples (250 mL) were collected with Nansen bottles and preserved with formaldehyde to a final concentration of 2% formaldehyde-sea water solution. Subsamples of 25 mL were settled in

counting chambers for at least 24 h. Counting was performed in one transect of the sedimentation chamber, using an inverted microscope with magnifications of ×200, and ×400 for different species, depending on their respective sizes. In the case of blooms or a high abundance of some species, counting was done in several randomly selected fields.

2.3. Data analysis

Analysis of variance (ANOVA) was used to determine the difference between the stations considering the specific nutrients.

The impact assessment of anthropogenic influence on land in the study area was determined by calculating the LUSI index (Land Uses Simplified Index), using the Croatian CORINE (Coordination of Information on the Environment) digital database that assesses the environmental pressure. CORINE has been accepted and evaluated by the European Union as a fundamental reference data set for spatial and territorial analysis. The LUSI index is quantifying potential anthropogenic pressures according to the percent of land used in various anthropogenic activities such as urbanization, industrialization, and proximity to large urban and agricultural areas. In this study, the LUSI index was calculated in accordance with Flo et al. (2011) with a small modification, which relates to a radius being taken into account. A radius of 5 km from the investigated points was taken to insure that all the stations are included in the calculation.

The biological data was tested for normality by the Kolmogorov–Smirnov and Liliefor tests, which showed that it does not have a normal distribution and was analyzed with nonparametric methods.

The Bray–Curtis similarity coefficient was used to determine the similarity of the phytoplankton community structure regarding the abundance of species (Bray and Curtis, 1957). Total abundances were used, and the input data were transformed using a logarithm (Clarke, 1993; Field et al., 1982). The obtained data gave the similarity matrix, and using the method of cluster analysis, the dendrogram of average similarity between stations was made. For a graphical representation, MDS (Multidimensional Scaling) was used with vectors of phytoplankton groups (Clarke and Warwick, 2001).

SIMPER (Similarity Percentage analysis) was used to determine how much individual species affect the diversity observed between the investigated stations. This analysis identifies species that are typical in terms of regularity of occurrence in a constant for most samples. The analysis was used to compare the phytoplankton community at the stations that are in areas of highest anthropogenic pressure in this investigation.

Non-parametric Spearman rank order correlations were used to determine the relationship between biomass and abiotic parameters.

The relationship between biomass and phytoplankton abundance was determined through ABC-plots, a simple graphic way to determine the level of disturbance in the investigated area.

Biodiversity was presented through the curves of cumulative dominance of species with k-dominance plots and different types of diversity indexes, of which the most significant proved to be Menhinick's diversity index (D).

3. Results and discussion

3.1. Environmental parameters in the bays

During this study in Šibenik Bay area, the sea temperature ranged from 7.35 to 23.47°C. Both extreme values were observed in the surface layer at station SB103, where the minimum temperature was recorded in January and the maximum in September. The salinity of this area ranged from 4.42 to 38.71 in December at the surface and in August at the bottom, respectively. Both extremes were found at the same station (SB103), indicating the strong influence of the freshwater inflow of the Krka River at this station. This assertion is confirmed by the maximum values of orthosilicate (9.59 mmol m^{-3}) and nitrate (TIN 57.93 mmol m^{-3}) recorded at that station. Orthophosphate concentrations in this area ranged from 0.002 to 0.12 mmol m^{-3} recorded at SB203 and SB103, respectively. The oxygen saturation of this area ranged from 78 to 125%.

The sea temperature in the Kaštela Bay area ranged from 9.45 to 26.93°C, recorded at the surface at stations ST101 in March and ST103 in July, respectively. The salinity ranged from 34.16 to 38.71, and both extremes were recorded at station ST101, in May at the surface and in July at 5 m of depth, respectively. The maximum values of orthosilicate and nitrate were recorded at station ST103, which is under direct influence of the Jadro River. The highest value of orthosilicates (12.32 mmol m^{-3}) was recorded in December on the surface, and the maximum value of nitrates was measured in August at a depth of 5 m (TIN 24.90 mmol m^{-3}). These findings have confirmed the influence of the freshwater inflow of the Jadro River at this station. Orthophosphate concentrations in this area had the highest range of all investigated areas, from 0.002 mmol m^{-3} at station CJ007, which is under the lowest influence from the land, to 1.5 mmol m^{-3} at station ST103, which is closest to land and under the direct influence of urban wastewaters. Oxygen saturation in the Kaštela Bay area ranged from 84 to 133%.

In the Mali Ston Bay area, the sea temperature ranged from 10.54 to 23.65°C at station PL105 in January and PL102 in August, respectively. Both extremes were recorded at the surface. Salinity in this area ranged from 26.47 to 38.62. These values were recorded at station PL102, strongly influenced by land, submarine springs and freshwater inflow of the Neretva River, which is confirmed by the large range of recorded values of orthosilicates (0.37–21.93 mmol m^{-3}) and TIN (0.34–38.85 mmol m^{-3}). The maximum value of orthosilicates was recorded in December at the surface and of nitrates in November at a depth of 5 m. Orthophosphate concentrations in this area had the lowest range of all investigated areas, from 0.01 to 0.11 mmol m^{-3}, indicating a week anthropogenic influence. Oxygen saturation in this area ranged between 94 and 127%.

The seasonal distribution of temperature and salinity at the surface layer at all investigated stations is presented in Fig. 2. It is evident that the influence of the seasons and freshwater inflow were great at stations closest to the mouth of the rivers and land. The abiotic parameters of the investigated areas were studied in detail in earlier research and have been presented in Bužančić et al. (2012).

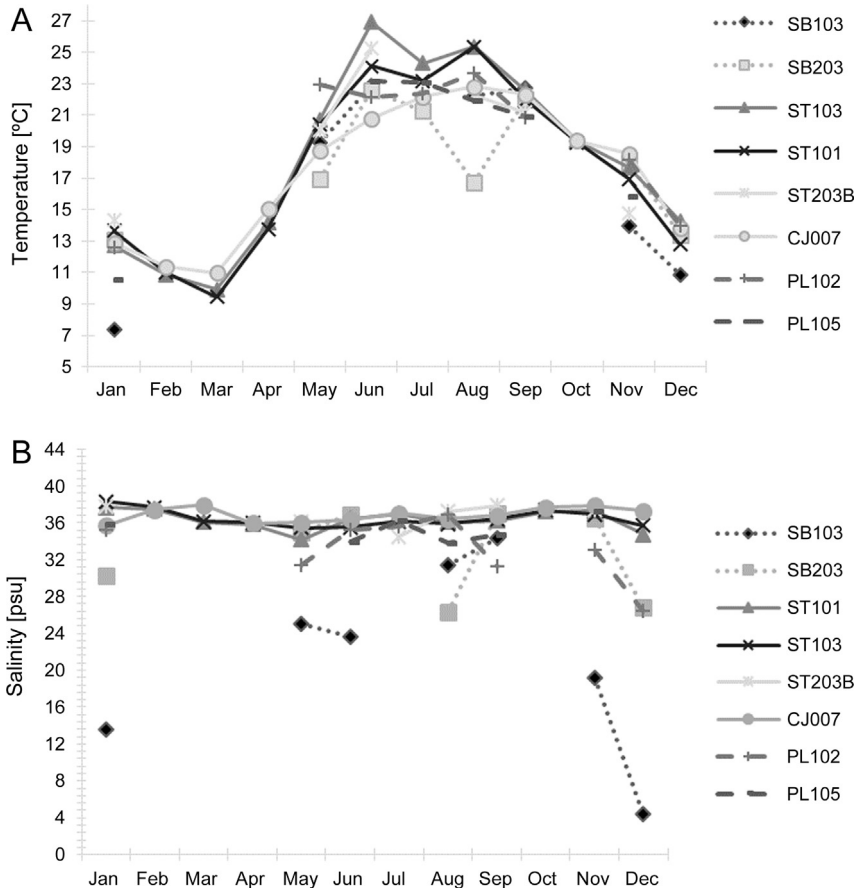

Figure 2 Seasonal distribution of temperature [°C] (A) and salinity [psu] (B) in the surface layer at all investigated stations.

The difference between the stations considering the specific nutrients was determined by an analysis of variance (ANOVA).

A statistically significant difference ($p < 0.001$) with respect to salinity was observed between stations SB103 and all other investigated ones. This station, given the very low salinity, describes the transitional waters while all other stations belong to the coastal waters (Kušpilić et al., 2011; Ninčević Gladan et al., 2015). At the stations in the coastal waters, the salinity was lowest in the Šibenik Bay area (outer station), followed by Mali Ston Bay and Kaštela Bay (inner stations), while the Kaštela Bay area (outer stations) was characterized by higher salinity. The difference in salinity between Kaštela Bay (inner stations) and the Šibenik Bay area (outer station) is statistically significant.

The highest nitrate concentration was recorded at station SB103 where the fresh water inflow from the Krka River is the greatest. Statistically significant ($p < 0.05$) higher concentrations of nitrate were found at station SB103, in contrast to stations CJ007 and ST203B, which were weakly influenced by fresh water inflow. At the other investigated stations, the nitrate concentration was lower in comparison to station SB103, but this difference was not statistically significant. The reason for this is the influence of the fresh water inflow of the Jadro and Neretva Rivers and the influence of submarine springs.

The highest concentration of orthosilicates was observed in the transitional waters of Šibenik Bay and the inner part of Mali Ston Bay, which is under a stronger influence of submarine springs. Statistically significant ($p < 0.01$) higher concentrations of orthosilicates were observed at stations SB103 and PL105 in relation to all other stations (ST103, SB203 and PL102). The lowest statistically significant correlations were observed at stations CJ007, ST101 and ST203B, which are located furthest from the river mouth.

A statistically significant ($p < 0.001$) higher concentration of orthophosphates was recorded at station ST103, which is under the strongest anthropogenic influence, compared to all other investigated stations.

Regarding the concentration of ammonium salts, a significant difference ($p < 0.05$) was observed between stations SB103, characterized by the highest concentration, and stations CJ007, ST203B, SB203 and PL102, characterized by the lowest concentration of ammonium salts. The remaining stations (ST102, ST103, PL105) had increased concentrations of ammonium ions but were not statistically different.

The proximity and intensity of the rivers' inflow and the influence of activities from the land mainly condition the physical and chemical characteristics of the investigated areas. The impact of agricultural activities on water quality in most European rivers is manifested through increased concentrations of nitrates (Crouzet et al., 1999; Ludwig et al., 2009). Rivers and groundwater bring the bulk of total nitrogen to the sea (nitrates, nitrites, ammonium salts), as confirmed by our research. The maximum concentrations of TIN were recorded at all stations in the surface layer through

Table 1 LUSI index of the investigated stations.

Impact	Station							
	SB103	SB203	ST101	ST103	ST203B	CJ007	PL102	PL105
Urban	1	1	2	2	3		1	
Industrial				1			1	
Agricultural	1	1	1	1			1	1
Harbour	1		1	1	1		1	
LUSI index	3	2	4	5	4	0	4	1

the winter–spring season, at the time of increased freshwater inflow and precipitation. The urban influence is manifested through an increased gradient of orthophosphate and ammonium ions. Previous research in the northwestern Mediterranean Sea shows the same association between the physical and chemical parameters (Flo et al., 2011).

3.2. Anthropogenic influence on the investigated stations

The Land Uses Simplified Index (LUSI) was used to determine the anthropogenic influence on the investigated stations (Table 1).

The greatest anthropogenic influence on the body of water was found in Kaštela Bay at ST103 situated in the eastern part. A relatively high LUSI index was established at station ST203B, which is under strong urban pressure, but as it is located in the channel area with strong current dynamics, there is no pronounced impact of human activity. At the referent station, CJ007 is located outside of Kaštela Bay, furthest from the coast and anthropogenic influence, and LUSI was 0. The lowest index was found in Mali Ston Bay at PL105. At station PL102, which is under a strong influence of agricultural land in the valley of the Neretva River, harbour and urban pressures from the city Ploče, the LUSI index was high. At the same station, the anthropogenic influence was not expressed as in Kaštela Bay, which is probably due to the hydro-geomorphological characteristics of its location. The Šibenik Bay area had a moderate anthropogenic pressure on the body of water.

3.3. Phytoplankton biomass

The highest phytoplankton biomass expressed as chlorophyll *a* concentration was recorded in Šibenik Bay at SB103 (4.73 mg m^{-3}), followed by Kaštela Bay at ST103 (2.79 mg m^{-3}), as both stations are directly influenced by freshwater inflow and high anthropogenic pressure. At all other stations, the recorded values of chlorophyll *a* were generally below 1 mg m^{-3} (Fig. 3).

In the Šibenik Bay area, the range of chl *a* data varied from 0.07 to 4.73 mg m^{-3}. The highest value was measured in May at SB103 on the surface layer, and the minimum one was recorded in July at SB203 in the bottom layer. In this area, the highest values of chl *a* have been recorded in the surface layer during the whole investigated period at both stations. The seasonal distribution of the phytoplankton biomass has shown a big difference between these two stations, where much higher concentrations were recorded at SB103 due to the positive impact of freshwater inflows and anthropogenic eutrophication (Fig. 3).

In the Kaštela Bay area, the phytoplankton biomass varied from 0.01 to 2.79 mg m^{-3} (Fig. 3). The maximum values of chl *a* were recorded at ST103 in September throughout the water column (2.17–2.79 mg m^{-3}), while the minimum one (0.01 mg m^{-3}) was recorded at station CJ007. Higher biomasses were recorded at stations inside of Kaštela Bay (ST101, ST103) opposed to stations just outside of the bay (ST203B, CJ007). The seasonal distribution of chl *a* in this area followed the distribution of nutrients with a marked increase in the autumn–winter period. Such regularity was much more pronounced at stations inside of the bay. Higher values at the surface in relation to the bottom and the vertical distribution of the biomass during the summer period indicate an inflow of nutrients at the surface layer due to the anthropogenic influence on stations placed in Kaštela Bay.

The maximum value of chlorophyll *a* (1.26 mg m^{-3}) in the Mali Ston Bay area was recorded at station PL105 in November, and the minimum value (0.04 mg m^{-3}) was recorded at PL102 in July. A strong anthropogenic influence on PL102 was not reflected on the phytoplankton biomass, probably due to the hydro-geomorphological characteristics of this area (Viličić, 1989). The seasonal distribution in the Mali Ston Bay area was in accordance with the distribution of nutrients and has shown that maximum values of chl *a* occurred in the autumn–winter period (Fig. 3).

According to the seasonal distribution of biomass, there were well pronounced differences between bays. Šibenik Bay is characterized by the highest values of chl *a* and the significantly more frequent appearance of higher biomasses compared to other areas. Although the greatest human impact was recorded in the eastern part of Kaštela Bay, the largest biomass was recorded in Šibenik Bay, largely due to natural eutrophication by the strong influence of the Krka River along with anthropogenic load. The eutrophication of this area was determined in earlier research (Cetinić et al., 2006; Legović et al., 1994; Svensen et al., 2007; Viličić et al., 1989) and confirmed by this study. Besides Šibenik Bay, Kaštela Bay was also characterized by a greater incidence of high concentrations of chl *a*, opposed to Mali Ston Bay, which was characterized by small concentrations of chl *a*. This finding confirms the significantly lower trophic level of this area, determined in earlier research studies (Jasprica et al., 2012; Skejić et al., 2015; Viličić et al., 1998).

3.4. Phytoplankton community composition

With the qualitative analysis of phytoplankton composition at the investigated area of Šibenik Bay, 114 phytoplankton taxa

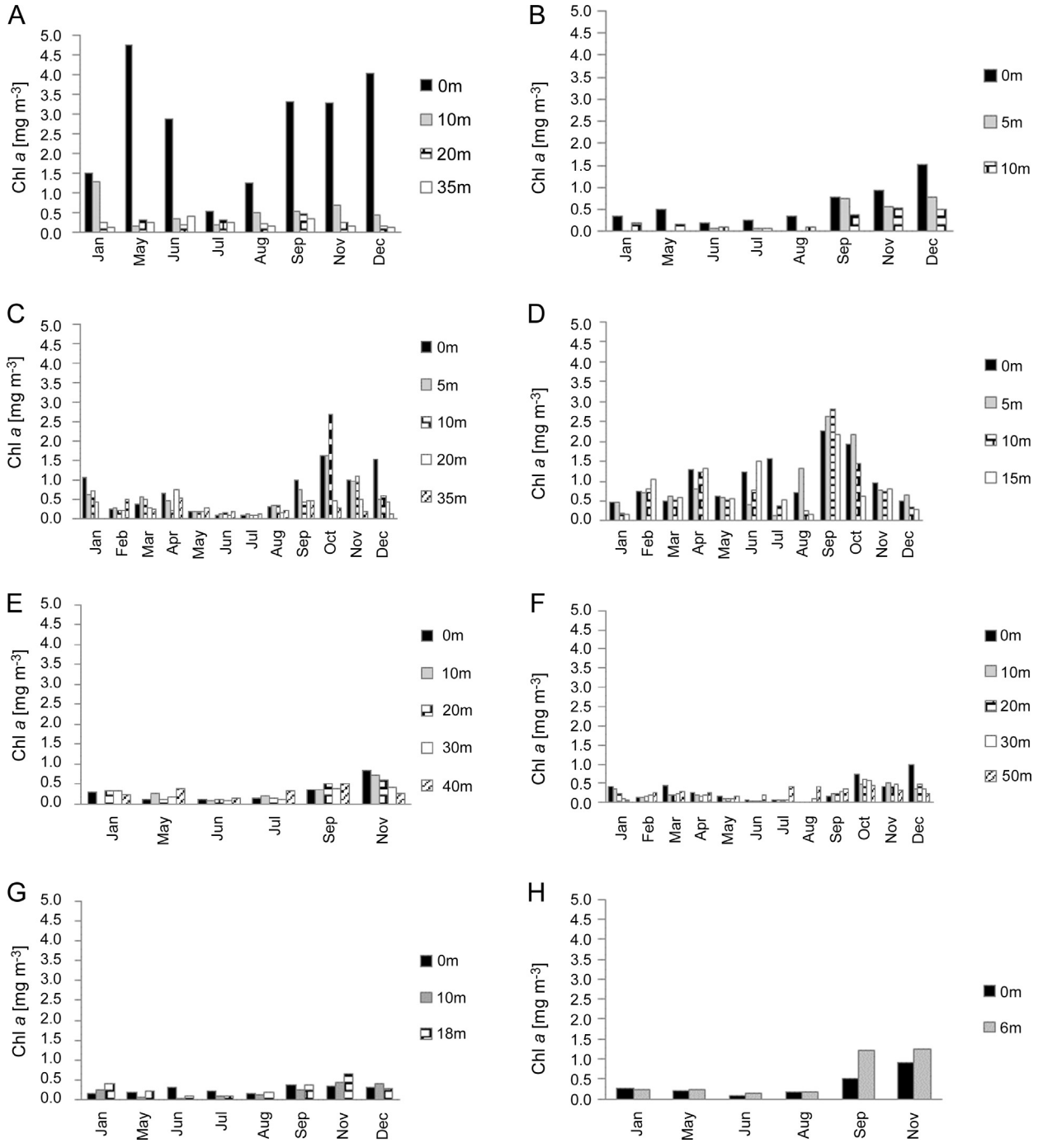

Figure 3 Seasonal distribution of chlorophyll *a* concentrations [mg m^{-3}] at the station SB103 (A), the station SB203 (B), the station ST101 (C), the station ST103 (D), the station ST203B (E), the station CJ007 (F), the station PL102 (G) and the station PL105 (H).

have been determined. The most diverse functional groups were diatoms (61) and dinoflagellates (37). Coccolithophorids contributed with 6, cryptophytes with 3, and silicoflagellates, euglenophytes, chlorophytes with 2 taxa each. The diverse flagellate group of phytoplankton, which is placed by size in the microflagella group, was present in the whole area with a high frequency of findings (96%). The most diverse station in this area with 100 recorded taxa was SB103, located in the Šibenik harbour, which is under a strong influence of urban waste waters and the city port and marina. At station SB203, 66 phytoplankton taxa were found.

In the investigated area of Kaštela Bay, a total of 193 phytoplankton taxa have been recorded. The dinoflagellate functional group was the most diverse one with 92 taxa, followed by diatoms (80), coccolithophorids (9), silicoflagellates and euglenophytes (4), cryptophytes (2) and chlorophyte (1). The microflagella group also had a high frequency of findings in this area (99%). The station with the most

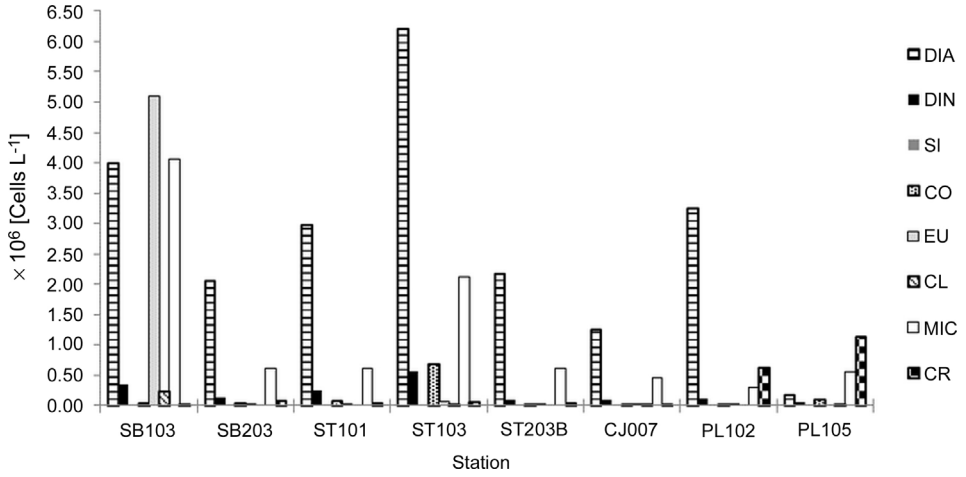

Figure 4 Total abundance of phytoplankton groups [cells L^{-1}] in the surface layer at all investigated stations (DIA, diatoms; DIN, dinoflagellates; SI, silicoflagellates; CO, coccolithophorids; EU, euglenophytes; CL, chlorophytes; MIC, microflagellates; CR, cryptophytes).

recorded phytoplankton taxa was ST103 (140), situated deepest in the bay and under a direct influence of the Jadro River and strong anthropogenic pressure. A somewhat smaller number of taxa were recorded at station ST101 (108), located further away from the freshwater influence but under strong anthropogenic pressure. Stations ST203B with 84 and CJ007 with 82 recorded taxa had the lowest diversity in this area, presumably because they are influenced by canal waters and currents, preventing nutrient retention at these stations.

In the Mali Ston Bay area, a total of 88 phytoplankton taxa have been found: 39 diatoms, 36 dinoflagellates, 4 coccolithophorids, 3 chrisophyte, 2 silicoflagellates and euglenophytes and 1 chlorophyte taxa. A diverse microflagella group had the highest frequency of findings in this area (100%). Station PL102, under the direct influence of the Neretva River, was the more diverse one, with 72 taxa recorded, compared to PL105 where 49 taxa were found.

The complete list of all phytoplankton taxa determined in the investigated areas with their frequency of findings was presented in Bužančić et al. (2012).

Diatoms were the most abundant component of the phytoplankton community at all stations except SB103, where euglenophytes prevailed and PL105, where cryptophytes were the most significant group (Fig. 4). Dinoflagellates were a second significant component of the phytoplankton community, whose contribution was most evident at stations SB103 and ST103 under the highest trophic load, followed by SB203, ST101 and PL102. The lowest contribution was at the stations under the lowest trophic load: ST203B, CJ007 and PL105. A diverse microflagella group was represented with great abundance in all areas with an increase in the spring–summer period.

The maximum abundance in the diatom group was reached by *Leptocylindrus minimus* (4,480,000 cells L^{-1}) in Kaštela Bay at ST103, followed by *Skeletonema marinoi* (3,870,000 cells L^{-1}) in Šibenik Bay, at SB103, and *Chaetoceros* spp. taxa (2,770,000 cells L^{-1}) in the Mali Ston Bay area at PL102. The maximum abundance of the dinoflagellate group was reached by *Prorocentrum triestinum* (489,000 cells L^{-1}) in Kaštela Bay at station ST103, followed by *Gymnodinium* spp. taxa with 88,100 cells L^{-1} and 42,600 cells L^{-1}, in Šibenik Bay (SB103) and Mali Ston Bay (PL102), respectively.

Dinoflagellates were most abundant at the stations that were under the greatest anthropogenic influence and generally more abundant in the warmer part of the year, which is in accordance with previous studies (Ninčević Gladan et al., 2009; Skejić et al., 2012; Smayda, 2000). Previous research indicates that diatoms are positively correlated with nitrates and silicates, and dinoflagellates with phosphates (Svensen et al., 2007).

It is also noteworthy to indicate the monospecific bloom of euglenophyta *Eutreptia lanowii* (5,090,000 cells L^{-1}) at station SB103, which occurred after a sudden rise in temperature of the surface layer. That is characteristic for diluted, warm and eutrophicated waters, and this taxon is used as a biological indicator of organic pollution (Ninčević Gladan et al., 2015; Stonik and Selina, 2001). Blooming of euglenophyta was replaced by blooming of diatom *S. marinoi* at the beginning of July, characterized by strong growth due to the increase of nitrate (DeManche et al., 1979; Ninčević Gladan et al., 2015). This makes it a better competitor among diatoms in eutrophicated conditions, so it is a good indicator species for eutrophication (Collos et al., 1997; Lagus et al., 2004).

It is interesting to point out that the Mali Ston Bay area, in contrast to the other two investigated bays, was characterized by a greater abundance of cryptophytes, which is according to many authors (Pick and Caron, 1987; Skejić et al., 2015; Watson et al., 1997; Willen et al., 1990) common in oligotrophic systems. In addition, coccolithophorids contributed more to community composition in the Mali Ston Bay area than in all other areas of research.

3.4.1. Multi-dimensional scaling of the phytoplankton community structure

The similarity of the phytoplankton community structure in the investigated bays, regarding the abundance and distribution of species, is shown in a MDS diagram with vectors of the phytoplankton taxonomic groups (Fig. 5). The stress value of 0.01 confirms the statistical significance of the

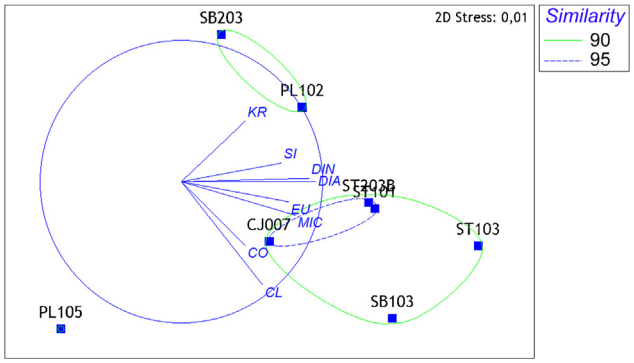

Figure 5 MDS diagram of the distance between the stations considering the groups of phytoplankton (DIA, diatoms; DIN, dinoflagellates; SI, silicoflagellates; CO, coccolithophorids; EU, euglenophytes; CL, chlorophytes; CR, cryptophytes; MIC, microflagellates).

MDS presentation. The similarity percentage of all stations, with regard to the identified groups, is over 80%.

This analysis connected stations in areas of high trophic levels, which are directly influenced by rivers' inflow and anthropogenic load (SB103, ST103), with more than 90% similarity (Fig. 6). There is a strong connection between stations ST101 and ST203B in the Kaštela Bay area with a similarity of over 95%, which are not directly influenced by river inflows, but are, according to the LUSI index, under a strong anthropogenic load. The analysis grouped stations SB203 and PL102, strongly influenced by river inflow and with high LUSI index, but because of their geomorphological features, the stations were not eutrophicated. Station PL105 was significantly different from all other investigated stations because it was not directly influenced by the Neretva River; it had the smallest pronounced anthropogenic eutrophication, and the smallest number of taxa was recorded. Diatoms, dinoflagellates and euglenophytes were mainly responsible for such grouping of the investigated stations.

3.4.2. SIMPER analysis of the phytoplankton community

The phytoplankton community was compared by SIMPER analysis at stations that have the highest value of LUSI index in the investigated areas (SB103, ST103, PL102). The analysis can point out those species that most affect the diversity at stations under a strong anthropogenic eutrophication. The phytoplankton community recorded at station ST103 in Kaštela Bay differs slightly more from the community recorded at PL102 (64.2%) rather than the community at station SB103 (61.63%). The species that contribute the most to the average differences between communities at these stations were proved to be *L. minimus* at station ST103, *S. marinoi* at SB103 and *Chaetoceros* spp. at PL102. Šibenik Bay and Kaštela Bay were characterized by a greater abundance of species *L. minimus* and *S. marinoi*, confirming the eutrophic characteristics of these areas and strong anthropogenic pressure.

3.5. Relationship between biomass and abiotic parameters

Non-parametric Spearman rank order correlations were used to determine the relationship between biomass and abiotic factors in the investigated areas. The analysis includes eight variables throughout the water column: temperature, salinity, nitrate, nitrite, ammonium salts, TIN, orthophosphates and orthosilicates. Results are shown in Table 2.

The negative correlation of phytoplankton biomass with salinity indicates the significant influence of freshwater inflow on the biomass in Šibenik Bay and at the stations located within Kaštela Bay. The stations located outside of Kaštela Bay and those in the Mali Ston Bay area do not exhibit such dependence. The phytoplankton biomass in the Mali Ston Bay area had a statistically significant and positive correlation with all nutrients except orthophosphates. This is associated with the lower trophic level of the area and the weaker anthropogenic influence so that any increase in nutrient concentrations has a positive effect on the biomass of phytoplankton. A similar correlation was observed in the Kaštela Bay area at stations located outside of the bay, where salinity along with nutrients and temperature, positively and significantly affected the growth of biomass. This indicates the lower impact of freshwater inflow to these stations and a greater dependence of biomass with nutrients. The negative correlation of biomass with orthophosphate is expected because as the development of phytoplankton spends orthophosphates, orthophosphate concentration decreases so the phytoplankton biomass increases.

3.6. Relationship between biomass and abundance: ABC-plots

The level of disturbance in the phytoplankton community, whether caused by natural process or anthropogenic load,

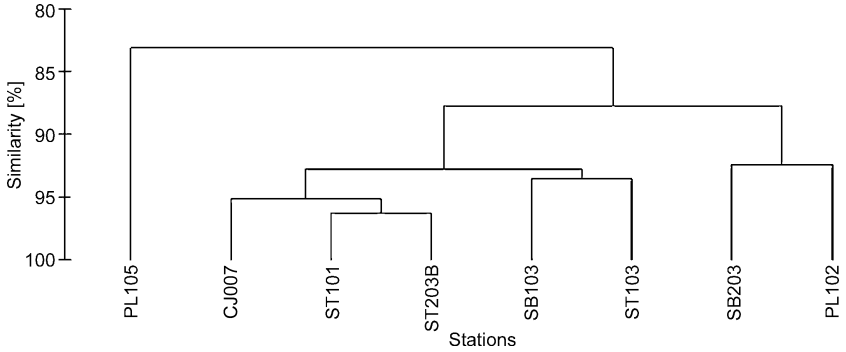

Figure 6 Dendrogram display of the relationship between the stations (similarity [%]) with respect to the phytoplankton groups.

Table 2 Spearman rank order correlations between phytoplankton biomass and abiotic factors (temperature, salinity, nitrates, nitrites, ammonium salts, TIN, orthophosphates and orthosilicates) in the investigated areas.

	Temperature	Salinity	NO_3^-	NO_2^-	NH_4^+	TIN	PO_4^{3-}	SiO_4^{4-}
The Šibenik Bay area SB103, SB203	0.06	−0.49[a]	0.17	0.16	0.16	0.19	−0.30[a]	0.44[a]
Kaštela Bay, inner stations ST101, ST103	0.09	−0.34[a]	−0.12	0.01	0.04	−0.02	−0.05	−0.08
Kaštela Bay, outer stations ST203B, CJ007	0.50[a]	0.42[a]	0.55[a]	0.59[a]	0.57[a]	0.61[a]	0.51[a]	0.53[a]
The Mali Ston Bay area PL102, PL105	−0.17	0.15	0.36[a]	0.53[a]	0.42[a]	0.58[a]	−0.33	0.55[a]

[a] Statistically significant.

was determined by the comparison method of phytoplankton abundance and biomass-abundance/biomass comparison plots (ABC-plots). The *W* index, visible on the graphs, is a practical measure of the trophic status of the particular area. Positive values of the *W* index, indicating the oligotrophic and unpolluted ecosystems, were recorded at the stations located outside Kaštela Bay (ST203B, CJ007) as well at station PL105 in Mali Ston Bay. Negative values of the *W* index, indicating the eutrophic or polluted ecosystems, were recorded at all other stations (SB103, SB203, ST101, ST103, PL102). In the graphic representation of these stations (Fig. 7), there is an evident difference between mesotrophic and eutrophic areas. At stations SB203 and ST101 abundance and biomass curves are closely matched and even intersected, indicating mesotrophic areas, while at stations SB103, ST103 and PL102, the abundance curve on the graph is located above the curve of the biomass, indicating eutrophic condition of these areas.

Kamenir and Dubinsky (2012) have also reported this comparison method of phytoplankton abundance and biomass. In unloaded ecological systems, the k-type species prevail because they are larger and have the capability of storing nutrients. They are slow growing, with abundance rarely dominant, but because of the cell size, those species form the bulk of the biomass. Altisan (2006) confirms a higher concentration of chlorophyll *a* in times when larger phytoplankton organisms prevailed in the community. With an increase of eutrophication, the r-type species are beginning to prevail in the phytoplankton community. Characterized by small size cells, which quickly respond to the increase in nutrient concentrations, they have a rapid growth so abundances become dominant and often create intense blooming. The results obtained in this study confirm the purpose of this method because the stations are under a strong natural or anthropogenic eutrophication (SB103, ST103, PL102), show a dominance of abundance compared to the biomass and a dominance of opportunistic species. The relationship between trophic levels, abundance of the community and cell size is well documented in many works (Cohen, 1991; Cohen et al., 2003; Kamenir and Dubinsky, 2012). In addition, the *W* index at station ST203B indicates an unpolluted condition although the station is under an anthropogenic influence according to the LUSI index (Table 1). That is a consequence of the distance from the coast, which is marked in previous studies (Flo et al., 2011; Ninčević Gladan et al., 2015).

3.7. Biodiversity in the investigated bays

3.7.1. Biodiversity indices

In this paper, we tried to define the characteristics of the community by using the ratio of number of taxa and the total abundance of phytoplankton in the investigated areas.

The maximum of total phytoplankton abundance was observed in Šibenik Bay, but the largest number of species in the total number of cells was noted in Kaštela Bay. The total phytoplankton abundance in the Šibenik and Kaštela Bay area was similar, while in the Mali Ston Bay area, it was considerably lower. We have calculated more types of diversity indices (Margalef's index (*d*), Menhinick's index (*D*), Pielou index (*J'*), Shannon's index (*H'*) and Simpson index (1 − Lambda')) to better define biodiversity in the investigated areas (Table 3).

Spearman's correlation between the abundance of phytoplankton and various diversity indexes shows that Margalef's ($d = 0.574$*), Pielou ($J' = -0.385$*) and Menhinick's ($D = -0.637$*) diversity indexes had a statistically significant correlation with abundance ($p < 0.05$), while Shannon's ($H'(\log) = 0.010$) and Simpson's ($1 - \text{Lambda}' = 0.019$) indexes did not. Although Shannon's diversity index is a commonly used index in biodiversity assessments, recent studies show that it is not linearly related to the trophic gradient (Spatharis and Tsirtsis, 2010). The most significant index is proved to be Menhinick's diversity index (*D*) due to its strong and significant correlation with the abundance of phytoplankton. The obtained negative correlation is expected because in the areas of higher trophic levels an increase in the number of phytoplankton cells is anticipated. A reduction in the diversity of the community is also expected due to opportunistic species that reproduce quickly and occupy the ecological niche, thus reducing the diversity of the phytoplankton community. The effectiveness of Menhinick's diversity index due to its consistent and linear change through the trophic gradient has been documented (Spatharis and Tsirtsis, 2010). Fig. 8 is presenting a seasonal distribution of Menhinick's index in the surface layer for all investigated sites. In the Šibenik and the Kaštela Bay areas, Menhinick's index was generally higher at stations located outside of the bays, in the areas of lower trophic levels, compared to stations located within the bays, areas of higher trophic levels. The Mali Ston Bay area, characterized as a moderate eutrophicated system, has a uniform distribution at both stations. These findings confirmed Menhinick's index

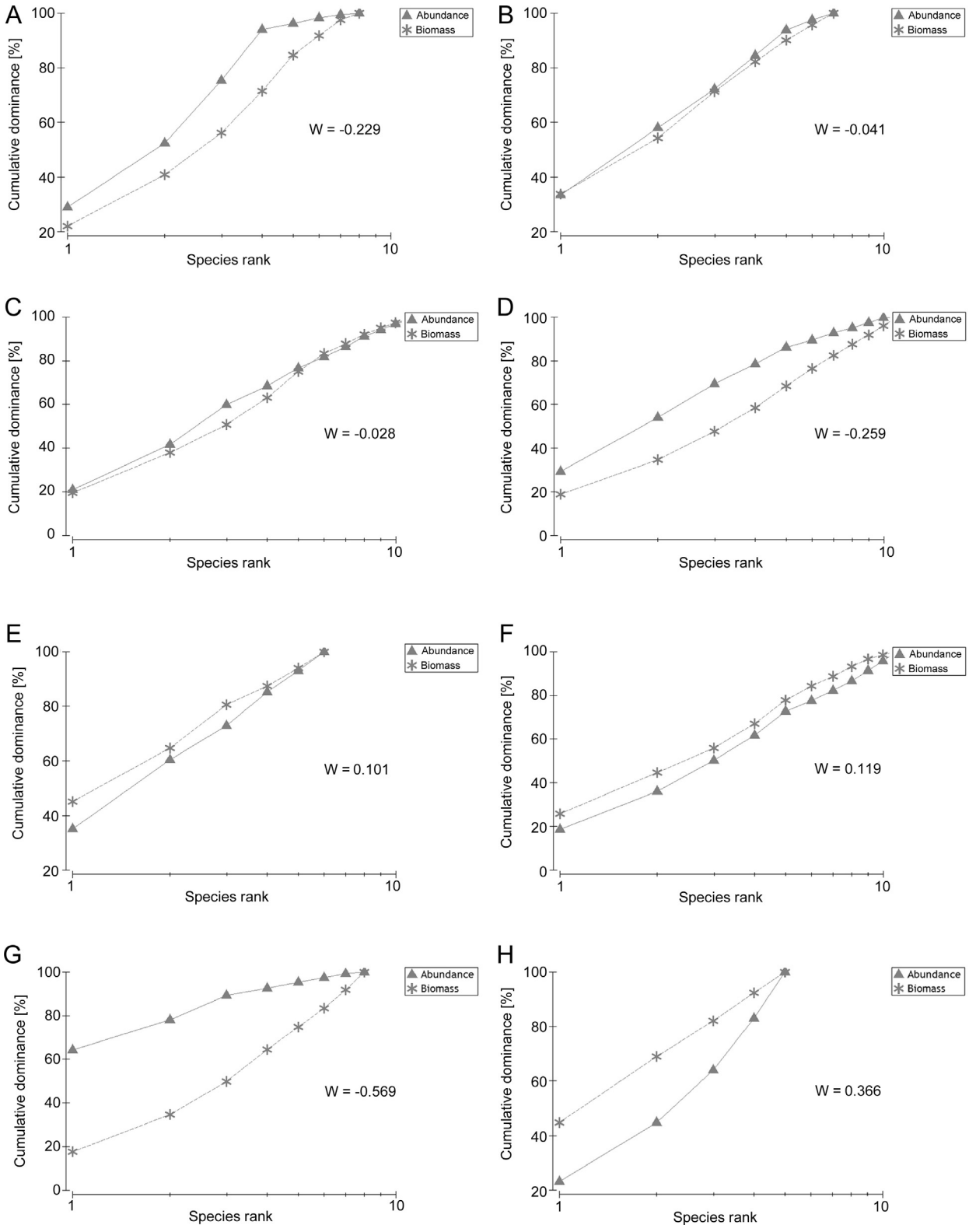

Figure 7 Abundance/biomass comparison plots of phytoplankton in the surface layer at the station SB103 (A), the station SB203 (B), the station ST101 (C), the station ST103 (D), the station ST203B (E), the station CJ007 (F), the station PL102 (G) and the station PL105 (H).

as a good indicator of biodiversity, which is highest in moderately eutrophic conditions because it is directly linked to the abundance of species that prove to be most numerous in moderately eutrophic areas. When assessing biodiversity, one must take into consideration that the phytoplankton community composition is highly sensitive to variation in their environment, which is reflected in the biodiversity assessment. The phytoplankton community consists of a very large

Table 3 Diversity indexes in the investigated areas (including number of species (*S*), the number of cells (*N*), Margalef's index (*d*), Menhinick's index (*D*), Pielou index (*J′*), Shannon's index (*H′*(log)) and Simpson index (1 – Lambda′)); their mean value (mean), the maximum (max) and minimum (min) values.

Diversity indexes	The Šibenik Bay area			The Kaštela Bay area			The Mali Ston Bay area		
	mean	max	min	mean	max	min	mean	max	min
S	15	23	7	15	37	6	12	21	5
N	599,340	5,407,290	35,130	478,606	5,064,990	21,970	238,024	2,891,840	41,030
d	1.090	1.773	0.538	1.129	2.448	0.434	0.878	1.521	0.355
D	0.031	0.052	0.009	0.029	0.058	0.010	0.030	0.057	0.011
J′	0.666	0.894	0.107	0.620	0.887	0.147	0.597	0.801	0.091
H′(log)	1.739	2.382	0.331	1.655	2.528	0.306	1.426	2.150	0.263
1 – Lambda′	0.705	0.889	0.113	0.673	0.893	0.106	0.609	0.821	0.082

number of species, and many taxa simply cannot be identified to the species level by light microscopy of preserved samples (Ojaveer et al., 2010). Some of the taxa were identified at a higher taxonomic level than species, which may underestimate the biodiversity in cases where the genus or higher unit actually includes several species. Previous studies showed that the best option is to use all of the available data and accept the fact that the taxonomic units vary, since discarding parts of the data or aggregating those means losing information related to biodiversity (Uusitalo et al., 2013).

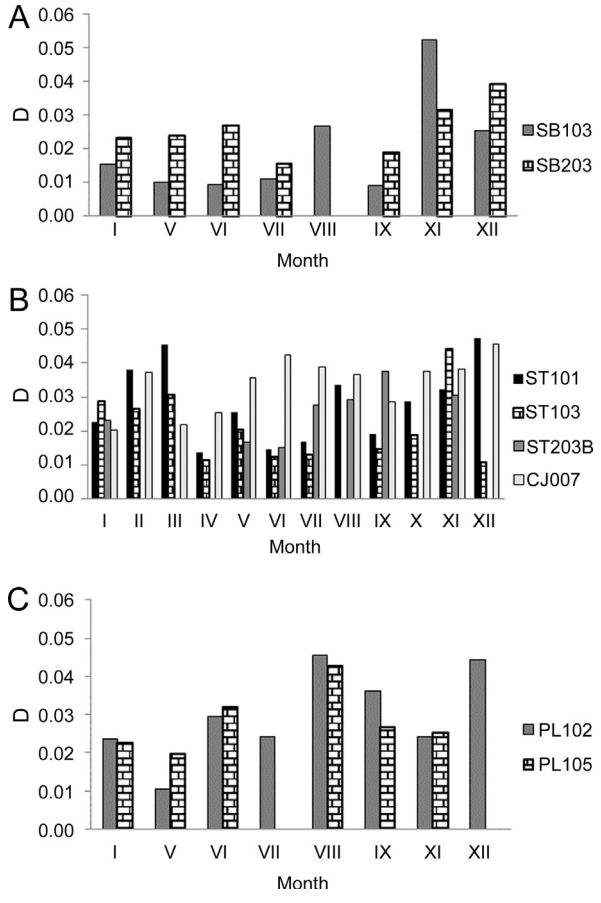

Figure 8 Seasonal distribution of Menhinick's diversity index (*D*) at the investigated stations in the surface layer of the Šibenik Bay area (A), the Kaštela Bay area (B) and the Mali Ston Bay area (C).

3.7.2. The cumulative dominance plots

In this paper, biodiversity is also presented through the curves of cumulative dominance of species (k-dominance plots) that represents the relationship between the number of organisms and the number of taxa found in the sample (Warwick and Clarke, 1991). The points on the graph indicate the percentage of the number of certain species in the phytoplankton community, and a curve that is placed highest on the graph has the lowest diversity.

The cumulative dominance curves in the surface layer for all investigated stations are presented in Fig. 9. There is a visible grouping of the stations placed in the area of higher trophic levels (SB103, ST101, ST103, PL102). These curves are placed higher on the chart, and they have a lower diversity from the stations (SB203, ST203B, CJ007, PL105) located further from the coast and away from sources of eutrophication, where the more diverse community was recorded.

Seasonal distribution of the k-dominance curves is a reflection of the seasonal distribution of the phytoplankton community, and the natural spring blooms are common and well documented in the subtropical seas (Carstensen et al., 2004; Spatharis et al., 2007; Zingone et al., 1995). Greater diversity in the winter period could be related to a moderate trophic condition caused by mixing of the water column and increasing concentrations of nutrients in the surface layer, which in addition to sufficient light during mild winters favour the grow of phytoplankton.

Previous studies show that a continuous inflow of nutrients results in communities dominated by species that are more competitive for limiting nutrients, while weaker competitor species are rare or non-existent in the community (Capblancq, 1990; Hardin, 1960; Sommer, 1985). The case of non-continuous inflow of nutrients increases the coexistence between species, leading to more species in the community (Harris, 1986; Margalef, 1978). However, by further eutrophication, the number of species drastically reduces, and the diversity rapidly decreases (Crossetti et al., 2008; Polishchuk, 1999), which is consistent with the hypothesis that the maximum number of species occurs in areas with moderate trophic levels (Connell, 1978). Spatharis et al. (2007) in the Aegean Sea and Aktan (2011) in the eastern Mediterranean obtained similar results. Crossetti et al. (2008) have also reported that biodiversity loss following trophic change was not a single dimension of a single factor, but rather a

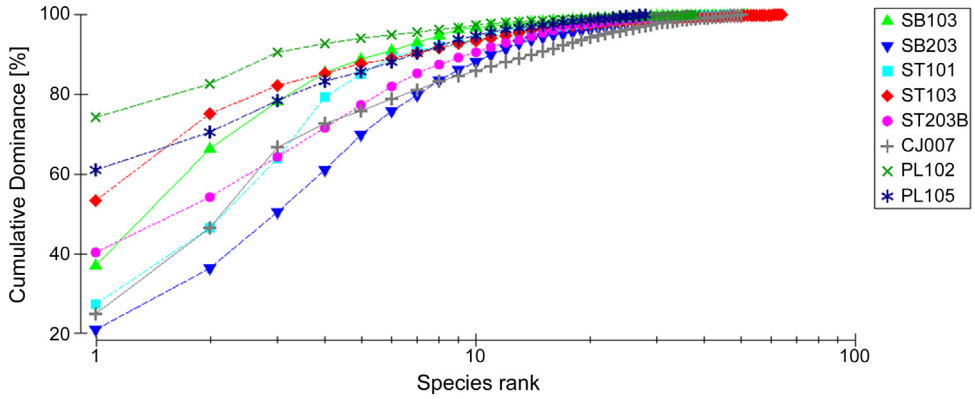

Figure 9 The k-dominance curves in the surface layer for all investigated stations.

template of factors co-varying in consequence of the larger levels of the biomass. Therefore, it is important to monitor the bays' area with a wide range of physical, chemical and biological parameters to make better ecological characterization of the study area.

4. Conclusion

This study confirms that biodiversity of the phytoplankton community is dependent on its spatial and temporal distribution in relation to environmental conditions, as well as its composition.

Diatoms were the most represented group of the phytoplankton community in all three bays. Species that were highlighted as significant for the specific area in this study were *S. marinoi* in Šibenik Bay, *L. minimus* in Kaštela Bay and the genus *Chaetoceros* spp. in Mali Ston Bay. Dinoflagellates were the second most significant group. A noticeably larger abundance of dinoflagellates was recorded in the Kaštela Bay area, characterized as the most influenced by anthropogenic pressure.

A MDS similarity analysis, based on the abundance of phytoplankton taxonomy groups, shows the close connection between stations strongly influenced by anthropogenic pressure. In addition, the k-dominance curves show the lowest biodiversity at these stations, and ABC curves with the negative *W* index at these stations indicate the conditions of stronger eutrophication.

Further monitoring of the bay areas is needed and an effort should be taken in order to keep the eutrophication at a moderate level, optimal for the phytoplankton community to maintain its great biodiversity, which is a good indicator of a balanced ecosystem.

Acknowledgements

The authors wish to thank H. Prelesnik bacc.ing. for analysing chlorophyll *a*, I. Pezo bacc.ing. for assistance with the fieldwork and all the people at the Laboratory of Plankton and Shellfish toxicity for their help and support.

This work has been fully supported/supported in part by Croatian Science Foundation under the project IP-2014-09-3606 (Marine plankton as a tool for assessment of climate and anthropogenic influence on the marine ecosystem).

References

Aktan, Y., 2011. Large-scale patterns in summer surface water phytoplankton (except picophytoplankton) in the Eastern Mediterranean. Estuar. Coast. Shelf Sci. 91 (4), 551—558, http://dx.doi.org/10.1016/j.ecss.2010.12.010.

Altisan, I.A.R., 2006. Effects on light and nutrient gradient on the taxonomic composition, size structure and physiological status of the phytoplankton community within a temperate eutrophic estuary. (Ph.D. thesis). Univ. Southampton, 205 pp.

Barić, A., Kušpilić, G., Matijević, S., 2002. Nutrient (N, P, Si) fluxes between marine sediments and water column in coastal and open Adriatic. Hydrobiologia 475—476 (1), 151—159, http://dx.doi.org/10.1023/A:1020386204869.

Barić, A., Marasović, I., Gačić, M., 1992. Eutrophication phenomenon with special reference to the Kaštela Bay. Chem. Ecol. 6 (1—4), 51—68, http://dx.doi.org/10.1080/02757549208035262.

Bonacci, O., Ljubenkov, I., 2005. New insights into the Krka river hydrology. Hrvatske Vode 13 (52), 265—281.

Bray, J.R., Curtis, J.T., 1957. An ordination of the upland forest communities of southern Wisconsin. Ecol. Monogr. 27 (4), 325—349, http://dx.doi.org/10.2307/1942268.

Brettum, P., Andersen, T., 2005. The Use of Phytoplankton as Indicators of Water Quality. NIVA Rep. SNO 4818-2004, 33 pp.

Bužančić, M., Ninčević Gladan, Ž., Marasović, I., Kušpilić, G., Grbec, B., Matijević, S., 2012. Population structure and abundance of phytoplankton in three bays on the eastern Adriatic coast, Šibenik Bay, Kaštela Bay and Mali Ston Bay. Acta Adriat. 53 (3), 413—435.

Capblancq, J., 1990. Nutrient dynamics and pelagic food web interactions in oligotrophic and eutrophic environments: an overview. Hydrobiologia 207 (1), 114, http://dx.doi.org/10.1007/BF00041435.

Carstensen, J., Conley, D.J., Henriksen, P., 2004. Frequency, composition and causes of summer phytoplankton blooms in a shallow coastal ecosystem, the Kattegat. Limnol. Oceanogr. 49 (1), 190—201, http://dx.doi.org/10.4319/lo.2004.49.1.0191.

Cetinić, I., Viličić, D., Burić, Z., Olujić, G., 2006. Phytoplankton seasonality in a high stratified karstic estuary (Krka. Adriatic Sea). Hydrobiologia 555 (1), 31—40, http://dx.doi.org/10.1007/s10750-005-1103-7.

Clarke, K.R., 1993. Non-parametric multivariate analyses of changes in community structure. Aust. J. Ecol. 18 (1), 117—143, http://dx.doi.org/10.1111/j.1442-9993.1993.tb00438.x.

Clarke, K.R., Warwick, R.M., 2001. Changes in Marine Communities: An Approach to Statistical Analysis and Interpretation, 2nd ed. Natur. Environ. Res. Coun., PRIMER-E, Plymouth, 234 pp.

Cohen, J.E., 1991. Report on the First International Conference on the Conservation and Biodiversity of Lake Tanganyika. B.S.P., Washington, DC, 128 pp.

Cohen, J.E., Jonsson, T., Carpenter, S.R., 2003. Ecological community description using the food web, species abundance, and body size. Proc. Natl. Acad. Sci. U.S.A. 100 (4), 1781–1786, http://dx.doi.org/10.1073/pnas.232715699.

Collos, Y., Vaquer, A., Bibent, B., Slawyk, G., Garcia, N., Souchu, P., 1997. Variability in nitrate uptake kinetics of phytoplankton communities in a Mediterranean coastal lagoon. Estuar. Coast. Mar. Sci. 44 (3), 369–375, http://dx.doi.org/10.1006/ecss.1996.0121.

Connell, J.H., 1978. Diversity in tropical rain forests and coral reefs. Science 199 (4335), 1302–1310, http://dx.doi.org/10.1126/science.199.4335.1302.

Crossetti, L.O., Bicudo, D.C., Bicudo, C.E.M., Bini, L.M., 2008. Phytoplankton biodiversity changes in a shallow tropical reservoir during the hypertrophication process. Braz. J. Biol. 68 (4), 1061–1067, http://dx.doi.org/10.1590/S1519-69842008000500013.

Crouzet, P., Nixon, S., Rees, Y., Parr, W., Laffon, L., Bogestrand, J., Kristensen, P., Lallana, C., Izzo, G., Bokn, T., Bak, J., Lack, T.J., Thyssen, N., 1999. Nutrients in European Ecosystems. Environ. Assess. Rep. 4. EEA, Copenhagen, 155 pp.

Čalić, M., Carić, M., Kršinić, F., Jasprica, N., Pećarević, M., 2013. Controlling factors of phytoplankton seasonal succession in oligotrophic Mali Ston Bay (south-eastern Adriatic). Environ. Monit. Assess. 185 (9), 7543–7563, http://dx.doi.org/10.1007/s10661-013-3118-2.

DeManche, J.M., Curl, J.H.C., Lundy, D.W., Donaghay, P.L., 1979. The rapid response of the marine diatom *Skeletonema costatum* to changes in external and internal nutrient concentration. Mar. Biol. 53 (4), 323–333, http://dx.doi.org/10.1007/BF00391615.

Edwards, V.R., Tetta, P., Jonesb, K.J., 2003. Changes in the yield of chlorophyll *a* from dissolved available inorganic nitrogen after an enrichment event – applications for predicting eutrophication in coastal waters. Cont. Shelf Res. 23 (17–19), 1771–1785, http://dx.doi.org/10.1016/j.csr.2003.06.003.

European Commission, 2008. Marine Strategy Framework Directive 2008/56/EC. Statute text: http://eur-lex.europa.eu/legal-content/EN/TXT/?uri=uriserv:OJ.L_.2008.164.01.0019.01.ENG&toc=OJ:L:2008:164:TOC.

Field, J.G., Clarke, K.R., Warwick, R.M., 1982. A practical strategy for analysing multispecies distribution patterns. Mar. Ecol. Prog. Ser. 8 (1), 37–52, http://dx.doi.org/10.3354/meps008037.

Flo, E., Garcés, E., Manzanera, M., Camp, J., 2011. Coastal inshore waters in the NW Mediterranean: physicochemical and biological characterization and management implications. Estuar. Coast. Shelf Sci. 93 (4), 279–289, http://dx.doi.org/10.1016/j.ecss.2011.04.002.

Gowen, R.J., Tetta, P., Jones, K.J., 1992. Predicting marine eutrophication: the yield of chlorophyll from nitrogen in Scottish coastal waters. Mar. Ecol. Prog. Ser. 85 (1–2), 153–161, http://dx.doi.org/10.3354/meps085153.

Grasshoff, K., 1976. Methods of Seawater Analysis. VCH, Weinheim, 307 pp.

Gržetić, Z., Precali, R., Degobbis, D., Škrivanić, A., 1991. Nutrient enrichment and phytoplankton response in an Adriatic karstic estuary. Mar. Chem. 32 (2–4), 313–331, http://dx.doi.org/10.1016/0304-4203(91)90046-Y.

Guinder, V.A., López-Abbate, M.C., Berasategui, A.A., Negrin, V.L., Zapperi, G., Pratolongo, P.D., Fernández Severini, M.D., Popovich, C.A., 2015. Influence of the winter phytoplankton bloom on the settled material in a temperate shallow estuary. Oceanologia 57 (1), 50–60, http://dx.doi.org/10.1016/j.oceano.2014.10.002.

Hardin, G., 1960. The competitive exclusion principle. Science 131 (3409), 1292–1297.

Harris, P., 1986. Phytoplankton Ecology: Structure, Function, and Fluctuation. Chapman and Hall, London, 384 pp.

Jasprica, N., Carić, M., 1994. Fine-scale distribution of dominant *Chaetoceros* species in Gruž and Mali Ston Bays (Southern Adriatic). In: Marino, D., Monteresor, M. (Eds.), Proc. 13th International Diatom Symp. Biopress Ltd., 207–218.

Jasprica, N., Carić, M., Kršinić, F., Kapetanović, T., Batistić, M., Njire, J., 2012. Planktonic diatoms and their environment in the lower Neretva River estuary (Eastern Adriatic Sea, NE Mediterranean). Nova Hedwigia 141, 405–430.

Kamenir, Y., Dubinsky, Z., 2012. Disturbance of opportunistic small-celled phytoplankton in Lake Kinneret. ISRN Botany 2012, http://dx.doi.org/10.5402/2012/123607, 7 pp., (Article ID 123607).

Kušpilić, G., 2005. Anthropogenic inputs, ecological state and impact of biodiversity in the marine environment. UNDP/GEF "Coast" project, Conservation and sustainable use of biodiversity in the Dalmatian Coast through greening coastal development, Project PDF B phase, Tech. Rep., Split, 50 pp.

Kušpilić, G., Precali, R., Dadić, V., Ninčević-Gladan, Ž., Šurmanović, D., Marjanović Rajčić, M., 2011. Prijedlog granica klasa fizikalno-kemijskih parametara unutar pokazatelja Fitoplankton za područje prijelaznih i priobalnih voda Republike Hrvatske. Hrvatske Vode 76, 101–110.

Lagus, A., Suomela, J., Weithoff, G., Heikkilä, K., Helminen, H., Sipura, J., 2004. Species-specific differences in phytoplankton responses to N and P enrichments and the N:P ratio in the Archipelago Sea, northern Baltic Sea. J. Plankton Res. 26 (7), 779–798, http://dx.doi.org/10.1093/plankt/fbh070.

Legović, T., Žutić, V., Gržetić, Z., Cauwet, G., Precali, R., Viličić, D., 1994. Eutrophication in the Krka estuary. Mar. Chem. 46 (1), 203–215, http://dx.doi.org/10.1016/0304-4203(94)90056-6.

Ljubenkov, I., 2015. Hydrodynamic modeling of stratified estuary: case study of the Jadro River (Croatia). J. Hydrol. Hydromech. 63 (1), 29–37, http://dx.doi.org/10.1515/johh-2015-0001.

Ludwig, W., Dumont, E., Meybeck, M., Heussner, S., 2009. River discharges of water and nutrients to the Mediterranean and Black Sea: major drivers for ecosystem changes during past and future decades? Prog. Oceanogr. 80 (3), 199–217, http://dx.doi.org/10.1016/j.pocean.2009.02.001.

Marasović, I., Gačić, M., Kovačević, V., Krstulović, N., Kušpilić, G., Pucher-Petković, T., Odžak, N., Šolić, M., 1991. Development of the red tide in the Kaštela Bay (Adriatic Sea). Mar. Chem. 32 (2–4), 375–385, http://dx.doi.org/10.1016/0304-4203(91)90050-7.

Marasović, I., Ninčević, Ž., 1997. Primary production – a basic factor in sea water quality assessment in the middle Adriatic. In: Rajar, R., Brebbia, C.A. (Eds.), Water Pollution IV: Modelling, Measuring and Prediction. Comput. Mech., Southampton, 649–658.

Marasović, I., Pucher-Petković, T., 1985. Effect of eutrofication on the structure of the coastal phytoplankton community. Rapp. Comm. Int. Mer. Medit. 29 (9), 137–139.

Margalef, R., 1978. Life-forms of phytoplankton as survival alternatives in an unstable environment. Oceanol. Acta 1 (4), 493–509.

McQuatters-Gollop, A., Gilbert, A.J., Mee, L.D., Vermaat, J.E., Artioli, Y., Humborg, C., Wulff, F., 2009. How well do ecosystem indicators communicate the effects of anthropogenic eutrophication? Estuar. Coast. Shelf Sci. 82 (4), 583–596, http://dx.doi.org/10.1016/j.ecss.2009.02.017.

Ninčević Gladan, Ž., Bužančić, M., Kušpilić, G., Grbec, B., Matijević, S., Skejić, S., Marasović, I., Morović, M., 2015. The response of phytoplankton community to anthropogenic pressure gradient in the coastal waters of the eastern Adriatic Sea. Ecol. Indic. 56, 106–115, http://dx.doi.org/10.1016/j.ecolind.2015.03.018.

Ninčević Gladan, Ž., Marasović, I., Grbec, B., Skejić, S., Bužančić, M., Kušpilić, G., Matijević, S., Matić, F., 2009. Inter-decadal variability in phytoplankton community in the middle Adriatic (Kaštela Bay) in relation to the North Atlantic Oscillation. Estuar. Coast. 33 (2), 376–383, http://dx.doi.org/10.1007/s12237-009-9223-3.

Ojaveer, H., Jaanus, A., MacKenzie, B.R., Martin, G., Olenin, S., Radziejewska, T., Telesh, I., Zettler, M.L., Zaiko, A., 2010. Status of biodiversity in the Baltic Sea. PLoS One 5 (9), pe12467, http://dx.doi.org/10.1371/journal.pone.0012467.

Orlić, M., Beg Paklar, G., Pasarić, Z., Grbec, B., Pasarić, M., 2006. Nested modeling of the east Adriatic coastal waters. Acta Adriat. 47 (Suppl.), 219—245.

Pick, F.R., Caron, D.A., 1987. Picoplankton and nanoplankton biomass in Lake Ontario: relative contribution of phototrophic and heterotrophic communities. Can. J. Fish. Aquat. Sci. 44 (12), 2164—2172, http://dx.doi.org/10.1139/f87-265.

Polishchuk, L.V., 1999. Contribution analysis of disturbance-caused changes in phytoplankton diversity. Ecology 80 (2), 721—725, http://dx.doi.org/10.1890/0012-9658(1999)080[0721:CAODCC]2.0.CO;2.

Richardson, K., Nielsen, T.G., Pedersen, F.B., Heilmann, J.P., Kokkegaardand, B., Kaas, H., 1998. Spatial heterogeneity in the structure of the planktonic food web in the North Sea. Mar. Ecol. Prog. Ser. 168, 197—211.

Skejić, S., Bojanić, N., Matijević, S., Vidjak, O., Grbec, B., Ninčević Gladan, Ž., Šestanović, S., Šantić, D., 2014. Analysis of the phytoplankton community in the vicinity of domestic sewage outflow during stratified conditions. Medit. Mar. Sci. 15 (3), 574—586, http://dx.doi.org/10.12681/mms.866.

Skejić, S., Marasović, I., Ninčević, Ž., 2012. Phytoplankton assemblages at fish farm in Maslinova Bay (the Island of Brač). Croat. J. Fish. 70 (2), 41—52.

Skejić, S., Vilibić, I., Matijević, S., Jozić, S., Ninčević Gladan, Ž., Morović, M., Prelesnik, H., 2015. Long-term regulating mechanisms of phytoplankton biomass in a traditional shellfish aquaculture area. Fresen. Environ. Bull. 24 (9), 3001—3013.

Smayda, T.J., 2000. Ecological features of harmful algal blooms in coastal upwelling ecosystems. S. Afr. J. Mar. Sci. 22 (1), 219—253, http://dx.doi.org/10.2989/025776100784125816.

Smith, V.H., 2006. Responses of estuarine and coastal marine phytoplankton to nitrogen and phosphorus enrichment. Limnol. Oceanogr. 51 (1 (pt. 2)), 377—384, http://dx.doi.org/10.3410/f.1031076.365427.

Sommer, U., 1985. Comparison between steady state and non-steady state competition: experiments with natural phytoplankton. Limnol. Oceanogr. 30 (2), 335—346, http://dx.doi.org/10.4319/lo.1985.30.2.0335.

Spatharis, S., Danielidis, D.B., Tsirtsis, G., 2007. Recurrent *Pseudonitzschia calliantha* (Bacillariophyceae) and *Alexandrium insuetum* (Dinophyceae) winter blooms induced by agricultural runoff. Harmful Algae 6 (6), 811—822, http://dx.doi.org/10.1016/j.hal.2007.04.006.

Spatharis, S., Tsirtsis, G., 2010. Ecological quality scales based on phytoplankton for the implementation of Water Framework Directive in the Eastern Mediterranean. Ecol. Indic. 10 (4), 840—847, http://dx.doi.org/10.1016/j.ecolind.2010.01.005.

Stonik, V., Selina, M.S., 2001. Species composition and seasonal dynamics of density and biomass of Euglenoids in Peter the Great bay, Sea of Japan. Russ. J. Mar. Biol. 27 (3), 174—176, http://dx.doi.org/10.1023/A:1016769519454.

Strickland, J.D.H., Parsons, T.R., 1972. A practical handbook of seawater analysis. Bull. Fish. Res. Bd. Can. 167, http://dx.doi.org/10.1002/iroh.19700550118, 310 pp.

Su, J., Tian, T., Krasemann, H., Schartau, M., Wirtz, K., 2015. Response patterns of phytoplankton growth to variations in resuspension in the German Bight revealed by daily MERIS data in 2003 and 2004. Oceanologia 57 (4), 328—341, http://dx.doi.org/10.1016/j.oceano.2015.06.001.

Svensen, C., Viličić, D., Wassmann, P., Arashkevich, E., Ratkova, T., 2007. Plankton distribution and vertical flux of biogenic matter during high summer stratification in the Krka estuary (Eastern Adriatic). Estuar. Coast. Shelf Sci. 71 (3), 381—390, http://dx.doi.org/10.1016/j.ecss.2006.07.022.

Utermöhl, H., 1958. Zur Vervollkommung der guantitativen Phytoplankton Methodik. Mitt. Int. Ver. Theor. Angew. Limnol. 9, 1—38.

Uusitalo, L., Fleming-Lehtinen, V., Hällfors, H., Jaanus, A., Hällfors, S., London, L., 2013. A novel approach for estimating phytoplankton biodiversity. ICES J. Mar. Sci. 70 (2), 408—417, http://dx.doi.org/10.1093/icesjms/fss198.

Viličić, D., 1989. Phytoplankton population density and volume as indicators of eutrophication in the eastern part of Adriatic Sea. Hydrobiologia 174 (2), 117—132, http://dx.doi.org/10.1007/BF00014060.

Viličić, D., Jasprica, N., Carić, M., Burić, Z., 1998. Taxonomic composition and seasonal distribution of microphytoplankton in Mali Ston Bay (eastern Adriatic). Acta Bot. Croat. 57, 29—48.

Viličić, D., Legović, T., Žutić, V., 1989. Vertical distribution of phytoplankton in a stratified estuary. Aquat. Sci. 51 (1), 31—46, http://dx.doi.org/10.1007/BF00877779.

Vollenweider, R.A., 1976. Advances in defining critical loading levels for phosphorus in lake eutrophication. Mem. Ist. Ital. Idrobiol. 33, 53—83.

Vollenweider, R.A., 1992. Coastal marine eutrophication: principles and control. In: Vollenweider, R.A., Marchetti, R., Viviani, R. (Eds.), Marine Coast. Eutroph. Elsevier, London, 1—20, http://dx.doi.org/10.1016/B978-0-444-89990-3.50011-0.

Warwick, R.M., Clarke, K.R., 1991. A comparison of some methods for analysing changes in benthic community structure. J. Mar. Biol. Assoc. U.K. 71 (1), 225—244, http://dx.doi.org/10.1017/s0025315400037528.

Watson, S.B., McCauley, E., Downing, J.A., 1997. Patterns in phytoplankton taxonomic composition across temperate lakes of differing nutrient status. Limnol. Oceanogr. 42 (3), 487—495, http://dx.doi.org/10.4319/lo.1997.42.3.0487.

Willen, E., Hajdu, S., Pejler, Y., 1990. Summer phytoplankton in 73 nutrient-poor Swedish lakes. Classification, ordination and choice of long-term monitoring objects. Limnologica 20 (2), 217—227.

Zingone, A., Casotti, R., Ribera d'Alcala', M., Scardi, M., Marino, D., 1995. 'St. Martin's Summer': the case of an autumn phytoplankton bloom in the Gulf of Naples (Mediterranean Sea). J. Plankton Res. 17 (3), 575—593, http://dx.doi.org/10.1093/plankt/17.3.575.

Žutić, V., Legović, T., 1987. A film of organic matter at the freshwater/seawater interface of an estuary. Nature 328 (6131), 612—614, http://dx.doi.org/10.1038/328612a0.

Oceanologia (2016) 58, 317—326

Available online at www.sciencedirect.com

ScienceDirect

journal homepage: www.journals.elsevier.com/oceanologia/

ORIGINAL RESEARCH ARTICLE

Performance of operational satellite bio-optical algorithms in different water types in the southeastern Arabian Sea

P. Minu [a], Aneesh A. Lotliker [b], S.S. Shaju [a], P. Muhamed Ashraf [a,*], T. Srinivasa Kumar [b], B. Meenakumari [c]

[a] *ICAR — Central Institute of Fisheries Technology, Kochi, India*
[b] *Indian National Centre for Ocean Information Services (INCOIS), Hyderabad, India*
[c] *Indian Council for Agricultural Research, New Delhi, India*

Received 31 October 2015; accepted 30 May 2016
Available online 16 June 2016

KEYWORDS
Remote sensing reflectance;
Algorithms;
Chlorophyll-*a*;
CDOM;
Arabian Sea;
SATCORE

Summary The *in situ* remote sensing reflectance (R_{rs}) and optically active substances (OAS) measured using hyperspectral radiometer, were used for optical classification of coastal waters in the southeastern Arabian Sea. The spectral R_{rs} showed three distinct water types, that were associated with the variability in OAS such as chlorophyll-*a* (chl-*a*), chromophoric dissolved organic matter (CDOM) and volume scattering function at 650 nm (β_{650}). The water types were classified as Type-I, Type-II and Type-III respectively for the three R_{rs} spectra. The Type-I waters showed the peak R_{rs} in the blue band (470 nm), whereas in the case of Type-II and III waters the peak R_{rs} was at 560 and 570 nm respectively. The shifting of the peak R_{rs} at the longer wavelength was due to an increase in concentration of OAS. Further, we evaluated six bio-optical algorithms (OC3C, OC4O, OC4, OC4E, OC3M and OC4O2) used operationally to retrieve chl-*a* from Coastal Zone Colour Scanner (CZCS), Ocean Colour Temperature Scanner (OCTS), Sea-viewing Wide Field-of-view Sensor (SeaWiFS), MEdium Resolution Imaging Spectrometer (MERIS), Moderate Resolution Imaging Spectroradiometer (MODIS) and Ocean Colour Monitor (OCM2). For chl-*a* concentration greater than 1.0 mg m^{-3}, algorithms based on the reference band ratios 488/510/520 nm to

* Corresponding author at: ICAR — Central Institute of Fisheries Technology, Matsyapuri P.O., Kochi 682029, India. Tel.: +91 4842412300; fax: +91 4842666845.
E-mail address: ashrafp2008@gmail.com (P.M. Ashraf).

Peer review under the responsibility of Institute of Oceanology of the Polish Academy of Sciences.

Production and hosting by Elsevier

http://dx.doi.org/10.1016/j.oceano.2016.05.005

547/550/555/560/565 nm have to be considered. The assessment of algorithms showed better performance of OC3M and OC4. All the algorithms exhibited better performance in Type-I waters. However, the performance was poor in Type-II and Type-III waters which could be attributed to the significant co-variance of chl-*a* with CDOM.

1. Introduction

Ocean colour remote sensing has been widely used as a tool to determine the surface chlorophyll-*a* (chl-*a*) concentration which acts as a proxy for phytoplankton biomass. Several empirical and semi-analytical algorithms have been proposed for the retrieval of chl-*a* from satellite ocean colour data. These algorithms were based on the non-linear relationship between oceanic reflectance and *in situ* measured chl-*a*, more precisely the ratios of reflectance in blue and green bands or their combinations (Lee et al., 2002; O'Reilly et al., 1998, 2000). These algorithms using the spectral ratios of reflectance were mainly attributed to Case 1 waters where the optical properties were determined mainly by phytoplankton and their accessory pigments. For Case 2 waters, apart from phytoplankton, other optically active substances (OAS) such as chromophoric dissolved organic matter (CDOM) and total suspended matter (TSM) contribute significantly to the reflectance (Morel and Prieur, 1977).

The development of ocean chlorophyll 2-band (OC2) and ocean chlorophyll 4-band (OC4) algorithms was done using SeaBAM data set. The OC2 algorithm was revised (OC2 v2) based on an extensive data set of 1174 *in situ* observations and thereafter with the SIMBIOS data set (McClain and Fargion, 1999). O'Reilly et al. (2000) updated OC2 and OC4 with 2853 *in situ* data sets (OC2v2 and OC4v4) and suggested the need to determine accuracy of these revised algorithms in lowest chl-*a* concentrations.

The characteristics of the reflectance spectrum, in terms of shape and magnitude, are largely influenced by the presence of OAS within the water column (Minu et al., 2014; Pierson and Strombeck, 2000). In other words, the apparent optical properties (AOP) of aquatic media, such as remote sensing reflectance (R_{rs}), largely affected by OAS and geometry of ambient light field can be quantified using inherent optical properties (IOPs) of the OAS (Mobley, 1994; Morel, 1991). The fundamental IOPs influencing the R_{rs} are absorption (a), scattering (b) and volume scattering function (β). The phytoplankton pigment, chl-*a*, has a tendency to absorb light in the blue and red bands of the visible electromagnetic spectrum (V-EMS) with the former being the primary peak. The CDOM also exhibits strong absorption in UV and the shorter wavelength band of V-EMS whereas the suspended matter usually scatters in the longer wavelength band. Apart from this, the water molecules themselves absorb strongly in the red part of V-EMS. Further, the volume scattering describes the angular distribution of light scattered from an incident beam. In the absence of inelastic scattering, IOP of a medium is completely determined by the absorption coefficient and β. These when combined with the angular and spectral distribution of the incident radiance field, just below the surface, the full radiative flux balance of the ocean can be simulated (Lee and Lewis, 2003). Studies using hyperspectral radiometers, on the relationship between IOP and concentration of OAS, indicated the presence of identifiable sub-types of coastal water within the conventional Case 2 classification (Mckee and Cunningham, 2006).

The ratio based empirical algorithms for the retrieval of chl-*a* from CZCS, MOS-B, IRS-P4-OCM and SeaWiFS have been already carried out in the southeastern Arabian Sea. Sathe and Jadhav (2001) studied retrieval of chl-*a* using sea-leaving radiance from MOS-B and showed that the single ratio of CZCS algorithm fails in the Arabian Sea. They also reported that the two factor algorithm of SeaWIFS fails in 30% of the cases. Further, Nagamani et al. (2008) reported that OC4v4 algorithm overestimates chl-*a* in the northern Arabian Sea when compared to MBR based OCM-2 algorithm. In addition to these, Chauhan et al. (2002) evaluated the accuracy, precision and suitability of different ocean colour algorithms for the Arabian Sea. According to their study, OC2 and OC4 algorithms performed well in Case 1 waters of the Arabian Sea. But both algorithms failed to estimate chlorophyll in *Trichodesmium* dominated waters. Tilstone et al. (2011) also assessed three algorithms, OC4v6, Carder and OC5, for retrieving chl-*a* in coastal areas of the Bay of Bengal and open ocean areas of the Arabian Sea. Based on the accuracy assessment, they recommended the use of the OC5 algorithm in the area of study. Most of these studies were confined to oligotrophic to mesotrophic waters. Assessment of MODIS-aqua chlorophyll-*a* algorithms in coastal and shelf waters of the southeastern Arabian Sea showed better performance of OC3M than GSM and GIOP (Tilstone et al., 2013). However, our study deals with mesotrophic to eutrophic waters. The problem with estimating chl-*a* from an ocean colour satellite sensor involves two critical steps. The first step is to eliminate the effect of the atmospheric contribution and the second step is to select a suitable bio-optical algorithm. In this study, we have focused on *in situ* bio-optical data, measured using hyperspectral radiometer, in the optically complex waters of the southeastern Arabian Sea, with the following objectives:

1. Analyzing the spectral remote sensing reflectance in the view of distribution of OAS.
2. Evaluation of operational empirical algorithm in different water types.

2. Study area

A part of the southeastern Arabian Sea forms the study area (Fig. 1). The area has a strong monsoonal influence resulting

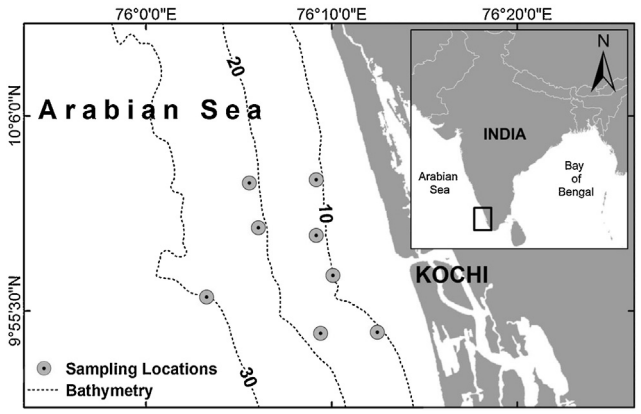

Figure 1 Map of study area showing the sampling stations.

in seasonal changes in hydrographic conditions influenced by river water discharge and surface circulation. During pre-monsoon season (February–May) wind-induced upwelling along with a northward undercurrent and a southward surface flow associated with strong vertical mixing are observed off Kochi waters (Kumar and Kumar, 1996). During the monsoon period, freshwater discharge from adjoining rivers increases the nutrient concentrations of the coastal waters along with the detrital load. These rapid changes often lead to very high production at primary and secondary levels (George et al., 2013). Upwelling process supported by the southerly current is also observed along the coastal waters during monsoon season (Joshi and Rao, 2012). The previous studies reported that freshwater discharge from the estuary and the high organic load of the bottom sediment are the potential factors affecting the biogeochemistry of the study area (Iyer et al., 2003; Srinivas and Dineshkumar, 2006).

3. Material and methods

3.1. *In situ* data

The data used for the present study was generated as a part of SATellite Coastal and Oceanographic REsearch (SATCORE) programme coordinated by Indian National Centre for Ocean Information Services (INCOIS). The data was generated, with monthly frequency, from eight stations, between April 2009 and 2011. The sampling was carried out using commercial purse seiner. Satlantic™ hyperspectral radiometer (HyperOCRII) was operated in all the stations. The instrument contains optical sensors which measure downwelling surface irradiance (E_s) and profiles of upwelling radiance (L_u) and downwelling irradiance (E_d). Apart from these the ancillary sensors measures tilt, pressure, temperature and conductivity. The radiometer was also equipped with ECO triplet sensor (Wetlabs™ ECO series) which measures chlorophyll fluorescence, CDOM fluorescence and β at 650 nm (β_{650}). The excitation and emission wavelengths to measure CDOM fluorescence were 370 and 460 nm respectively with a sensitivity of 0.28 ppb of quinine sulphate dihydrate equivalent (QSDE). The volume scattering function, β, when integrated in backward direction provides estimates of backscattering (Balch et al., 2001). The backscattering at longer wavelengths, especially in red, is more sensitive to the suspended matter. Hence in the present study β is considered as a measure of total suspended matter.

Utmost care was taken to avoid tilt, maintain profiling velocity and avoid shadows from sources. The data from hyperspectral radiometer was recorded using SatView™ software and multi-level processing was carried out using Prosoft™ software.

The spectral R_{rs} was computed as

$$R_{rs}(0^+,\lambda) = \frac{L_w(0^+,\lambda)}{E_d(0^+,\lambda)}, \quad (1)$$

where $L_w(0^+, \lambda)$ is water leaving radiance and $E_d(0^+, \lambda)$ is downwelling irradiance above the sea surface. Further the upwelling radiance and downwelling radiance were computed as follows:

$$E_d(0^+,\lambda) = \frac{E_d(0^-,\lambda)}{1-\alpha}, \quad (2)$$

where α is the Fresnel reflection albedo for irradiance from the sun and sky and

$$L_w(0^+,\lambda) = L_u(0^-,\lambda)\frac{[1-\rho(\lambda,\theta)]}{\eta_w^2(\lambda)}, \quad (3)$$

where $\rho(\lambda, \theta)$ is the Fresnel reflectance index of seawater and $\eta_w(\lambda)$ is the Fresnel refractive index of seawater.

The spectral R_{rs}, measured using radiometer, was then used as an input to derive the chlorophyll concentration from respective algorithms.

3.2. Empirical algorithms

Six operational empirical algorithms (OC3C, OC4O, OC4, OC4E, OC3M, OC4O2) were selected for this study. These algorithms have been operationally implemented as default algorithms for Costal Zone Colour Scanner (CZCS), Ocean Colour and Temperature Scanner (OCTS), Sea-viewing Wide Field-of-view Sensor (SeaWiFS), Medium Resolution Imaging Spectrometer (MERIS), Moderate Resolution Imaging Spectroradiometer (MODIS) and Ocean Colour Monitor (OCM2). The functional forms of these algorithms are given in Table 1.

These algorithms have undergone several revisions based on the *in situ* data generated from different water types. The OC2 algorithm, originally designed for CZCS, has undergone eight revisions (OC2a, OC2b, OC2c, OC2d, OC2e, OC2, OC2v2 and OC2v4). The latest of which is OC2v4 which has a modified cubic polynomial form. The OC4O algorithm, designed for OCTS, has undergone four revisions and emerged as 4th order polynomial function relating the maximum of three band ratios. The OC4 algorithm, designed for SeaWiFS, has two versions (OC4 and OC4v4). Both versions use maximum ratio of four bands. The first version of OC4 was a modified cubic polynomial and the current version uses a fourth order polynomial with five coefficients (O'Reilly et al., 1998, 2000). The OC4E algorithm, designed for MERIS, is the tuned version of OC4v4 and has the functional form of 4th order cubic polynomial. The OC3 algorithm, designed for MODIS had undergone two versions (OC3d, and OC3e). It is three banded maximum band ratio and uses fourth order polynomial function. The default algorithm for OCM-2 is third order modified cubic polynomial which used the maximum ratio of four bands (Nagamani et al., 2008).

Table 1 The functional forms of the algorithms used to generate chl-*a* from Coastal Zone Colour Scanner (CZCS), Ocean Colour and Temperature Scanner (OCTS), Sea-viewing Wide Field-of-view Sensor (SeaWiFS), Medium Resolution Imaging Spectrometer (MERIS), Moderate Resolution Imaging Spectroradiometer (MODIS) and Ocean Colour Monitor 2 (OC4O2).

Sensor	Algorithm	Functional form	Model type
CZCS	OC3C MBR	$R = \log_{10}\left\{\max\left[\left(\frac{R_{rs}443}{R_{rs}550}\right), \left(\frac{R_{rs}520}{R_{rs}550}\right)\right]\right\}$ $a = [0.3330, -4.3770, 7.6267, -7.1457, 1.6673]$ $C = 10^{(a_0+a_1R+a_2R^2+a_3R^3+a_4R^4)}$	Fourth order polynomial
OCTS	OC4O MBR	$R = \log_{10}\left\{\max\left[\left(\frac{R_{rs}443}{R_{rs}565}\right), \left(\frac{R_{rs}490}{R_{rs}565}\right), \left(\frac{R_{rs}520}{R_{rs}565}\right)\right]\right\}$ $a = [0.2399, -2.0825, 1.6126, -1.0848, -0.2083]$ $C = 10^{(a_0+a_1R+a_2R^2+a_3R^3+a_4R^4)}$	Fourth order polynomial
SeaWiFS	OC4 MBR	$R = \log_{10}\left\{\max\left[\left(\frac{R_{rs}443}{R_{rs}555}\right), \left(\frac{R_{rs}490}{R_{rs}555}\right), \left(\frac{R_{rs}510}{R_{rs}555}\right)\right]\right\}$ $a = [0.2515, -2.3798, 1.5823, -0.6372, -0.5692]$ $C = 10^{(a_0+a_1R+a_2R^2+a_3R^3+a_4R^4)}$	Fourth order polynomial
MERIS	OC4E MBR	$R = \log_{10}\left\{\max\left[\left(\frac{R_{rs}443}{R_{rs}560}\right), \left(\frac{R_{rs}490}{R_{rs}560}\right), \left(\frac{R_{rs}510}{R_{rs}560}\right)\right]\right\}$ $a = [0.2521, -2.2146, 1.5193, -0.7702, -0.4291]$ $C = 10^{(a_0+a_1R+a_2R^2+a_3R^3+a_4R^4)}$	Fourth order polynomial
MODIS	OC3M MBR	$R = \log_{10}\left\{\max\left[\left(\frac{R_{rs}443}{R_{rs}547}\right), \left(\frac{R_{rs}488}{R_{rs}547}\right)\right]\right\}$ $a = [0.2424, -2.7423, 1.8017, -0.0015, -1.2280]$ $C = 10^{(a_0+a_1R+a_2R^2+a_3R^3+a_4R^4)}$	Fourth order polynomial
OCM2	OC4O2 MBR	$R = \log_{10}\left\{\max\left[\left(\frac{R_{rs}443}{R_{rs}555}\right), \left(\frac{R_{rs}490}{R_{rs}555}\right), \left(\frac{R_{rs}510}{R_{rs}555}\right)\right]\right\}$ $a = [0.475, -3.029, 2.240, -1.253, -0.027]$ $C = 10^{(a_0+a_1R+a_2R^2+a_3R^3+a_4R^4)}$	Third order modified cubic polynomial

4. Results

The results of the present study have been described in the following three sections. The first section deals with the optical classification of coastal waters based on AOP. The second section deals with the association of OAS with spectral R_{rs} and the third section with the assessment of ocean colour algorithms in different water types.

4.1. Optical classification using remote sensing reflectance

The entire data sets exhibited three different types of R_{rs} spectra and their spectral variability is given in Fig. 2. Based on the variability in R_{rs} spectra, the coastal waters off Kochi are optically classified into three types. Type-I waters had spectra (Fig. 2a) with flatter curve between 400 and 450 nm which then increased to peak at 482 nm. After 482 nm, R_{rs} decreased gradually till 608 nm and then the curve flattened again till 700 nm indicating no reflectance in the region. The spectral R_{rs} in Type-II waters (Fig. 2b) was found to be distinct from that of Type-I. The average R_{rs} increased gradually from shorter wavelength (400 nm) and showed almost a flat peak between 532 and 566 nm with a marginally higher value at 560 nm. Beyond 560 nm, a steep valley was observed till 610 nm. After which the decrease was gradual till 670 nm. A secondary maximum was also observed at 681 nm. The R_{rs} spectra in Type-III waters (Fig. 2c) showed similarity to that of the Type-II at the longer wavelength. In this type, a steep increase in R_{rs} was observed from 400 to 570 nm. The peak R_{rs} was more prominent. The spectral behaviour of R_{rs} from 570 to 700 nm in this water type was similar to that of Type-II. However, the secondary maximum was more prominent (684 nm) and higher in magnitude.

4.2. Association of optically active substances with different water types

The analyses of spatio-temporal variability in OAS (chl-*a* and CDOM) and their IOP (β_{650}) have been carried out for the

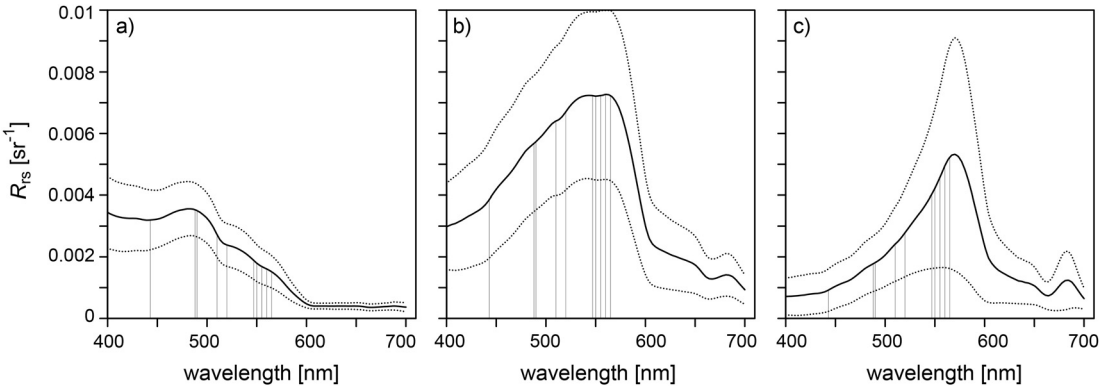

Figure 2 Spectral variability of remote sensing reflectance (R_{rs}) in the study area. The similar spectra have been clubbed together as (a) Type-I, (b) Type-II and (c) Type-III. The solid line represent mean and the dotted line represents the standard deviation. The *X*-axis represents wavelength [nm] and *Y*-axis represents R_{rs} [sr^{-1}] coefficients.

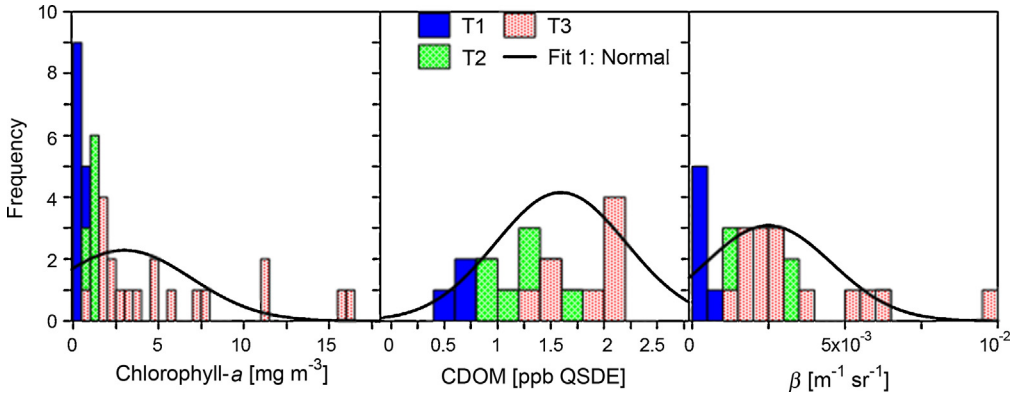

Figure 3 Frequency distribution of chlorophyll-*a* (chl-*a*), volume scattering function at 650 nm (β_{650}) and concentration of chromophoric dissolved organic matter (CDOM) in quinine sulphate dihydrate equivalent (QSDE) unit in different water types. The solid line indicates the normal distribution. The *X*-axis represents concentration of chl-*a*, β_{650} and CDOM. The *Y*-axis represents frquency distribution.

three water types based on the frequency distribution (Fig. 3). The frequency distribution plots were also superimposed with the normal Gaussian function to understand the trend. The frequency distribution showed large variability in the OAS for the three water types. The chl-*a*, which varied between the three water types, was 0.077 and 20.0 mg m^{-3} (Fig. 3a). The chl-*a* in Type-I and Type-II waters ranged from 0.77 to 1.0 mg m^{-3} and 1.0 and 2.0 mg m^{-3} respectively. The Type-III waters, chl-*a* ranged from 1 to 20 mg m^{-3} while the frequency was less at lower concentration.

The CDOM varied between 0.39 and 2.25 ppb QSDE (Fig. 3b). Type-I waters showed lower concentration of CDOM, between 0.3 and 0.75 ppb QSDE. The CDOM concentration in Type-II and Type-III waters are varied, from 0.75 to 1.25 and Hp1.25 to 2.25 ppb QSDE respectively. The concentration of CDOM was comparatively higher in Type-II waters. β_{650}, ranged between 0.16×10^{-3} and 9.5×10^{-3} m^{-1} sr^{-1} (Fig. 3c) with a higher frequency at the lower range between 0.16×10^{-3} and 0.19×10^{-3} m^{-1} sr^{-1}. In Type-II and Type-III waters, β_{650} was in the range from 1.3×10^{-3} to 6.1×10^{-3} m^{-1} sr^{-1} and 1.4×10^{-3} to 9.5×10^{-3} m^{-1} sr^{-1} respectively. The maximum value of β_{650} was encountered in Type-III waters.

4.3. Assessment of ocean chlorophyll algorithms

The scatter plots showing relation between *in situ* measured chl-*a* and that derived using OC4, OC3C, OC4O, OC4E, OC3M and OC4O2 algorithms is given in Fig. 4. The validation statistics have been computed using data from all water types. The corresponding statistical indicators are given in Table 2. The R^2 was better in case of OC4 (0.70), which was also comparable with that of OC3M (0.68). Further OC4 and OC3M showed least Log_{10}-RMSE (0.37). However, absolute percentage difference (APD) (35.9%) was better in case of OC4 whereas OC3M showed better slope (0.69), relative percentage difference (RPD) (4.8%) and unbiased percentage difference (UPD) (17.1%). The intercept (0.07) was least in the case of OC4O and '*r*' was closer to unity in case of OC4O2. The inverse transform ratios also showed that OC3M performs better at the median scale with F_{med} close to unity. The overall statistical analysis showed that OC3M and OC4 produced comparable results having least significant difference between estimated and measured chl-*a*.

Although the validation has been carried out for the entire data set, the accuracy of the algorithms was also evaluated in the different water types. The assessment of measured and

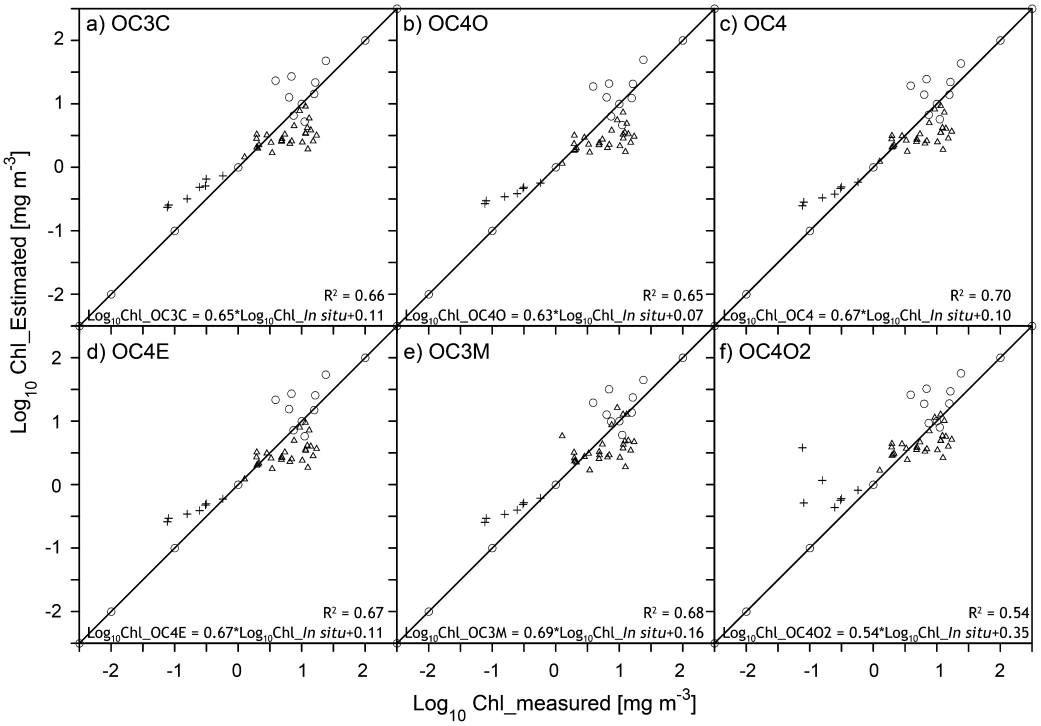

Figure 4 Correlation between *in situ* chlorophyll-*a* (chl-*a*) and that derived using OC4, OC3C, OC4O, OC4E, OC3M and OC4O2 algorithms in Type-I (plus), II (triangle) and III (circle) waters. The solid line indicate the trend and the dotted line corresponds to 1:1.

Table 2 Performance indices for relative errors between *in situ* measured and estimated chl-*a* from *in situ* R_{rs} using OC3C, OC4O, OC4, OC4E, OC3M and OC4O2 algorithms. These indices include correlation coefficient (R^2), slope (S), intercept (I), sumation of ratio of measured to estimated (r), root mean squared error (RMSE), absolute percentage difference (APD), relative percentage difference (RPD) and unbiased percentage difference (UPD). The geometric mean and one-sigma range of the ratio (F = $Value_{alg}/Value_{meas}$) are given by F_{med}, F_{min}, and F_{max}, respectively. The values closer to 1 are more accurate. Total 42 data points were used for the analysis.

Algorithm	R^2	S	I	r	RMSE	APD	RPD	UPD	F_{min}	F_{med}	F_{max}
OC3C	0.66	0.65	0.11	1.74	0.39	41.0	17.2	29.8	0.50	1.21	2.94
OC4O	0.65	0.63	**0.07**	1.95	0.41	40.3	23.6	36.5	**0.56**	1.36	3.34
OC4	**0.70**	0.67	0.10	1.69	**0.37**	**35.9**	16.3	26.7	0.53	1.22	2.82
OC4E	0.67	0.67	0.10	1.70	0.38	37.2	16.6	27.7	0.50	1.20	2.88
OC3M	0.68	**0.69**	0.16	1.47	**0.37**	50.4	**4.8**	**17.1**	0.44	**1.04**	2.45
OC4O2	0.54	0.54	0.35	**1.21**	0.45	47.1	3.26	30.1	0.29	0.82	2.29

estimated chl-*a* in Type-I waters showed a good agreement with a correlation coefficient (R^2) of 0.93 in the case of OC4O, OC4, OC4E and OC3M and 0.89 in the case of OC3C. Chl-*a* estimated using OC4O2 algorithm showed relatively lower correlation (R^2 = 0.74). However, the measured chl-*a* was lower in magnitude than the estimated chl-*a* having a slope of 1.06, 0.60, 0.68, 0.67, 0.71 and 0.68 for OC3C, OC4O, OC4, OC4E, OC3M and OC4O2 respectively. The result based on the statistical analysis indicated that OC3M performs better than other algorithms in Type-I waters. In Type-II waters, it was observed that a cluster of points having chl-*a* concentration between 9.0 and 13 mg m^{-3} showed a poor relation between estimated and measured chl-*a*. At these points, β_{650} was ten-fold higher than that in Type-I waters. In addition, the CDOM was higher than the average value (2.1—2.5 ppb QSDE). In the absence of this cluster, it was observed that estimated and measured chl-*a* had moderate agreement in case of OC3C (R^2 = 0.52), OC4 (R^2 = 0.67), OC4E (R^2 = 0.67), OC3M (R^2 = 0.67) and OC4O2 (R^2 = 0.67). In this water type, estimated chl-*a* was lower in magnitude than the measured with a slope of 0.59, 0.50, 0.63, 0.63, 0.90 and 0.88 for OC3C, OC4O, OC4, OC4E, OC3M and OC4O2 respectively. Based on the statistical analysis, comparable result was seen between OC3M and OC4O2. The performance of both these algorithms was better than other algorithms in Type-II waters. In Type-III waters, estimated chl-*a* was found to be higher in magnitude as compared to measured chl-*a*. The slope of regression was 1.46, 1.45, 1.39, 1.65, 1.44 and 1.84 for OC3C, OC4O, OC4, OC4E, OC3M and OC4O2 respectively. Although the estimated and measured chl-*a* was found to be variable in magnitude, the trend was in good agreement. The R^2 was 0.68, 0.63, 0.69, 0.66, 0.70 and 0.70 for OC3C, OC4O, OC4, OC4E, OC3M and OC4O2 respectively. The OC3M and OC4 algorithms performed better in Type-III waters.

An attempt has been also made to understand existence of any covariance between CDOM and errors associated with the

algorithms in Type-II and III waters. Hence a ratio of estimated chl-*a*, from various algorithms, to *in situ* chl-*a* was regressed with CDOM. The results showed that in Type-II waters, the covariance was 2.48, 1.42, 2.24, 2.48, 5.16 and 2.99% whereas in Type-III it was 39.64, 25.96, 27.09, 30.46, 25.41 and 35.86% respectively for OC3C, OC4O, OC4, OC4E, OC3M and OC4O2 algorithms.

5. Discussion

The retrieval of geophysical products from an ocean colour satellite sensor involves two critical steps. The first step is to eliminate the effect of the atmospheric contribution from the total radiance received by the satellite sensor (Hu et al., 2004). The second step is to select a suitable bio-optical algorithm which relates the signal leaving the water column with the concentration of the OAS. The present study aims towards the second step. In the present case, the empirical algorithms, used operationally to retrieve chl-*a* from CZCS, OCTS, SeaWiFS, MERIS, MODIS and OCM2, were applied to the *in situ* R_{rs} measured using hyperspectral radiometer. Further, an attempt has been also made to classify the waters based on the reflectance characteristics and to evaluate impact of OAS on these water types. Subsequently the performance of these algorithms was tested in these water types.

The data generated for the present study exhibited three distinct spectra for R_{rs}. The distribution of OAS within different water types also showed a remarkable difference. In Type-I waters, R_{rs} spectra showed the maximum in the blue (400–480 nm) region and was almost negligible in the red region (beyond 600 nm). The variability in concentration of chl-*a* and CDOM was very low in this water type with a standard deviation of less than 50% of the average value. The β_{650} also showed less variability in this water type. The low concentration in distribution of OAS in Type-I waters was responsible for least absorption in the shorter wavelength resulting in high R_{rs}. However, the lower R_{rs} in the longer wavelength may be attributed to the strong absorption due to water molecules. This indicates that the water molecules were the principal light absorbing component in this water type along with chl-*a*. This is in agreement with the previous studies carried out in oligotrophic waters of Lakshadweep Islands, hyperoligotrophic waters in the South Pacific gyre and in the Chesapeake Bay where the authors have shown that the water molecules are the major components responsible for the absorption in the longer wavelength resulting in minimal variability of R_{rs} (Menon et al., 2005; Morel et al., 2007; Tzortziou et al., 2007). The spectral signature of R_{rs} in Type-II waters showed significant difference in shorter wavelengths. In Type-II waters, chl-*a* concentration and β_{650} was ten-fold higher than in Type-I waters. Also, the CDOM concentration was almost twice in magnitude. The phytoplankton pigment, chl-*a*, has the primary absorption peak in the blue region (~440 nm). Apart from this, CDOM also has a tendency for strong absorption in UV and the blue region (Jorgenson, 1999; Menon et al., 2005; Siegal et al., 2002). Therefore, the respective signature of R_{rs} in Type-II waters was predominantly due to the combined effect of absorption due to chl-*a* and CDOM. In Type-III waters, the peak in the R_{rs} spectra shifted more towards the longer wavelength as compared to that in Type-II waters. In addition, the peak R_{rs} was more prominent as compared to Type-I and II waters. In this water type, β_{650} was comparable with Type-II waters. However, chl-*a* and CDOM concentration was found to be increased by 64% and 76% respectively. This indicates that the impact of chl-*a* and CDOM absorption has further increased which resulted in much lower R_{rs} at the shorter wavelength. Menon et al. (2006) showed that CDOM significantly influences the water leaving radiance at the shorter wavelengths and its impact can be spread up to 650 nm. Kutser et al. (2006) reported an 'abnormal' shape of the R_{rs} spectra when the concentrations of optically active substances were high. The study carried out by Cannizaro and Carder showed that, in non-coastal oligotrophic waters, the peak R_{rs} was at 400 nm which was shifted to ~490 nm in highly reflective, optically shallow, mesotrophic waters and ~560 nm in optically deep eutrophic waters. Ouillon and Petrenko (2005) also reported peak R_{rs} at 443 and 490 nm in Case 1 waters and at 560 nm in Case 2 waters.

The above discussion clearly indicates that distinct spectral signatures of R_{rs} were more attributed towards variability in OAS. Further, the distribution of these OAS could be controlled by hydrography of the study area. The study area is subjected to coastal upwelling and heavy fresh water discharge from the estuary of the Periyar River in the monsoon period which enhances nutrient upload resulting in increased biological production (Jyothibabu et al., 2006; Nair et al., 1992). Studies by Srinivas et al. (2003) also reported that the coastal waters of the southeastern Arabian Sea are the recipient of approximately 1.9×10^{10} m^3 of fresh water annually from the Cochin backwaters. We have also analyzed the inter-relationship of chl-*a* with CDOM and β_{650} in different water types (Fig. 5). The chl-*a* and CDOM did not show any significant relation in Type-I waters. This indicates that CDOM is independent of the variations in chl-*a* in these waters. However a large association was seen in Type-II and Type-III waters. Also in these waters, the concentration of chl-*a* and CDOM was very high. The co-variance of chl-*a* with CDOM indicates that the source of nutrients for phytoplankton growth, and organic matter is the same. Since the primary source of CDOM is from the river, it can be inferred that river discharges are one of the primary mechanisms for distribution of chl-*a* and CDOM in the study area. The β_{650} did not show any significant relationship with chl-*a* in any of the water types. This indicates that chl-*a* and suspended matter do not co-vary in water types. Hence, it can be inferred that river discharges are not the primary source of suspended matter in the study area. Some of the previous studies by Jyothibabu et al. (2006), Srinivas et al. (2003) and Thomas et al. (2004) also reported that continuous dredging process occurring throughout the year in the study area increases the nutrients and sediment loads into the estuary which is drained into the coastal waters.

The distribution of OAS thus significantly alters the spectral R_{rs} which is the input for the empirical algorithm for the retrieval of chl-*a*. In the present study, chl-*a* algorithms were evaluated in different water types having similar variability in spectral R_{rs}. Among all the algorithms, OC3M and OC4 performed better in the study area. In general, all algorithms showed that, in Type-I waters, the measured chl-*a* was less than that estimated using various algorithms. However measured and estimated chl-*a* showed the same trend with good correlation. These waters were having typical Case 1 characteristics. Also the R_{rs} signals dominated in 443 nm band. In

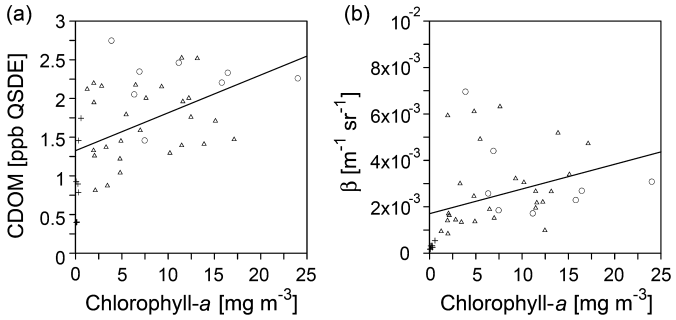

Figure 5 Scatter plot showing relation between (a) *in situ* chlorophyll-*a* (chl-*a*) and CDOM in QSDE unit and (b) *in situ* chl-*a* and β. The plus (+) sign corresponds to Type-I, open triangle (△) corresponds to Type-II and open circles (○) corresponds to Type-III waters.

Type-II waters, the cluster of points was found to be weakly correlated. Further in Type-II waters, the dominant signal in R_{rs} was from the blue-green band. In the case of OC4, OC4E and OC4O2 the dominant R_{rs} signal was from 510 nm, whereas it was 520 nm in the case of OC3C and OC4O. For OC3M, R_{rs} signal was dominated by the 488 nm band. Similar conditions were observed in Type-III waters. The performance of all the algorithms was poor in Type-II waters whereas it was comparatively better in Type-III waters. Although in Type-II and Type-III waters concentration of chl-*a* and CDOM was ten-fold higher than Type-I waters, the co-variance between chl-*a* and CDOM was significantly higher in Type-III waters. Desa et al. (2001) showed that the ratio of R_{rs} at 490—555 nm is a better indicator of chl-*a* in the eastern Arabian Sea. They illustrated significant improvement in R^2 (0.93), slope (0.96) and intercept (0.26) by modifying SeaWiFS OC4v4 coefficients. However Shanmugam (2011) suggested that although OC3 reliably estimates chl-*a* in the open ocean waters, it tends to fail in the coastal waters of the Arabian Sea. The chl-*a* and CDOM compete for absorption of light at almost similar wavelengths in the blue region. As a result, the signal emerging from the water column carries signatures of both chl-*a* and CDOM. The empirical algorithms take the ratio of the blue to the green band with an assumption that the water leaving radiance decreases in the blue band with an increase in chl-*a* concentration. However, if the water column is dominated by chl-*a* and CDOM, both significantly contribute to the decrease in the water leaving radiance in the blue band. In such a scenario, the performance of a ratio based algorithms weakens the retrieval of chl-*a*. In the earlier studies, Tzortziou et al. (2007) also reported that the failure of MODIS algorithm in inshore waters of the Chesapeake Bay was due to the large contribution of non-co-varying CDOM and non-algal particles to total light absorption in the blue region.

6. Conclusion

The present study primarily focused on the evaluation of six empirical algorithms (OC3C, OC4O, OC4, OC4E, OC3M and OC4O2), operationally used to retrieve chl-*a* from CZCS, OCTS, SeaWiFS, MERIS, MODIS and OCM-2. The algorithms were applied to the spectral R_{rs} measured *in situ* using hyperspectral radiometer with an intention to assess the functional form and the coefficients. The effect of atmospheric correction has been ignored in the present study. The R_{rs} showed three distinct water types based on the spectral variability. These water types were attributed to the variability in the concentration of OAS. In Type-I waters chl-*a*, CDOM and β_{650} were very low indicating that these were pure Case-I waters and the peak R_{rs} was in the blue band. In Type-II waters, the peak R_{rs} shifted to the green band which was attributed to elevated concentration of chl-*a*, CDOM and β_{650}. In Type-III waters, the peak R_{rs} further shifted to longer wavelengths due to an increase in chl-*a* and CDOM. Also chl-*a* was found to be associated with CDOM indicating that rivers are one of the primary sources for discharging essential parameters for the growth of phytoplankton. The overall statistical analysis showed that the performances of OC3M and OC4 were better as compared to other algorithms. Further in the case of chl-*a*, at more than 1.0 mg m^{-3} it was found that the ratio of higher wavelengths (488, 510 and 520 nm) dominates. The assessment of algorithms in different water types indicated better performance of all the algorithms in Type-I waters. The performance was poor in Type-II and Type-III waters. The errors associated with the estimation of chl-*a* were significantly co-varied with CDOM in Type-III waters. Therefore, in the regions where there is dominance of OAS other than chl-*a*, it is required to develop IOP-based algorithm that takes into account absorption and scattering due to individual OAS.

Acknowledgements

The study was funded by Indian National Centre for Ocean Information Services (INCOIS) (INCOIS:F&A:XII:D2:021), Ministry of Earth Sciences under SATellite Coastal Oceanographic REsearch (SATCORE) programme. The authors are thankful to the Director of INCOIS for encouragement. Thanks are also due to the Director of ICAR — Central Institute of Fisheries Technology, for support and encouragement. The authors are also grateful to the management and staff of MV 'Bharath Darshan', for their unrestricted support during the cruises.

References

Balch, W.M., Drapeau, D., Fritz, J., Bowler, B., Nolan, J., 2001. Optical backscattering in the Arabian Sea — continuous underway measurements of particulate inorganic and organic carbon. Deep-Sea Res. Pt. I 48 (11), 2423—2452, http://dx.doi.org/10.1016/S0967-0637(01)00025-5.

Chauhan, P., Mohan, M., Sarangi, R.K., Kumari, B., Nayak, S., Matondkar, S.G.P., 2002. Surface chlorophyll estimation in the Arabian Sea using IRS-P4 OCM Ocean Color Monitor (OCM) satellite data. Int. J. Remote Sens. 23 (8), 1663–1676, http://dx.doi.org/10.1080/01431160110075866.

Desa, E.S., Suresh, T., Matondkar, S.G.P., Desa, E., 2001. Sea truth validation of SeaWiFS ocean colour sensor in the coastal waters of the eastern Arabian Sea. Curr. Sci. India 80 (7), 854–860.

George, R., Muraleedharan, K.R., Martin, G.D., Sabu, P., Gerson, V. J., Dineshkumar, P.K., Nair, S.M., Chandramohanakumar, N., Nair, K.K.C., 2013. Nutrient biogeochemistry of the eastern Arabian Sea during the southwest monsoon retreat. Environ. Earth Sci. 68 (3), 703–718, http://dx.doi.org/10.1007/s12665-012-1772-2.

Hu, C., Montgomery, E.T., Schmitt, R.W., Muller-Karger, F.E., 2004. The dispersal of the Amazon and Orinoco River water in the tropical Atlantic and Caribbean Sea: observation from space and S-PALACE floats. Deep-Sea Res. Pt. II 51 (10–11), 1151–1171, http://dx.doi.org/10.1016/j.dsr2.2004.04.001.

Iyer, P.C.S., Sindhu, M., Kulkarni, S.G., Tambe, S.S., Kulkarni, B.D., 2003. Statistical analysis of the physic-chemical data on the coastal waters of Cochin. J. Environ. Monitor. 5 (2), 324–327, http://dx.doi.org/10.1039/B209219K.

Jorgenson, S.V., 1999. Standard Case 1 algorithms in Danish coastal waters. Int. J. Remote Sens. 20 (7), 1289–1301, http://dx.doi.org/10.1080/014311699212731.

Joshi, M., Rao, A.D., 2012. Response of Southwest monsoon winds on shelf circulation off Kerala coast, India. Cont. Shelf Res. 32, 62–70, http://dx.doi.org/10.1016/j.csr.2011.10.015.

Jyothibabu, R., Madhu, N.V., Jayalakshmi, K.V., Balachandran, K.K., Shiyas, C.A., Martin, G.D., Nair, K.K.C., 2006. Impact of fresh water influx on microzooplankton mediated food web in a tropical estuary (Cochin backwaters – India). Estuar. Coast. Shelf Sci. 69 (3–4), 505–518, http://dx.doi.org/10.1016/j.ecss.2006.05.013.

Kumar, H.P.V., Kumar, M.N., 1996. On the flow and thermohaline structure off Cochin during pre-monsoon season. Cont. Shelf Res. 16 (4), 457–468, http://dx.doi.org/10.1016/j.ecss.2006.05.013.

Kutser, T., Vahtma, E., Martin, G., 2006. Assessing suitability of multispectral satellites for mapping benthic macroalgal cover in turbid coastal waters by means of model simulations. Estuar. Coast. Shelf Sci. 67 (3), 521–529, http://dx.doi.org/10.1016/j.ecss.2005.12.004.

Lee, M.E., Lewis, M.R., 2003. A new method for the measurement of the optical volume scattering function in the upper ocean. J. Atmos. Ocean. Tech. 20 (4), 563–571, http://dx.doi.org/10.1175/1520-0426(2003)20<563:ANMFTM>2.0.CO;2.

Lee, Z., Carder, K.L., Arnone, R.A., 2002. Deriving inherent optical properties from water color: a multiband quasi-analytical algorithm for optically deep waters. Appl. Opt. 41 (27), 5755–5772, http://dx.doi.org/10.1364/AO.41.005755.

McClain, M.E., Fargion, G.S., 1999. Simbios project annual report. Document ID: 20000013962, Report/Patent Number: NASA/TM-1999-209486, NAS 1.15:209486 Rept-2000-00655. Goddard Space Flight Center, Greenbelt, Maryland, 132 pp.

Mckee, D., Cunningham, A., 2006. Identification and characterization of two optical water types in the Irish Sea from in situ inherent optical properties and seawater constituents. Estuar. Coast. Shelf Sci. 68 (1), 305–316, http://dx.doi.org/10.1016/j.ecss.2006.02.010.

Menon, H.B., Lotliker, A.A., Moorthy, K.K., Nayak, S.R., 2006. Variability of remote sensing reflectance and implications for optical remote sensing – a study along the eastern and northeastern waters of Arabian Sea. Geophys. Res. Lett. 33, L15602, http://dx.doi.org/10.1029/2006GL026026.

Menon, H.B., Lotliker, A.A., Nayak, S.R., 2005. Pre-monsoon bio-optical properties in estuarine, coastal and Lakshadweep waters. Estuar. Coast. Shelf Sci. 63 (1), 211–223, http://dx.doi.org/10.1016/j.ecss.2004.11.015.

Minu, P., Lotliker, A.A., Shaju, S.S., SanthoshKumar, B., Ashraf, P.M., Meenakumari, B., 2014. Effect of optically active substances and atmospheric correction schemes on remote-sensing reflectance at a coastal site off Kochi. Int. J. Remote Sens. 35 (14), 5434–5447, http://dx.doi.org/10.1080/01431161.2014.926420.

Mobley, C.D., 1994. The optical properties of water. In: Bass, M. (Ed.), Handbook of Optics, 2nd ed., vol. I. McGraw-Hill, New York, 1248 pp.

Morel, A., 1991. Light and marine photosynthesis: a spectral model with geo-chemical and climatological implications. Prog. Oceanogr. 26 (3), 263–306, http://dx.doi.org/10.1016/0079-6611(91)90004-6.

Morel, A., Claustre, H., Antoine, D., Gentili, B., 2007. Natural variability of bio-optical properties in Case 1 waters: attenuation and reflectance within the visible and near-UV spectral domains, as observed in South Pacific and Mediterranean waters. Biogeosci. Discuss. 4 (4), 2147–2178.

Morel, A., Prieur, L., 1977. Analysis of variations in ocean color. Limnol. Oceanogr. 22 (4), 709–720.

Nagamani, P.V., Chauhan, P., Dwivedi, R.M., 2008. Development of chlorophyll *a* algorithm for Ocean Colour Monitor onboard OCEANSAT-2 satellite. IEEE Geosci. Remote Sens. Lett. 5 (3), 527–531, http://dx.doi.org/10.1109/LGRS.2008.923213.

Nair, V.E., Devassy, V.P., Madhupratap, M., 1992. Blooms of phytoplankton along the coast of India associated with nutrient enrichment and the response of zooplankton. In: Vollenweider, R.A., Marchetti, R., Viviani, R. (Eds.), Marine Coastal Eutrophication. Elsevier, Amsterdam, London, New York, Tokyo, 819–828.

O'Reilly, J.E., Maritorena, S., Mitchell, B.G., Siegel, D.A., Carder, K. L., Garver, S.A., Kahru, M., McClain, C.R., 1998. Ocean colour chlorophyll algorithms for SeaWiFS. J. Geophys. Res. 103 (C11), 24937–24953, http://dx.doi.org/10.1029/98JC02160.

O'Reilly, J.E., Maritorena, S., Siegel, D., O'Brien, M.C., Toole, D., Mitchell, B.G., et al., 2000. Ocean color chlorophyll *a* algorithms for SeaWiFS, OC2, and OC4: Version 4. In: Hooker, S.B., Firestone, E.R. (Eds.), SeaWiFS postlaunch technical report series. SeaWiFS post-launch calibration and validation analyses, Part 3, vol. 11 NASA/GSFC. 9–23.

Ouillon, S., Petrenko, A., 2005. Above-water measurements of reflectance and chlorophyll-*a* algorithms in the Gulf of Lions, NW Mediterranean Sea. Opt. Exp. 13 (7), 2531–2548, http://dx.doi.org/10.1364/OPEX.13.002531.

Pierson, D.C., Strombeck, N., 2000. A modelling approach to evaluate preliminary remote sensing algorithms: use of water quality data from Swedish Great Lakes. Geophysica 36 (1–2), 177–202.

Sathe, P.V., Jadhav, N., 2001. Retrieval of chlorophyll from the sea-leaving radiance in the Arabian Sea. J. Indian Soc. Remote Sens. 29 (1–2), 97–106.

Shanmugam, P., 2011. A new bio-optical algorithm for the remote sensing of algal blooms in complex ocean waters. J. Geophys. Res.-Oceans 116, C04016, http://dx.doi.org/10.1029/2010JC006796.

Siegal, D.A., Maritorena, S., Nelson, N.B., Hansel, D.A., Lorenzi-Kayser, M., 2002. Global distribution and dynamics of colored dissolved and detrital organic materials. J. Geophys. Res. 107, 3228, http://dx.doi.org/10.1029/2001JC000965.

Srinivas, K., Dineshkumar, P.K., 2006. Atmospheric forcing on the seasonal variability of sea level at Cochin, South west of India. Cont. Shelf Res. 26 (10), 1113–1133, http://dx.doi.org/10.1016/j.csr.2006.03.010.

Srinivas, K., Revichandran, C., Maheswaran, P.A., Ashraf, M.T.T., Murukesh, N., 2003. Propagation of tides in the Cochin estuarine system, South west coast of India. Indian J. Mar. Sci. 32 (1), 14–24.

Thomas, J.V., Premlal, P., Sreedevi, C., Kurup, M.B., 2004. Immediate effect of bottom trawling on the physicochemical parameters in the inshore waters (Cochin-Munambum) of Kerala. Indian J. Fish. 51 (3), 277–286.

Tilstone, G.H., Ingrid, M., Benavides, A., Pradhan, Y., Shutler, J.D., Groom, S., Sathyendranath, S., 2011. An assessment of chlorophyll-*a* algorithms available for SeaWiFS in coastal and open areas of the Bay of Bengal and Arabian Sea. Remote Sens. Environ. 115 (9), 2277—2291, http://dx.doi.org/10.1016/j.rse.2011.04.028.

Tilstone, G.H., Lotliker, A., Miller, P.I., Ashraf, P.M., Kumar, T.S., Suresh, T., Ragavan, B.R., Menon, H.B., 2013. Assessment of MODIS-Aqua chlorophyll *a* algorithms in coastal and shelf waters of the eastern Arabian Sea. Cont. Shelf Res. 65 (1), 14—26, http://dx.doi.org/10.1016/j.csr.2013.06.003.

Tzortziou, M., Subramaniam, A., Herman, J.R., Gallegos, C.L., Neale, P.J., Harding Jr., L.W., 2007. Remote sensing reflectance and inherent optical properties in the mid Chesapeake Bay. Estuar. Coast. Shelf Sci. 72 (1), 16—32, http://dx.doi.org/10.1016/j.ecss.2006.09.018.

Oceanologia (2016) 58, 327—335

Available online at www.sciencedirect.com

ScienceDirect

journal homepage: www.journals.elsevier.com/oceanologia/

ORIGINAL RESEARCH ARTICLE

UV filters are an environmental threat in the Gulf of Mexico: a case study of Texas coastal zones

Hamidreza Sharifan [a,*], **David Klein** [b,1], **Audra N. Morse** [a,2]

[a] *Department of Civil, Environmental, and Construction Engineering, Texas Tech University, Lubbock, TX, United States*
[b] *Department of Environmental Toxicology, Institute of Environmental and Human Health, Texas Tech University, Lubbock, TX, United States*

Received 15 February 2016; accepted 15 July 2016
Available online 30 July 2016

KEYWORDS
Coastal zones;
UV filters;
Water pollution;
Texas;
Gulf of Mexico;
Estuaries

Summary UV filters are the main ingredients in many cosmetics and personal care products. A significant amount of lipophilic UV filters annually enters the surface water due to large numbers of swimmers and sunbathers. The nature of these compounds cause bioaccumulation in commercial fish, particularly in estuarine areas. Consequently, biomagnification in the food chain will occur. This study estimated the amount of four common UV filters (ethylhexyl methoxycinnamate, EHMC; octocrylene, OC; butyl methoxydibenzoylmethane, BM-DBM; and benzophenone-3, BP3), which may enter surface water in the Gulf of Mexico. Our data analysis was based on the available research data and EPA standards (age classification/human body parts). The results indicated that among the 14 counties in Texas coastal zones, Nueces, with 43 beaches, has a high potential of water contamination through UV filters; EHMC: 477 kg year^{-1}; OC: 318 kg year^{-1}; BM-DBM: 258 kg year^{-1}; and BP by 159 kg year^{-1}. Refugio County, with a minimum number of beaches, indicated the lowest potential of UV filter contamination. The sensitive estuarine areas of Galveston receive a significant amount of UV filters. This article suggests action for protecting Texas estuarine areas and controlling the number of tourists and ecotourism that occurs in sensitive areas of the Gulf of Mexico.

* Corresponding author at: Department of Civil, Environmental, and Construction Engineering, Texas Tech University, Office # 018, Lubbock, TX 79409-1023, United States. Fax: +1 806 742 3493.
E-mail addresses: hamidreza.sharifan@ttu.edu, hsharifan@gmail.com (H. Sharifan).
[1] Address: 1207 Gilbert Drive, Box 41163, Lubbock, TX 79409-1163, United States.
[2] Address: Department of Civil, Environmental, and Construction Engineering, Texas Tech University, Box 41023, Lubbock, TX 79409-1023, United States.
Peer review under the responsibility of Institute of Oceanology of the Polish Academy of Sciences.

Production and hosting by Elsevier

http://dx.doi.org/10.1016/j.oceano.2016.07.002

1. Introduction

Ultraviolet (UV) filters are common ingredients in many cosmetics and personal care products such as sunscreens, soap, shampoos, and hair sprays (Li et al., 2007; Sharifan et al., 2016; Silvia Díaz-Cruz et al., 2008). UV filters and their transformation products, which are washed off from the skin and clothes during swimming and bathing, enter the surface water (Giokas et al., 2007; Li et al., 2007; Nakajima et al., 2009; Plagellat et al., 2006; Poiger et al., 2004; Ramos et al., 2016) and are considered to be a source of surface water contamination (Ekpeghere et al., 2016; Poiger et al., 2004; Ramos et al., 2016). UV filters are added to consumer sunscreen products at different concentrations due to sunscreen formulations (Amine et al., 2012; Kupper et al., 2006; Li et al., 2007; Plagellat et al., 2006; Silvia Díaz-Cruz et al., 2008). The water contamination by UV filters is an increasing public concern due to the secondary effects (i.e. bioaccumulation) of pharmaceuticals and personal care products (PPCPs) in receiving waters, which may reach detectable and potentially toxic concentration levels (Gago-Ferrero et al., 2013; Sharifan et al., 2016).

Furthermore, due to the lipophilic characteristics of UV filters, they can bioaccumulate and biomagnify through the food chain, and their presence is associated with estrogenic effects (Broniowska et al., 2016; Mueller et al., 2003; Vila et al., 2016). Ultimately, these filters can bioaccumulate in humans (Broniowska et al., 2016; Valle-Sistac et al., 2016). Due to a high log octanol–water partition coefficient (log-K_{ow}) of UV-filters (3.8–5.9), these compounds are associated with a high accumulation rate in fish (Broniowska et al., 2016; Ekpeghere et al., 2016; Kim and Choi, 2014).

Fish has a strong tendency to accumulate UV filters (Giokas et al., 2007; Liu et al., 2015). Reported concentrations of UV filters in fish ranged from 9 to 2400 ng g^{-1} lipid weight (Gago-Ferrero et al., 2015). For example, two fish species of perch and roach accumulated UV filters, respectively, by 2000 ng g^{-1} and 500 ng g^{-1} lipids (Li et al., 2007). Though the accumulation rate of UV-filters in fish has been studied both in the field and in laboratories (Blüthgen et al., 2014; Gago-Ferrero et al., 2013; Liu et al., 2015), the toxicokinetic mechanisms of these compounds in fish remain unclear.

In addition to accumulating in the food chain, UV filters have shown severe effects on coral reefs by bleaching corals at very low concentrations (Danovaro et al., 2008). Recently, the UV filters were detected at concentration levels greater than 3700 ng L^{-1} along the coastal areas of South Carolina in the USA (Bratkovics et al., 2015). This concentration may actively link to the life of U.S. endangered coral species such as *Acropora palmata* at the Flower Garden Banks National Marine Sanctuary in the northwestern Gulf of Mexico (Zimmer et al., 2006).

The long shoreline in South Texas (approximately 367 miles/590 km) is a center of recreational activities throughout the year. All 14 counties of this shoreline have 169 beaches for water activities (EPA, 2013). Every year, due to millions of beach visitors and swimmers, significant amounts of UV filters directly or indirectly (i.e. through mistreatment of wastewater, contamination of sand, etc.) enter the surface water in the Gulf of Mexico. However, UV filter concentration information is geographically restricted to some European and Asian countries, as well as Australia, whereas data from other regions, namely the Americas, is missing (Ramos et al., 2016). The potential release of these compounds has never been studied in the Gulf of Mexico. A major challenge for the potential risk effects of UV filters on aquatic life and the food chain is the availability of reliable analytical procedures that determine these substances in aquatic systems (Giokas et al., 2004, 2005; Rodil and Moeder, 2008). However, the empirical research (laboratory experiments and field surveys) is strictly limited due to financial and practical constraints (Arnot and Gobas, 2003; Korsman et al., 2015).

In order to fill the knowledge gap on the ecotoxicity of UV filters in the Gulf of Mexico region, this study aims to identify potentially hazardous substances in an effective and conservative manner. The objective of this study is to estimate the amount of UV filters: ethylhexyl methoxycinnamate (EHMC), octocrylene (OC), butyl methoxydibenzoylmethane (BM-DBM), and benzophenone-3 (BP3) entering the Gulf waters from Texas beaches.

2. Material and methods

2.1. Study area of Gulf of Mexico (Texas)

Based on an EPA report, the total number of beaches in the Texas shoreline, all 14 counties, contain 169 beaches (EPA, 2013), which are aquatic centers for swimmers and beachgoers. The counties of Nueces and Galveston have the highest number of beaches, 43 and 36, respectively. Since 1970, the population of this region increased more than 50% by 2003 based on available statistical data (Lynch et al., 2003). Texas coastal zones have the second largest number of beach visitors (3.8 million) and swimmers (3.07 million) in the entire USA (Lynch et al., 2003). Fig. 1 shows the geographical distribution of Texas counties along the Gulf of Mexico.

2.2. Chemicals

Currently, 14 organic UV filters are authorized in the USA (Ao et al., 2015; Rodil et al., 2009). Four commonly-used UV filters, which are authorized in the USA were studied herein (Santos et al., 2012; Scalia and Mezzena, 2009). The chemical structures of these four compounds, BP3, EHMC, OC and BM-DBM, are described in Table 1, which are presenting the typical structure of chemical UV filters with an aromatic moiety and a side-chain indicating different degrees of unsaturation (Silvia Díaz-Cruz et al., 2008).

2.3. Concentration of UV filters

The average content of each UV filter in cosmetic products (Table 1) was calculated as a weighted average from the composition of individual products via Eq. (1), which was developed by Poiger et al. (2004). The data of UV filter content in sunscreen products used in this study were extracted from a study by Poiger et al. (2004).

$$c_{j,\mathrm{av}} = \frac{\sum n_j c_{j,i}}{\sum n_j}. \quad (1)$$

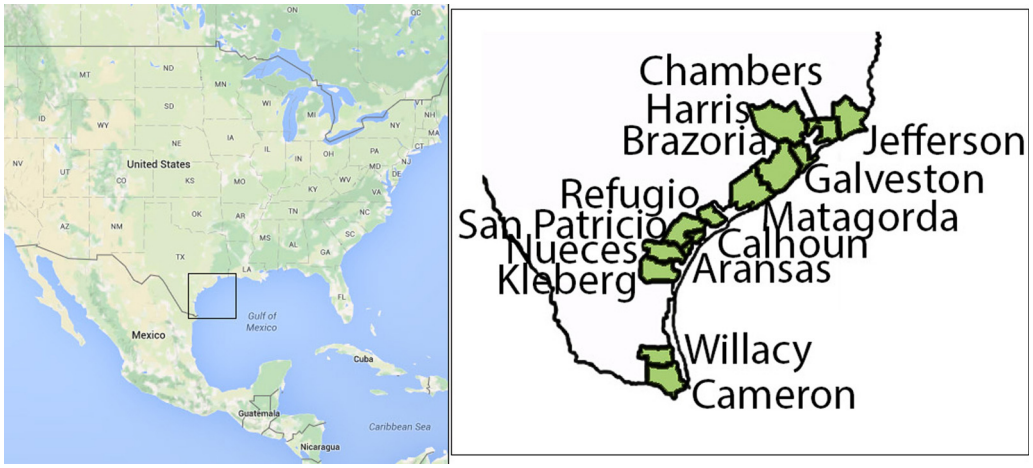

Figure 1 The map of the beaches in 14 counties along the Gulf coast of Texas.
Source: EPA (EPA, 2013), Google.

In this equation $c_{j,\mathrm{av}}$ is the average content of UV filter j in the products used during the survey, n_i is the number of people using product i, and $c_{j,i}$ is the concentration of UV filter j in product i.

2.4. Surface area of the body

In this study, the surface area of the body parts for different standard age groupings as recommended by the EPA (Table 2) was applied to estimate how much each individual body part could contribute to the release of UV filters into the surface water. The age classes between 1 and 21 are combined by gender. Both genders of male and female are classified from age 21 to 80 (EPA, 2011).

2.5. Release estimation

The direct input of UV filters to the surface water is a function of the fraction of UV filters released from the skin (wash-off rate) during swimming and sunbathing at the beach. The

Table 1 Chemical characteristics, structures and corresponding abbreviations of the surveyed UV filters.

INCI name[a]	Abbreviation	Solubility ([mg L^{-1}] at 25°C)[b]	Average UV filter content in sunscreen products [mg g^{-1}]	Log K_{ow}	Structure
Ethylhexyl methoxycinnamate	EHMC	0.15	2.4	5.8	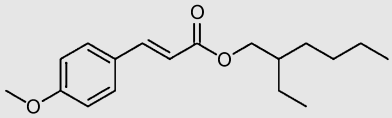
Octocrylene	OC	0.02	1.6	6.88	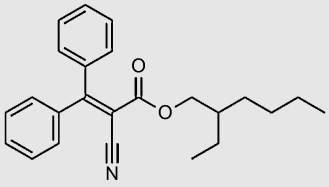
Benzophenone-3	BP3	68.56	0.8	3.79	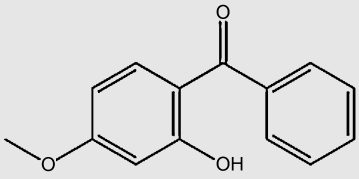
Butyl methoxydibenzoylmethane	BM-DBM	2.2	1.3	4.51	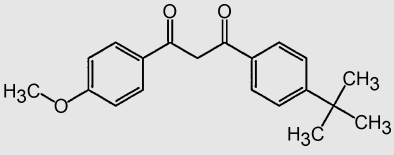

[a] International Nomenclature of Cosmetic Ingredients.
[b] *Source*: https://pubchem.ncbi.nlm.nih.gov.

Table 2 Surface area of each individual body part [m^2] for different age classifications.

Age class	Face	Trunk	Arms	Hands	Legs	Feet
1–<2	0.029	0.188	0.069	0.03	0.122	0.033
2–<3	0.017	0.25	0.088	0.028	0.154	0.038
3–<6	0.02	0.313	0.106	0.037	0.195	0.049
6–<11	0.022	0.428	0.151	0.051	0.311	0.073
11–<16	0.024	0.63	0.227	0.072	0.483	0.105
16–<21	0.025	0.759	0.269	0.083	0.543	0.112
>21 male	0.045	0.827	0.314	0.107	0.682	0.137
>21 female	0.038	0.654	0.237	0.089	0.598	0.122

lipophilic and hydrophilic UV filters account for 50 and 100% fraction rate (wash-off rate from the skin), respectively. Such a high fraction rate was studied on swimmers on beaches in Galveston County, Texas (Wright et al., 2001). In order to estimate the amount of release in each beach – because of a lack of demographical data on age classification of visitors to beaches – the average surface body of each adult swimmer, 1.94 m^2 recommended by the EPA (>21 years), was applied in this study to account for the worst case of water contamination with all adult swimmers (EPA, 2011). The empirical formula used for this estimation is shown in Eq. (2), which was developed in the previous study by author (Sharifan et al., 2016).

$$c_{j,\mathrm{rel}} = c_{j,\mathrm{av}} \times \alpha \times \beta \times S \times A. \quad (2)$$

The index $c_{j,\mathrm{rel}}$ indicates an estimation of the UV filters released from skin surface area for an adult swimmer (average of male and female), α is the amount of sunscreen cm^{-2} of skin, β is the application rate (dimensionless), S represents the surface area of the body and A represents the percentage of body which was covered by sunscreen products. Table 3 presents the experimental values of these parameters used by researchers in recent studies. In this study, A = 87%, α = 2 and β = 1.5 have been assumed (Poiger et al., 2004; Sharifan et al., 2016; Wright et al., 2001).

The number of swimmers on each beach was estimated by evenly distributing the total number of swimmers in Texas. The potential release rate of UV filters to the surface water in the Gulf of Mexico (index $c_{j,\mathrm{rel,p}}$) was calculated based on experimental Eq. (3), which was developed in this study.

$$c_{j,\mathrm{rel,p}} = c_{j,\mathrm{rel}} \times \emptyset \times P. \quad (3)$$

In this equation, $\emptyset$ indicates the fraction of UV filter (50%) and index P shows the number of swimmers or bathers who are visiting the beach during the swimming season (Sharifan et al., 2016). The annual number of swimmers in Texas was estimated to be approximately 3.07 million (Lynch et al., 2003).

3. Results and discussion

3.1. Release of UV filters from the body parts

The body surface area data (Table 2) and Eq. (2) that was used to calculate the potential release of UV filters from the surface area of swimmers is presented in Fig. 2, highlighting the impact of the different body parts on UV filter release. Evaluation of the data achieved from Eq. (3) showed that the release of UV filters significantly increased proportionately with the age of the groups. An adult male has the greatest majority of UV filter release from their skin due to higher surface area. Adult females show a significant rate of release except for the amount of EHMC, which is greater for the age group of 16–21. This difference can be explained by a larger surface area for teenagers. EHMC has the highest potential of release among the three other UV filters, which can be explained by a higher content in sunscreen products compared to other UV filter ingredients. OC showed greater value than BM-DBM, and BP3 indicated a lower value than BM-DBM in all average surface body parts in all ages. OC has higher K_{ow} (6.8) and has the highest content amount after EHMC compound. The trunk of the body has the largest surface area and shows the maximum potential for release. The hands and feet, respectively, have the lowest potential for release in the water. Trunk surface of the body for an adult can release a considerable concentration of UV filters that for EHMC could be the maximum level of approximately 200 mg per square meter of skin. Both hands and feet for a child (between 1 and 11 years) may release the minimum amount of UV filters due to smaller surface areas of the body.

Table 3 Experimental parameters for the application of sunscreens, which may vary in different studies.

References	Experimental parameters		
	α (amount of sunscreen [mg] cm^{-2} of skin)	β (application rate)	A (percentage of body [%])
Giokas et al. (2007); Poiger et al. (2004)	2, 3, 8	–	–
Poiger et al. (2004)	1	1.5	87
Neale et al. (2002)	1.5	1.03	80
Wright et al. (2001)	0.5, 1.5, 2	–	–

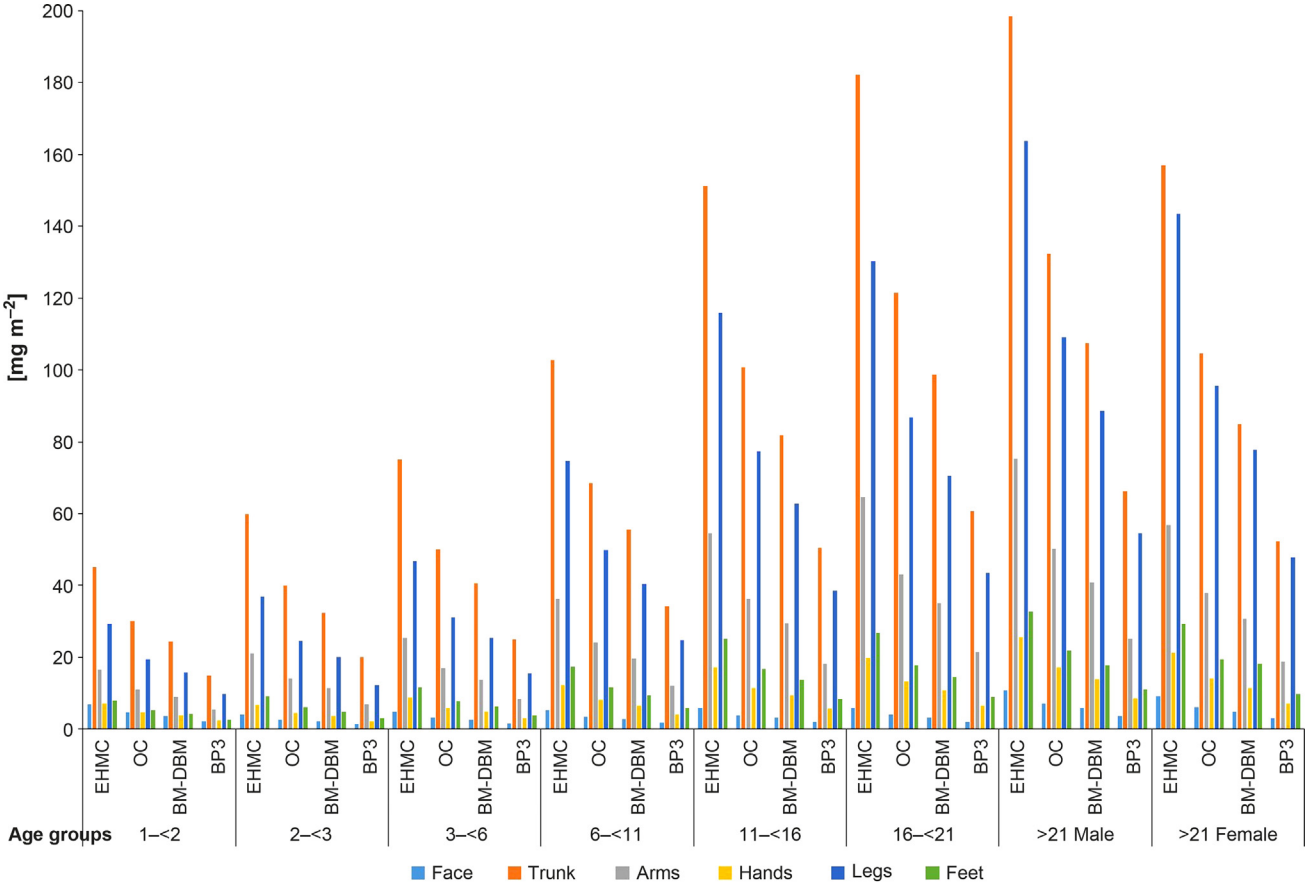

Figure 2 Results for UV filter release per body parts for different age classifications.

With respect to solubility, BP3 has the highest solubility in water (68.5 mg L^{-1}) among the other UV filters studied; therefore, it may have more potential for release in the surface water. However, BP3 may indicate a lower lipophilicity and bioaccumulation rate.

Fig. 3 shows that all UV filters have a higher potential release from the body surface of an adult male, and the age grouping of 16–21 has the second largest potential to release UV filters in surface water. This potential is due to the greater size of the body compared to other age classifications. Though there was no statistical data on the number of male and female visitors to the Gulf of Mexico in Texas, if women have a more than 50% higher tendency than men to apply sunscreens (Wright et al., 2001) on their body, the rate of release may significantly increase. However, regardless of a tendency to apply sunscreens, this analysis indicated that an average surface body of an adult female, after a male body, has a relatively high potential to release UV filters.

Due to the higher solubility of BP3 in the water, it may wash off faster than any other UV agents and may require reapplying the sunscreens. BP3 is approximately 4500 times more soluble in water than EHMC; and, at the same concentration levels, BP3 may enter the water at significantly larger amounts compared to EHMC. A study on beachgoers in Texas shows that half of beach visitors are more likely to stay in the sun longer when applying sunscreen, and approximately 70% of them believe the sunscreen will last at least 3 h without reapplying (Wright et al., 2001). Therefore, preference to stay longer periods of time on the beach may strengthen the hypothesis of higher wash-off rate from skin, as long as exposure times to the sunlight increase.

3.2. Release of UV filters to the surface water

The amount of UV filters that directly enters the Gulf further depends on the amount of UV filters released from the skin during swimming/bathing. The results of this analysis were used to estimate the average input of UV filters discharged to surface water in Texas coastal zones including 14 counties. Estuarine areas of the Texas coastline are productive aquatic systems for providing recreational and commercial marine species such as crabs, shrimp, and fish (Cai et al., 2007; Sager, 2002). For example, the Galveston Bay area has the second greatest number of beaches after Nueces, which is in the vicinity of the second largest populated region in Texas. This area has been contaminated by organic and inorganic aromatic compounds through anthropogenic sources (Glenn and James Lester, 2010; Liu et al., 2016). Therefore, an evaluation of the number of swimmers and potential release of organic UV filters from their body to the surface water is critical for the protection of the marine ecosystem of the Gulf and estuarine areas of the Texas region.

The results of this study (Table 4) estimated the Nueces with 43 beaches has the highest amount of sunscreen release to the water by 477 kg of EHMC, 318 kg of OC, 258 kg of BM-DBM and 159 kg of BP3. The county of Refugio with minimum

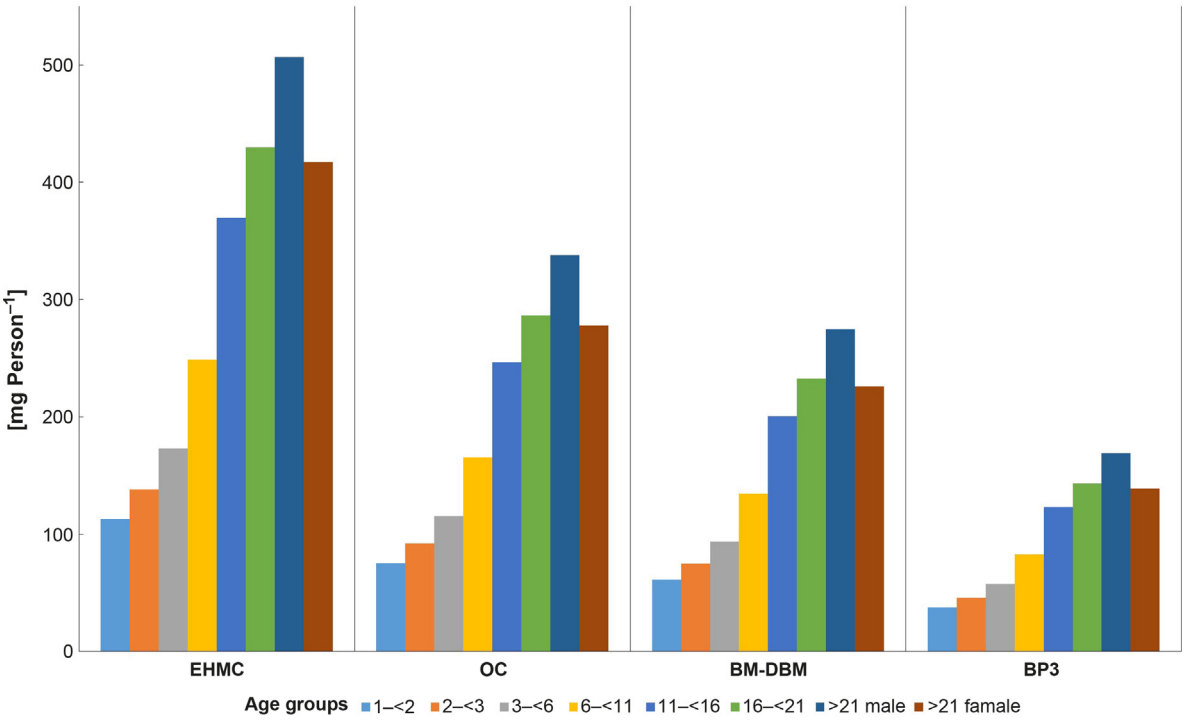

Figure 3 Results of releasing UV filters from the whole surface of a human body at different ages to the receiving water.

beach areas indicated the lowest potential of contamination with sunscreen products at the rate of approximately EHMC = 11 kg, OC = 7.5 kg, BM-DBM = 6 kg and BP3 = 4 kg. The quantity of sunscreen released during the swimming season could be far higher than what was estimated in this study because the number of beachgoers in Texas was greater than three million per year, which was not considered in this analysis. In addition, due to water activities (e.g. swimming, surfing, etc.) in the upstream of discharging rivers to the Gulf, a significant amount of UV filters may enter the water through a variety of streams, which increases the concentrations of UV filters in the Gulf.

Table 4 Estimated input of UV filters to surface water from swimmers in each county on the Texas coastline.

County	No. of beaches[a]	Beach percentage[b]	Swimmers (million)[c]	Estimated input of UV filters to surface water from swimmers [kg][d]			
				EHMC	OC	BM-DBM	BP3
Aransas	9	0.05	0.16	99.8	66.5	54.1	33.3
Brazoria	10	0.06	0.18	110.9	73.9	60.1	37.0
Calhoun	18	0.11	0.33	199.6	133.1	108.1	66.5
Cameron	12	0.07	0.22	133.1	88.7	72.1	44.4
Chambers	2	0.01	0.04	22.2	14.8	12.0	7.4
Galveston	36	0.21	0.66	399.2	266.1	216.2	133.1
Harris	8	0.05	0.15	88.7	59.1	48.0	29.6
Jefferson	2	0.01	0.04	22.2	14.8	12.0	7.4
Kleberg	7	0.04	0.13	77.6	51.7	42.0	25.9
Matagorda	12	0.07	0.22	133.1	88.7	72.1	44.4
Nueces	43	0.25	0.78	476.8	317.8	258.3	158.9
Refugio	1	0.01	0.02	11.1	7.4	6.0	3.7
San Patricio	6	0.04	0.11	66.5	44.4	36.0	22.2
Willacy	3	0.02	0.05	33.3	22.2	18.0	11.1
Total	169	1.00	3.08	1873.8	1249.2	1015.0	624.6

[a] Data from EPA report on Texas Beaches (EPA, 2013).
[b] Percentage of the beaches based on the EPA report on Texas Beaches.
[c] Calculated based on total population of swimmers in Texas reported by Lynch et al. (2003) and assumption of even distributions between beaches.
[d] Extrapolated from calculated data of potential release of UV filters from an adult (average of male and female) from the EPA report (EPA, 2015) and estimation of swimmers in a year.

However, the concentration of a variety of pyrogenic polyaromatic compounds (PAH) in the Gulf of Mexico has been increasing during the last decades (Ruiz-Fernández et al., 2016). The high concentration of UV filters released from the human body along with significant amounts of other PAH may have accumulative effects in estuarine areas of the Gulf coast of Texas. Due to chemical/microbiological stability, low water solubility, lipophilic properties, and vapor pressure, these aromatic-based compounds may accumulate highly in both aquatic and terrestrial estuary areas (Adhikari et al., 2016; Park et al., 2001). As an interpretation, the combination of both UV filter compounds and residues of petroleum pollution to the marine ecosystem may transform the oil into compounds with less volatility and longer residence time in the sediment. The carcinogenic, toxic, mutagenic and persistent nature of PAHs (Adhikari et al., 2016; Singleton et al., 2016) and the high tendency of UV filters to bioaccumulate (Giokas et al., 2007; Liu et al., 2015) may adversly affect the large fishing industry (e.g. mutagenic and estrogenic) in the Gulf of Mexico (Klimová et al., 2015; Ozáez et al., 2016), and make them a critical group of organic pollutants that need to be monitored thoroughly.

4. Conclusion

This study was a scientific approach based on the analysis of the available research data and EPA standards (age classification/body parts of human). Through this method, the release of UV filters from the surface body was estimated and the release of UV filters in susceptible coastal areas in Texas was predicted to provide bioaccumulation data. This information can be used to determine the hazard risks to aquatic wildlife of the region, which is linked to the food web.

Texas coastal zones consist of several sensitive estuarine that may be significantly affected by cumulative effects of UV filter release and contamination by PAHs. Rather than direct release through wash off from the skin, a considerable amount of UV filters may be released through showering or rubbing off with towels or clothes. This number may increase more during laundering or showering by using other personal care products containing UV filters (i.e. shampoos, cosmetics, etc.) and indirectly be discharged to the surface bodies through wastewater. Further studies are needed to investigate the ecotoxicological effects of the UV filters in aquatic organisms, particularly the cumulative effects of PAH compounds in estuarine areas of Texas coastal zones. Therefore, several bay areas in Texas can be considered as a sensitive ecosystem which are exposed to a significant amount of UV filters. Research on this issue may affect the environmental policies for the protection of the reservoirs such as zoning of marine areas as well as make markets reconsider the sunscreen formulation for a safe combination of ingredients.

Acknowledgments

We would like to thank Mr. John C. Korsman, a Ph.D. student at the Institute for Water and Wetland Research, Department of Environmental Science, Radboud University, The Netherlands for his comments and suggestions. Also, we would like to express our deep gratitude to Mrs. Shella Bibb Baccus for the editing and the English manuscript proofreading service.

Appendix A. Supplementary data

Supplementary data associated with this article can be found, in the online version, at doi:10.1016/j.oceano.2016.07.002.

References

Adhikari, P.L., Maiti, K., Overton, E.B., Rosenheim, B.E., Marx, B.D., 2016. Distributions and accumulation rates of polycyclic aromatic hydrocarbons in the northern Gulf of Mexico sediments. Environ. Pollut. 212, 413–423, http://dx.doi.org/10.1016/j.envpol.2016.01.064.

Amine, H., Gomez, E., Halwani, J., Casellas, C., Fenet, H., 2012. UV filters, ethylhexyl methoxycinnamate, octocrylene and ethylhexyl dimethyl PABA from untreated wastewater in sediment from eastern Mediterranean river transition and coastal zones. Mar. Pollut. Bull. 64 (11), 2435–2442, http://dx.doi.org/10.1016/j.marpolbul.2012.07.051.

Ao, J., Gao, L., Yuan, T., Jiang, G., 2015. Interaction mechanisms between organic UV filters and bovine serum albumin as determined by comprehensive spectroscopy exploration and molecular docking. Chemosphere 119, 590–600, http://dx.doi.org/10.1016/j.chemosphere.2014.07.019.

Arnot, J.A., Gobas, F.A.P.C., 2003. A generic QSAR for assessing the bioaccumulation potential of organic chemicals in aquatic food webs. QSAR Comb. Sci. 22 (3), 337–345, http://dx.doi.org/10.1002/qsar.200390023.

Blüthgen, N., Meili, N., Chew, G., Odermatt, A., Fent, K., 2014. Accumulation and effects of the UV-filter octocrylene in adult and embryonic zebrafish (*Danio rerio*). Sci. Total Environ. 476–477, 207–217, http://dx.doi.org/10.1016/j.scitotenv.2014.01.015.

Bratkovics, S., Wirth, E., Sapozhnikova, Y., Pennington, P., Sanger, D., 2015. Baseline monitoring of organic sunscreen compounds along South Carolina's coastal marine environment. Mar. Pollut. Bull. 101 (1), 370–377, http://dx.doi.org/10.1016/j.marpolbul.2015.10.015.

Broniowska, Ż., Pomierny, B., Smaga, I., Filip, M., Budziszewska, B., 2016. The effect of UV-filters on the viability of neuroblastoma (SH-SY5Y) cell line. Neurotoxicology 54, 44–52, http://dx.doi.org/10.1016/j.neuro.2016.03.003.

Cai, Y., Rooker, J.R., Gill, G.A., Turner, J.P., 2007. Bioaccumulation of mercury in pelagic fishes from the northern Gulf of Mexico. Can. J. Fish. Aquat. Sci. 64 (3), 458–469, http://dx.doi.org/10.1139/f07-017.

Danovaro, R., Bongiorni, L., Corinaldesi, C., Giovannelli, D., Damiani, E., Astolfi, P., Greci, L., Pusceddu, A., 2008. Sunscreens cause coral bleaching by promoting viral infections. Environ. Health Perspect. 116 (4), 441, http://dx.doi.org/10.1289/ehp.10966.

Ekpeghere, K.I., Kim, U.-J., O., S.-H., Kim, H.-Y., Oh, J.-E., 2016. Distribution and seasonal occurrence of UV filters in rivers and wastewater treatment plants in Korea. Sci. Total Environ. 542 (Part A), 121–128, http://dx.doi.org/10.1016/j.scitotenv.2015.10.033.

EPA, 2013. EPA's BEACH Report: Texas 2012 Swimming Season. United States, EPA, 2 pp., https://www.epa.gov/sites/production/files/2013-10/documents/tx2012.pdf.

EPA, 2015. Dermal exposure factors. In: Agency, T.U.S.E.P. (Ed.), Exposure Factors Handbook. EPA 6 pp., http://www.epa.gov/sites/production/files/2015-06/documents/efh_highlights_chap7.pdf.

EPA, U., 2011. Exposure factors handbook: 2011 Edition (Final), Washington, DC, 1466 pp., http://www.nrc.gov/docs/ML1400/ML14007A666.pdf.

Gago-Ferrero, P., Díaz-Cruz, M.S., Barceló, D., 2015. UV filters bioaccumulation in fish from Iberian river basins. Sci. Total Environ. 518–519, 518–525, http://dx.doi.org/10.1016/j.scitotenv.2015.03.026.

Gago-Ferrero, P., Mastroianni, N., Díaz-Cruz, M.S., Barceló, D., 2013. Fully automated determination of nine ultraviolet filters and transformation products in natural waters and wastewaters by on-line solid phase extraction-liquid chromatography–tandem mass spectrometry. J. Chromatogr. A 1294, 106–116, http://dx.doi.org/10.1016/j.chroma.2013.04.037.

Giokas, D.L., Sakkas, V.A., Albanis, T.A., 2004. Determination of residues of UV filters in natural waters by solid-phase extraction coupled to liquid chromatography–photodiode array detection and gas chromatography–mass spectrometry. J. Chromatogr. A 1026 (1–2), 289–293, http://dx.doi.org/10.1016/j.chroma.2003.10.114.

Giokas, D.L., Sakkas, V.A., Albanis, T.A., Lampropoulou, D.A., 2005. Determination of UV-filter residues in bathing waters by liquid chromatography UV-diode array and gas chromatography–mass spectrometry after micelle mediated extraction-solvent back extraction. J. Chromatogr. A 1077 (1), 19–27, http://dx.doi.org/10.1016/j.chroma.2005.04.074.

Giokas, D.L., Salvador, A., Chisvert, A., 2007. UV filters: from sunscreens to human body and the environment. TrAC Trends Anal. Chem. 26 (5), 360–374, http://dx.doi.org/10.1016/j.trac.2007.02.012.

Glenn, S.M., James Lester, L., 2010. An analysis of the relationship between land use and arsenic, vanadium, nitrate and boron contamination in the Gulf Coast aquifer of Texas. J. Hydrol. 389 (1–2), 214–226, http://dx.doi.org/10.1016/j.jhydrol.2010.06.002.

Kim, S., Choi, K., 2014. Occurrences, toxicities, and ecological risks of benzophenone-3, a common component of organic sunscreen products: a mini-review. Environ. Int. 70, 143–157, http://dx.doi.org/10.1016/j.envint.2014.05.015.

Klimová, Z., Hojerová, J., Beránková, M., 2015. Skin absorption and human exposure estimation of three widely discussed UV filters in sunscreens – in vitro study mimicking real-life consumer habits. Food Chem. Toxicol. 83, 237–250, http://dx.doi.org/10.1016/j.fct.2015.06.025.

Korsman, J.C., Schipper, A.M., de Vos, M.G., van den Heuvel-Greve, M.J., Vethaak, A.D., de Voogt, P., Hendriks, A.J., 2015. Modeling bioaccumulation and biomagnification of nonylphenol and its ethoxylates in estuarine–marine food chains. Chemosphere 138, 33–39, http://dx.doi.org/10.1016/j.chemosphere.2015.05.040.

Kupper, T., Plagellat, C., Brändli, R., de Alencastro, L.F., Grandjean, D., Tarradellas, J., 2006. Fate and removal of polycyclic musks, UV filters and biocides during wastewater treatment. Water Res. 40 (14), 2603–2612, http://dx.doi.org/10.1016/j.watres.2006.04.012.

Li, W., Ma, Y., Guo, C., Hu, W., Liu, K., Wang, Y., Zhu, T., 2007. Occurrence and behavior of four of the most used sunscreen UV filters in a wastewater reclamation plant. Water Res. 41 (15), 3506–3512, http://dx.doi.org/10.1016/j.watres.2007.05.039.

Liu, H., Sun, P., Liu, H., Yang, S., Wang, L., Wang, Z., 2015. Hepatic oxidative stress biomarker responses in freshwater fish *Carassius auratus* exposed to four benzophenone UV filters. Ecotoxicol. Environ. Saf. 119, 116–122, http://dx.doi.org/10.1016/j.ecoenv.2015.05.017.

Liu, Z., Liu, J., Gardner, W.S., Shank, G.C., Ostrom, N.E., 2016. The impact of Deepwater Horizon oil spill on petroleum hydrocarbons in surface waters of the northern Gulf of Mexico. Deep Sea Res. Part II: Top. Stud. Oceanogr. 129, 292–300, http://dx.doi.org/10.1016/j.dsr2.2014.01.013.

Lynch, T.A., Harrington, J., O'Brien, J.J., 2003. Economic Impact Analysis of Coastal Ocean Observing System in the Gulf Coast Region. US Department of Commerce, National Oceanic and Atmospheric Administration, Office of Program Planning and Integration.

Mueller, S.O., Kling, M., Firzani, P.A., Mecky, A., Duranti, E., Shields-Botella, J., Delansorne, R., Broschard, T., Kramer, P.-J., 2003. Activation of estrogen receptor α and ERβ by 4-methylbenzylidene-camphor in human and rat cells: comparison with phyto- and xenoestrogens. Toxicol. Lett. 142 (1–2), 89–101, http://dx.doi.org/10.1016/S0378-4274(03)00016-X.

Nakajima, M., Kawakami, T., Niino, T., Takahashi, Y., Onodera, S., 2009. Aquatic fate of sunscreen agents octyl-4-methoxycinnamate and octyl-4-dimethylaminobenzoate in model swimming pools and the mutagenic assays of their chlorination byproducts. J. Health Sci. 55 (3), 363–372, http://dx.doi.org/10.1248/jhs.55.363.

Neale, R., Williams, G., Green, A., 2002. Application patterns among participants randomized to daily sunscreen use in a skin cancer prevention trial. Arch. Dermatol. 138 (10), 1319–1325, http://dx.doi.org/10.1001/archderm.138.10.1319.

Ozáez, I., Aquilino, M., Morcillo, G., Martínez-Guitarte, J.-L., 2016. UV filters induce transcriptional changes of different hormonal receptors in *Chironomus riparius* embryos and larvae. Environ. Pollut. 214, 239–247, http://dx.doi.org/10.1016/j.envpol.2016.04.023.

Park, J.-S., Wade, T.L., Sweet, S., 2001. Atmospheric distribution of polycyclic aromatic hydrocarbons and deposition to Galveston Bay, Texas, USA. Atmos. Environ. 35 (19), 3241–3249, http://dx.doi.org/10.1016/S1352-2310(01)00080-2.

Plagellat, C., Kupper, T., Furrer, R., De Alencastro, L.F., Grandjean, D., Tarradellas, J., 2006. Concentrations and specific loads of UV filters in sewage sludge originating from a monitoring network in Switzerland. Chemosphere 62 (6), 915–925, http://dx.doi.org/10.1016/j.chemosphere.2005.05.024.

Poiger, T., Buser, H.-R., Balmer, M.E., Bergqvist, P.-A., Müller, M.D., 2004. Occurrence of UV filter compounds from sunscreens in surface waters: regional mass balance in two Swiss lakes. Chemosphere 55 (7), 951–963, http://dx.doi.org/10.1016/j.chemosphere.2004.01.012.

Ramos, S., Homem, V., Alves, A., Santos, L., 2016. A review of organic UV-filters in wastewater treatment plants. Environ. Int. 86, 24–44, http://dx.doi.org/10.1016/j.envint.2015.10.004.

Rodil, R., Moeder, M., 2008. Development of a method for the determination of UV filters in water samples using stir bar sorptive extraction and thermal desorption–gas chromatography–mass spectrometry. J. Chromatogr. A 1179 (2), 81–88, http://dx.doi.org/10.1016/j.chroma.2007.11.090.

Rodil, R., Moeder, M., Altenburger, R., Schmitt-Jansen, M., 2009. Photostability and phytotoxicity of selected sunscreen agents and their degradation mixtures in water. Anal. Bioanal. Chem. 395 (5), 1513–1524, http://dx.doi.org/10.1007/s00216-009-3113-1.

Ruiz-Fernández, A.C., Betancourt Portela, J.M., Sericano, J.L., Sanchez-Cabeza, J.-A., Espinosa, L.F., Cardoso-Mohedano, J.G., Pérez-Bernal, L.H., Garay Tinoco, J.A., 2016. Coexisting sea-based and land-based sources of contamination by PAHs in the continental shelf sediments of Coatzacoalcos River discharge area (Gulf of Mexico). Chemosphere 144, 591–598, http://dx.doi.org/10.1016/j.chemosphere.2015.08.081.

Sager, D.R., 2002. Long-term variation in mercury concentrations in estuarine organisms with changes in releases into Lavaca Bay, Texas. Mar. Pollut. Bull. 44 (8), 807–815, http://dx.doi.org/10.1016/S0025-326X(02)00064-4.

Santos, A.J.M., Miranda, M.S., Esteves da Silva, J.C.G., 2012. The degradation products of UV filters in aqueous and chlorinated aqueous solutions. Water Res. 46 (10), 3167–3176, http://dx.doi.org/10.1016/j.watres.2012.03.057.

Scalia, S., Mezzena, M., 2009. Incorporation in lipid microparticles of the UVA filter, butyl methoxydibenzoylmethane combined with the UVB filter, octocrylene: effect on photostability. AAPS PharmSciTech 10 (2), 384–390, http://dx.doi.org/10.1208/s12249-009-9217-2.

Sharifan, H., Klein, D., Morse, A.N., 2016. UV filters interaction in the chlorinated swimming pool, a new challenge for urbanization, a need for community scale investigations. Environ. Res. 148, 273—276, http://dx.doi.org/10.1016/j.envres.2016.04.002.

Silvia Díaz-Cruz, M., Llorca, M., Barceló, D., Barceló, D., 2008. Organic UV filters and their photodegradates, metabolites and disinfection by-products in the aquatic environment. TrAC Trends Anal. Chem. 27 (10), 873—887, http://dx.doi.org/10.1016/j.trac.2008.08.012.

Singleton, B., Turner, J., Walter, L., Lathan, N., Thorpe, D., Ogbevoen, P., Daye, J., Alcorn, D., Wilson, S., Semien, J., Richard, T., Johnson, T., McCabe, K., Estrada, J.J., Galvez, F., Velasco, C., Reiss, K., 2016. Environmental stress in the Gulf of Mexico and its potential impact on public health. Environ. Res. 146, 108—115, http://dx.doi.org/10.1016/j.envres.2015.12.019.

Valle-Sistac, J., Molins-Delgado, D., Díaz, M., Ibáñez, L., Barceló, D., Silvia Díaz-Cruz, M., 2016. Determination of parabens and benzophenone-type UV filters in human placenta. First description of the existence of benzyl paraben and benzophenone-4. Environ. Int. 88, 243—249, http://dx.doi.org/10.1016/j.envint.2015.12.034.

Vila, M., Lamas, J.P., Garcia-Jares, C., Dagnac, T., Llompart, M., 2016. Ultrasound-assisted emulsification microextraction followed by gas chromatography—mass spectrometry and gas chromatography—tandem mass spectrometry for the analysis of UV filters in water. Microchem. J. 124 (5), 530—539.

Wright, M.W., Wright, S.T., Wagner, R.F., 2001. Mechanisms of sunscreen failure. J. Am. Acad. Dermatol. 44 (5), 781—784, http://dx.doi.org/10.1067/mjd.2001.113685.

Zimmer, B., Precht, W., Hickerson, E., Sinclair, J., 2006. Discovery of *Acropora palmata* at the flower garden banks national marine sanctuary, northwestern Gulf of Mexico. Coral Reefs 25 (2), 192, http://dx.doi.org/10.1007/s00338-005-0054-9.

Oceanologia (2016) 58, 336—340

Available online at www.sciencedirect.com

ScienceDirect

journal homepage: www.journals.elsevier.com/oceanologia/

SHORT COMMUNICATION

Colonies of *Gyrosigma eximium*: a new phenomenon in Arctic tidal flats

Józef Wiktor [a,*], **Agnieszka Tatarek** [a], **Jan M. Węsławski** [a], **Lech Kotwicki** [a], **Michel Poulin** [b]

[a] *Institute of Oceanology PAN, Sopot, Poland*
[b] *Research and Collections Division, Canadian Museum of Nature, Ottawa, Canada*

Received 5 February 2016; accepted 22 April 2016
Available online 16 May 2016

KEYWORDS
Tidal flat;
Tube-dwelling diatoms;
Spitsbergen

Summary For the first time at Svalbard, a colonial form of the tube-dwelling diatom *Gyrosigma eximium* was found in summer 2010 in the tidal flats on Spitsbergen at 78°N. The colonies take the form of conical, green structures that are 1—2 cm high and are associated with other diatom taxa and cyanobacteria (Oscillatoriaceae). The diatom colonies were associated with rich meiofauna and apparently act as cohesive factors for the fine sediment. In the Arctic tidal flats, this represents the first observation of long-term sediment stabilization and biological enrichment. Since this first observation, this species has apparently colonized broader areas in Advenentelva's tidal flat.

1. Introduction

Arctic tidal flats are unique habitats in which the winter freezes down to the upper 10—20 cm of sediment and forms a solid ice (80—110 cm) cover on the surface that breaks and moves apart in spring with the tides, removing the frozen sediment layer (Węsławski et al., 1999). The removal of this upper layer of sediment causes seasonal defaunation of the seabed and random recolonization of this very unstable fine sediment. The Adventfjorden tidal flat, which is located near Longyearbyen (Spitsbergen) at 78°N, 15°E (Fig. 1), is one of the most intensively studied Arctic coastal habitats (Dobrzyn et al., 2005; Węsławski and Szymelfenig, 1999; Węsławski et al., 1999; Węsławski et al., 1993; Zajączkowski et al.,

* Corresponding author at: Institute of Oceanology PAN, Marine Ecology, Powst. Warszawy 55, 81-712 Sopot, Poland.
Tel.: +48 587311785.
E-mail address: wiktor@iopan.gda.pl (J. Wiktor).
Peer review under the responsibility of Institute of Oceanology of the Polish Academy of Sciences.

Production and hosting by Elsevier

http://dx.doi.org/10.1016/j.oceano.2016.04.007

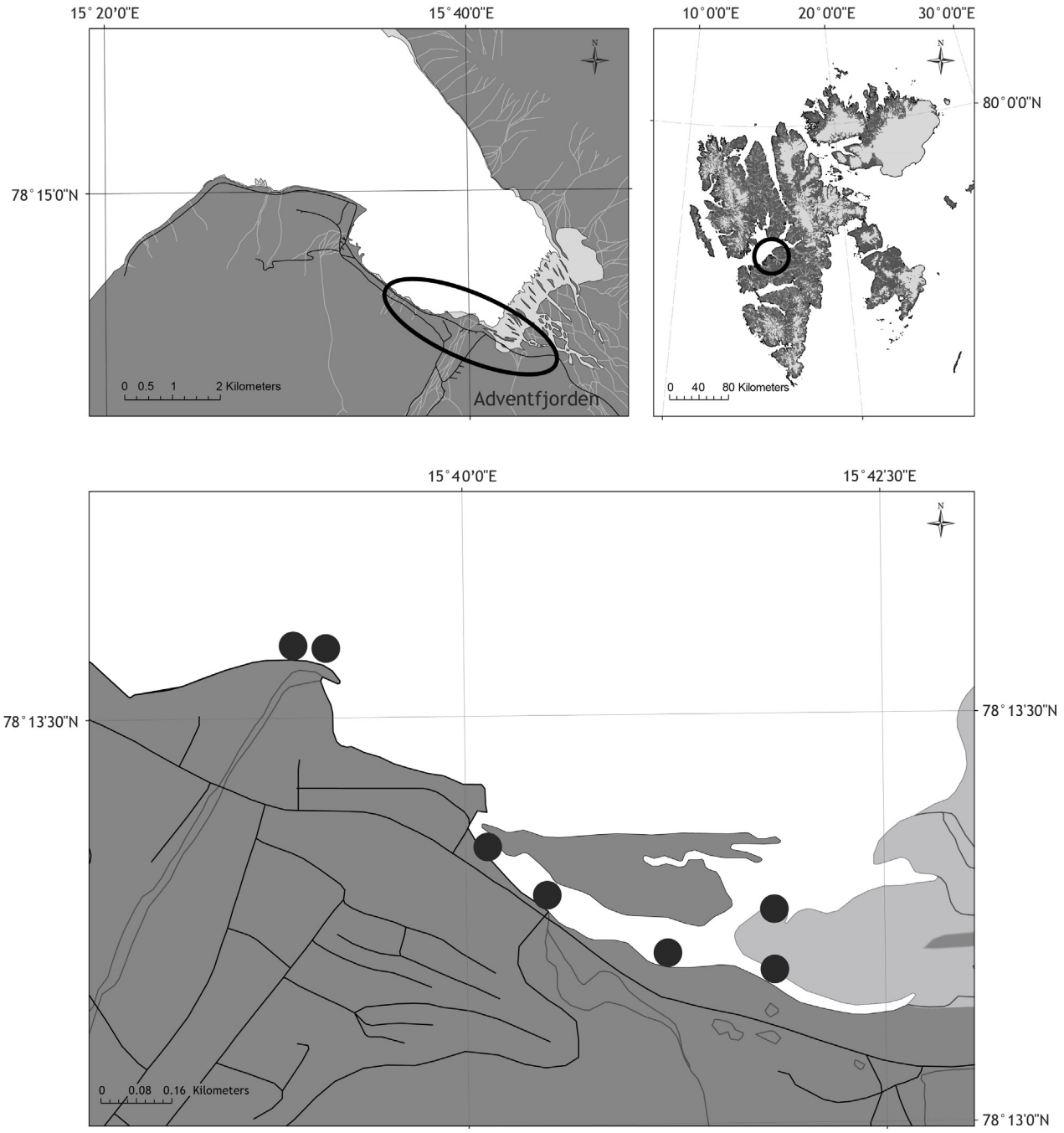

Figure 1 Area of interest and sampling points.

2008). This area is strongly influenced by Adventelva, a river with a flow rate as high as 3.6 $m^3 s^{-1}$ that is loaded with 132–486 g dm^{-3} of mineral suspended matter (Zajączkowski et al., 2004). During low tide, at least the highest parts of the bottom are exposed for approximately 4 h per cycle of regular M2 semidiurnal tide. In this frequently visited (every summer) area, we noted a new and distinctive feature in late summer 2010. This phenomenon seems to be recurrent, and we observed it in consecutive years. During the observation period, the area populated by colonies increased, and green, conical structures cover large parts of this area during low tide (Fig. 2). Since then, the structures have been observed in the same area every summer (July to September). This paper presents the details of our examination of this new phenomenon.

2. Material and methods

Surface sediment samples from areas with green structures were collected from 7 locations in the Adventfjorden tidal flat in the summers of 2010–2013. In 2010, sampling was performed using corers (3.6 cm in diameter). The upper 5 cm were collected and immediately fixed in 4% formaldehyde. In 2011–2013, samples were collected only qualitatively using tweezers and were also fixed in 4% formaldehyde.

Figure 2 General view of the area covered by *Gyrosigma eximium* colonies (a) and a close-up view of the colonies (b).

For algological analysis, a microscope equipped with differential interference contrast (DIC) and phase contrast and with 10, 40 and 60× (water-immersion) objectives was initially used. To perform a detailed taxonomical determination, diatom frustules that had been cleaned in 30% hydrogen peroxide (H_2O_2) were analysed under a light microscope (magnification 600×) and a scanning electron microscope (SEM). For SEM analyses, few drops of cleaned diatom material were put on aluminum stubs, air-dried, coated with gold and examined under a Philips environmental SEM operating at 10 kV.

Prior to meiofauna analyses, the LUDOX HS silica density gradient centrifugation technique (density of 1.18 g cm^{-3}) was used to extract meiofaunal organisms from the sediment (Heip et al., 1985). After centrifugation, the supernatant was sieved through 500 μm and 38 μm sieves. The samples retained on the 38 μm sieve were stained with Rose Bengal. Subsequently, meiofaunal organisms were identified to the higher taxa level (phylum, class or order), and the abundances of particular taxa were expressed per 10 cm^2.

3. Results and discussion

The structures, which were of a 1—2 cm height and basal width, grew on the higher parts of the tidal flats that emerged during low-tide above the sediment (Fig. 2). They remained exposed for 2—3 h during each tidal cycle. The structure density was approximately 100—160 per m^2, and the estimated biomass (wet weight) was 50 g m^{-2}.

Analyses conducted using high-power light microscopy revealed that these structures consisted of branched tubes that were densely packed with *Gyrosigma eximium* (Thwaites) Boyer arranged in single or multiple rows of cells (Fig. 3).

3.1. Description of the *Gyrosigma eximium*

The valves are linear with obliquely rounded ends. Their length ranges from 53.4 μm to 75.9 μm and the width from 8.8 μm to 12.8 μm. The valves are straight, nearly central, and slightly sigmoid at the ends. The central area is rather large and rounded. Transverse striae (23—25 in 10 μm) and longitudinal striae (27—28 in 10 μm) were observed. The frustules in the gelatinous tubes differed from those of *G. scalproides* (Rabenhorst) Cleve and *G. obtusatum* (Sullivant & Wormley) Boyer in their linear outline and from those of *G. obliquum* (Grunow) Boyer in their rounded ends (Fig. 4).

Type locality: England. Distribution: fresh and brackish water. Rare and local. Reported from the Demerara River, Guiana, and occurs at Rio de Janeiro. It may occur northward.

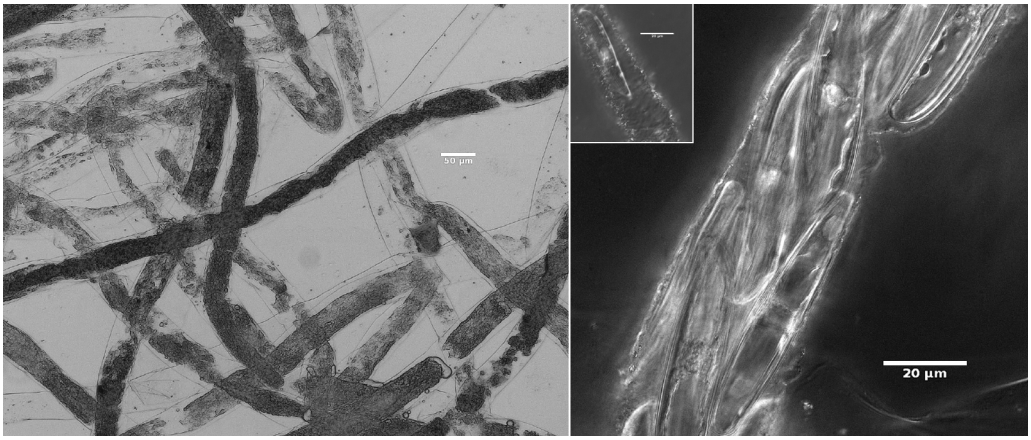

Figure 3 Magnified view of the *Gyrosigma eximium* tubes.

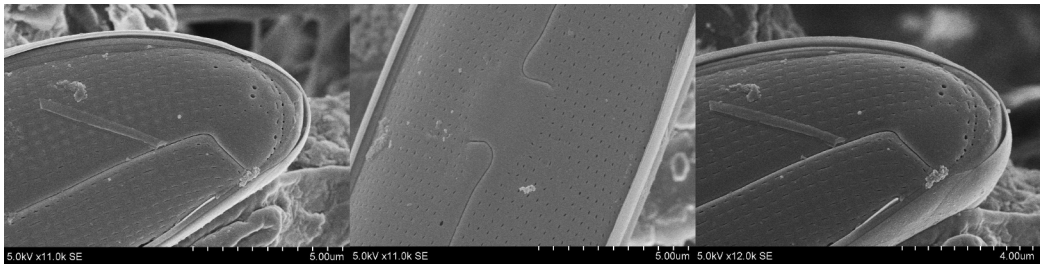

Figure 4 SEM picture of *Gyrosigma eximium* from Adventfjorden tidal flat.

Its ornamentation is characteristic for the section Strigiles (Peragallo, 1890–1981). The longitudinal striae (32–35 in 10 μm) are less spaced and less visible than the transapical ones (22–24 in 10 μm). Although the linear valve outline resembles that of *G. balticum* (Ehrenberg) Rabenhorst or *G. pensacolae* Sterrenburg, the latter two species are longer and broader (200 μm; 25 μm). All three taxa, however, have equal numbers of longitudinal and transapical striae (11–14 in 10 μm). Unlike *G. limosum* Sterrenburg & Underwood, as discussed here, *Gyrosigma* presents linear valves with parallel margins (in contrast to the nearly linear to slightly lanceolate ones of *G. limosum*). Additionally, it has a somewhat median raphe with a tendency to be off centred when approaching the apices; in *G. limosum*, the raphe is practically median throughout the entire valve. Finally, as presented here, *Gyrosigma* has a small terminal hyaline area, triangular in shape and displaced towards the terminal, strongly deflected raphe fissure, whereas that of *G. limosum* is only slightly deflected (Sterrenburg and Underwood, 1997).

3.2. Distribution

Gyrosigma is also known to be a component of ice-associated communities (Poulin, 1991). In tidal flats, this genus was reported by Asmus and Bauerfeind (1994) in the Wadden Sea, whereas Jesus et al. (2009) identified *G. fasciola* (Ehrenberg) Griffith & Henfrey as a microbenthic diatom with 'muddy' preferences. To date, only *G. obliquum* has been noted at sites located outside of the Arctic, as far as the Gulf of Mexico (Krayesky et al., 2009), Samoa (Sterrenburg, 1989) and South China (UNEP, 2008). Some *Gyrosigma* taxa are known for their ability to form tube structures and were previously found further south (45°N), in the Canadian salt marshes of the Bay of Fundy (*G. orbitum* Thaler & Kaczmarska) by Thaler and Kaczmarska (2009), and in western European mudflats (*G. limosum*) by Underwood et al. (1998). According to Sterrenburg (1989), only *G. eximium* exists as tube-dwelling forms. For example, *G. orbitum*, which was described by Thaler and Kaczmarska (2009), forms uniseriate tubes, whereas in Adventfjorden, *G. eximium* forms multiseriate branched tubes.

3.3. Ecological impact

Diatom colonies and their associated cyanobacterial mats constitute a potential factor increasing the transfer of organic carbon to heterotrophic parts of tidal flats. The relatively very high density of meiofauna, exceeding in average 3000 ind. 10 cm^{-2} in comparison with typical for Adventfjorden tidal flat densities of 100 ind. 10 cm^{-2}, in extreme case 1941 ind. 10 cm^{-2} (Table 1) seems to be a confirmation of this statement.

The taxonomic structure of the meiofauna associated with *G. eximium* structures shows a predominance of harpacticoid copepods over nematodes and relatively high density of tardigrades, whereas in previous studies in this region, a clear predominance of nematodes was observed. The most numerous harpacticoid species was the newly described *Nannopus didelphis* Fiers and Kotwicki (2013), which confirms that *Nannopus palustris auct.* is a complex of pseudo-cryptic species (Fiers and Kotwicki, 2013). In general, the Svalbard intertidal meiofauna displayed low density and diversity, with nematodes dominating in total abundance. However, specific microhabitats can create favourable conditions for

Table 1 Abundance [ind. cm^{-2}] of intertidal meiofauna in Isfjorden, Adventfjorden and this study.

Site	Isfjorden mean of 30 sampling points	Adventfjorden only			This study
Taxon	[b]	[a]	[b]	[c]	
Nematoda	113	116	23	1640	1428
Harpacticoida	43	0	3	30	1575
Copepoda nauplii	22	0	0	267	26
Tardigrada	1	0	0	1	38
Polychaeta	1	0	0	0	19
Others	61	0	0	3	0
Total	241	133	26	1941	3086

[a] Włodarska-Kowalczuk et al. (2007).
[b] Szymelfenig et al. (1995).
[c] Węsławski and Szymelfenig (1999).

abundant meiofaunal communities dominated by other taxa. Besides their nutritional influence, the observed high density of tube-dwelling diatoms may act as an important stabilizer of the surface sediment of tidal flats because excreted extracellular polymeric substances may glue the sediment particles together (Decho, 2000).

Acknowledgements

This study was supported by NCN-funded grants: GAME, PicMac, UMO-2015/17/B/NZ8/02473 and Norwegian Funding Mechanism GLARE.

References

Asmus, R., Bauerfeind, E., 1994. The microphytobenthos of Königshafen – spatial and seasonal distribution on a sandy tidal flat. Helgol. Meeresunters. 48 (2–3), 257–276.

Decho, A.W., 2000. Microbial biofilms in intertidal systems: an overview. Cont. Shelf Res. 20 (10), 1257–1273.

Dobrzyn, P., Keck, A., Tatur, A., 2005. Sedimentation of chlorophylls in an Arctic fjord under freshwater discharge. Hydrobiologia 532 (1–3), 1–8.

Fiers, F., Kotwicki, L., 2013. The multiple faces of *Nannopus palustris auct.* reconsidered: a morphological approach (Copepoda: Harpacticoida: Nannopodidae). Zool. Anz. 253 (1), 36–65.

Heip, C., Vincx, M., Vranken, G., 1985. The ecology of marine nematodes. Oceanogr. Mar. Biol. Ann. Rev. 23, 399–489.

Jesus, B., Brotas, V., Ribeiro, L., Mendes, C., Cartaxana, P., Paterson, D., 2009. Adaptations of microphytobenthos assemblages to sediment type and tidal position. Cont. Shelf Res. 29 (13), 1624–1634.

Krayesky, D.M., Meave del Castillo, E., Zamudio, E., Norris, J.N., Fredericq, S., Tunnell Jr, J., Felder, D., Earle, S., 2009. Diatoms (Bacillariophyta) of the Gulf of Mexico. In: Felder, D.L., Camp, D. K. (Eds.), Gulf of Mexico Origin, Waters, and Biota: Biodiversity. Vol. 1. Texas A&M Univ. Press, College Station, 155–185.

Peragallo, H., 1890–1981. Monographie du genre *Pleurosigma* et des genres alliés. Vol. 1 of Le Diatomiste, Tempère, 96 pp.

Poulin, M., 1991. Sea ice diatoms (Bacillariophyceae) of the Canadian Arctic. 2. A taxonomic, morphological and geographical study of *Gyrosigma concilians*. Nord. J. Bot. 10 (6), 681–688.

Sterrenburg, F., 1989. Studies on tube-dwelling *Gyrosigma* populations. Diatom Res. 4 (1), 143–150.

Sterrenburg, F., Underwood, G.J., 1997. Studies on the Genera Gyrosigma and Pleurosigma (Bacillariophyceae). The marine "*Gyrosigma spenceri*" records: *Gyrosigma limosum* Sterrenburg et Underwood nov. sp. Proc. Acad. Nat. Sci. Philadelphia 165–169.

Szymelfenig, M., Kwaśniewski, S., Węsławski, J.M., 1995. Intertidal zone of Svalbard. Polar Biol. 15 (2), 137–141.

Thaler, M., Kaczmarska, I., 2009. *Gyrosigma orbitum* sp. nov. (Bacillariophyta) from a salt marsh in the Bay of Fundy, eastern Canada. Bot. Mar. 52 (1), 60–68.

Underwood, G., Phillips, J., Saunders, K., 1998. Distribution of estuarine benthic diatom species along salinity and nutrient gradients. Eur. J. Phycol. 33 (2), 173–183.

UNEP, 2008. National Reports on Mangroves in the South China Sea. UNEP/GEF/SCS Technical Publication No. 14.

Węsławski, J., Szymelfenig, M., 1999. Community composition of tidal flats on Spitsberg: consequence of disturbance. In: Gray, J., Ambrose, W., Szaniawska, A. (Eds.), Biogeochemical Cycling and Sediment Ecology. Vol. 59 of NATO ASI Series. Springer Science +Business Media B.V., Dordrecht, 185–193.

Węsławski, J.M., Szymelfenig, M., Zajączkowski, M., Keck, A., 1999. Influence of salinity and suspended matter on benthos of an Arctic tidal flat. ICES J. Mar. Sci. (56), 194–202.

Węsławski, J., Wiktor, J., Zajączkowski, M., Swerpel, S., 1993. Intertidal zone of Svalbard. Polar Biol. 13 (2), 73–79.

Włodarska-Kowalczuk, M., Szymelfenig, M., 2007. Dynamic sedimentary environments of an Arctic glacier-fed river estuary (Adventfjorden, Svalbard). II: Meio- and macrobenthic fauna. Estuar. Coast. Shelf Sci. 74 (1–2), 274–284.

Zajączkowski, M., 2008. Sediment supply and fluxes in glacial and outwash fjords, Kongsfjorden and Adventfjorden, Svalbard. Polish Polar Res. 29 (1), 59–72.

Zajączkowski, M., Szczuciński, W., Bojanowski, R., 2004. Recent changes in sediment accumulation rates in Adventfjorden, Svalbard. Oceanologia 46 (2), 217–231.

Oceanologia (2016) 58, 341—352

Available online at www.sciencedirect.com

ScienceDirect

journal homepage: www.journals.elsevier.com/oceanologia/

SHORT COMMUNICATION

How do differences in the nutritional and hydrological background influence phytoplankton in the Vistula Lagoon during a hot summer day?

Marek Kruk [a,*], **Bożena Jaworska** [a], **Izabela Jabłońska-Barna** [a], **Agata Rychter** [b]

[a] *University of Warmia and Mazury, Department of Applied Ecology, Olsztyn, Poland*
[b] *State University of Applied Sciences in Elbląg, Institute of Technology, Elbląg, Poland*

Received 18 October 2015; accepted 13 May 2016
Available online 28 May 2016

KEYWORDS
Lagoon;
Soluble Reactive Phosphorus;
Dissolved Inorganic Nitrogen;
Phytoplankton;
Biomass

Summary The aim of this work was to find out whether the difference between the central Vistula Lagoon (the southern Baltic Sea) and the western lagoon was reflected in the relationships between nutrients and phytoplankton during one-day hot summer conditions when the water temperature exceeded 20°C. Significant differences in Soluble Reactive Phosphorus (SRP) and Dissolved Inorganic Nitrogen (DIN) concentrations, and also in the biomass of the dominant phytoplankton assemblage of Cyanoprokaryota, were noted in the studied parts of the lagoon. No such differences were found for the nitrogen to phosphorus ratio (N:P) or for the biomasses of Bacillariophyta and Chlorophyta. The very low values of N:P (on average 2.8 and 3.4) indicated strong nitrogen limitation. The Correspondence Canonical Analysis (CCA) showed that the central part of the lagoon could be defined as positively related to DIN and to N:P, and western part could be characterized by correlation with temperature, dissolved oxygen and SRP concentrations. Competition for the limited resources of Dissolved Inorganic Nitrogen in the western, shallower part of the lagoon was in favour of Cyanoprokaryota, to the detriment of other phytoplankton assemblages. In contrast, the Cyanoprokaryota biomass in the central part of the lagoon, where DIN concentrations were increased, was lower, and Bacillariophyta in particular prospered at their expense. Here, the competition for Soluble Reactive Phosphorus was not so clear-cut.

* Corresponding author at: University of Warmia and Mazury, Department of Applied Ecology, Oczapowskiego 2, 10-957 Olsztyn, Poland. Tel.: +48 89 523 32 24; fax: +48 89 523 39 69.
E-mail address: mkruk@uwm.edu.pl (M. Kruk).
Peer review under the responsibility of Institute of Oceanology of the Polish Academy of Sciences.

Production and hosting by Elsevier

http://dx.doi.org/10.1016/j.oceano.2016.05.004

1. Introduction

The eutrophication of shallow coastal lagoons and bays has recently become a leading topic in the ecology and biogeochemistry of temperate shelf seas (Lloret et al., 2008; Nixon, 1995; Su et al., 2015; Vidal et al., 1999). A number of research projects focus on the relations between nutrients like phosphorus (P) and nitrogen (N), and the consequent rapid increase in the primary production of phytoplankton, which manifests itself in blooms of Cyanoprokaryota, undesirable from the sanitary and economic state of seas worldwide (Nixon et al., 2001), including shallow coastal waters of the Baltic Sea (Pliński, 2005). The present work addresses this global phenomenon and attempts to demonstrate the spatial differentiation in the nutrient supply and its consequences for the relations between the main phytoplankton assemblages in the summer phase of their reproductive cycles in shallow coastal waters, which are characteristic for such shelf, semi-closed and catchment-dependent seas as the Baltic Sea. This study also refers to a number of publications on the effects of eutrophication in Baltic Sea coastal waters (Pilkaitytė and Razinkovas, 2006; Seppälä and Balode, 1999; Włodarska-Kowalczuk et al., 2014), and points out the spatial hydrological aspect of relationships between the distribution of nutrients and phytoplankton production and structure.

The horizontal distribution of algae in open oceanic waters is regulated by hydrodynamic processes like Kelvin waves and advection, chemical ones such as the differences in nutrient concentrations, and biological ones associated with the dynamics of grazing (Bidigare and Ondrusek, 1996; Lucas et al., 1999). The differences in the phytoplankton assemblage biomasses can also be found as an effect of competition among them for resources (Carey et al., 2014; Chakraborty and Feudel, 2014). The spatial distribution of phytoplankton structure and biomass in shallower coastal sea waters, like the Gulf of Riga (Baltic Sea), depends above all on the levels of nutrients supplied by river waters and subsequently disseminated by sea currents (Seppälä and Balode, 1999).

The general aim of the present work was to show the effect of the uneven distribution of assimilable P and N forms on the relations between the biomasses of the main phytoplankton taxonomic groups. It was achieved by comparing the various levels of N and P species in the two parts of the lagoon with the differences in the phytoplankton assemblage. The particular objectives of this work were to verify a hypothesis on whether the differentiation in water exchange between two parts of the shallow Baltic lagoon was reflected: (1) in the distribution patterns of biomass and dominant species, Cyanoprokaryota, Bacillariophyta and Chlorophyta correlated with N and P compounds and other basic environmental parameters, (2) in the relations between Dissolved Inorganic Nitrogen (DIN) and Soluble Reactive Phosphorus (SRP) and the biomass of the main phytoplankton assemblages during a hot summer day, when the water temperature in the lagoon exceeds 20°C.

The areas of the Vistula Lagoon to be compared in this respect were its shallower western part, influenced by inflows of inland waters but relatively isolated from the effects of the open sea, and its central part, which is deeper and whose waters are exchanged rather more quickly with the open Baltic. We expected to find different nutritional factors responsible for phytoplankton structure, including Cyanoprokaryota domination, in relation to varied exchange of waters in shallow lagoons in the Baltic Sea. This can serve to expand our knowledge of the spatial hydrological causes of harmful algal blooms in shallow coastal water bodies and to find pointers for eliminating these undesirable phenomena.

2. Material and methods

2.1. Study area

The Vistula Lagoon is a shallow coastal water body with specific hydrodynamic and trophic properties. A characteristic feature of the water exchange between the lagoon and the Baltic Sea is the presence of the only connection, the Baltiysk Strait, which cuts through the northern end of the Vistula Spit. The velocity of water movement in and out of the lagoon differs strongly: it is relatively fast mainly in the Russian part of the lagoon, but slow in the more enclosed Polish part. According to Bielecka and Kaźmierski (2003), the speed of inflowing or outflowing lagoon waters off Mamonovo (Kaliningrad Oblast) is 0.04–0.05 m s^{-1}, off Frombork ca. 0.02 m s^{-1} and near the Żuławy Wiślane (Vistula Delta lowlands) less than 0.01 m s^{-1}. One consequence of this slowing down of current flows coming in from the sea and the flows of freshwater from the land is the salinity gradient in the Polish part of the lagoon (Bielecka and Kaźmierski, 2003). The depth of the lagoon and the nature of the bottom sediments are different too: in the deeper (3–4 m) eastern and central parts the sediments consist mainly of mineral matter such as sands and clays, whereas in the shallower (ca. 2 m) western part the emphasis shifts to organic alluvial deposits (Uścinowicz and Zachowicz, 1996).

2.2. Field and laboratory methods

The fieldwork in the Vistula Lagoon was carried out in August 2011, a year with a typical hot summer when water temperature exceeded 20°C from July to the beginning of September: mean water temperature in August amounted 21.5°C near Nowa Pasłęka according to an ecohydrodynamical model simulation (Institute of Oceanography, University of Gdańsk) and phytoplankton growth was intensive. Samples were taken on one day (15 August) in the same meteorological condition and hydrodynamic relations, which guaranteed the high comparability of samples. Twenty-one sampling stations were designated in the two areas of the Polish part of the lagoon. Eleven sampling stations were located in the eastern area, between Frombork and Tolkmicko on the southern shore and Piaski and Krynica Morska on the northern one, and ten such stations were situated in the shallower western area bordering on the Vistula Delta lowlands (Fig. 1). Depth, Secchi Disc visibility, water temperature and dissolved oxygen content (by Hach LDO oxygen probe) were measured at each sampling station in situ.

The volume of 1 dm^3 of surface water (0–0.5 m depth) was taken using a vertical point water sampler at each point for chemical analysis in the laboratory. Samples were collected into dark bottles and cooled. Then, no more than a dozen or so hours later, the water samples were passed through a GF/C (1.2 μm) Whatman glass fibre filter. The

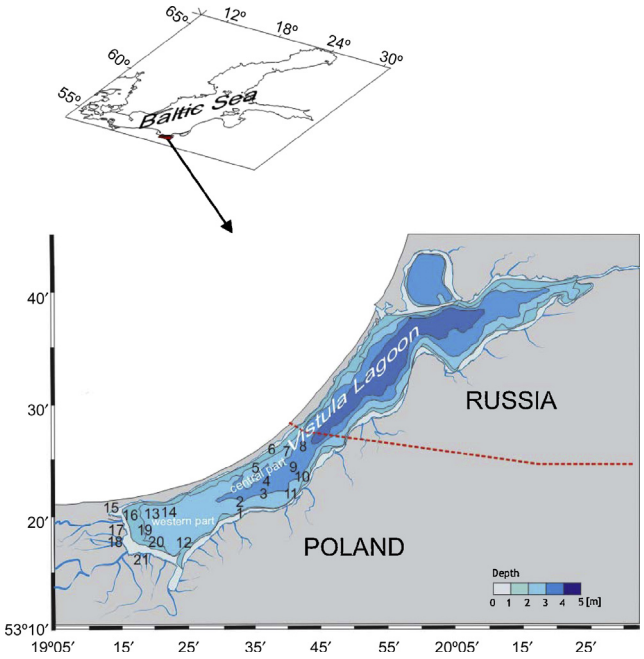

Figure 1 Vistula Lagoon bathymetry and location of sampling sites in the Vistula Lagoon in August 2011 with delimitation of western and central parts; points with numbers indicate sampling sites.

sediment deposited on the filter was analyzed for its content, and the chlorophyll *a* level was estimated spectrophotometrically using the acetone method (Lorenzen, 1967). Soluble Reactive Phosphorus (SRP) was determined with the molybdate blue method, and total phosphorus (TP) by combustion in perchloric acid. Dissolved Inorganic Nitrogen (DIN) was defined as the sum of nitrate and ammonium nitrogen. Nitrate nitrogen (NO_3-N) was determined by reduction to nitrite and ammonium nitrogen (NH_4-N) using Kudeyarov's modification of Solerzano's method. Total nitrogen (TN) was obtained as the sum of Kjeldhal nitrogen as determined by combustion in sulphuric acid and of the nitrate content (APHA, 1996; Golterman et al., 1969).

For the phytoplankton analysis another 1 dm^3 of water was taken from the same depth as that for chemical analysis; in addition, the phytoplankton were sampled for qualitative analysis by hauling a 30 μm plankton net through the water. Lugol's solution was used for sample preservation (Wetzel and Likens, 2000). The quantitative analysis was done on research material which was obtained from the 1 dm^3 samples of water and densified by the sedimentation method (Hötzel and Croome, 1999). The counting units were cells, cenobia or trichomes 100 μm in length. The quantitative analysis was done in accordance to APHA (1996) methodology using 1 cm^3 Sedgwick-Rafter cells. Magnifications of 1 × 10 × 40 and 1 × 10 × 63 (Carl Zeiss Axio Imager A1) were used for the microscopic analysis. The phytoplankton biomass was estimated by measuring cell volumes according to the recommendations of the Baltic Monitoring Programme (HELCOM). Dominant taxa in biomass on a specific site were those with shares in the total biomass of phytoplankton greater than 5%.

2.3. Statistical methods

Canonical Correspondence Analysis (CCA) was used to show the distribution pattern of the phytoplankton groups (Cyanoprokaryota, Bacillariophyta and Chlorophyta) biomass, dominant species of these assemblages in relation to basic physical (temperature, Secchi Disc visibility, dissolved oxygen concentration) and nutrient (SRP, DIN, N:P) parameters, as well as in relation to sampling stations and two parts of the Vistula Lagoon. Prior to CCA, Detrended Correspondence Analysis (DCA) was performed to determine the gradient length of phytoplankton composition. Results of DCA allow subsequent CCA performance due to the results of gradient length for the axes: 3.875 standard deviation. It is recommended to use unimodal methods as CCA when the gradient length is >3 standard deviation (ter Braak and Šmilauer, 2002). Environmental variables were transformed logarithmically (ter Braak and Šmilauer, 2002) and analyzed with forward selection of the Monte Carlo permutation test (499 unrestricted permutations). CANOCO 4.5 software was used for the above ordination analyses. Two-factor correlation and regression analysis was used to demonstrate relationships among nutrients (SRP and DIN) and biomass of three dominant groups of phytoplankton in the western and central parts of the Vistula Lagoon. Test *t* for equality of means was used to compare environmental parameters of two parts of the Vistula Lagoon.

3. Results

3.1. Differences in physicochemical characteristics

The two areas of the Vistula Lagoon selected for this study (Fig. 1) differed above all in their bathymetry. They shared some physicochemical characteristics but differed in others. Table 1 shows that the differences in location, depth and hydrodynamics between the two areas were the most likely reason for the statistically significant ($p < 0.05$) differences in salinity and dissolved oxygen (DO) concentration. The O_2 concentration in the central area of the lagoon (7.35 mg dm^{-3}) was significantly lower than in the western area (9.12 mg dm^{-3}) (Table 1).

Despite a number of significant differences in several physicochemical parameters, the two parts of the lagoon did not differ significantly with respect to levels of chlorophyll *a* (40–42 μg dm^{-3}); moreover, the Secchi Disc visibility was no greater than 50 cm in both parts.

The concentrations of N and P forms in the lagoon waters in summer 2011 differed widely. Mean TP and SRP levels in the shallower, western part of the lagoon were very high at 233 and 34 μg dm^{-3} respectively. These values were significantly higher than the equally fairly high mean levels noted in the central area of the lagoon: 179 μg dm^{-3} TP and 23 μg dm^{-3} SRP (Table 2). Total nitrogen (TN) levels were the same at ca. 0.6 mg dm^{-3} in both areas of the lagoon. But the mean level of Dissolved Inorganic Nitrogen (DIN) was significantly higher in the centre of the lagoon (44 μg dm^{-3} DIN) than in its western part (29 μg dm^{-3} DIN) (Table 2). The stoichiometric relationships between N and P did not differ significantly in the two parts of the lagoon and were very low

Table 1 General characteristics of the two studied parts of the Vistula Lagoon in August 2011: *m* – mean, SD – standard deviation, *p* – significance level of test *t* for equality of means. Significance level $p < 0.05$ in bold font.

Parameter Unit		Depth [m]	Salinity[a] [PSU]	Temperature [°C]	Visibility of Secchi Disc [m]	O_2 dissolved [mg dm^{-3}]	Chlorophyll *a* [μg dm^{-3}]
Central part	*m*	3.3	2.5–4.0	20.2	0.44	7.35	42.0
(*n* = 11)	SD	0.8		0.4	0.08	0.48	24.4
Western part	*m*	2.2	1.5–2.5	21.0	0.47	9.12	40.1
(*n* = 10)	SD	0.4		0.5	0.03	0.95	24.8
p		***0.0024***		***0.0004***	*0.1999*	***0.0001***	*0.8587*

[a] Multiyear ranges of mean salinity (Institute of Meteorology and Water Management data, 2011).

Table 2 Nutrient concentrations in the two studied parts of the Vistula Lagoon in August 2011: *m* – mean, SD – standard deviation, *p* – significance level of test *t* of equality of means. Significance level $p < 0.05$ in bold font.

Parameter Unit		SRP [μg dm^{-3}]	TP [μg dm^{-3}]	DIN [μg dm^{-3}]	TN [mg dm^{-3}]	TN:TP
Central part	*m*	23	179	44	0.60	3.4
(*n* = 11)	SD	9	15	14	0.12	0.6
Western part	*m*	34	233	29	0.64	2.8
(*n* = 10)	SD	13	31	9	0.20	0.9
p		***0.03711***	***0.00024***	***0.01115***	*0.59622*	*0.11558*

in both. The N:P ratio in the water column was ca. 3 in both areas (Table 2).

3.2. Differences in phytoplankton

The dominant taxa in biomass were Cyanoprokaryota, Bacillariophyta and Chlorophyta. Among Cyanoprokaryota, the dominant genera were Aphanocapsa, Aphanothece, Chroococcus, Gloeocapsa, Gomphosphaeria, Microcystis, Dolichospermum, Woronichinia, Snowella and Merismopedia. Identified species were dominant on individual sites of each part of the lagoon. *Microcystis viridis* was the dominant species on sites 1–11 in the central part, but in the western part it dominated on sites 12–16 and 21. Other dominant species on different sites were *Microcystis flos-aquae*, *Microcystis botrys*, and *Microcystis aeruginosa*. The most significant differences in dominant *Microcystis* spp. were found on site 3. *Aphanocapsa holastica* dominated on sites 6–7 and 10–11 of the central lagoon, and on sites 13–21 in the western lagoon. The greatest taxonomic diversity of dominant Aphanocapsa species was found on site 6 in the central part of the lagoon and on sites 17 and 19 in the western part. These were the only sites where biomass was formed by dominant Aphanocapsa species such as *A. holastica*, *A. delicatissima* and *A. incerta*. *Dolichospermum spiroides* and *Dolichospermum flos-aqae* were dominant in biomass only on sites 8, 9 and 10, in the central lagoon. *Worionichinia compacta*, *Woronichinia elorante* and *Snowella lacustris* dominated in biomass only on sites 2, 5 and 7 in the central lagoon. *Gomphosphaeria salina* was also dominant on sites 4 and 9 of this part of the lagoon. Merismopedia species were dominant on sites 12–18 and 19–21 in the western lagoon. The greatest diversity of dominant Merismopedia species (*M. glauca*, *M. punctata*, *M. tenuissima*) was found on site 14. Bacillariophyta dominant in biomass were represented by *Actinocyclus* spp. and *Camphylodiscus* spp. They were dominant on sites 1 and 2. *Camphylodiscus* spp. was also dominant in biomass on sites 3 and 4, and *Actinocyclus* spp. on sites 8–10 in the central lagoon. In the western part the only dominant was *Camphylodiscus* spp. on sites 17–21. Dominant Chlorophyta were represented by Pediastrum and Scenedesmus species. *Pediastrum boryanum* was dominant on sites 1, 2 and 6. In the central part *Scennedesmus* spp. was dominant in biomass on site 20 in the western part (Table 3).

The distribution of dominant species varied in different parts of the lagoon. Species from genera Dolichospermum, Woronichinia, Snowella, Pediastrum and Actinocyclus were dominant in phytoplankton biomass only in the central area. Species representing Merismopedia and Senedesmus were dominant only in the western area. Species representing Aphanocapsa, Aphanothece, Chroococcus, Gloeocapsa, Gomphosphaeria, Microcystis and Campylodiscus were dominant in both lagoon areas, but their distribution on individual sites varied in different parts of the lagoon (Table 3).

The dominant group of algae in the Vistula Lagoon in August 2011 was Cyanoprokaryota, with a mean biomass of 12.9 mg dm^{-3} in the central area and 15.1 mg dm^{-3} in the west. The respective mean biomasses of Bacillariophyta were distinctly lower at 2.4 and 2.9 mg dm^{-3}, but more than those of Chlorophyta (1.3 and 1.6 mg dm^{-3}). Only very low biomasses of species from the other groups were present (Table 4). The differences in the biomasses of the identified

Table 3 List of taxa dominating in the phytoplankton biomass on sites in the central and western parts of the Vistula Lagoon in August 2011. Codes of taxa are used in the CCA plot (Fig. 2).

Taxa	Code	Sites																			
		Central part											Western part								
		1	2	3	4	5	6	7	8	9	10	11	12	13	14	15	16	17	18	19	20	21
Cyanoprokaryota																						
Aphanocapsa delicatissima W. et G.S. West	A del	+				+	+									+	+	+	+	+	+	+
Aphanocapsa holastica (Lemm.) Cromb. et Kom.	A hol						+	+			+	+		+	+	+	+	+	+	+	+	+
Aphanocapsa incerta (Lemm.) Cromb. et Kom.	A inc						+				+	+						+		+		
Aphanothece spp.	Apha								+							+					+	
Chroococcus spp.	Chro						+		+													+
Dolichospermum flos-aquae (Lyngb.) Breb. ex Born. et Flah.	D flaq								+	+	+											
Dolichospermum spiroides Kleb.	D sp								+	+	+											
Gloeocapsa spp.	Gloe			+	+															+	+	
Gomphosphaeria salina Kom. et Hind.	G sal		+		+	+		+		+			+									
Merismopedia glauca (Ehr.) Kutz.	M gla													+	+	+					+	
Merismopedia punctata Meyen	M pun												+	+	+							+
Merismopedia tenuissima Lemm.	M ten												+		+	+	+	+	+			
Microcystis aeruginosa (Kütz.) Kütz.	Mic aer			+									+				+			+	+	
Microcystis botrys Teil.	Mic bot	+		+	+													+	+			+
Microcystis flos-aquae (Witt.) Kirch.	Mic fla	+		+	+	+				+		+		+			+		+			
Microcystis viridis (A. Br.in Raben.) Lemm.	Mic vir	+	+	+	+	+	+	+	+	+	+	+	+	+	+	+	+					+
Snowella lacustris (Chodat) Kom. et Hind.	S lac		+			+		+														
Woronichinia compacta (Lemm.) Strom.	W com		+																			
Woronichinia elorantae Kom. et Kom.-Leg.	W elo					+		+														
Bacillariophyta																						
Actinocyclus spp.	Acti	+	+						+	+	+											
Camphylodiscu spp.	Cam	+	+	+	+													+	+	+	+	+
Chlorophyta																						
Pediastrum boryanum (Turp.) Meneg.	P bor	+	+				+															
Scenedesmus spp.	Scen																				+	

Table 4 Biomass [mg dm^{-3}] of main phytoplankton taxonomic groups in the two parts of the Vistula Lagoon in August 2011. *m* – mean, SD – standard deviation, *p* – significance level of test *t* of equality of means. Significance level $p < 0.05$ in bold font.

Parameter		Share of phytoplankton taxonomic groups				
Phytoplankton Group		Cyanoprokaryota	Euglenophyta	Pyrrophyta	Bacillariophyta	Chlorophyta
Central part	*m*	12.9	0.03	0.17	2.4	1.3
(*n* = 11)	SD	2.0	0.05	0.07	0.9	0.4
Western part	*m*	15.1	0.03	0.16	2.9	1.6
(*n* = 10)	SD	0.9	0.05	0.07	1.0	0.4
p		***0.0132***	*1.00000*	*1.00000*	*0.17199*	*0.11690*

groups of algae in the two areas of the lagoon were statistically significant only in the case of Cyanoprokaryota at the $p < 0.05$ level (Table 4).

3.3. Relationships between phytoplankton and environmental parameters

The CCA ordination method was used to analyze distribution features of the phytoplankton groups' (Cyanoprokaryota, Bacillariophyta and Chlorophyta) biomass, their taxonomic composition and set of environmental parameters, including N and P compounds. The eigenvalues of first two axes were 0.120 and 0.104, and these axes explained 19.5 and 16.8% of the variation, respectively. The Monte Carlo test confirmed that the CCA model was significant with F ratio = 4.35 ($p = 0.002$).

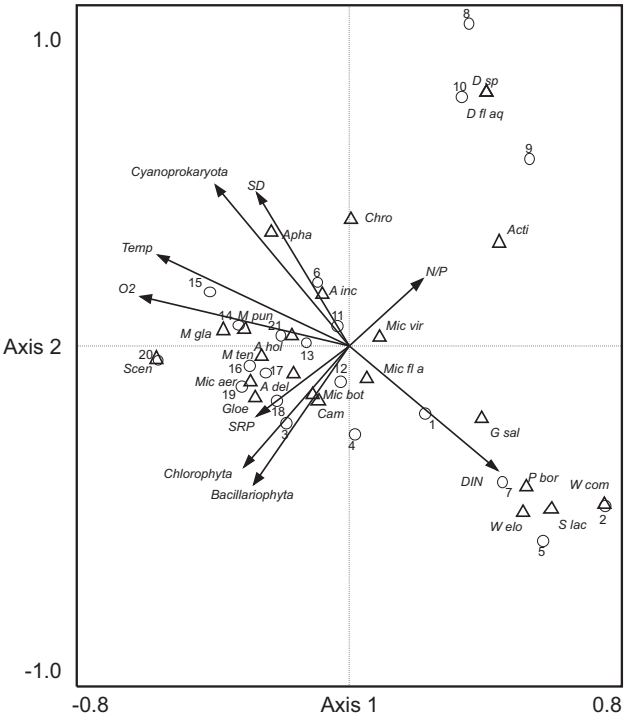

Figure 2 Ordination diagram of Canonical Correspondence Analysis (CCA) including phytoplankton groups Cyanoprokaryota, Bacillariophyta and Chlorophyta biomass (arrows), dominant taxa (triangles – codes are given in Table 3), environmental variables (arrows, bold font – codes are given in Table 5) and sampling sites (circles). The position of sampling sites is divided into the western part (limited by a cluster) and the central part of the Vistula Lagoon.

The CCA 1 axis was interpreted as a gradient of temperature (Temp), Dissolved Oxygen concentration (DO) and Dissolved Inorganic Nitrogen concentration (DIN) (Fig. 2, Table 5). The second axis was much more weakly defined by correlation with environmental variables. Only Secchi Disc visibility (SD) and biological variable Cyanoprokaryota biomass (Cyano) showed significant relations with this axis (Table 5).

The ordination analysis clearly showed an environmental separation between the main phytoplankton groups occurring in the Vistula Lagoon. Bacillariophyta and Chlorophyta biomass had significant positive relationships with SRP concentration and significant negative relationships with the nitrogen to phosphorus ratio (N:P). By contrast, Cyanoprokaryota biomass correlated significantly with the majority of physical-chemical parameters: Secchi Disc visibility (SD), water temperature (Temp), Dissolved Oxygen concentration (DO) (positively) and DIN (negatively), but did not correlate significantly with SRP and N:P (Fig. 2, Table 5).

The present CCA ordination analysis also allowed the identification and delimiting of a cluster of sampling stations belonging to the shallower western part of the Vistula Lagoon (Fig. 2). Assemblages in a limited and coherent area of cluster sampling stations from this part of the lagoon showed that the environmental, taxonomic and biomass relationships of phytoplankton were similar in this region. This contrasted, however, with a wider dispersion on the scatterplot distribution of sampling stations belonging to the deeper central part of the Vistula Lagoon (Fig. 2). Generally, the central part of the lagoon could be defined as positively related to DIN and N:P, and the western part could be characterized by a SRP, as well as by DO and Temp (Fig. 2).

Inside the delimited cluster area on the scatter plot of CCA analysis, referred to as the western part of the Vistula Lagoon, we can find a number of phytoplankton species occurring only in this region (Table 3) as belonging to Cyanoprokaryota *M. punctata* (M pun), *M. glauca* (M gla), *M. tenuissima* (M ten) or Chlorophyta genus *Scenedesmus* spp. (Scen) (Fig. 2).

Table 5 Correlations between environmental and biological (phytoplankton groups biomass) variables and CCA axes (Fig. 2) in the Vistula Lagoon: $p < 0.5$, $p < 0.01$ (with asterisk), $n = 21$.

Variables	Axis 1	Axis 2	SD	Temp	DO	SRP	DIN	N/P	Cyano	Bac	Chlo
Secchi Disc visibility (SD)		0.45					−0.57*		0.62*		
Temperature (Temp)	−0.56*		0.54*		0.93*		−0.66*		0.77*		
Dissolved Oxygen (DO)	−0.61*						−0.58*		0.69*		
Soluble Reactive Phosphorus (SRP)							−0.41	−0.60*		0.61*	0.59*
Dissolved Inorganic Nitrogen (DIN)	0.44								−0.74*		
Nitrogen to phosphorus ratio (N/P)										−0.43	−0.42
Cyanoprokaryota (Cyano)		0.47								−0.46	
Bacillariophyta (Bac)											0.90*
Chlorophyta (Chlo)											

3.4. The influence of nutrient spatial differentiations on phytoplankton biomass

It is evident from Table 2 that the statistically significant differences in nutrient levels in the two parts of the lagoon with respect to algal biomass were accompanied by a similar difference only in the case of Cyanoprokaryota (Table 4). The CCA results also confirmed differences in SRP and DIN directly assimilated by phytoplankton, with biological parameters between the central and western parts of the lagoon. Given the dominance in the biomass of Cyanoprokaryota and also of Bacillariophyta and Chlorophyta, the two groups with the

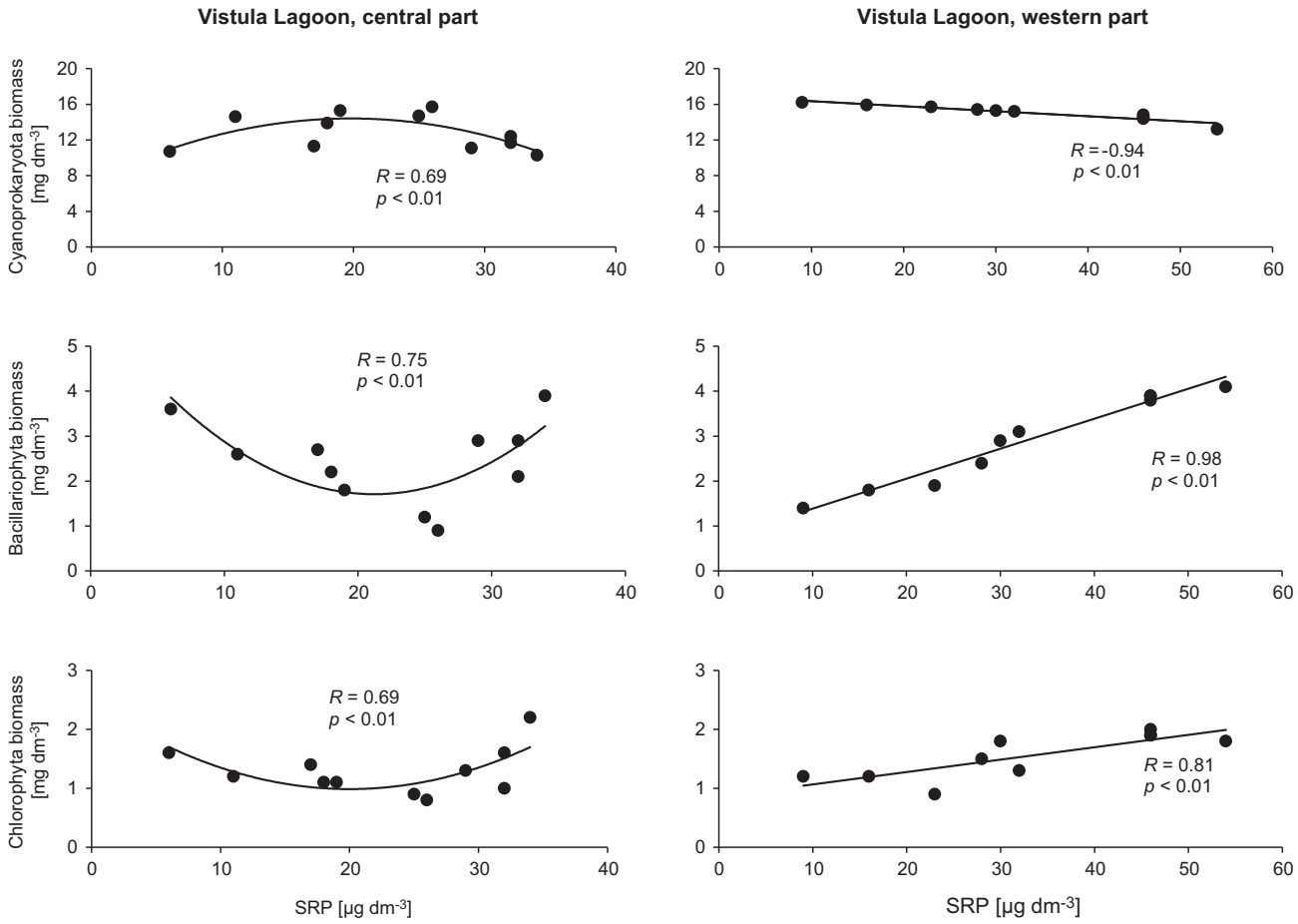

Figure 3 The relationship between concentrations of Soluble Reactive Phosphorus (SRP) [µg dm^{-3}] and Cyanoprokaryota, Bacillariophyta and Chlorophyta biomass [mg dm^{-3}] in the central and western parts of the Vistula Lagoon in August 2011.

next-highest biomasses, we analyzed how the variability in the different SRP and DIN contents in the two lagoon areas affected the biomass of these groups of algae. It turned out that there were distinct differences in the reactions of Cyanoprokaryota on the one hand, and those of Bacillariophyta and Chlorophyta on the other, to changing nutrient levels in the two areas of the Vistula Lagoon.

SRP levels in the western lagoon were relatively high (mean = 34 μg dm^{-3}, Table 2). The relationships between the biomass of Cyanoprokaryota and this nutrient were such that for lower SRP levels the biomass of Cyanoprokaryota was at its highest, whereas that of Bacillariophyta and Chlorophyta was low. Conversely, when SRP levels were higher, the biomass of Cyanoprokaryota was lower, and that of Bacillariophyta and Chlorophyta higher. The relationships between these taxa and SRP levels are described by high correlation coefficients: $R = -0.94$ for Cyanoprokaryota, $R = 0.98$ for Bacillariophyta and $R = 0.81$ for Chlorophyta at a significance level of $p < 0.01$ (Fig. 3). In contrast, in the central part of the lagoon, where SRP levels were lower (mean = 23 - μg dm^{-3}, Table 2), the relationships between the variability in SRP concentrations and the biomass of these three groups of algae were not linear; they can be described by a polynomial function. As in the western part of the lagoon, a higher biomass of Cyanoprokaryota coincided with a minimal biomass of Bacillariophyta and Chlorophyta, whereby the most Cyanoprokaryota were present at SRP levels between 20 and 30 μg dm^{-3} and relatively fewer at higher and lower concentrations. These non-linear relationships between the biomass of phytoplankton groups and SRP levels are described by correlation coefficients of $R = 0.69$ for Cyanoprokaryota, $R = 0.79$ for Bacillariophyta and $R = 0.69$ for Chlorophyta at a significance level of $p < 0.01$ (Fig. 3).

The relationships between DIN and the biomass of the dominant groups of algae in the Vistula Lagoon were different. In the western part the DIN content was distinctly lower than in the central part (mean = 29 μg dm^{-3}) (Table 2). Under such conditions the algal assemblages occurred mainly (in 8 cases out of 10) where DIN levels were higher (30—40 μg dm^{-3}). Here, at higher DIN levels the biomass of Cyanoprokaryota rose but that of Bacillariophyta and Chlorophyta fell. These relationships are described by correlation coefficients of $R = 0.68$ for Cyanoprokaryota, $R = -0.67$ for Bacillariophyta and $R = -0.65$ for Chlorophyta at a significance level of $p < 0.05$ (Fig. 4). However, if DIN levels were higher (mean = 44 μg dm^{-3}) (Table 2), as it was in the central part of the lagoon, lower DIN levels (up to ca. 20 μg dm^{-3}) correspond to maximum biomass of Cyanoprokaryota (ca. 16 mg dm^{-3}) and to minimum that of Bacillariophyta and Chlorophyta. And vice versa: when DIN concentrations were

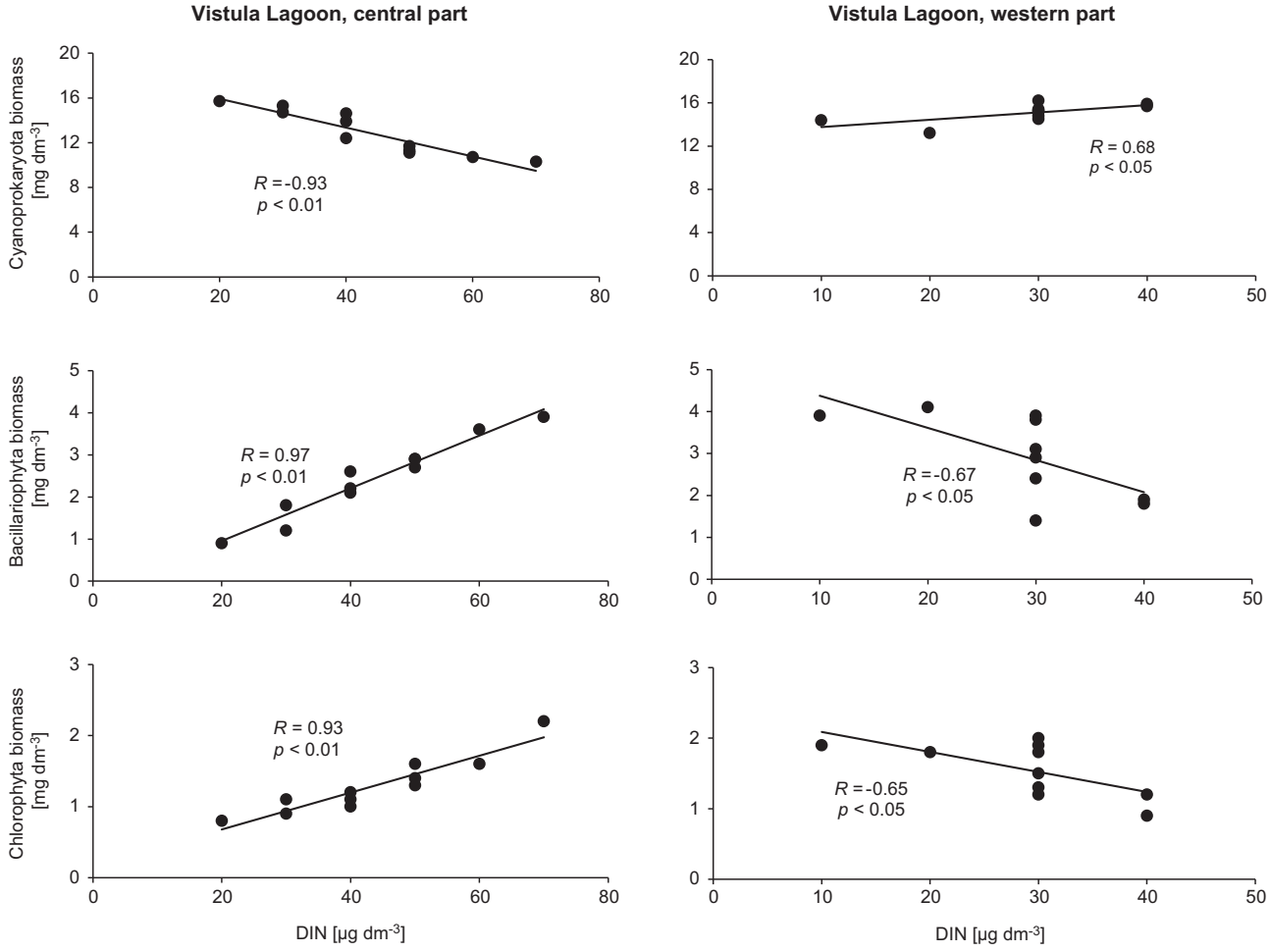

Figure 4 The relationship between concentrations of Dissolved Inorganic Nitrogen (DIN) [mg dm^{-3}] and Cyanoprokaryota, Bacillariophyta and Chlorophyta biomass [mg dm^{-3}] in the central and western parts of the Vistula Lagoon in August 2011.

higher (over 50 μg dm^{-3}), the biomass of Cyanoprokaryota fell to ca. 10 mg dm^{-3} but that of Bacillariophyta rose to ca. 4 mg dm^{-3} and that of Chlorophyta to ca. 2 mg dm^{-3}. These relationships are strongly correlated with one another: $R = 0.93$ for Cyanoprokaryota, $R = 0.97$ for Bacillariophyta and $R = -0.93$ for Chlorophyta at a significance level of $p < 0.01$) (Fig. 4).

4. Discussion and conclusions

The waters of the Vistula Lagoon are enriched principally by N and P compounds entering from point sources (sewage outfalls) and rivers, and released from bottom sediments that have been accumulating pollutants for many decades at least (Kruk, 2012; Pliński, 2005). One result of the presence of N and P loads in the Lagoon's waters is the regular occurrence of Cyanoprokaryota blooms, especially on summer days (Rybicka, 2005). The Lagoon has long been classified as a hypertrophic water body (Nawrocka and Kobos, 2011; Pliński, 2005). However, hydrodynamic differences between the more shallow western part and the deeper part, with faster water exchange, cause various nutrient distributions and may imply differences in eutrophication effects.

In what way do the differences in the spatial distribution of nutrient concentrations affect the biomass of the phytoplankton assemblage under the special conditions of a hot summer day in the shallow Vistula Lagoon? To answer this question, it is important first of all to note that in the areas of the Lagoon we studied, there were significant differences both in SRP and DIN levels, and in the biomass of the dominant phytoplankton assemblage of Cyanoprokaryota. In contrast, no such differences were recorded for the N:P ratio or the biomasses of Bacillariophyta and Chlorophyta. The very low N:P ratios, ranging from barely 2.8 to 3.4, indicated unequivocally that nitrogen was very strongly limited in both areas of the lagoon. At the same time, the western area of the lagoon exhibited distinctly higher SRP and lower DIN levels in relation to the central area. The question therefore arises as to why, despite the similar stoichiometric relations, the spatial distribution of nutrients gave rise to a significantly higher biomass of Cyanoprokaryota in the shallower, less saline and more stagnant waters of the western Vistula Lagoon (Bielecka and Kaźmierski, 2003) than in the central area, which receives more inflows of water from the open Baltic Sea. As shown in the Canonical Correspondence Analysis (CCA), environmental differences between both parts of the Vistula Lagoon, described above, influenced the biomass of dominant phytoplankton assemblages and the taxonomic composition of these groups.

The phytoplankton community acquires nutrients from the water in accordance with Monod's (1942) model, and their assimilation into algal cells under good thermal and light conditions — and such were the conditions prevailing during our study — can take from a matter of minutes to one day (Olsen et al., 2013). The stimulator of algal cell growth, inter alia of ribosomal RNA, is above all assimilable phosphorus (Arrigo, 2005), which is not limited in the Vistula Lagoon. Under such benign conditions, the only possible limitation to the growth of the assemblage of algae living in the lagoon's waters appears to be competition between the various taxonomic groups of algae (and also bacteria) for the available nitrogen.

For simplification, the present study took no account of the range of nutrient assimilability, different in various taxa (Tilman, 1982), the possibility that phytoplankton can assimilate tiny fractions of organic nutrient elements (Davidson et al., 2012; Glibert et al., 1991), or the additional effects of competitive displacement by Cyanoprokaryota such as allelopathy (Suikkanen et al., 2005) or shading (Zevenboom et al., 1982). It was not ruled out, however, that the conspicuously different levels of salinity in the two areas of the lagoon could affect the biomass of algae, including that of Cyanoprokaryota (Rakko and Seppälä, 2014). Moreover, the consumption of phytoplankton by zooplankton seems to be an insignificant factor in the Vistula Lagoon, which is indicated by the lack of proportional relation between the phytoplankton biomass recorded in our study and zooplankton biomass (Cladocera species feeding on algae) in the central and western parts of the Vistula Lagoon (Paturej and Kruk, 2011).

Some species of Cyanoprokaryota are said to be capable of enzymatically fixing atmospheric nitrogen, which in this way makes up for the deficit of nitrogen in algal cells due to the lower N:P ratio (Knuuttila et al., 1994; Smith, 1982). Even though exceptionally low N:P ratios were recorded in our study, the participation of Cyanoprokaryota species potentially capable of binding atmospheric nitrogen appears to be marginal. Here, we have only *D. flos-aquae*, *D. spiroides* (at 3 sampling stations in the central basin). Even under conditions of nitrogen limitation in eutrophic water bodies, the share of Cyanoprokaryota assimilating atmospheric N is no more than a few per cent: this was estimated on the basis of incubational and isotopic studies by Ferber et al. (2004). Therefore, the binding of atmospheric nitrogen by Cyanoprokaryota in the waters we studied was probably of marginal significance in the assimilation of this element and did not affect the relations between these algae and the forms of Dissolved Inorganic Nitrogen in the water.

In the light of our results and the above considerations regarding the part played by different environmental factors capable of modifying the relations between nutrient supply and phytoplankton biomass in a shallow, oligohaline lagoon (Paturej, 2005), we can now put forward the following scheme for the different reactions of the phytoplankton assemblage to the varying supply of assimilable N and P in the central and western areas of the Vistula Lagoon. In the western part, where SRP levels are quite considerable, there is competition for P between Cyanoprokaryota and Bacillariophyta and Chlorophyta, especially when those levels are low. The biomass of Cyanoprokaryota peaks at SRP levels from 15 to 30 μg dm^{-3}; when SRP is higher. However, competition on the part of Cyanoprokaryota weakens, and the biomasses of Bacillariophyta and Chlorophyta then increase.

Bacillariophyta and Chlorophyta require higher SRP concentrations for growth than Cyanoprokaryota (Watson et al., 1997; Zhu et al., 2010). The latter begin to age and die off only when the P supply is completely exhausted (Lafforgue et al., 1995). Moreover, the P resources in the water can maintain Cyanoprokaryota at a relatively constant level, enabling them to grow even when SRP is low. This is because they can accumulate P in larger amounts than other algae (Jensen and Andersen, 1992). As their phosphatase activity is greater, they can assimilate organic P more efficiently (Giraudet et al., 1997; Hadas et al., 1999; Shapiro, 1990), this being a product of their own metabolism, as well as of

competing algae and the excreta of zooplankton (Elser et al., 1987; Keating, 1977).

In the western lagoon there was also a relatively lower supply of DIN; this probably elicits stiff competition for this nutrient. An increase in its concentration led to an almost equivalent increase in the biomass of Cyanoprokaryota at the expense of the biomass of the subdominant algae.

In the conditions of shallow, stagnant waters of the western lagoon, favouring the growth of Cyanoprokaryota, these algae could win the competition for N resources against other phytoplankton groups by bringing into play their specific physiological adaptation mechanisms. In consequence, by producing gas vacuoles and controlling their turgor Cyanoprokaryota are capable of vertical migrations in the water; this enables them to choose habitats that are optimal not only with regard to temperature and illumination, but also to food resources (Dokulil and Teubner, 2000; Humphries and Lyne, 1988). The ability of vertical migration in the stagnating waters of the western lagoon, where the penetration of light to the deeper layers of water was limited by the intense growth of phytoplankton, frequently dominated by the Cyanoprokaryota themselves, also gave them an advantage in their development over other algae (Dokulil and Teubner, 2000; Ganf et al., 1989). A strong correlation between the Cyanoprokaryota biomass and Secchi Disc visibility demonstrated in the study suggests a decisive effect of these algae on water transparency in the Vistula Lagoon.

The competition between the algal groups in the central area of the lagoon, where relatively less SRP and more DIN were recorded, takes on a different aspect. Here, the competition for phosphorus (SRP) was non-linear: in the SRP range from ca. 15 to 25 $\mu g\ dm^{-3}$, Cyanoprokaryota appeared to be the winners, but above and below this range Bacillariophyta and Chlorophyta came into their own. In contrast, increasing levels of DIN in this part of the lagoon favoured the growth of Bacillariophyta in particular (a fourfold increase) but Chlorophyta to a lesser extent; the biomass of Cyanoprokaryota decreased in these conditions. This means that Bacillariophyta found better conditions for growth in the water flowing in from the open sea, probably because the silica content in this water was higher; in addition, its higher salinity might retard the growth of some species of Cyanoprokaryota.

The basic factor limiting the growth of Cyanoprokaryota is the movement of water masses: these algae grow best when the mixing of waters is weak (Berman and Shteinman, 1998; Lafforgue et al., 1995; Lindenschmidt and Chorus, 1998). A change in weather conditions, strong winds, intense rainfall, stronger wave action and other water movements often cause the growth of Cyanoprokaryota to break down. The aquatic environment of the central part of the Vistula Lagoon, periodically affected by the inflow of brackish waters through the Baltiysk Strait and more exposure to air movements, was far less static than the stagnant western part. Under such conditions, the chances of algae other than Cyanoprokaryota ones growing here were much greater. The pressure on the part of Cyanoprokaryota, thus attenuated, could benefit diatoms arriving with the inflows of water from the sea. The most common diatoms are typically brackish-water species, which do not occur in fresh waters. These propitious environmental conditions could have given Bacillariophyta a competitive advantage in the acquisition of food resources and in utilizing the high DIN levels in this part of the lagoon for their growth.

The CCA ordination analysis showed differences between the two parts of the Vistula Lagoon by delimitation a cluster of sampling sites belonging to the shallower western part. Environmental, taxonomic and biomass relationships in sampling stations were similar in this region in comparison with the deeper central part. Generally, the central part of the lagoon could be defined as positively related to nitrogen compounds and to the N to P ratio, and the western part could be characterized by a correlation with a wider range of environmental variables, in which SRP play a significant role.

The differences in the levels of assimilable N and P available to algae between the more 'closed' western area of the Vistula Lagoon and the more 'open' central area, may be shaping the competition for resources between Cyanoprokaryota on the one hand and Bacillariophyta and Chlorophyta on the other; they may explain the differences between these two areas as regards the intensity of Cyanoprokaryota blooms during a hot summer. The biomass of Cyanoprokaryota was greater than that of the other groups of algae when they were competing for the meagre resources of Dissolved Inorganic Nitrogen in the western area of the Lagoon. By contrast, the biomass of Cyanoprokaryota was smaller in the more open central area of the Lagoon, with its higher DIN levels, where the growth of Bacillariophyta superseded that of Cyanoprokaryota. Competition for SRP was not so clear-cut; this was due to the very low N:P ratio characteristic of the trophic status of the entire Vistula Lagoon.

Acknowledgements

The work was supported by the project “System of environmental and spatial information as the background for the sustainable management of the Vistula Lagoon” (VISLA), PNRF 82-AI-01/07.

References

APHA, 1996. Standard Methods for the Examination of Water and Waste Water, 19th ed. APHA, New York, 1274 pp.

Arrigo, K.R., 2005. Marine microorganisms and global nutrient cycles. Nature 437 (7057), 349—355.

Berman, T., Shteinman, B., 1998. Phytoplankton development and turbulent mixing in Lake Kinneret (1992—1996). J. Plankton Res. 20 (4), 709—726.

Bidigare, R.R., Ondrusek, M.E., 1996. Spatial and temporal variability of phytoplankton pigment distributions in the central equatorial Pacific Ocean. Deep-Sea Res. II 43 (4—6), 809—833.

Bielecka, M., Kaźmierski, J., 2003. A 3D mathematical model of Vistula Lagoon hydrodynamics — general assumptions and results of preliminary calculations. In: Diffuse Pollution Conference, ECSA 8, Dublin, 140—145.

Carey, C.C., Wheathers, K.C., Ewing, H.A., Greer, M.L., Cottingham, K.L., 2014. Spatial and temporal variability in recruitment of the cyanobacterium *Gloeotrichia echinulata* in an oligotrophic lake. Freshw. Sci. 33 (2), 577—592, http://dx.doi.org/10.1086/675734.

Chakraborty, S., Feudel, U., 2014. Harmful algae blooms: combining excitability and competition. Theor. Ecol. 7 (3), 221—237, http://dx.doi.org/10.1007/s12080-014-0212-1.

Davidson, E.A., David, M.B., Galloway, J.N., Goodale, C.L., Haeuber, R., Harrison, J.A., Howarth, R.W., Jaynes, D.B., Lowrance, R.R.,

Nolan, B.T., 2012. Excess nitrogen in the U.S. environment: trends, risks, and solutions. Issues Ecol. 15, 1–16.

Dokulil, M., Teubner, K., 2000. Cyanobacterial dominance in lakes. Hydrobiologia 438, 1–12.

Elser, J.J., Goff, N.C., McKay, N.A., Amand, A.L.S., Elser, M.M., Carpenter, S.R., 1987. Species-specific algal responses to zooplankton: experimental and field observations in three north temperate lakes. J. Plankton Res. 9 (4), 699–717.

Ferber, I.R., Levine, S.N., Lini, A., Livingston, G.P., 2004. Do cyanobacteria dominate in eutrophic lakes because they fix atmospheric nitrogen? Freshw. Biol. 49 (6), 690–708.

Ganf, G.G., Oliver, R.L., Walsby, A.E., 1989. Optical properties of gas-vacuolate cells and colonies of *Microcystis* in relation to light attenuation in a turbid, stratified reservoir (Mount Bold Reservoir, South Australia). Aust. J. Mar. Freshw. Res. 40 (6), 595–611.

Giraudet, H., Berthon, J.L., Buisson, B., 1997. A comparison of the daily alkaline phosphatase activity of a cyanobacterium (*Microcystis aeruginosa*) and a diatom (*Synedra capitata*). Biochemistry 320 (6), 451–458.

Glibert, P.M., Garside, C., Fuhrman, J.A., Roman, M.R., 1991. Time-dependent coupling of inorganic and organic nitrogen uptake and regeneration in the plume of the Chesapeake Bay estuary and its regulation by large heterotrophs. Limnol. Oceanogr. 36 (5), 895–909.

Golterman, H.L., Clymo, R.S., Ohnstad, M.A.M., 1969. Methods for Chemical Analysis of Fresh Waters. Blackwell Scientific Publications, Oxford/Edinburgh/London/Melbourne, 172 pp.

Hadas, O., Pinkas, R., Delphine, E., Vardi, A., Kaplan, A., Sukenik, A., 1999. Limnological and ecophysiological aspects of an *Aphanizomenon ovalisporum* bloom in Lake Kinneret, Israel. J. Plankton Res. 21 (8), 1439–1453.

Hötzel, G., Croome, R., 1999. A Phytoplankton Methods Manual for Australian Freshwaters. Land Water Resour. Res. Develop. Corp., Canberra, 58 pp.

Humphries, S.E., Lyne, V.D., 1988. Cyanophyte bloom: the role of cell buoyancy. Limnol. Oceanogr. 33 (1), 79–91.

Jensen, H.S., Andersen, F.O., 1992. Importance of temperature, nitrate, and pH for phosphate release from sediments of four shallow, eutrophic lakes. Limnol. Oceanogr. 37 (3), 577–589.

Keating, K.I., 1977. Allelopathic influence on green-blue sequence in an eutrophic lake. Science 196 (4292), 885–886, http://dx.doi.org/10.1126/science.196.4292.885.

Knuuttila, S., Pietilainin, P., Kauppi, L., 1994. Nutrients balance and phytoplankton dynamics in two agriculturally loaded shallow lakes. Hydrobiologia 275/276, 359–369.

Kruk, M., 2012. The Vistula Lagoon between land and sea. Troublesome consequences. In: Kruk, M., Rychter, A., Mróz, M. (Eds.), The Vistula Lagoon. Environment and its Research in VISLA Project. Wyd. PWSZ, Elbląg, 21–52.

Lafforgue, M., Szeligiewicz, W., Devaux, J., Poulin, M., 1995. Selective mechanisms controlling algal succession in Aydat Lake. Water Sci. Technol. 34 (4), 117–127.

Lindenschmidt, K.E., Chorus, I., 1998. The effect of water column mixing on phytoplankton succession, diversity and similarity. J. Plankton Res. 20 (10), 1927–1951.

Lloret, J., Marín, A., Marín-Guirao, L., 2008. Is coastal lagoon eutrophication likely to be aggravated by global climate change? Estuar. Coast. Shelf Sci. 78 (2), 403–412, http://dx.doi.org/10.1016/j.ecss.2008.01.003.

Lorenzen, C., 1967. Determination of chlorophyll and pheo-pigments: spectrophotometric equations. Limnol. Oceanogr. 12 (2), 343–346.

Lucas, L.V., Koseff, J.R., Cloern, J.E., Monismith, S.G., Thompson, J. K., 1999. Processes governing phytoplankton blooms in estuaries: I. The local production-loss balance. Mar. Ecol. -Progr. Ser. 187, 1–15.

Monod, J., 1942. Recherches sur la croissance des cultures bacteriennes. Hermann, Paris, 210 pp.

Nawrocka, L., Kobos, J., 2011. The trophic state of the Vistula Lagoon: an assessment based on selected biotic and abiotic parameters according to the Water Framework Directive. Oceanologia 53 (3), 881–894, http://dx.doi.org/10.5697/oc.53-3.881.

Nixon, S.W., 1995. Coastal marine eutrophication: a definition, social causes, and future concerns. Ophelia 41 (1), 199–219.

Nixon, S.W., Buckley, B., Granger, S., Bintz, J., 2001. Responses of very shallow marine ecosystems to nutrient enrichment. Hum. Ecol. Risk Assess. 7 (5), 1457–1481.

Olsen, Y., Reinertsen, H., Sommer, U., Vadstein, O., 2013. Responses of biological and chemical components in North East Atlantic coastal water to experimental nitrogen and phosphorus addition – a full scale ecosystem study and its relevance for management. Sci. Total Environ. 473–474, 262–274, http://dx.doi.org/10.1016/j.scitotenv.2013.12.028.

Paturej, E., 2005. The relationships between the zooplankton structure of some coastal lakes and their trophic states. Bull. Sea Fish. Inst. 3 (166), 79–93.

Paturej, E., Kruk, M., 2011. The impact of environmental factors on zooplankton communities in the Vistula Lagoon. Oceanol. Hydrobiol. Stud. 40 (2), 37–48.

Pilkaitytė, R., Razinkovas, A., 2006. Factors controlling phytoplankton blooms in a temperate estuary: nutrient limitation and physical forcing. Hydrobiologia 555 (1), 41–48, http://dx.doi.org/10.1007/s10750-005-1104-6.

Pliński, M., 2005. The hydrobiological characteristics of the Polish part of the Vistula Lagoon: a review. Oceanol. Hydrobiol. Stud. 34 (Suppl. 3), 287–294.

Rakko, A., Seppälä, J., 2014. Effect of salinity on the growth rate and nutrient stoichiometry of two Baltic Sea filamentous cyanobacterial species. Estonian J. Ecol. 63 (2), 55–70, http://dx.doi.org/10.3176/eco.2014.2.01.

Rybicka, D., 2005. Potentially toxic blue-green algae (Cyanoprokaryota) in the Vistula Lagoon. Oceanol. Hydrobiol. Stud. 34 (Suppl. 1), 161–173.

Seppälä, J., Balode, M., 1999. Spatial distribution of phytoplankton in the Gulf of Riga during spring and summer stages. J. Mar. Syst. 23 (1), 51–67.

Shapiro, J., 1990. Current believes regarding dominance of blue-greens: the case of the importance of CO_2 and pH. Verh. Int. Verein Limnol. 24, 38–54.

Smith, V.H., 1982. The nitrogen and phosphorus dependence of algal biomass in lakes: an empirical and theoretical analysis. Limnol. Oceanogr. 27 (6), 1101–1112.

Su, J., Tian, T., Krasemann, H., Schartau, M., Wirtz, K., 2015. Response patterns of phytoplankton growth to variations in resuspension in the German Bight revealed by daily MERIS data in 2003 and 2004. Oceanologia 57 (4), 328–341, http://dx.doi.org/10.1016/j.oceano.2015.06.001.

Suikkanen, S., Fistarol, G.O., Granéli, E., 2005. Effects of cyanobacterial allelochemicals on a natural plankton community. Mar. Ecol. -Prog. Ser. 287, 1–9.

ter Braak, C.J.F., Šmilauer, P., 2002. CANOCO Reference Manual and CanoDraw for Windows User's Guide: Software for Canonical Community Ordination (version 4.5). Microcomputer Power, Ithaca, 283 pp.

Tilman, D., 1982. Resource Competition and Community Structure. Princeton Univ. Press, Princeton, 296 pp.

Uścinowicz, S., Zachowicz, J., 1996. Atlas Geochemiczny Zalewu Wiślanego. Państwowy Instytut Geologiczny, Warszawa, 27 pp.

Vidal, M., Duarte, C.M., Sanchez, M.C., 1999. Coastal eutrophication research in Europe: progress and imbalances. Mar. Pollut. Bull. 38 (10), 851–854.

Watson, S.B., McCauley, E., Downing, J.A., 1997. Patterns in phytoplankton taxonomic composition across temperate lakes of differing nutrient status. Limnol. Oceanogr. 42 (3), 487—495.

Wetzel, R.G., Likens, G.E., 2000. Limnological Analyses, 3rd ed. Springer-Verlag, New York, 429 pp.

Włodarska-Kowalczuk, M., Balazy, P., Kobos, J., Wiktor, J., Zajączkowski, M., Moskal, W., 2014. Large red cyanobacterial mats (*Spirulina subsalsa* Oersted ex Gomont) in the shallow sublittoral of the southern Baltic. Oceanologia 56 (3), 661—666, http://dx.doi.org/10.5697/oc.55-3.661.

Zevenboom, W., Bij de Vaate, A., Mur, L.R., 1982. Assessment of factors limiting growth rate for *Oscillatoria agardhii* in hypertrophic Lake Wolderwijd by use of physiological indicators. Limnol. Oceanogr. 27 (1), 39—52.

Zhu, S.H., Guo, J.A., Aldonaldo, M.T.M., Green, B.R., 2010. Effects of iron and copper deficiency on the expression of members of the light-harvesting family in the diatom *Thalassiosira pseudonana* (Bacillariophyceae). J. Phycol. 46 (1), 974—981.